Max-Planck-Institut
für Meteorologie

MAX-PLANCK-GESELLSCHAFT

Influence of different permafrost processes on the large-scale energy and water cycles over Siberia

Tanja Blome

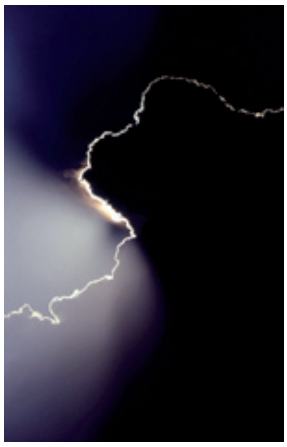

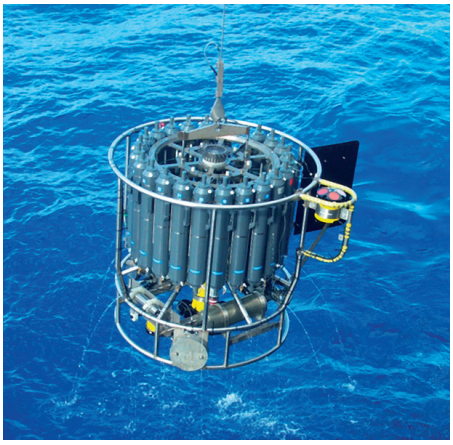

Berichte zur Erdsystemforschung 150
2014

Reports on Earth System Science

Hinweis

Die Berichte zur Erdsystemforschung werden vom Max-Planck-Institut für Meteorologie in Hamburg in unregelmäßiger Abfolge herausgegeben.

Sie enthalten wissenschaftliche und technische Beiträge, inklusive Dissertationen.

Die Beiträge geben nicht notwendigerweise die Auffassung des Instituts wieder.

Die "Berichte zur Erdsystemforschung" führen die vorherigen Reihen "Reports" und "Examensarbeiten" weiter.

Notice

The Reports on Earth System Science are published by the Max Planck Institute for Meteorology in Hamburg. They appear in irregular intervals.

They contain scientific and technical contributions, including Ph. D. theses.

The Reports do not necessarily reflect the opinion of the Institute.

The "Reports on Earth System Science" continue the former "Reports" and "Examensarbeiten" of the Max Planck Institute.

Anschrift / Address

Max-Planck-Institut für Meteorologie
Bundesstrasse 53
20146 Hamburg
Deutschland

Tel.: +49-(0)40-4 11 73-0
Fax: +49-(0)40-4 11 73-298
Web: www.mpimet.mpg.de

Layout:

Bettina Diallo, PR & Grafik

Titelfotos:
vorne:
Christian Klepp - Jochem Marotzke - Christian Klepp
hinten:
Clotilde Dubois - Christian Klepp - Katsumasa Tanaka

Berichte zur Erdsystemforschung 150 2014

Influence of different permafrost processes on the large-scale energy and water cycles over Siberia

Tanja Blome

aus Marburg/Lahn, Deutschland

Hamburg 2014

Reports on Earth System Science 150 2014

ISSN 1614-1199

Tanja Blome
Max-Planck-Institut für Meteorologie
Bundesstrasse 53
20146 Hamburg

Als Dissertation angenommen
vom Department Geowissenschaften der Universität Hamburg

auf Grund der Gutachten von
Professor Dr. Martin Claußen
und
Dr. Stefan Hagemann (habilitiert an der Universität Hamburg)

Hamburg, den 21. Juni 2013
Prof. Dr. Jürgen Oßenbrügge
Leiter des Departments für Geowissenschaften

ISSN 1614-1199

Influence of different permafrost processes on the large-scale energy and water cycles over Siberia

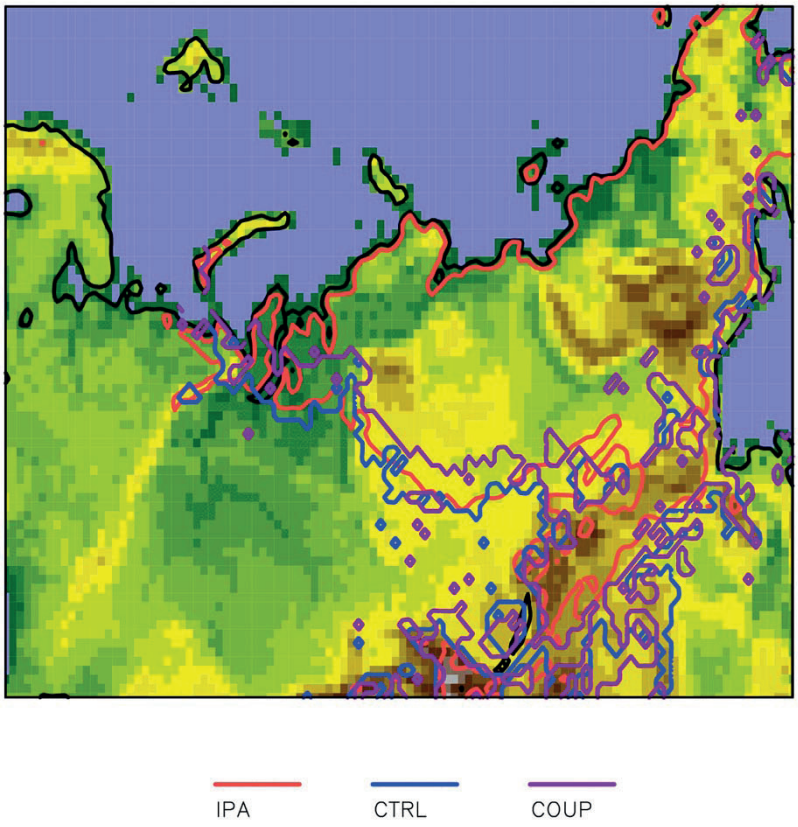

Tanja Blome

Hamburg 2014

Contents

List of used symbols (units given in text) and acronyms

A_{surf}	Amplitude of temperature oscillation at the surface
A	area
C	volumetric heat capacity
C_{froz}	volumetric heat capacity of frozen material
C_{ice}	volumetric heat capacity of ice
C_{unfroz}	volumetric heat capacity of unfrozen material
C_{water}	volumetric heat capacity of water
ET	evapotranspiration
FI	Frost Index
G	ground heat flux
$Infil$	infiltration of surface water into the ground
$Infil_{red}$	reduced infiltration of surface water due to frozen ground
Ke	Kersten number
Ke_{fr}	Kersten number of frozen soils
Ke_{unfr}	Kersten number of unfrozen soils
L_f	latent heat of fusion of water
L	latent turbulent heat flux
$Precip$	precipitation
P	sourc/sink term in energy balance
RO	surface runoff
R_{net}	net radiative flux
$R_{s,net}$	net shortwave radiative flux
$R_{l,net}$	net longwave radiative flux
S	sensible turbulent heat flux

T	temperature
T_{air}	near surface air temperature
T_{soil}	soil temperature
$\bar{T}_{surf}$	mean annual temperature at the surface
U	internal energy
V	volume
a	thermal diffusivity
a_{froz}	thermal diffusivity of frozen material
a_{unfroz}	thermal diffusivity of unfrozen material
ACIA	Arctic Climate Impact Assessment report
ALD	Active Layer Depth
AL	Active Layer
AR2	Second Assessment Report
CH_4	Methane
CMIP5	Coupled Model Intercomparison Project Phase 5
CO_2	Carbondioxide
c	specific heat
C	Carbon
$\dot{Q}$	heat flux
DWD	German weather service
ECHAM	Atmospheric circulation model of the Max-Planck-Institute for Meteorology, Hamburg
ERA40	ECMWF Reanalysis dataset (40 years)
ESM	Earth System Model
fc	soil field capacity
fc_{bucket}	field capacity of bucket scheme
fr_{froz}	fraction of frozen ground in a model grid cell

GCM	Global Circulation Model
GHG	Greenhouse gas
GlobSnow	GlobSnow SWE data
HCE	heat conduction equation
IIASA	International Institute for Applied Systems Analysis
IPA	International Permafrost Association
IPCC	Intergovernmental Panel on Climate Change
IPY	International Polar Year
i	soil layer index
JFP	Johansen-Farouki Parameterization of thermal conductivity
JSBACH	land surface scheme of ECHAM
λ	thermal condcutivity
λ_{dry}	thermal conductivity of dry soil
λ_{froz}	thermal conductivity of frozen material
λ_{ice}	thermal conductivity of ice
λ_{sat}	thermal conductivity of saturated, i.e. moist soil
λ_s	thermal conductivity of soil solids
λ_{unfroz}	thermal conductivity of unfrozen material
λ_{water}	thermal conductivity of water
LSP2	Land Surface Parameter Dataset 2
LSS	land surface scheme
MAAT	mean annual air temperature
MAGT	mean annual ground temperature
MPI-M	Max Planck Institute for Meteorology
$\boldsymbol{n}$	normal vector
PFP	Permafrost Processes

por	soil porosity
$\dot{\boldsymbol{q}}$	heat flux density
RCM	Regional Climate Model
REMO	REgional MOdel
ρ_w	density of water
ρ	density
Sat	soil saturation
Sat_{bucket}	soil saturation from bucket scheme
Sat_{froz}	soil saturation, frozen case
Sat_{unfroz}	soil saturation, unfrozen case
SEB	surface energy balance
SOM	soil organic matter
SWE	Snow Water Equivalent
τ	period of temperature oscillation
θ	volumetric soil moisture content
θ_{ice}	volumetric soil ice content
TSP	Thermal State of Permafrost
t	time
u	specific internal energy
w	actual absolute moisture content
w_{bucket}	absolute water content in soil bucket
w_{liq}	absolute content of liquid soil moisture
w_{sol}	absolute content of solid soil moisture
w_{total}	absolute content of total soil moisture
WFD	WATCH forcing data
$\boldsymbol{x}$	position vector
z	depth

Abstract

Permafrost is an important phenomenon of the land surface in the high northern latitudes. Perenially frozen ground covers one quarter of the terrestrial land surface, and is located in regions where anthropogenic climate change is more pronounced than elsewhere. Observational evidence of this Arctic amplification is supported by theoretical knowledge and from global climate model studies. As permafrost soils store large amounts of organic matter and thus carbon, the large scale thawing of deep-frozen soil carbon could lead to a positive feedback through outgassing of additional greenhouse gases.

Furthermore, model studies suggest that in the high northern latitudes land surface-atmosphere interactions on larger scales are dominated by processes that are specific to permanently or seasonally frozen ground. It is therefore decisive to have these processes incorporated in the soil schemes of the land surface part of climate models. However, many models do not or not fully include frozen ground physics and even with permafrost physics included the uncertainty range in simulations is still large.

In order to study such feedbacks between land surface and climate on the larger scale, the regional climate model REMO was extended with relevant permafrost process formulations as part of this PhD study. Due to the step-wise implementation of the new formulations, it was possible to attribute changes in simulated climate to individual frozen ground processes.
It could be shown for spring and summer, that the near-surface climate was altered mainly by the reduced infiltration of surface water into the ground due to the implementation of soil freezing. This led to a lower state of soil moisture, and influenced the related atmospheric variables, such as 2m air temperature, cloud cover, and total precipitation via surface heat fluxes. Successive incorporation of other frozen ground processes did not show such a strong impact on the atmosphere. Winter climate was not affected due to the insulation of snow.

The soil variables, however, reacted to the implementation of the different physical formulations, and, as expected, were influenced also in the cold season.
The new REMO version with permafrost processes included is able to simulate specific permafrost features, such as the thermal offset effect that tends to stabilize permafrost, and the pronounced freezing and melting during the transition seasons. Moreover, the implemented permafrost processes improved the simulated climate with respect to large-scale characteristics of the high northern latitudes, as surface fluxes of energy and water are now controlled by the thermal state of the ground.

1 Introduction

1.1 Definition

Permafrost is defined as all sub-surface material, be it soil, water, ice, bedrock and/or mixtures of these, that remains at or below 0°C for at least two consecutive years (Riseborough et al., 2008). Almost one quarter of the Earth's land surface is underlain by permafrost (J. Brown et al., 1998), most of which is situated in the high northern latitudes (Figure 1.1). Its spatial distribution is usually mapped in terms of zones or classes, which are described in Section 2.2. In the first place, it is a thermal phenomenon such that permafrost can develop and be sustained where air temperature is low enough to keep ground constantly frozen below a near-surface, seasonally thawing layer, the Active Layer (AL) (French, 2007). Its occurance is thus controlled by climate on the large (regional or hemispheric) scale, while it is modulated by environmental aspects on the local scale. Permafrost is important in the context of climate change and climate modelling due to two important aspects, which will be explained in the following.

1.2 Permafrost and the global Carbon cycle

Earth's climate is determined by the amount of several greenhouse gases, most importantly water vapor, in the atmosphere, which influence the radiation budget and thus the energy balance of the planet. Since fluxes of these gases, namely the biologically produced and consumed gases Carbondioxide (CO_2) and Methane (CH_4), between atmosphere, ocean, vegetation and soils are interrelated and depend on the conditions of the respective component of the Earth's system, it is desirable to represent sinks, sources and the fluxes between them within an Earth System Model (ESM).

In recent years, estimates for the amount of carbon stored in soils have attracted more and more attention, and especially the estimates for the carbon storage in the vast permafrost regions increased numbers drastically (McGuire et al., 2009; Tarnocai et al., 2009; Zimov et al., 2006)). Permafrost is assumed to store between 1400 and 1800 Pg of carbon in the upper few meters of the soil (Schuur et al., 2008), which would be twice the amount of the atmosphere's content. The high northern latitudes are one of the critical regions of anthropogenic climate change, where the observed warming is clearly above average due to the Arctic Amplification (Intergovernmental Panel on Climate Change IPCC, 2007; Arctic Climate Impact Assessment report ACIA, 2005). Climate model simulations project this trend to continue. The combination of the high carbon stocks in

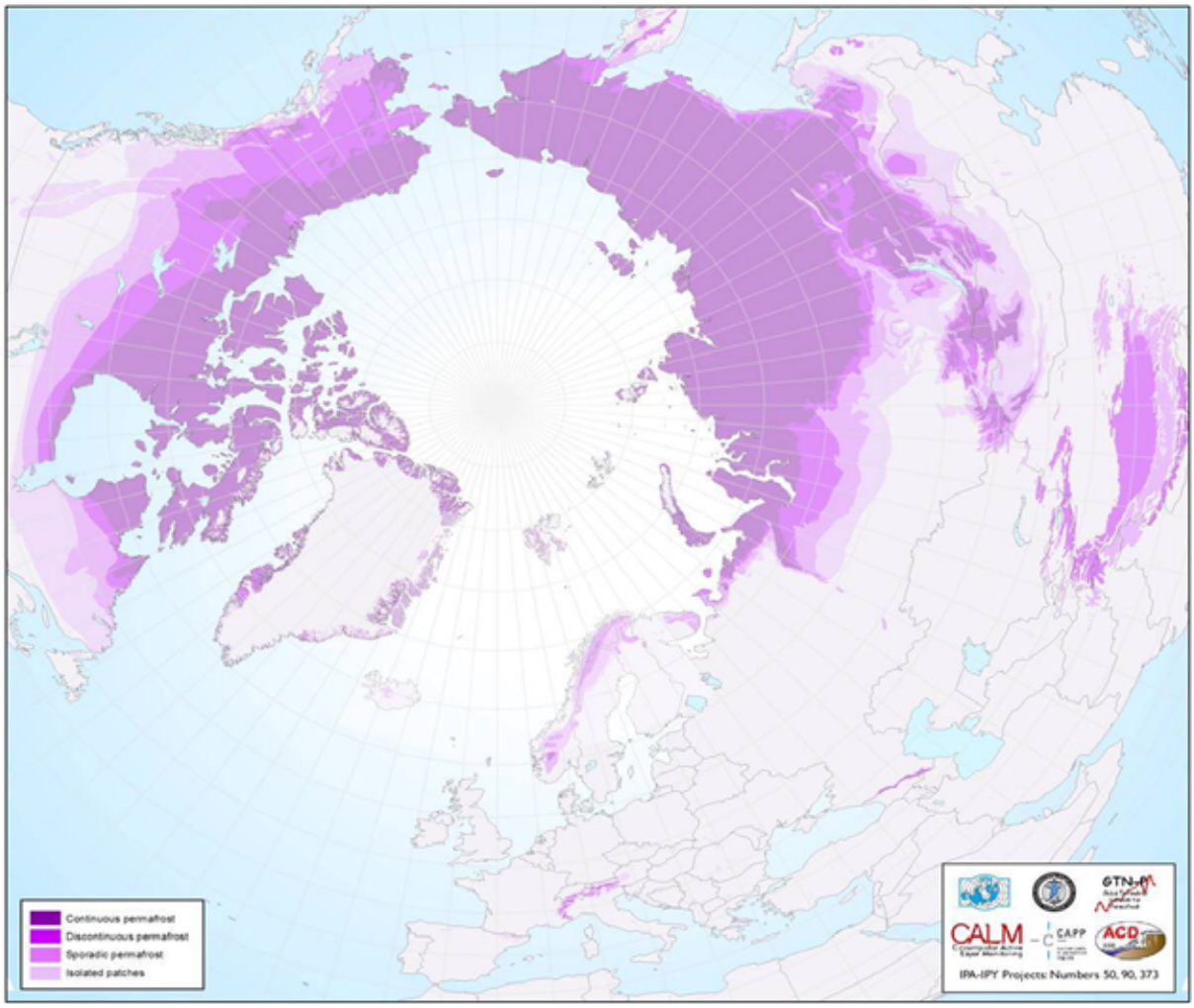

Figure 1.1: Circumpolar view of permafrost distribution on the northern hemisphere according to International Permafrost Association (IPA).

sub-arctic and arctic soils with the pronounced warming in the affected regions could thus lead to a positive feedback through the release of formerly trapped, deep-frozen carbon into the atmosphere, when near-surface permafrost thaws. Hereby, it is less questionable if this feedback will occur, but to which extent additional carbon will be released from permafrost soils.

A possible tool to address this open question are global climate models that incorporate the processes of carbon accumulation and decomposition in their land surface modules. These simulate carbon pools in the individual parts of the land surface (i.e. vegetation and soil), which react on climatic conditions, while climate reacts on changes of the atmospheric carbon concentration. The incorporation of such feedback processes in Global Circulation Model (GCM)s, instead of prescribing carbon concentrations, is part of the development from climate models towards comprehensive ESMs. The processes are represented within land surface schemes (LSS) in biogeochemical models.

The microbial decomposition of soil organic matter (SOM) depends on soil states of temperature, moisture and nutrient supply, which therefore are input parameters for biogeochemical models. For the biogeochemistry in soils, it is decisive whether dry or wet conditions predominate: Aerobic decomposition leads to CO_2, while anaerobic decomposition leads to CH_4 as the main product of the decomposition of SOM. Since CH_4 is roughly 20 times more potent as a Greenhouse gas (GHG) than CO_2, values of both soil temperature and moisture are needed for modelling the biogeochemical response to changes in climatic conditions, and thus should be represented in models in a realistic and process-based manner.

1.3 Permafrost processes in climate models

The land surface influences climate, e.g. through the partitioning of the incoming radiative energy into ground heat flux and latent and sensible turbulent heat fluxes towards the atmosphere. It thus affects the atmosphere in terms of temperature and moisture. Feedback mechanisms were found to work between land surface and atmosphere, as e.g. the soil moisture - atmosphere feedback discussed in Seneviratne et al. (2010), or the snow albedo temperature feedback (Hall and Qu, 2006).

The aim of this work was to study interactions between land surface and atmosphere in permafrost regions, and to better understand the respective relevance of individual processes. For this purpose, a climate model was chosen, as it is able to simulate the feedbacks between climate and land surface. The model climate reacts on changes in the physical formulations of its soil scheme, thereby simulating differences in atmospheric variables that in turn act on the soil. These back-and-forth reactions can not be treated with an off-line land surface model.

The land surface scheme (LSS) of a climate model should be able to reproduce land-atmosphere interactions "as coupled processes, rather than as boundary conditions as was the case with earlier models." (Sushama et al., 2007). These interactions depend on the processes that act on the land surface and in the ground, and these processes should thus be represented by a model in a way that they include the specific and controlling factors. Therefore, studying permafrost regions by using a climate model requires the representation of cold regions' processes in the model's soil.

Permafrost processes have been implemented into the LSSs of several climate models in recent years (more details are given in Section 3.4). Important processes are e.g. freezing and melting of soil moisture and reduced soil water infiltration (Riseborough et al., 2008). However, not all of the Intergovernmental Panel on Climate Change (IPCC) GCMs include the necessary formulations, and the degree of sophistication varys greatly between them. A recent intercomparison study by Koven et al. (2013) analysed the Coupled Model Intercomparison Project Phase 5 (CMIP5) GCMs in terms of their simulated permafrost characteristics. They showed that these diverge to a large degree between the models, even for models that incorporate the same frozen ground processes (Figure 1.2). Thus, the adequate representation of permafrost processes is a necessary and challenging task in climate modelling (Hagemann et al., 2013).

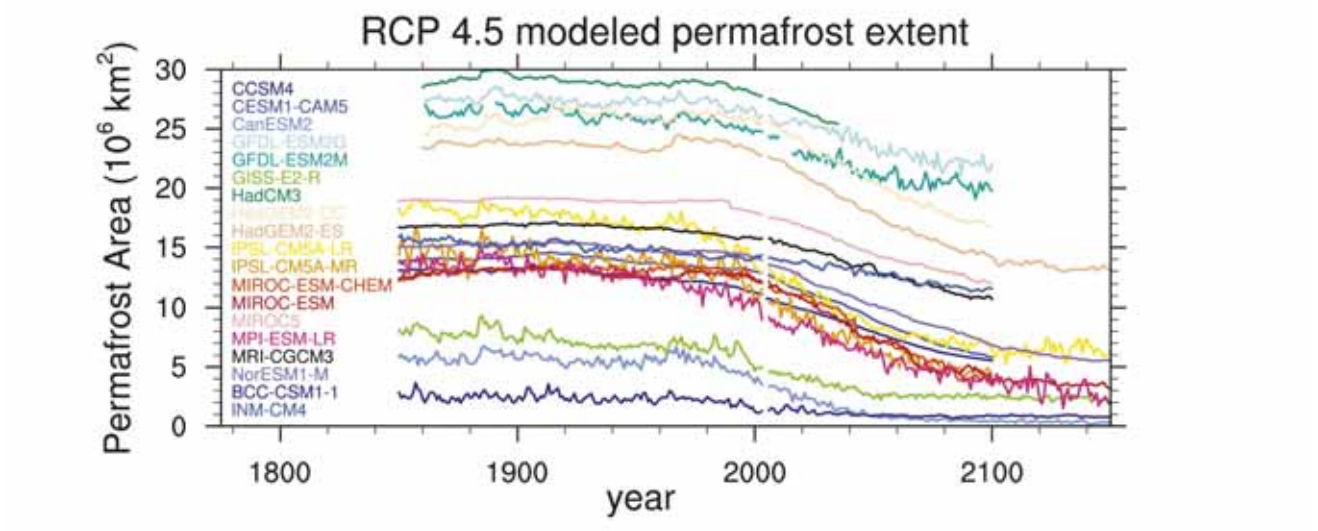

Figure 1.2: Simulated total permafrost area for historical 20^{th} century and future climate following the RCP8.5 scenario for various CMIP5 models. Figure is taken from Koven et al. (2013).

It was decided to implement physical processes that are known to be important for cold regions soil physics into a Regional Climate Model (RCM), as a high spatial resolution is advantageous for studying land surface-atmosphere interactions (Sushama et al., 2007). Using an RCM, it is possible to conduct experiments at a high resolution, which would be much more time consuming and computationally expensive with a global model.

A second reason was a principle difference between global and regional models. The latter are driven at their lateral boundaries with climate data, while global models compute the atmosphere state for the whole globe and, due to the non-linear nature of climate, can drift to its own climatic state. This may complicate the tracing of impacts of changes to a model, while a regional model is constraint to its driving climate, therefore differences must originate in the altered model physics. Moreover, using reanalysis data for driving data ties the simulated climate as close as possible to observed climate ("perfect boundary conditions" (Jacob, 2001)).

The REgional MOdel REMO has been developed as the RCM of the Atmospheric circulation model of the Max-Planck-Institute for Meteorology, Hamburg (ECHAM). Several extensions of soil physical processes were needed to be implemented; the respective details about the theoretical background as well as about their model formulation can be found in Chapters 3 and 4, respectively.

1.4 Research questions

With the above mentioned aim of studying land surface - atmosphere interactions over permafrost regions, the following scientific questions are answered within this thesis:

1. How do different simulated permafrost properties and/or processes influence states of energy and water in the soil and at the land surface?

2. How does permafrost impact seasonal variations of energy and water fluxes on the regional scale?

3. How well does the new REMO model simulate cold regions' soil processes?

These questions can better be answered in a meaningful way if the process implementation is conducted such that changes in the simulated climate that evolve due to altered model physics are attributable to individual processes.
The process implementation was thus conducted in a step-wise manner, as this enabled the attribution of changes in model climate to individual processes; it is therefore possible to analyse their respective impact. This provided reliability of the new soil scheme, which should also improve the LSS of REMO for studies in the high northern latitudes.

Siberia was chosen as experimental region as it covers a large land mass, which implies that interactions between land and atmosphere play an important role in the regional climate; moreover it builds the largest area on earth underlain with permafrost.

1.5 Structure of the thesis

The thesis is structured as follows:
In **Chapter 2**, permafrost as a complex phenomenon of the land surface is described in more detail. It gives an overview of the history of permafrost research and of current knowledge on the phenomenon (Sections 2.1 and 2.2). Section 2.3 explains how the development and characteristics of permafrost are influenced by regional, i.e. climatic, and more local, i.e. environmental, factors. Systems that are in turn influenced by permafrost, such as carbon and water cycles as well as vegetation, are described in Section 2.4.

In **Chapter 3**, the theoretical background of soil physics is introduced in order to understand which processes are important for the representation of frozen ground in climate models (Section 3.3). It also gives an overview of work that has been done so far with other models, and methods that are used when questions related to permafrost and climate are addressed (Section 3.4).

In **Chapter 4**, the status of the soil scheme of REMO at the beginning of the thesis is described (Section 4.2), as well as the implemention of frozen ground processes in REMO and their adaption (Section 4.3).

In **Chapter 5**, results of the experiments conducted with the original and the modified model versions are presented and discussed. In order to answer the above stated research questions, the respective impacts which the step-wise implementation of frozen ground processes had on the simulated climate were first analysed for the soil thermal regime and the surface water balance (Section 5.3.1). Thereafter, the investigation focussed more on characteristics of the larger scale related to cold regions soil processes (Section 5.3.2). Both of these sections give answers to the first two research questions.
In Section 5.3.3, the new REMO version was compared to observational and reanalysis data in order to evaluate both the representation of atmospheric variables on the larger scale, as well as its ability to reproduce properties and processes that are specific to permafrost.

In **Chapter 6**, the findings of the work are summarized and conclusions are given, as well as an outlook to future work.

2 About Permafrost or: Permafrost, climate, and land surface

2.1 History of permafrost science

This section gives a brief overview of the history of permafrost science, and is based on publications by Shiklomanov (2005), Heginbottom (2002), and Riseborough et al. (2008). Since nearly 70 % of the Russian territory is underlain by permafrost, it is not surprising that first written documents on perennially frozen ground originate from Russia, and that Geocryology as an own branch of science formed there (Shiklomanov, 2005).

The report to the Russian zar on the unsuccesfull trial to bore a well in Yakutsk in 1686 was the first written document on the phenomenon of permanent frost, or permafrost. The drilling ceased in a depth of 30.5 m, since it did not seem to be possible to penetrate through the frozen layers and reach an aquifer with the available means (Shiklomanov, 2005).
The 17th century was a period of Russian expansion towards the East, and of fostering of colonisation and of establishment of new cities in Siberia. Many remnants of ice age animals which had been conserved in the frozen ground were recovered during this time. This gave rise to the idea that the ground had not been thawed since the pleistocene.
At the beginning of the 19th century, Russian government decided to enhance trade with and colonisation of the East, therefore the first expeditions were undertaken that had a focus also on permafrost. Among these, the "Voyage to the North and the East of Siberia" from 1842 until 1845 lead by Middendorf was the most important and most recognized. It was the first expedition for which a dedicated report on the actual status of knowledge about permafrost was ordered beforehand, and for which a special instrument, a borer for drilling in frozen soils, was constructed.
Middendorf managed to sample a timeseries of periodic soil temperature measurements for deep permafrost.
He instrumented 'Shergin's well', a shaft that had been drilled as the second try to establish a well in Yakutsk between 1828 and 1837, when work was ceased in a depth of 116.4m, in still frozen ground. Middendorf installed thermometers in secondary, perpendicular boreholes down to the full depth of the shaft. These temperature records can be regarded as the first proof of permafrost by measurements. Middendorf also analysed the observations and extrapolated permafrost depth in Yakutsk, using the temperature gradient he found, to 189.6m. However, there was much debate on his findings; the differing contributions reveal that there was already awareness of the dilemma of disturbing a

phenomenon through observing it. Nervertheless, Middendorf's record remained the only series of temperature measurements in deep permafrost for the rest of the 19th century.

The demand for a map of permafrost distribution increased, and since observational data was scarce, attempts to link air and ground temperatures on the basis of theoretical findings were made (see also Section 2.3.1).

Lopatin was another important pioneer in permafrost research. He conducted thorough investigations of ground ice, and was the first to report on the most important features. He described the most abundant forms of ground ice, but also speculated on the mechanisms behind their development, and on the relationships between landforms, ground ice, and climatic changes. Doing so, he could link, e.g., untypical series of geological layers in England to former glacial periods and collapsing of ice-rich soils due to subsequent warming.
Thoughts about permafrost and its responses to climatic change thus already emerged as early as 1880.

Yarchevskyi compiled the state-of-the-art knowledge at the end of the 19th century. He brought important inputs as he proposed the existence of 'global factors' for permafrost development, such as air temperature and precipitation, which would determine the regional-scale distribution of frozen ground, and of 'local factors', such as soil properties, which decide for a specific site if and how strong permafrost develops. Thus it was seen already at that time that local conditions can prevent or foster permafrost for the same climatic conditions.

The 20th century with its large migration and industrial development brought about a shift in permafrost research towards more practical questions. The next decades lead to substantial increase in data coverage and process understanding. Seven research stations were established all over Siberian territory, and the Permafrost Research Institute in Yakutsk was founded in 1938.

On the other side of the planet, in North America, permafrost research started to evolve with some delay. The second World War can be seen as an ignition for the USA and Canada to put more emphasis on exploring the High North, and, as holds for Russia too, the increasing need for resources, namely fossil fuels, fostered investigation of frozen ground phenomena.

At the end of the 20th century, the rising concern about anthropogenically driven climate change lead to increasing interest in permafrost soils and their relation to climate. This was especially the case since permafrost areas are affected by the Arctic Amplification, therefore facing higher warming rates than other regions on the planet. Complex feedback mechanisms, such as e.g. the ice-albedo feedback, lead to enhanced temperature increase in high Northern latitudes, which is being observed, and which climate models project to continue in the future (IPCC, 2007). Already the IPCC report of 1990 featured a

section on permafrost and its observed and possible reactions to anthropogenic warming. However, changes of permafrost environments through the relatively fast climatic change were seen as problematic solely under socio-economical and ecological aspects, e.g. coastal erosion and destruction of human infrastructure due to melting of soil ice.

In the 1990's, reported values of carbon stored in permafrost soils as deep-frozen SOM rose continuously, and it became clear that perennially frozen ground holds at least twice as much carbon as the atmosphere (Schuur et al., 2008). This brought about the hypothesis of a sofar not considered feedback within the Earth system if large areas of these soils would thaw, thus releasing additional greenhouse gases to the atmosphere. The IPCC had raised the issue of such a feedback in its Second Assessment Report (AR2) (IPCC, 1995).
Permafrost therefore became an important issue for climate modelling, since such a feedback could best be assessed quantitatively using global climate, or ESMs. Section 3.4 will report in more detail on various models and their approaches.

2.2 Contemporary knowledge on permafrost

Permafrost zonation

Permafrost is classified according to its spatial distribution into two to three main zones that reflect the portion of a given land surface underlain by perennially frozen ground (J. Brown et al., 1998; Heginbottom, 2002). Sub-categories have been defined, that in part not only incorporate the percentage of permafrost occurance, but also additional information such as soil ice content. Unfortunately, no clear consensus exists within the permafrost scientific community on how exactly to define these classes. The widest agreement is on the distinction between "continuous" and "discontinuous" zones. These refer to regions with more than 90 % and less than 90 % of the land surface, respectively. Translation of permafrost maps from Russian to English versions, and the in part relatively enclosed development of permafrost research in East and West during many decades may have been reasons for the traditionnally different usage of nomenclatures (Heginbottom, 2002). Table 2.1 shows the attribution of permafrost zones and their respective percentages.

Permafrost Zone	Continuous	Discontinuous	Sporadic	Isolated Permafrost
Surface ratio	$> 90\%$	50 - 90 %	10 - 90 %	< 10 %

Table 2.1: Permafrost zones, representing areal percentage (acc. to Heginbottom (2002)).

Figure 1.1 gives a circum-polar view of contemporary permafrost distribution using these classes. It can be seen that spread and strength of permafrost follow a latitudinal gradient, so that the most continuous permafrost can be found in high latitudes; but also that regional differences modify this latitudinal dependency. Land-sea distribution steers ocean and atmospheric currents in such a way that more maritime conditions develop in some parts, which lead to less severe climate in regions such as, e.g. south and south-western Alaska and Greenland, northern Scandinavia, or the North of the European part of Russia (Romanovsky et al., 2010).

Permafrost depth

A view into the ground reveals that permafrost has its origin to some extent in past climates. The observed depth of the permanently frozen layers in some regions can only be explained if past climatic conditions are considered. During glacial periods, climate was substantially colder than today, and precipitation rates were significantly lower, especially in higher latitudes. Binding of water in the large glacial iceshelfs resulted in lower sea levels than today, thus large continental land masses were exposed to the cold of the overlying air, and could freeze down to depths of more than 1200m (Nelson, 2003).

Ground ice

Although climate for the above mentioned reasons is often very dry, high soil ice contents are observed in many permafrost regions. The reason again can be found in the low temperatures, which lead to freezing of any soil moisture during the cold months. Soil moisture is 'trapped' through freezing, and not readily available for evapotranspiration nor soil water movement at the beginning of the warm season, but needs to be melted first. Thus its resting time is prolongued; cracks in the soil through freezing deliver pathways for infiltration of water from the surface, where refreezing over time yields to the growth of large bodies of ice. These ice bodies thus form storages of water which must not necessarily be in equilibrium with the actual climate, since a large amount of energy would be required to fully melt it.

Water enters the soils through frost cracks and, through volume expansion during freeze-up, further increases the cavities in the ground. Cryosuction leads to movement of unfrozen water towards the freezing front, and, over time, the ice body can grow several meters in height and thickness. This process is slow and lasts many years to decades (French, 2007). As a consequence, permafrost soils often show oversaturated ice contents. This can be seen as long-term storage of both energy and water in the climate system.

Permafrost temperatures

An international initiative for the promotion of geophysical research on key processes in polar regions, the International Polar Year (IPY), also focussed on observations of permafrost temperatures and their possible changes. One of the outcomes of the third IPY, running from 2007 until 2009, was the establishment of a network for monitoring the Thermal State of Permafrost (TSP), which brought about a synthesis of the actual status permafrost is observed in, as well as of trends for the last two to three decades (Romanovsky et al., 2010).
The measurements revealed that soils are warming in many permafrost regions in combination with warmer air temperatures and/or changed snow conditions (Figure 2.1). Warming rates reach from a few tenths of a degree for warm permafrost, where latent heat effects dampen temperature increase, to almost 2 K for colder permafrost areas, where the thermal distance of the ground to the threshold of melting is large enough, and thus all of the additional heat inflow can warm the soil. Due to regional differences both in changes of air temperatures and in precipitation patterns (namely snow), also the observed changes in permafrost temperature vary regionally (Smith et al., 2010; Christiansen et al., 2010; Romanovsky et al., 2010).
Considering other observations, such as from landscape forms (e.g., thermokarst lakes), hydrology, or vegetation, it can be confirmed that permafrost regions and permafrost itself are undergoing a rapid and substantial change (Arctic Climate Impact Assessment report (ACIA), 2005).

Climate change and Permafrost

The response of permafrost to (anthropogenic) climate change is thought to be a possible triggering factor within the complex of GHG induced climate warming (IPCC, 2007).
Its nature is that it is bound to the threshold of melting. Crossing this threshold is possible towards one and the other direction; thus permafrost as a purely thermal feature of the land surface recovers, if temperatures decrease. However, the large amounts of water and carbon stored in permafrost have accumulated in the sub-surface during millenia. Time scales of anthropogenic warming are very short compared to these, and it is impossible to 'recharge' permafrost with similar amounts of carbon than they show today within the short time scales that current climate change is acting on. An optimistic scenario which projects cooling after a century of warming would thus enable permafrost to re-establish in areas where it will decrease over the next decades. Yet this permafrost will hold water and carbon to a much lesser extent (DeConto et al., 2012; Zech et al., 2011).

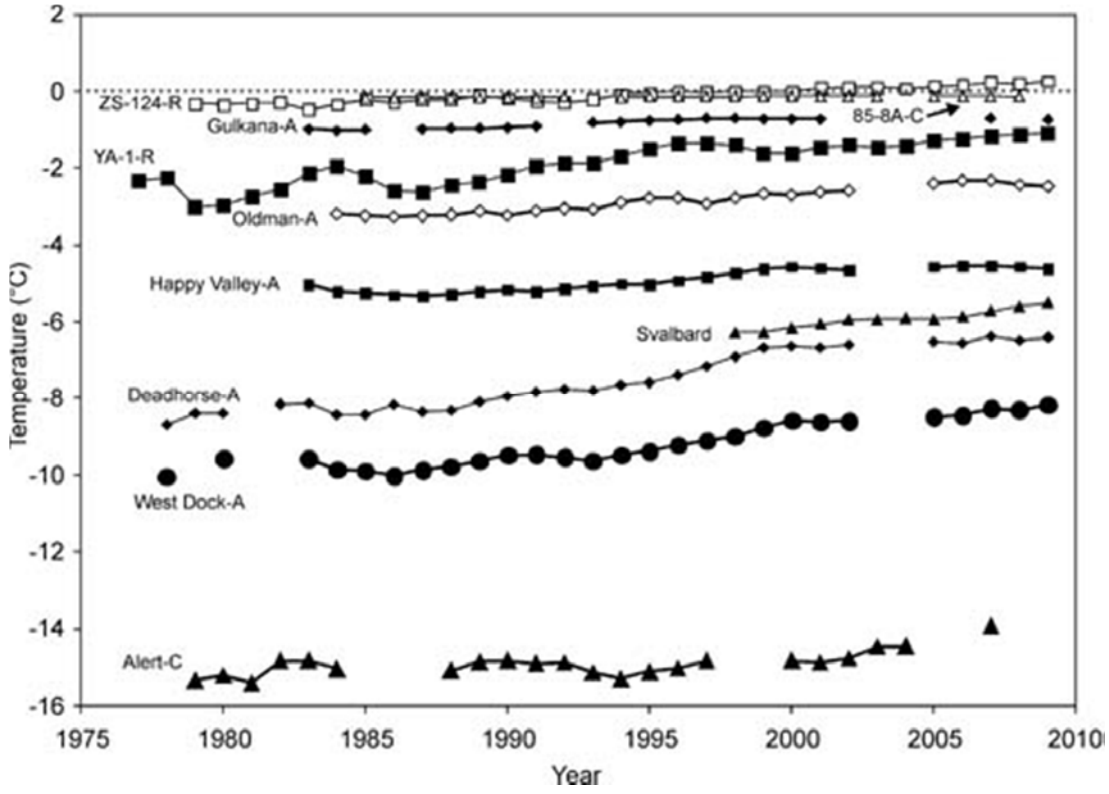

Figure 2.1: Observed permafrost temperatures at different northern hemisphere sites. Figure is taken from Romanovsky et al. (2010).

2.3 What is influencing permafrost?

2.3.1 Climate: Air temperature

Permafrost is a thermal phenomenon, and thus depends on the temperature of the overlying air masses (Nelson, 2003). Many studies have tried to find unambiguos relationships between mean annual air temperatures and the southern margin of permafrost. The presence of permafrost is mainly dependent upon the air temperature being low enough. Nevertheless, for a particular location, many more factors determine the ground thermal regime, as is explained in Sections 2.3.2 and 2.3.3. It is therefore not possible to find a relationship that predicts permafrost occurance based on air temperature allone.

In earlier stages of permafrost research, these approaches were yet the only methods to draw maps of permafrost distribution and of its southern boundary. Examples of these can be found, e.g., in R. Brown (1960). The very first attempt was undertaken as early as 1882 by Wild, who constructed a correlation between air and ground temperatures, basing his assumptions on empirical data (Shiklomanov, 2005). At the end of the 1920's, Nikiforoff hypothesized that permafrost development had taken place north of the -2 °C isotherm (Shiklomanov, 2005). Later studies used the 0°C isotherm, e.g by Terzhagi in the middle of the 20^{th} century (Shiklomanov, 2005), but it rapidly became clear that this would widen predicted permafrost areas too much; obviously, air temperatures needed to be lower than 0°C in order to establish and keep permafrost.
As Russian scientists had stated already in the 19th century (see Section 2.1), local conditions such as snow cover or soil properties modify the climatic, or thermal, signal significantly. Therefore Black in 1950 proposed a range between -1.1 and -4.4 °C for the mean annual air temperature at maximum which allows permafrost to exist (R. Brown, 1960).

The concurrence of permafrost zones' boundaries with certain values of freeze and thaw indices is another method for estimating the spatial distribution of permafrost via relating it to air temperatures. Extensions of these 'index models' exist that also incorporate effects of surface and sub-surface conditions on the ground thermal regime. An overview of the respective approaches and of their use in the context of mapping as well as of climate modelling can be found in Section 3.4.

These approaches link permafrost to contemporary climate and thus cannot predict the full range of observed permafrost. A belt of discontinuos permafrost exists, e.g., in Southern Siberia, the Northern Outer Mongolia, and Manchuria, but its occurance is very patchy, and the islands lay buried within the ground. This permafrost is not in equilibrium with current climate but originates from past cold periods, since it is situated in regions south of the -2 °C isotherm, while no or less permafrost is observed in other regions with the same mean annual air temperatures (R. Brown, 1960).
It is observed, however, that trees seem to suffer from increased drought stress in this region, which is attributed to shrinking sub-surface permafrost (V. Romanovsky, pers.

comm. Nov. 2012). Thus, the above mentioned ancient permafrost might already be substantially degraded today.

2.3.2 Climate: Snow

The second steering climatic factor for the development of the ground thermal regime is the presence and character of a snow cover. A synthesis of the physical effects due to snow will be given in this subsection, following a review by T. Zhang (2005), and references therein.In general, three physical properties or processes related with snow are important modulators of the ground temperature profile:

- snow influences the surface energy balance through its radiative characteristics;
- via its insulating properties, snow controls the energy transfer into the ground;
- the large latent heat consumed during melting forms an energy sink in the surface energy balance (SEB).

These aspects will be explained in more detail in the following.

Radiative properties of snow

Snow cover can modify a land surface's albedo significantly. The strength of this effect depends on the snow grains' specific shape and size, on the solar zenith angle and on cloud conditions, and, up to a certain threshold of melting, on the albedo of the material below. The effect is in most cases a reduction, since snow has one of the highest albedo values amongst natural land surface materials, ranging from 0.6 for old, wet snow to 0.85 for fresh snow (up to > 0.9 for cloudy conditions). The net effect due to albedo varies, depending on geographical area and season:
during autumn, albedo of the fresh snow is high, whilest elevation of the sun is reduced - in consequence, the developing snow cover further decreases energy input for the land surface.
During spring, the albedo of the old snow is reduced, compared to autumn, while elevation angle of the sun is already almost at its yearly maximum. The cooling effect of snow cover therefore is shown to be larger for spring than for autumn.

Snow is almost a black body in the infrared spectrum, which is reflected in its very high emissivity (0.96 - 0.99). This affects the emission of thermal radiation and therefore surface temperatures. It leads to a cooling of the land surface for the case of snow covered ground in comparison to bare surfaces, if the same amount of energy is emitted by longwave radiation.
A high emissivity in turn requires a high absorptivity. These specific longwave radiative properties lead to differences in how a snow covered surface reacts on cloudy conditions

in contrast to clear-sky weather situations:
The letter often result in the development of near-surface temperature inversions because of the strong radiative cooling, whereas moist, cloudy conditions with their high portion of back-scattered longwave radiation bring about higher snow surface temperatures.

Thermal conductivity of snow

Snow has a very low density due to its high content of air. Values of thermal conductivity as well as of density are displayed in Table 2.2.

substance	$\rho[kg/m3]$	$\lambda[w/mK]$
ice	917	2.24
air	1.2	0.025

Table 2.2: Values of density and thermal conductivity for air and ice (Haeckel, 2008).

It is thus an excellent insulator with thermal conductivities ranging between $\lambda_{snow} < 0.1W/mK$ and $\lambda_{snow} > 0.5W/mK$; values for mineral soils are by a factor of 5 to 20 higher. A snow cover on the ground therefore effectively decouples air and soil temperatures.

Latent heat of snow

The latent heat of fusion of water is $334J/g$, whereas the volumetric heat capacity of ice is only $2.1J/gK$. The melt of snow cover during spring is thus a large sink of energy, although it lasts only two weeks or even less. The effects on the SEB to date are still not fully understood. It is yet a rather short period, so that mean annual ground temperature (MAGT) is not influenced strongly by this effect.

Impacts of snow

General statements on the net effects of the different physical characteristics of snow on the surface are possible:

- high albedo and emissivity rather lead to a cooling of the snow surface;
- the latent heat effect during snow melt season, the insulating properties and high absorptivity rather lead to a warming of the surface

The overall effect of a snow cover depends strongly on aspects like begin and end of snow season, the temperature of the surface and ground before snow fall, atmospheric

conditions and elevation of the sun.

Soil temperatures are impacted by a snow cover in different ways. The net effects depend on temporal and spatial details of the snow cover as well as of the ground, and cannot be seen isolated from atmospheric conditions.
The consequences of the above listed physical properties of snow for ground temperatures will be explained in the following more specific.

The cooling effect due to high albedo affects surface temperatures at the beginning of the snow season, when snow cover is still thin. As soon as snow thickness increases, its insulating qualities come into play and soils are rather warmed. For a $T_{surf} = -15.C$, T_{air} can be in the range of 0 to -50. °C when snow cover is present, yet it must be between 0 and -25. °C for the case of no snow cover.
Also the amplitude of daily temperature fluctuations at the surface are reduced by snow due to insulation, which helps to identify beginning and ending of the snow season in observational time series.
On short time scales, also actual weather situations decide whether snow insulates soil from cooling or from warming, since frontal activity can induce downward sensible heat fluxes.
The MAGT can be raised substantially through a snow cover:
In regions on the North-slope of Alaska, $T_{air} = -13.C$, whereas T_{ground} ranges between -5 and -10. °C because snow cover prevents a more effective heat loss from the ground.

One of the main factors snow is effective through is its depth. The thicker a snow cover, the better its insulating properties can work. A maximum of this effect is reached at approximately 40 cm; greater snow depths do not significantly strengthen insulation any more.
If snow thickness is large enough to let snow cover endure until the next spring, it then can have a cooling effect due to latent heat consumption.
MAGT can be > 0°C, which means absence of permafrost, although mean air temperatures are as low as -6 to -8 °C. Thus the ability of snow to hold summer warmth inside the ground can keep locations unfrozen despite of very cold mean annual air temperature (MAAT)s.

As mentioned, the low thermal conductivities of snow originate from its low densities. Measurements revealed yet how strongly these parameters can vary for snow types of different age and/or history. Two distinct types of snow that are abundant in the Arctic are the so-called depth hoar and wind slab snow, which have contrasting properties. Depth hoar shows very low densities, thus low thermal conductivities, and vice versa for the case of wind slab. The letter develops in Arctic regions with low vegetation and high wind speeds, which leads to thin snow covers that often densify ('tundra snow'). The development of depth hoar depends on high temperature gradients in the snow cover and on low wind speeds, conditions that can be found in regions with rather calm weather conditions and a not too sparse vegetation.

The above listed properties of snow have effects on the establishment and characteristics of permafrost, as can be seen in attributes as spatial distribution, thickness, and temperature of permafrost:

Continuous PF

The Northern coast of Alaska, e.g., features permafrost that is about 4 °C colder and 250 m thicker than in the interior of Alaska, whilest MAATs are the same for both regions. The differences can easily be attributed to different environmental factors which lead to a thin, well conducting snow cover in the North, while in the interior a thicker and less dense snow cover can develop.
Comparisons of MAGT's in forest and taiga ecozones with such in tundra areas in Canada showed that the tundra soils were significantly colder than the forest sites.
Observational studies showed an increase of shrub abundance in the Arctic over the last 50 years. This could be one reason for the concomittand warming of soils.

Discontinuous and sporadic PF

In the discontinuous and sporadic PF zone, snow is an important driver for the presence or absence of permafrost at all. The less widespread permafrost occurs in any region, the more its presence depends on the characteristics of the snow cover.
Sporadic permafrost oftenly is only enabled where relict, ice-rich permafrost occurs, in combination with thin snow cover and isolating peat layers.

To summarize, snow with its unique physical properties is decisive for the ground thermal regime. The development of soil temperatures and thus permafrost depends strongly on snow cover parameters, which can vary significantly between locations even in close vicinity. Therefore these parameters have an important impact on the actual permafrost occurance and peculiarity especially in the non-continuous permafrost areas.

2.3.3 Conditions and characteristics of surface and sub-surface

Surface

The land surface can be seen as a boundary that has to be passed by the intruding heat wave signal. Thus the strength of insulation of the surface material is decisive for the amount of thermal energy that can enter the ground. In this respect, timing, duration and characteristics of snow cover are the most important factors, as is pointed out in section 2.3.2.
Another important insulator is a layer of organic material on top of the soil, since organic material has a very low thermal conductivity. This is especially true for dry organic matter, which conducts heat one order of magnitude worse than the wet material.

Similar effects evolve through typical tundra vegetation types such as moss and lichen, which show a distinct behaviour with respect to their water holding capacity:
Mosses with their sponge-like structure can hold almost their own volume of water, which leads to good conductive properties especially for the frozen case. In contrast, they are excellent insulators when they are dry, as is commonly the case at the end of summer. Non-vascular vegetation types like mosses and lichen therefore tend to 'protect' permafrost through their specific seasonal thermal impacts on the ground, in contrast to vascular vegetation types such as grasses and shrubs, which enhance summer warming and deepen the Active Layer (AL) (Beringer et al., 2001; Canone et al., 2006; Rinke et al., 2008).

Vegetation can also impact heat transport into the ground via its interactions with snow. The high Arctic's most abundant vegetation types, mosses and lichen, are only few centimeters high at maximum, and thus cannot trap snow to a similar extent as higher vegetation types such as tussock grasses do. Cooling in winter is thus more efficient than in shrub-dominated regions.
However, also the reverse effect is observed: A thicker snow cover that persists until late in spring retards soil warming at the beginning of the warm season, thereby relatively cooling the ground in comparison to adjacent locations with a thinner snow cover.
Trees trap substantial amount of snow in their canopy, which tends to decrease snow depths at the ground; this leads to lower soil temperatures. Moreover, forested areas produce more litter, which builds up thick layers of organic matter, only poorly decomposing due to the cold climatic conditions. In combination with the shading effect of the canopy, and a thus reduced solar energy input, forests in general stabilize permafrost.

Sub-surface

In the sub-surface, physical properties of the ground material play an important role, as they determine the quality of heat flow within the soil.
Herein, the distinction of the ground materials themselves might be most decisive. Subsurface materials can consist of bedrock, unconsolidated sediments, mineral and organic

soils. All of these types can, but do not necessarily have to, contain water (and thus ice). Bedrock has the highest thermal conductivities, followed by coarse grained materials such as gravel or unconsolidated sediments of sandy types. Mineral soil texture types in general show higher values than organic ones, and within the class of mineral types, coarser soils conduct better than fine-grained soils. Thermal conductivities of organic material are of a factor of 3 to 4 lower than that of mineral soil texture types (for the moist case). Sections 3.3.2 and 4.3.2 treat this parameter in more detail.

Water and ice in the soil modify its thermal properties significantly, as especially ice has a high thermal conductivity. Ice in soils in general leads to increased thermal conductivities as compared to the same soil without ice; signs and degree of the modification depend on the soil material itself, and on the amount of ice in it. As can be seen in the case of organic material (see above for mosses), already the presence of water can change a soil's thermal properties markedly; letting soil water change its phase can introduce even stronger modifications.

Another important aspect of the thermal state of the ground is the latent heat introduced with the presence of ice. Water is a substance with a very high latent heat of fusion, and as environmental temperatures often vary close to the threshold of melting, it plays an important role in the climate system through transporting energy and delaying temperature variations. The large amount of energy needed to melt ice acts as an additional heat capacity, which leads to the so-called zero-curtain effect during every autumn and spring in permafrost soils:
Soil temperatures stay at 0°C until the full amount of soil water (ice) is frozen (melted), although air temperatures have already decreased (increased) substantially lower (higher). The same process introduces high thermal inertia also on longer time-scales wherever ice (water) contents are high. This explains, e.g., why permafrost areas with soil temperatures close to 0°C only warm slowly with observed climate warming in comparison to cold permafrost regions, where warming rates are higher (Romanovsky et al., 2010).

As explained, water and ice within the sub-surface material have strong impacts on the ground's thermal behaviour. Since bedrock is completely different from soil insofar as water, if at all, is abundant in large but few vains, consequently latent heat effects can appear less widespread. In nature, their occurance is bound to distinct (small with respect to total area/volume) areas, where water over time could open channels to flow through. If and to what extent this happens depends on the type of bedrock, since some materials (like granite) block entering of water completely, others (like limestone) are more permeable.
Therefore, heat transfer in bedrock is dampened to a much lesser extent through latent heat effects. Combined with the high thermal conductivities, heat transfer is in general much more efficient in bedrock than in soils.

2.4 What is influenced by permafrost?

Permafrost on his part is important for the Earth system. It modulates cycles of heat, water, and matter at the surface and below through its distinct characteristics,. This can have implications on many different scales, from local to global.

2.4.1 Carbon cycle

The gaseous carbon compostitions CO_2 and CH_4 are important drivers within the global climate system, as their radiative properties make them effective greenhouse gases. Nevertheless, the surplus of CO_2 due to anthropogenic use of fossil fuels has lead to an increase of mean global temperature. This increase was detected in measurements; modelling studies have shown that the warming rate of the last decades to 150 years can only be explained and reproduced if anthropogenic carbon emmissions are considered in the experiments. The amount of carbon added to the atmopshere as CO_2, and as CH_4, which is roughly 23 times more potent than CO_2, over the next decades is thus crucial for the development of global climate (IPCC, 2007).

Permafrost regions are important in this respect as their soils build large carbon pools. Mechanisms that lead to the high observed carbon contents can be found in the specific conditions that arose through cycles of glacials and interglacials. In general, colder climatic conditions lead to reduced biological activity, thus also less carbon storage via plant growth. However, this is modified when freezing and thawing of the land surface come into play:
Due to short growing seasons in high northern latitudes and deep freezing during every winter, considerable amounts of organic material is trapped from (re-)cycling.
A process that has worked effectively through deep-freezing organic material in the sub-surface is the development of thick, loess type soils, called Yedoma. Wind-driven dust deposition ontop of mostly grass-covered steppe-tundra helped to bury organic material in the permafrost due to fast deposition rates. Since steppe-tundra like conditions predominated the mid-to-high northern latitudes over such long periods considering the whole pleistocene, large amounts of almost un-decomposed organic material could accumulate. This is especially noticeable since Yedoma still is a mineral soil (McGuire et al., 2009; Zimov et al., 2006).

Zech et al. (2011) studied Siberian soils with respect to the age of the stored carbon. They could link observed paleo-temperatures of the probes with their respective age, and concluded that carbon storage rates were high during cold periods, and vice versa. They pointed out that according to their findings and with a synopsis of other investigations, the implementation of permafrost into biogeochemical and climate models is not only important with respect to anthropogenic warming, but also for the correct simulation of the carbon cycle on glacial-interglacial time-scales. Therefore today's large observed amounts of carbon in permafrost soils have a long history, and tapping into this pool brings carbon back into the atmosphere that has not contributed to cycling for centuries or even millenia.

Zimov et al. (2006) have investigated soil probes with a variety of methods in order to verify the mechanism that builds up Yedoma, and to assess the amount of stored carbon for Yedoma soils and the rates at which this carbon would be decomposed. They found that when simulating the loess deposition ontop of grass vegetation in the laboratory, in combination with freeze-thaw-cycles, similar SOM contents as in reality were reached, therefore the mechanism used to explain the development of Yedoma is meaningful. Moreover, carbon emmision rates were measured using in-situ soil probes from several Siberian sites along a climatic transect. Doing so, emmission rates after the initial thawing (for estimation of the vulnerability to decomposition) were measured as well as after several thawing and freezing cycles (in order to observe how fast most of the stored carbon is depleted). Based on their results, they estimate accumulated carbon contents in Yedoma soils to reach up to 450GT; this amount corresponds to more than half of the atmospheric carbon content. In addition to this, SOM is of old, pleistocene origin, and is highly labile, thus rapidly decomposed when brought to thawing. Moreover, even after several thaw-freeze cycles carbon emmissions are still noticeable.

It is known from observations as well as from modelling studies that the high northern latitudes form one of the 'hot spots' of anthropogenic climate change, due to the Arctic Amplification (IPCC, 2007). Observed changes in climate, namely reduction in sea-ice cover, warming and changes in atmospheric water content and thus precipitation patterns are already observed to a stronger degree than in other regions (ACIA, 2005). Model studies project these trends to continue (IPCC, 2007). Permafrost regions are part of these areas and are thus threatened by warming rates of 2.8 - 7.8 K until the end of the 21st century. Such an intense increase in air temperature would mean bringing significant parts of permafrost areas above the threshold of melting. The combination of such high temperatures with the high but labile soil carbon contents imply a positive feedback via decomposition of large amounts of SOM, and thus outgassing of additional CO_2 and CH_4.

Since a considerable portion of this carbon would be of pleistocene origin, its emmission into the atmosphere over relatively short time scales, i.e., decades, is irreversible on the same time scales. Permafrost of course can be re-built, yet it is not possible to recover the high water and ice contents that were accumulated over millenia. For this reason, it is of major concern to what extent permafrost soils will thaw, and how much of its stored soil carbon will be decomposed and emitted into the atmosphere.

2.4.2 Hydrology

General behaviour of hydrology: characteristics and links to frozen ground

Siberia features a strongly continental climate with a large amplitude of air temperatures. The seasonal precipitation patterns are typical for Sub-Arctic and Arctic regions, as winter precipitation is low, most of the snow falls in the beginning of the cold season, and precipitation maxima are observed in summer. The range of precipitation classifies large parts of Siberia as cold-arid, with yearly amounts are very low. It could thus be expected to observe rather low soil moisture, which is not the case - on the contrary, Siberian landscapes often feature wet soils and frequent water bodies. A reason behind this can be found in the low air temperature.

First, it leads to low evaporation rates - a large portion of the soil water cannot leave the ground due to the low energy supply.
Second, the cold temperatures lead to a soil moisture regime that is specific to the permafrost regions, and which is regulated through freezing and melting processes.

Some general features of high Northern latitudes in terms of soil and surface hydrology can be found on the basis of observations, as reviewed e.g. by Swenson et al. (2012). They result from the above mentioned physical peculiarities of the region:

- soil moisture values in upper layers are often high;
- stagnant water in surface layers and/or on top of the soil is frequent;
- river discharge and surface runoff show distinct seasonal cycles:
- sharp spring/early summer peak,
- low base flow (cold season river streamflow);
- observed changes in e.g. river discharge hint to ongoing impact from climate warming;
- non-linear processes on different time scales, e.g. thermokarst, erosion or landslide events.

Typical observed features of the seasonal cycle of hydrological variables will be described in the following, linking them to basic physical understanding of cold regions hydrology. The snow melt, which is usually constrained to a very short period of sometimes less then two weeks, delivers a large water input to the land surface, which at this time of the year is still frozen. Infiltration capacity is thus low, and much of the snow melt water is channelled into surface runoff. The beginning of soil melting coincides with high surface moisture values, and ice melting in near-surface layers occurs on top of still frozen, and thus less permeable, deeper layers. Consequently, drainage is weak, and high soil moisture values develop within the still thin thawed upper layers. Refreezing of infiltrated snow

melt water also contributes to this (Swenson et al., 2012). As the warm season proceeds and the AL deepens, water storage capacity increases. The permafrost table still forms a barriere in the deeper soil, so that a lateral flow can develop, which forms the slow subsurface runoff part. Due to the enlarged water storage and improved drainage, upper soil layers can become drier at this part of the year. Autumn precipitation often coincides with the start of the freezing season, thus again high surface runoff rates are produced, yet much lower than in spring. During winter, immobility of soil moisture and decreased hydraulic conductivity of frozen soils lead to the observed low winter baseflow.

Apart from these effects of the soil processes on hydrological quantities, perennially frozen ground shows some unique features, that are examples for processes acting on both long and short time scales, and that are often highly non-linear.
One of these features are the massive ice wedges that occur in permafrost dominated landscapes (French, 2007), which lead to the oversaturated ice contents often observed in permafrost soils (see Section 2.2).

Specific periglacial processes act on short times scales and can stronlgy alter the morphology. Among these are abrupt changes, occuring when large ice bodies in the soil, after a period of relatively slow and constant warming, collapse in sudden events, e.g. due to intense rain events that bring high heat inputs into the ground. This might lead to considerable change in the landscape through severe soil subsidence, opening of channels, and coastal erosion. Belonging to these phenomena are the so-called thermokarst lakes, that develop when formerly stable permafrost thaws at the top due to perturbation (e.g. a fire event), and soil subsidence and melting ground ice lead to the formation of a lake (French, 2007). Cycles of slow build-up of ice masses in the ground and relatively short-termed collapses in conjunction with the implied morphological changes have happenend ever since. Yet since the atmosphere is warming, and since the atmospheric moisture transport from mid- to high northern latitudes and precipitation and circulation patterns are believed to change with anthropogenic climate change, these events might become more frequent in the future. This again has implications for the carbon cycle, as erosion events bring formerly bound carbon back into the cycle.

Relevance of cold regions' hydrology and implications of climate change

The freshwater input into the Arctic Ocean is depending to a large part on the tributaring rivers' discharge, which is different to oceans in tropical latitudes, where a much higher amount is supplied by precipitation (Serreze et al., 2002). The portion of freshwater is one of the factors controlling sea-ice building, and thus a significant increase or decrease in the amount delivered from the continent could alter this process. Another process that is influenced by the Ocean's stratification is the formation of deep water, which may be perturbed by the surplus of melting ground ice (Peterson et al., 2002).
PF is a sub-surface phenomenon and it is impossible to observe the response to climatic changes inside the ground, apart from point measurements. What can be observed and

measured, however, are variables such as river discharge and runoff, which are linked to PF and seasonal frozen ground and integrate over larger areas, thus reflecting regional climatic changes.
Many studies investigated the influence of permafrost and/or seasonally frozen ground on larger scale hydrological variables, and some found indications/evidence for changes due to climate warming.
They have found, e.g., earlier spring snow melt (D. Yang et al., 2002), and, related to that, an earlier spring peak of the surface runoff (D. Yang et al., 2002). The amounts of winter discharge from large Siberian rivers have increased, the summer values have decreased, with an overall increase of river discharge (Serreze et al., 2002; D. Yang et al., 2002). The positive trend in the total amount of streamflow is detectable since several decades (D. Yang et al., 2002). The patterns of changes of discharge hold for basins with and without human river management, and therefore indicate that they originate in changed physical processes within the earth system (McClelland et al., 2004). A warming of air temperatures was found over Siberia (D. Yang et al., 2002), and in some parts a warming of permafrost temperatures and a deepening of the AL (Romanovsky et al., 2010). The terrestrial water storage seems to have increased in recent years (Landerer et al., 2010). It has been tried to separate effects from human management, fires, permafrost, and increased atmospheric moisture transport, and several investigators conclude that the latter is the main reason for the increase in streamflow from the large Arctic river basins (McClelland et al., 2004), and for the enlarged terrestrial water storage (Landerer et al., 2010). Still, a deeper AL and changes in PF seem to be detectable (Landerer et al., 2010).

2.4.3 Vegetation

Section 2.3.3 gave an overview of the effects of the surface characteristics on the ground thermal regime, and how different vegetation types strengthen or weaken the exchange of energy between atmosphere and sub-surface. This section explains the relevance of permafrost for vegetation, and feedbacks between them with respect to today's and future climatic conditions. Several mechanisms are observed, and for some of these aspects, no consensus yet has been found on the sign of a possible signal with climate warming.

Sections 2.3.3 and 2.3.2 hinted at the interactions between vegetation and snow. Greenhouse induced warming seems to enhance the atmospheric water vapor transport and could increase snow fall in the High Northern latitudes, which would bring about stronger insulation of the ground. As also the snow melt appears to occur earlier, the first order effect of a warmer climate would be a warming of the soil. However, the latter factor can be reversed if shrubs enter formerly tundra-type areas, and snow melt is retarded due to larger amounts of snow trapped by the vegetation. Therefore, a negative feedback between vegetation and snow on permafrost is also postulated, and observed. The actual sign of the signal depends on the specific features of the area, which determine if snow cover is actually increasing, how long it persists on the ground, and how its thermal properties develop during the snow season. These factors depend also on climatic variables such as wind speed (see Section 2.3.2).

Interdependencies between vegetation, snow and soil microbiology are also discussed:
Due to the thicker snow cover around shrubs and the thus higher soil temperatures, soil microbial activity is less stronlgy dampened during winter in the root zones of these plants. This leads to a better nutrient supply at the start of the new growing season, which is advantageous for these species (Sturm et al., 2001, 2005).

Yi et al. (2007) project permafrost to degrade less strongly in the next decades as compared to many modelling studies, since large parts of the Arctic and Sub-Arctic regions feature organic layers on top of the soil, which dampen the warming. This peculiarity is often not represented in climate models, which would lead to an overestimation of ground warming and permafrost shrinking in future warming scenarios.

Through cold soil temperatures, low nutrient supply, and the restriction of the root zone to the thin AL, permafrost is a harsh environment for larger plants to grow in. Taller trees that depend on deep roots, such as aspen, therefore prefer discontinuous permafrost zones where the AL is deep. Other species such as black spruce are better adapted and can survive farther north.
The Siberian larch taiga is an ecosystem where trees and permafrost seem to interdepend such that one is sustaining the other: Larch loose their needles every autumn, thus the insulating organic topping is regularly maintained, and the canopy shades the ground so that radiative warming is reduced; the permafrost on his part forms a reliable water supply during summer, which protects the trees from drought stress.

This coupling has been shown to function in observational studies (Sugimoto et al., 2002), as well as with numerical modelling methods (N. Zhang et al., 2011). The latter study could show that air temperature warming of more than 2 °C could substantially disturb the system through permafrost degradation, and the dominant vegetation type would shift from larch to species that are more resistent to drought stress. Displacing larch with coniferous and decidious forest species has implications for the regional energy and water cycles, as this would change evapotranspiration and thus the partitioning of energy into sensible and latent heat fluxes.

3 Theory and modelling approaches

3.1 The Energy balance of the surface

The energy balance of the surface is written as follows:

$$R_{net} = S + L + G \tag{3.1}$$

where the net radiative flux (R_{net}) is the sum of net shortwave ($R_{s,net}$) and longwave ($R_{l,net}$) radiative fluxes, S and L are the sensible and latent turbulent heat fluxes, respectively, and G is the ground heat flux [W/m^2]. The incoming energy is provided by the solar radiation. This is balanced by the thermal or longwave radiation emitted by the surface according to its emissivity and absolute temperature, and by the turbulent heat fluxes at the surface, S and L, which represent energy transport through atmospheric processes. Part of the incoming energy is transported into the ground, which is called the ground heat flux, denoted by G. The ground heat flux can be defined as the "sum of the energy fluxes below the respective surface" (Kraus, 2008).
Halliwell and Rouse (1987) state that as a general orientation ground heat fluxes sum up to about 10% of the incoming radiation at the surface; for permafrost soils, however, this value can be subtantially higher due to the consumption and release of latent heat during melting and freezing.

3.2 Ground heat flux

In general, three mechanisms for transport of thermal energy, or heat, exist:

1. conduction or diffusion,
2. convection,
3. radiation.

The first two are bound to a transport medium, whereas radiation occurs independently of a carrying substance.
Diffusion is the most important process for heat transfer in soils, therefore its concepts and mathematical formulations will be described in the following. Non-conductive heat transport in soils takes place via convection through water vapor transport, but since this process is of second-order importance on the spatial scales and vertical resolutions

of RCM's (V. Romanovsky, pers. comm. 2010), it will not be included here.

In physics (and physical chemistry), diffusion describes the process through which a fluid medium tends to balance a concentration gradient in order to reach equilibrium, or a statistically homogenous distribution of all fluids and/or solutes over a given space. Thus movement from regions of higher to regions of lower concentrations can be observed, which is ultimately driven by the molecular movement of each particle (Baehr and Stephan, 2010).
The diffusion equation describes the change of concentration with time, and shows that it depends on the strength of the concentration gradient on one hand, and on the material's specific ability to diffuse, or the diffusion coefficient, on the other.
Heat conduction is often referred to as heat diffusion, since the underlying process can be treated equivalent to that of diffusion. A medium intends to achieve equilibrium over a given space, in this case treating heat content or temperature in the same sense as concentration, and a flux of heat from warmer to colder parts results. While in original diffusion the compensating movements are bound to movement of matter, thermal energy wanders through the carrier substance without displacement; yet both processes share molecular movement as their basic driving force.
Although this description is originally valid for solid media, the diffusion process takes place in fluids as well, yet here it is superimposed mainly by convective heat transport, which is by orders of magnitude larger than diffusion (Kraus, 2008).

3.2.1 Heat conduction equation

The derivation of the heat conduction equation (HCE) is based on the first law of thermodynamics (which describes conservation of energy) and on Fourier's law (or "law of heat conduction"). It can be found, e.g. in Baehr and Stephan (2010). Fourier's law is written as follows:

$$\dot{\boldsymbol{q}}(\boldsymbol{x}, t) = -\lambda \nabla T(\boldsymbol{x}, t), \tag{3.2}$$

where $\dot{\boldsymbol{q}}$ denotes the heat flux density $[W/m^2]$, or rate of heat flux, $\boldsymbol{x}$ is the position vector, T is temperature [°C], λ is the thermal condcutivity $[W/mK]$ and t is time $[s]$.
Heat flows in a material with a given temperature gradient, opposite to the direction of the gradient, i.e. from warmer to colder parts. The strength of the flow depends on the strength of the gradient, and on the thermal conductivity, which is specific to all materials and has the unit $[W/(mK)]$. Fourier could thus generalise his observations that, given a certain, constant difference in temperature within a body, this gradient was balanced over time due to heat flowing from the warmer to the colder parts, and that this heat flow is fast in 'good conductors' and where gradients are large, and vice versa.

We imagine a solid, incompressible, homogeneous probe of material with volume V and surface A.
With the first law of thermodynamics one can state that heat content, or internal energy, of the probe changes with time due to heat flow into or out of the probe, and due to internal heat sources/sinks:

$$dU/dt = \dot{Q}(t) + P(t), \tag{3.3}$$

where U is the internal energy $[J]$, or heat, $\dot{Q}$ is heat flux $[W/s]$ (i.e., change in heat content per unit time due to transport of thermal energy through the surface), and P $[J]$ denotes for sources or sinks in the system. These can comprise of chemical or nuclear energy, e.g., or stand for latent heat due to phase change within the probe.
Equation 3.3 states that the amount of energy contained in a given material U changes with time t due to heat flux into or out of the probe, and due to internal processes that lead to increase or decrease of internal energy.
The derivation will be conducted without the additional source/sink term P; the contribution of phase change will be explained later in Section 3.3.1.

Assuming ρ = constant, it can be stated that

$$dU/dt = d/dt \int_V \rho u dV = \rho \int_V \frac{\partial u}{\partial t} dV, \tag{3.4}$$

where u is the specific internal energy $[J/g]$, which is a function of temperature.
Equation 3.4 simply states that the total amount of internal energy U changes with time as the sum of the changes in specific internal energy u of the infinitesimal small parts in the respective volume.

The specific heat capacity c $[J/(gK)]$ is introduced:

$$du = c \cdot dT, \tag{3.5}$$

which describes that the difference in internal energy of a substance depends on the imposed difference in temperature, but is specific to any material through the parameter c. More details on this paramter can be found in sections 3.3.2 and 4.3.3.
Substituting du in Equation 3.4 gives

$$dU/dt = \rho \int_V c \cdot \frac{\partial T}{\partial t} dV, \tag{3.6}$$

where the change in temperature with time appears.

In order to determine the heat flux $\dot{Q}$ through a surface A, we consider a section of the surface, dA, with the normal vector $\boldsymbol{n}$ directed towards the outside.
The heat flux into the volume V through the surface section dA is considered to be

$$d\dot{Q} = -\dot{\boldsymbol{q}}\boldsymbol{n} dA. \tag{3.7}$$

Integrating all fluxes from 3.7 over dA gives the heat flux $\dot{Q}$:

$$\dot{Q} = -\int_A \dot{\boldsymbol{q}}\boldsymbol{n}dA = -\int_V div\dot{\boldsymbol{q}}dV, \tag{3.8}$$

where use was made of the Gauss theorem in order to achieve a volume integral instead of an area integral.

Now resulting terms for dU/dt and for $\dot{Q}$ are used for substitution in Equation 3.3 in order to assess the energy balance:

$$\int_V (\rho c\frac{\partial T}{\partial t} + div\dot{\boldsymbol{q}})dV = 0. \tag{3.9}$$

which leads to

$$\rho c\frac{\partial T}{\partial t} = -div\dot{\boldsymbol{q}} \tag{3.10}$$

In the last part, Fourier's law is recalled in order to substitute $\dot{\boldsymbol{q}}$ in Equation 3.10, which leads to

$$\rho c\frac{\partial T}{\partial t} = div(\lambda gradT) \tag{3.11}$$

It was assumed throughout the derivation that c and λ are constant, which is not fully valid as they depend on temperature in reality. For readability, this was omitted during the derivation, as it is negligible within the temperature ranges of interest for this work. Nevertheless, there are important differences in these parameters when phase change takes place, as is occuring in freezing and melting soils. The related principles will be explained in Section 3.3.2.

In reality, fluxes of heat, and of matter, occur in all three dimensions in the soil. However, vertical heat transport is dominating over lateral fluxes for many problems considering energy exchange between atmosphere and ground (Kraus, 2008). This is especially true for climate models, where the horizontal, i.e. grid cell, scale is much larger than the vertical scale, i.e. the depth and resolution of the soil scheme. Therefore spatial dimensions two and three are omitted, and, again assuming constant thermal conductivity λ, the general HCE is obtained in its one-dimensional form:

$$\rho c\frac{\partial T}{\partial t} = \lambda\frac{\partial^2 T}{\partial z^2}. \tag{3.12}$$

Interpretation of the heat conduction equation with respect to land surface processes

The HCE relates the rate of change of internal energy over time of a substance with the heat flux density into or out of the probe. This heat flux density, or change in heat content, is controlled by the strength of the heat flux (the gradient), and by the material properties, the thermal properties c and λ. General aspects on soils' thermal properties can be found in textbooks, as e.g. Hillel (1980).

The heat capacity C is defined as the amount of energy that is required to warm a unit mass for one K and has the unit $[J/(gK)]$. It is often used in its volumetric form:

$$C = \rho c, \tag{3.13}$$

where ρ is the density of the material $[kg/m^3]$.

The thermal conductivity λ determines how fast heat is distributed within a material. It depends on the material's ability to pass over kinetic momentum on the molecular/atomic level, and is a specific parameter $[W/(mK)]$. In general, the closer the molecules of a substance are, the better heat can be conducted; thus, it is low for gases, higher for liquids, and shows the largest values for solid materials that are organized in a grid-like structure. Therefore, crystalline substances like quartz are good conductors; for the same reason, ice has a high thermal conductivity.

The integration of the HCE using suitable boundary and initial conditions gives solutions for T and G in z and t. These can be found, e.g. in Carslaw and Jaeger (1959). For the purpose of land surface processes, a harmonic, sinusoidal temperature forcing at the surface is assumed and sets the boundary conditions. Temperature at the surface T_{surf} oscillates with amplitude A_{surf} around a mean temperature $\bar{T}_{surf}$. This assumption can be made due to the sinusoidal forcing through solar incoming energy during the annual cycle. Another such oscillation is the daily temperature wave (though it is not truly sinusoidal).
The solution of Equation 3.12 using these assumptions for given $\bar{T}_{surf}$, angular frequency $\omega = 2\pi/\tau$, period of the oscillation τ, soil thermal diffusivity a, and amplitude of the oscillation $A_{surf} = (T_{max} - T_{min})/2$ is

$$T(z = 0, t) = \bar{T}_{surf} + A_{surf} sin\omega t \tag{3.14}$$

The temperature oscillation propagates into the ground, which increasingly dampens the amplitude of the oscillation with depth.
Dampening of the amplitude as well as the depth to which a signal intrudes are functions of the soil diffusivity: well conducting soils show temperature signals in larger depths than weak conducting soils.

Moreover, the damping depth, i.e. the depth at which the amplitude has decreased to $1/e$ of A_{surf}, is a function of the inverse of the angular frequency ω:
Temperature oscillations with high angular frequency, thus short periods, intrude to a smaller depth into the ground than oscillations with the opposite properties. This is reflected in shallow intrusion of the daily temperature wave to only a few centimeters, while the annual temperature fluctuation is detectable down to more than ten meters depth. The temperature wave is subject to a phase lag with depth, so that e.g. the annual maximum, occuring in summer in near-surface zones of the ground, is observed with several months delay in the deeper soil.

3.3 Coupled energy and water in soils

Soils form a matrix, comprising of the soil material, water and/or ice, solutes, and air. They thus react more complex to changes in energy than the pure substances would do, as materials with such different properties are involved and interact (Hillel, 1980). Energy and water budgets within soils are effectively coupled, which to a large part can be attributed to the peculiarities of water. Processes that link energy and water in the ground are:

- the high latent heat of fusion of water (see Section 3.3.1);
- the dependency of the thermal properties on water and ice content (see Section 3.3.2);
- a reduced infiltration of surface water for frozen soils;
- the restriction of water movement to the liquid phase in frozen soils;
- a decreased permeability when soil ice is present;
- cryosuction.

The latter four aspects will be explained in section 3.3.3.

3.3.1 Latent heat of fusion

Freezing (or melting) is the process that occurs when a substance changes phase from liquid to solid (or vice versa). The latent heat of fusion is the amount of energy required to break up the inter-particle bonds in order to melt a substance. The same amount of energy is released when the bonds of the solid phase build up. During phase change, any adding or detraction of energy to or from the substance will not induce a change in temperature. The amount of energy consumed (released) as a substance is warmed (cooled) during the phase change without a change in temperature is thus called the latent heat. It is specific to any material and has the unit $[kJ/kg]$. The HCE including the additional source/sink term is written as follows:

$$\rho c \frac{\partial T}{\partial t} = \lambda \frac{\partial^2 T}{\partial z^2} + L_f \rho_w \frac{\partial \theta_{ice}}{\partial t}, \tag{3.15}$$

where L_f is the latent heat of fusion of water $[kJ/kg]$, ρ_w is the density of water $[kg/m^3]$, and θ_{ice} $[m^3/m^3]$ is the amount of ice that freezes or melts within time t [s].

3.3.2 Thermal properties

Conductivity

Studies in field as well as in the laboratory investigated soil thermal conductivities with respect to their dependencies on material composition, moisture and solutes content (Abu-Hamdeh and Reeder, 2000), or influence of freezing (Farouki, 1981). The principle knowledge of soil thermal conductivity is well based and can be found in textbooks (e.g. Carslaw and Jaeger (1959)). The thermal conductivity of soils is influenced by the thermal and hydrological states of the ground. The main influencing factors for this parameter are the following:

1. soil moisture,
2. thermal state of the ground (through presence of ice),
3. the dry soil's thermal conductivity,
4. bulk density.

Heat flow in soils occurs via the points of contact between the single soil particles. Thus the thermal conductivity of a dry soil is influenced by the number and form of these points of contact, and by the conductive quality of the soil particles themselves. The first aspect is referred to as the 'dry soil conductivity' and is depending on the bulk density: In dense soils, more points of contact exist, and heat can be passed over more easily between single particles.
The second aspect is also called the soil solids' conductivity, as it reflects how high the pure soil material's conductivity would be. For example, sandy soils have a high quartz fraction, which shows highest conductivities of all materials; compared to this, clay soils have high percentages of silicate minerals, and thus heat conduction is weaker in this type of soil.
The largest difference can be observed between mineral and organic soils, due to the much lower conductivity of organic material (Kraus, 2008).

Variations in soil moisture have a large influence on the thermal conductivity of soil. When a dry soil is slowly wetted, water films begin to form on the particles' surfaces, surrounding the contacts between single grains and building meniscii that bridge the air-filled, isolating gaps. This leads to a strong increase of thermal conductivity at the beginning of wetting, since the water films and meniscii are good conductors themselves, but also since they provide an enlarged surface for heat conduction between soil particles. λ increases only weakly at higher saturation values, since then a small surplus of moisture does not impose noticeable changes on the overall λ.
At very low moisture values, however, these general statements do not hold, as then λ is dominated by the dry soil conductivity.

thermal conductivity of ice (λ_{ice}) is about four times higher than thermal conductivity of water (λ_{water}), therefore soil freezing tends to noticeably increase the soil thermal conductivity (Farouki, 1981; Gouttevin et al., 2012; Moelders and Romanovsky, 2006).

As is obvious from the dicussion of the HCE above, soil thermal conductivity is an important parameter for the soil thermal regime. Soil temperatures' response to changes in this parameter is known to be very sensitive from field and laboratory studies (refer to the literature review in Tarnawski and Wagner (1993), which was found also when using climate models (Moelders and Romanovsky, 2006; Saha et al., 2006). Therefore its implementation in a model should be treated with care.

Measurements of the soil thermal conductivity are relatively time-consuming (Tarnawski and Wagner, 1993) and show large variablity, for which reason it is difficult to create spatial data sets of this parameter that in the same time provide a high degree of detail and of accuracy (Saha et al., 2006).

Different parameterizations exist that try to model soil thermal conductivity for different soils, for varying soil moisture values, and also for different thermal states of the ground (Mickley, 1951; Kersten, 1949; De Vries, 1963; Johansen, 1975, and others, see Tarnawski and Wagner, 1993). Some of them are built for certain conditions in terms of the moisture range and/or the soil texture (type), and there seems to be no general formulation for this parameter which covers all possible configurations.
Soil freezing complicates the situation, in many cases increasing thermal conductivities in soils, as explained above (Moelders and Romanovsky, 2006; Tarnawski and Wagner, 1993).

The listed model approaches have been developed on the point scale, and were later brought to small geographic scales. As the governing principles are well understood and since these point models are driven with input parameters collected directly for the location of interest, these models deliver good simulations of what is observed in reality. The aspect of input parameters, however, complicates or prohibits a transfer of these models to the larger scale, as often not all of the needed input parameters can be obtained in spatial distribution. For this reason, e.g. no widespread use is made of the DeVries model in climate models, althoug it proved to work well for frozen and unfrozen soils (Tarnawski and Wagner, 1993).
To the contrary, the model proposed by Johansen (1975) and reviewed by Farouki (1981) is used widely in models with a focus on cold regions' soils (Moelders and Romanovsky, 2006; V. Romanovsky, pers. comm. 2010). For details on this parameterization the reader is referred to Section 4.3.2, where its implementation into REMO is described.

Heat capacity

As λ, soil volumetric heat capacity (C) is a function of the soil texture type and of water and ice contents.
It also increases with increasing water content, yet in a more linear behaviour. Since volumetric heat capacity of ice (C_{ice}) is roughly half as large as the one for water (C_{water}), the heat capacity decreases in soils when they freeze (De Vries, 1963; Gouttevin et al., 2012).

Thermal diffusivity

Dividing λ by C leads to the thermal diffusivity a $[m/s^2]$. It behaves somewhat different with wetting of the soil than the thermal conductivity does:
Since λ increases with added soil water at low saturation values, yet this increase levels off at medium to high saturation values while C increases steadily, the diffusivity shows an increase at the beginning of wetting, but decreases in moist soils when they are further wetted (Warnecke, 1997).
With soil freezing, a increases compared to the unfrozen diffusivity for a given moisture content. Since $\lambda_{froz} > \lambda_{unfroz}$ while $C_{froz} < C_{unfroz}$, in consequence $a_{froz} > a_{unfroz}$ (see Gouttevin et al. (2012), e.g.).

3.3.3 Soil hydrology

Incoming water at the land surface is supplied by precipitation and snow melt. It's partitioning into different fluxes ontop of and into the ground as well as towards the atmosphere is sketched schematically in Figure 3.1.

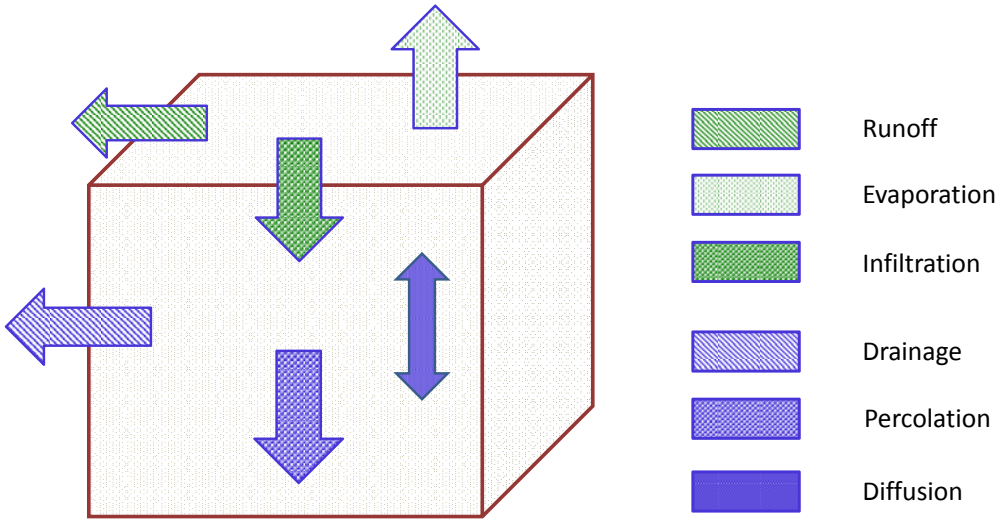

Figure 3.1: Schematic diagram of different hydrological fluxes at the land surface.

Part of the supplied water enters the soil as infiltration. It is controlled by the available volume within the soil, therefore is determined largely by pore space and therefore texture type, and by the saturation history of the ground, i.e. how much of the pore space was already filled. Infiltration capacity varies substantially on small scales, as variation in topography (slope) as well as irregularities in the soil structure (e.g., fissures in the ground material due to worm holes etc.) lead to inhomogeneities.
As soon as soil pores are filled, infiltration capacity is reached, and surplus water flows off laterally towards lakes, rivers, and finally the ocean as surface runoff.

Infiltrated water forms part of the soil matrix, i.e. of the combination of soil solid material, water, maybe ice, solutes, and air. Soil water is confined to the particles of the ground material in adhesive films, and in the network of pores as capillary water.
The degree to which the pore space is filled is called the saturation Sat:

$$Sat = \theta/\theta_{sat} = \theta/por, \tag{3.16}$$

where $\theta = w/V$ $[m^3/m^3]$ is the actual volumetric water content, obtained from absolute water content w $[m^3]$ and V being the considered soil volume $[m^3]$.

Capillary forces enable soil water to be retained in the pores against gravitation up to a certain degree (suction), which is a function of saturation and of the soil texture type.

The specific behaviour of a soil in terms of the balance between capillary and gravitational forces is observed in the differences between soils as they are dried or wetted.
A common method for characterising soils is the retention curve, which shows the increase of water potential, i.e. suction of soil water against gravitation, with decreasing moisture content, and vice versa. A consequence of high suction values is a low ability of the soil to conduct water, whereas wet soils provide good conditions for water flow due to low surface tension.

Percolation is the amount of soil water that exceeds field capacity and cannot be retained by the soil against gravitation. It thus percolates into deeper layers, or, if blocking zones are reached, is channelled into a lateral flow. This sub-surface, slow runoff compartment is called drainage.

Water movement due to gravitation and suction in climate models usually is formulated using the one-dimensional form of the Richards equation for soil water movement. It describes vertical diffusion, which is controlled by the soil moisture gradient and the transport coefficient, the diffusivity. The latter depends on both the actual soil saturation and on the soil texture type: coarse grained materials show rather high diffusivities, whereas fine grained soils retain water more effectively. Organic soils have high diffusivities as their pore space is large. The diffusivity is calculated with the use of the method of Clapp and Hornberger, while percolation is described using the Van-Genuchten parameterization (Hagemann and Stacke, 2013) (in review). Sources or sinks in the system are evapotranspiration or infiltration.

Influence of frozen ground on soil and surface hydrology

In terms of cold regions' soil hydrology, the most important effect that needs to be implemented in a land surface scheme is the phase change of soil water. This is usually done using the additional source/sink term in the heat diffusion equation in order to satisfy the energy balance (Equation 3.15), by which solid and liquid soil moisture contents are obtained. Obviously, only liquid water can move within or out of the ground.

Moreover, the permeability for liquid water flow is reduced in frozen soils, as soil ice retards liquid water movement (Niu and Z.-L. Yang, 2006). According to Staehli et al. (1999), there are two possible pathways for the flow of liquid water when soil temperature is below 0°C. A 'slow' path through the thin films of adsorptive and capillary water, that, depending in their amount mainly on soil texture type, still exist in liquid phase, provides transport channels for water flow, while a 'fast' path through air-filled macropores is supplied due to structural variations like cracks, holes and channels. The reduction of permeability has consequences for two processes:

- **infiltration** at the surface,
- movement of water within the soil, i.e. **percolation**, **drainage**, and **diffusion**.

The decrease of the **infiltration** capacity at the surface is horizontally highly variable, as the above mentioned inhomogeneities increase with soil freezing. Frost cracks, e.g., provide excellent channels for infiltration of water, and the horizontal variations of the snow cover lead to areas with more favorable or more restricting conditions for infiltration. Neighboured regions with the same climatic conditions can therefore show blocking properties in one area, and provide sinks for water inflow in others.

The most simple method to incorporate effects from soil freezing sets infiltration to zero at temperatures below 0°C, which is too strict, as explained above. Another approach is the linear scaling of infiltration with the fraction of near-surface frozen ground. This is also applied in REMO, as is explained in Section 4.3.4 (Equation 4.20). To date, the best method seems to be the use of power-based parameterizations that produce less-than-linear decrease of infiltration. The effect is a less strong blocking when soils are frozen. A larger amount of snowmelt water, e.g., can infiltrate and recharge soil moisture storage in spring. Such effects are reported by e.g. Finney et al. (2012); Gouttevin et al. (2012); Swenson et al. (2012), and references therein.
Soil ice also reduces **percolation**, **drainage**, and **diffusion** of soil water. The presence of ice in the pores reduces the volume available for liquid water movement, and liquid water films are thinner than they would be in an unfrozen soil with the same total water content. Therefore, they have a higher surface tension, which increases suction. This in turn leads to decreased diffusivities.

In order to parameterize the effect on the diffusivity in models, an analogon between drying/wetting and freezing/thawing can be used, which represents the dependency of suction on saturation for frozen soils.
The soil characteristic curve is considered, but hereby taking the liquid for the total water content. Resulting suction (potential) and thus diffusivity can be obtained from the retention curve.
Figure 3.2 illustrates the effect on the saturation for a frozen soil when using the liquid soil moisture content w_{liq} instead of the total soil moisture content w_{total} for the computation of diffusivity. It becomes clear that, especially for high total moisture contents and strongly frozen soils (thus $w_{liq} << w_{total}$), the difference between Sat_{froz} and Sat_{unfroz} can be substantial for the same w_{total}.

Also, taking w_{liq} in place of w_{total} produces a soil moisture gradient in the region of freezing. Movement of liquid water towards the freezing front is resulting, where it crystallizes, and thickens existing ice. The region of phase change can therefore be seen as a water sink in the soil, which induces liquid water migration towards the freezing front. This so-called cryosuction leads to high soil moisture contents in near-surface layers, as well as it explains the growth of large ice bodies and of extensive frost heave. The degree to which a soil can hold unfrozen water depends on its texture type (Farouki, 1981; Romanovsky and Osterkamp, 2000). Fine grained soils have larger capillary forces than coarse soils and show higher unfrozen water contents. The above explained phenomena are thus observed in these regions featuring fine texture types. Coarse grained soils,

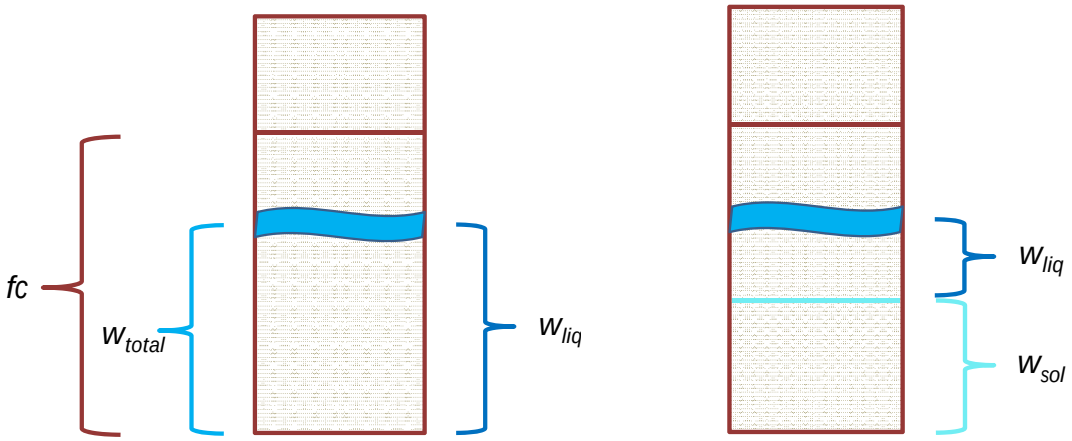

(a) Unfrozen case (b) Frozen case

Figure 3.2: Schematic diagram of effect of considering liquid instead of total water content for computation of hydraulic diffusivity: Unfrozen (a), frozen (b) case of soil with given field capacity fc (corresponds to maximum possible water content), w_{total}, w_{liq}, and w_{sol}. Considering w_{liq} instead of w_{total} for the determination of θ leads to lower values of Sat, i.e. $Sat_{unfroz} < Sat_{froz}$.

to the contrary, tend to simply 'run empty' before notable moisture migration towards the freezing front, against gravitation, could occur.
The analogon between freezing/melting and drying/wetting is useful for modelling, as the same parametrizations for the diffusivity can be employed for frozen than for non-frozen soils.

The liquid water content can be obtained from the energy balance (Equation 3.15). It is also possible to compute liquid water content at $T < 0°C$ with the use of a freezing point depression equation. For a range of mineral texture type soils it limits freezing through allowing more water to stay liquid than the energy supply would determine.

Approaches that combine freezing point depression equation and the use of only the liquid water content for the hydrological parameterizations are more and more common in the LSSs of climate models. They 'automatically' lead to decreased hydraulic conductivities for cold ground materials, and may simulate cryosuction.

3.4 Overview of permafrost modelling methods and state of the art in climate models

3.4.1 Overview of permafrost modelling methods

Permafrost as an important aspect of land surface-atmosphere interactions was noticed in the First Assessment Report of the IPCC in 1990, where also the peculiarity of permafrost as an indicator of climatic change was perceived. Warming of permafrost had been observed in borehole ground temperature measurements, which was mainly due to climatic warming since the end of the Little Ice Age. A statement on whether this warming was also anthropogenically driven was not possible at that time (IPCC, 1990). This had changed already in the next IPCC report, for which observational evidence had been collected for persistent warming as well as for its partly anthropogenic causes (IPCC, 1995). Permafrost was recognized as an important factor within the cycles of energy, water and matter between atmosphere and the land surface. Changes in the ground's thermal regime can have various implications as it induces thicker AL depths, possible melting of ground ice, and/or shrinking of the permafrost area. All of these effects change the conditions for soil microbial activity, hydrology at and below the surface, geomorphology, vegetation, and partitioning of energy fluxes at the surface. Melting of large ice bodies in the sub-surface also impacts human infrastructure, as the ground material is destabilized. In this report also the link between permafrost and global climate through the large carbon pools of the High Northern latitudes was pointed out, as well as the need to incorporate the interactions between carbon and climate into climate models.

In the following years the amount of estimated carbon content in high latitudes' soils rose continuously, meanwhile land surface schemes for the use in climate models increased their complexity. While roughly 25 years ago supplying the lower boundary conditions for the atmosphere in a simplifying manner, e.g. by use of a bucket scheme for soil hydrology, they have developed to dynamically reacting schemes for cycles of energy, water, and nutrients (Pitman, 2003).

Several possibilities of different complexity exist to model the distribution of near-surface permafrost for a given climate on human timescales. Not all of them are suitable for transient climate change experiments, and not all of them can be used within the framework of climate models. They differ in horizontal resolution, the representation of processes, vertical structure, needed input data, and output variables.

Simple models

Permafrost as a thermal phenomenon depends in the first place on the climate of the overlying air masses. The first, simple permafrost models thus tried to find relationships between ground and air temperatures based on empirical knowledge. They were used to

extrapolate from points to the larger scale in order to produce spatial maps of permafrost distribution. First attempts were made as early as 1882 by G. Wild (Shiklomanov, 2005). During the first decades of the 20th century this method remained common in permafrost mapping (Heginbottom, 2002). Thus early permafrost studies used the -2°C-isotherm as boundary between permafrost and non-permafrost regions, and placed the continuous permafrost zone poleward of the -6°C-isotherm.

Process-based models

This type of models can be sub-divided in equilibrium and numerical models, following a review of methods on permafrost modelling from Riseborough et al. (2008).
The main feature of these models is the use of mathematical formulations for the physical processes. Permafrost models form a sub-class of geothermal models, and are based on the theory of heat conduction in order to describe heat transport in soils. The governing equation of heat diffusion can be solved either analytically or numerically, both with use of specified initial and boundary conditions. Since freezing and melting of soil water is important when adressing permafrost, the pure diffusion equation is not sufficient, and the additional source/sink term for the energy released or consumed during the phase change is incorporated. Analytical solutions for diffusion with phase change only exist for idealised cases, as e.g. for stady-state heat fluctuation at the surface, or constant thermal parameters.

An important group of models are the so-called Stefan models. Stefan (1889) formulated an analytical solution to the problem of a moving boundary of phase change, where latent heat of fusion of water, the thermal property of the material, and the driving temperature oscillation at the surface determine the position of the phase change boundary (French, 2007).

It can be used to determine how deep the freeze/thaw front intrudes into the ground, which would represent the AL when the yearly cycle of surface temperature oscillations is chosen. Since in reality the characterisitics of this oscillation are not constant over time, the term 'equilibrium models' is frequently used for Stefan based formulations. It points to their largest disadvantage with respect to the use for climate models, as one specific oscillation is assumed for the Stefan approach. This precludes non-equilibrium, changing climatic conditions.

An advantage of Stefan models is its output variable, as the freezing/thawing front is a parameter in which especially impact modellers are interested, dividing the ground into frozen and non-frozen parts. As pointed out in sect. (3.3.2.), this is decisive for the soil's biogeochemistry. Applications are often GIS based when spatial modelling is aimed for, and give good results especially when used with well determined input parameters.

Index models

This type of model uses frost and thaw indices, resp., to create maps with permafrost distribution on regional to hemispheric scales. The underlying principle is based on the dependency of permafrost occurance on climatic factors, namely air temperature in the most simple versions, but extensions exist that incorporate also snow cover and soil conditions. The basic 'frost number' or Frost Index (FI) is computed using the freezing and thawing degree-days, i.e. the sums of degrees below and above freezing for any point location. Possible extensions are presented by Nelson and Outcalt (1987), who first include the effects of snow cover duration and density on the surface temperature, and in a second step incorporate the Stefan solution, which leads to an index that also considers subsurface conditions. Using these approaches, the index takes into account that the absence or presence of permafrost is determined not only by air temperature, but is strongly modified by snow cover and soil properties, such as water content and presence of ice.
Advantages of the FI method are that they can be applied over larger areas; moreover, there is no need for detailed input data for the soil, such as porosity, field capacity, or hydraulic conductivity. It is possible to use it with observed climate data, but also with data provided from atmospheric circulation models or from paleoreconstructions. In principle, it is applicable for climate change studies, since different climatic states generate altered permafrost distributions via the use of air temperatures in the degree-day formula; yet this holds only for step-wise changes in climate, and it is not possible to conduct transient climate change experiments. The frost indices use the mean climatic status input for the thermal state of the ground, and thus thermal inertia during a shift of mean air temperatures is not treated.
Index models are thus rather diagnostic tools, which explains their widespread use in the context of permafrost mapping. They provide a valid tool for the assessment of questions that base on the climatic factor of permafrost distribution.
However, they have been and still are applied in combination with climate models in order to investigate the impact of climate change on permafrost, if the respective climate model lacks a comprehensive formulation of permafrost processes (Anisimov and Nelson, 1997; Rinke et al., 2012).

Numerical models

Numerical models have been used more and more in recent years (Riseborough et al., 2008). They use a numerical solution to the HCE, thereby accepting small errors, while gaining the advantage of a model that delivers vertical soil temperature profiles and that is suitable for transient climate experiments. The numerical method has clear advantages, as this type of model describes the physical process of heat transport from the ground surface into deeper layers, basing on the HCE. It thus delivers a temperature profile for several depths in the ground, which is needed e.g. by biogeochemical modules of LSS's, where information about soil moisture and temperature are decisive input variables. Since it computes the transport of heat from the surface through the soil, it

allows to conduct experiments with changing climate - no correlations or dependencies between climate and ground thermal regime are used which themselves depend on climate.

Disadvantages of the numerical solution are their need of spatial input data that are often not available and bring additional uncertainty. Moreover, numerical solutions to differential equations contain errors, and these models are often used on a coarse resolution. With respect to the biogeochemistry, a disadvantage is that the depth of the AL cannot be located exactly. It is necessary to interpolate this variable, or to assume the deepest node with $T \geq 0°C$ as a proxy for the ALD (Koven et al., 2013).

3.4.2 State of the Art of permafrost in climate models

The previous section explained that only numerical modelling is suitable for the use in climate models, if the aim is to model permafrost in its physical values, and if transient climate change experiments should be possible. In recent years, improvement has been achievevd in climate modelling with repsect to the implementation of permafrost processes into the land surfaces of climate models (Riseborough et al., 2008). However, e.g. the GCMs which are used for CMIP experiments show a noticeable range in the sophistication of the implemention of land surface processes. It is thus not surprising that simulations of permafrost-related quantities differ substantially between the models (Koven et al., 2013; Slater and D. Lawrence, 2013). The most comprehensive models include freezing and melting of soil water, soil thermal properties' dependency on water and ice content, multi-layer snow schemes with snow on top of the soil instead of blending upper soil layers and snow, and the representation of soil organic matter (D.M. Lawrence et al., 2011; Volodin et al., 2010)). Some others miss one or two of the above mentioned processes (e.g. Verseghy (1991); Takata et al. (2003); Dunne et al. (2012)). In contrast, in some models almost all of these processes are still missing (e.g. Krinner et al. (2005); Raddatz et al. (2007)), but their implementation is under progress (Ekici et al. (2014); Gouttevin et al. (2012)).

It is important to notice that also for models that include the same processes the results may diverge markedly. This is attributable to differences in details of the schemes, e.g.

- the discretization of the vertical column that represents the soil in the model (depth and resolution),
- the formulations for the thermal properties that control heat transfer in the ground,
- the horizontal resolution of the model grid, which differs between 25 km edge length for some RCMs to more than 250 km for GCM studies,
- the formulation of latent heat effects in the soil, i.e. the effect of freezing and melting of soil moisture on the energy balance,
- effects of frozen soil on the soil's hydrology,

as is stated by Koven et al. (2013); Riseborough et al. (2008); Slater and D. Lawrence (2013).
This was demonstrated e.g. with an intercomparison study by Luo et al. (2003), who investigated the quality of land surface schemes with respect to their ability to capture cold regions' hydrology, validated with observations from West Russia. They found that even if frozen ground physics were implemented in the models in a similar way, the results could diverge noticeably.

With respect to GCMs, Koven et al. (2013); Slater and D. Lawrence (2013) analysed the ability of the CMIP5 GCMs to simulate permafrost related quantities such as permafrost distribution and AL characteristics. Their detailed listing of the frozen ground processes implemented in the models reveals that many of them miss one or more of theses processes; some even do not incorporate freezing and melting of soil moisture. Therefore, modelled contemporary permafrost characteristics differ to a large degree between the models, and the range of permafrost extent calculated for an intermediate future emission scenario is large (Figure 1.2). It was concluded by the authors that the incorporation of the same processes did not necessarily lead to agreement in the results.
In order to assess the problem that a large part of the explained uncertainty may originate from the range of uncertainty in the CMIP5 models, i.e. the spread of mean states between the used models, Slater and Lawrence (2013, subm.) conducted an analysis that tried to disentangle climatic and soil physical factors for simulated permafrost characteristics. To do so, they derived "climatic permafrost" on the basis of model output of e.g. near-surface air temperature, which gives information on how stronlgy permafrost could develop due to climate.
Moreover, they introduced quantities that reflect how a model's soil reacts on climate due to its physical properties and formulations, e.g. the strength of dampening of the heat wave with depth in the ground. They can thus judge how a model transmits the driving climate into the soil, which is decisive for actual permafrost occurance and specifics on the local scale (Section 2.3). This distinction enables them to analyse how 'cold' a model climate is, and how wide 'climatic permafrost' would be distributed, and to compare this to the permafrost distribution that would develop due to the model's soil and surface physics. Using this method, they found that models with similar climatic conditions can simulate very different permafrost in terms of distribution and strength. Moreover, they showed that for several individual models their 'climatic' and their 'soil physical' permafrost differed markedly.

Within the context of regional climate modelling, still only few RCMs include the relevant processes for studying regions with extensive seasonal freezing and/or permafrost (Matthes et al., 2012).
Saha et al. (2006) found that Arctic and Sub-Arctic simulated climate is strongly dependent on the choice of the LSS. Process representation had a marked influence not only on modelled soil variables, but also impacted near-surface air temperature and even remote areas over the ocean. In consequence, results for future climate change scenarios differed between the experiments due to the use of different LSSs.

One can summarize that albeit many models already have Permafrost Processes (PFP)s included in their LSSs, it is still a field where much is left to do. Albeit many climate models nowadays have cold regions' soil processes incorporated, there often lacks one or more of the decisive processes (see above in this section); some of the studies that have relatively comprehensive soil physics exaggerate certain processes and are on very coarse horizontal grid resolution (Takata and Kimoto, 2000), some models do not fully couple atmospheric and land surface model (Matthes et al., 2012), and others have very shallow soil columns (Sushama et al., 2007). Therefore the effects of climate change on permafrost are still being investigated also with offline configurations, either with use of detailed, sophisticated permafrost models such as the GIPL model of the Geophysical Institute of the University of Alaska in Fairbanks, which are fed with climate model data as input (Sazonova et al., 2004; Sushama et al., 2006), or via calculating large-scale permafrost distribution using index models, also driven with climate model output (Rinke et al., 2012).
In order to study effects of permafrost on climate change, or modulations of climate change due to PFPs, it is necessary, however, to model the processes online within the climate model.

4 Model description and development

4.1 The regional climate model REMO

REMO (Jacob, 2001; Jacob and Podzun, 1997) is an RCM that was developed at the Max Planck Institute for Meteorology (MPI-M) jointly with the German Weather Service (DWD), starting from a numerical weather prediction model (Majewski, 1991). The parameterization package of the ECHAM4 model has been implemented later on, in which combination the model has shown reliability in simulating present day's climate on the regional scale. It is a three-dimensional, hydrostatic, atmospheric circulation model, that solves the dicretised primitive equations for atmospheric motion. These are horizontal wind components, specific humidity, surface pressure, and cloud liquid water. The lateral boundary conditions for REMO can either be delivered by GCM ouput data, or by other climate data, as e.g. reanalysis datasets. This was the case within the present work, as it was necessary to use an experimental setup that ensures simulations that are as near to observed climate as possible. The lateral driving is organised such that within a buffer zone of eight grid boxes the boundary data are exponentially dampened, so that inside this buffer layer, the RCM simulates 'its own climate'.
Lower boundary over seas is obtained mostly by prescribing the seas surface temperature and sea ice cover; however model versions exist that enable to compute them online.
In recent years, several studies worked with the LS in REMO (Kotlarski (2007); Preuschmann (2012)), e.g. investigating the influence of vegetation cycles on the regional climate over Europe (Rechid, 2009), or disentangling problems that arise from the derivation of albedo for the surface library used in REMO (Preuschmann, 2012). Semmler (2002) extended the LSS with a fractional land, water and sea ice cover, and implemented a simplified formulation for cold regions' soils processes (see Section 4.2). Also working on sub-grid scale heterogeneity, Kotlarski (2007) developed a dynamical glacier scheme for use in REMO. For the purpose of this study a layered soil hydrology was essential; this was developed by Hagemann and Stacke (2013) (in review).

4.2 Status of the REMO soil scheme at the beginning of the thesis

At the start of this PhD project, the thermodynamic and hydrological parts of the soil had different structures. Figure 4.1 illustrates the increasingly thick layers for thermal diffusion, whereas due to the bucket only one value is determined by the hydrology scheme. The depth of the bucket in a particular grid cell is derived from the Land Surface Parameter Dataset 2 (LSP2) dataset is part of the soil library.

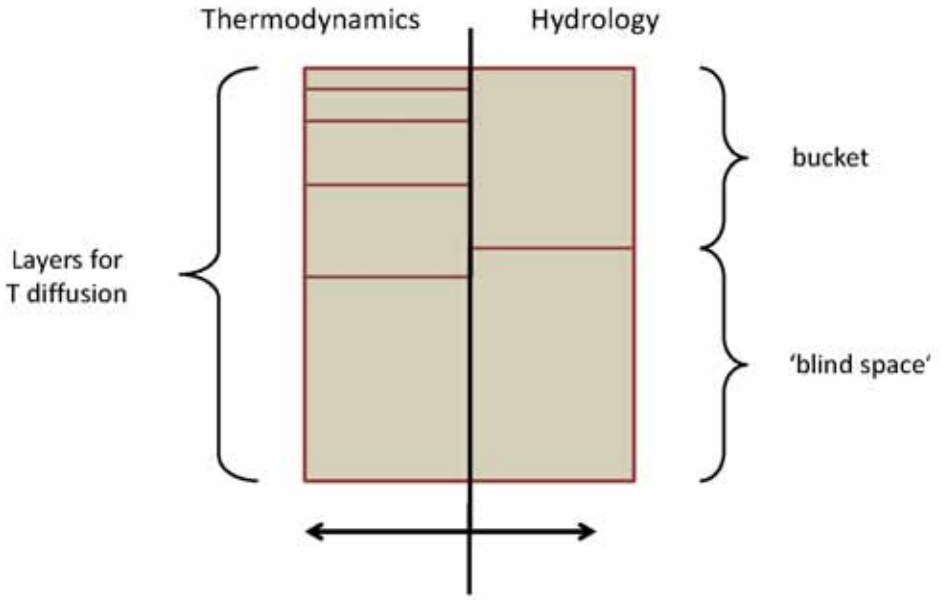

Figure 4.1: Schematic diagram of thermodynamic and hydrological schemes in soil columns of the original REMO version.

The HCE is solved numerically using the Richtmeyer-Morton scheme. A zero-heat-flux condition is applied at the lower boundary, which is at the depth of roughly $10m$. As pointed out in Section 3.3, thermodynamics and hydrology in reality are tightly coupled, which was not represented in the LSS of ECHAM, JSBACH, until recently (Ekici et al., 2014).
In REMO, however, a simplifying formulation existed for the effect of latent heat of fusion, which had been implemented by Semmler (2002). It included the influence of soil water on the energy balance of the soil, yet did not treat the backward impact of the soil's thermal status on hydrology (details on this formulation can be found in Section 4.3.4).

The dependency of the thermal properties on soil water content was introduced also by Semmler (2002). A parameterization originating from the German weather service (DWD) was used, for which a further, i.e. original reference could not be found (Semmler, pers. comm. 2008). It was decided to nevertheless work on the topic of the thermal

conductivity and implement a new parameterization for four reasons:

1. the parameterization seemed to have been developed by the DWD, thereby designed it for the use in mid-latitudes,

2. the impact of varying soil moisture contents was introduced using a correction factor which depends on soil texture type, thus adding uncertainty,

3. the correction factor existed for five soil texture types plus peat - a possible extension of a soil library with more detailed texture types is difficult, and

4. soil ice is not represented in this parameterization.

The snow scheme is different in REMO as compared to ECHAM/JSBACH. Semmler (2002) introduced a layered snow module, and a dependency of the snow density and thus thermal conductivity on snow temperature. The main difference between the two schemes is the blending of snow and soil properties for the case of ECHAM/JSBACH, which means that snow is part of the upper soil layers,whereas the new REMO scheme sets snow on top of the soil. The experiments conducted for this work all use the REMO snow scheme.

A pre-requisite for the work done within this thesis was the development of a layered scheme for the soil hydrology. This was conducted by Hagemann and Stacke (2013) (in review). The new layered soil hydrology treats water movement between layers using the Richards equation for vertical diffusion.

4.3 Model development: Implementation of Permafrost processes

The following sections explain how the discussed processes were implemented into REMO. The subscript i was used as an index for soil variables; please note that because of the one-dimensional treatment of soil porcesses in the LSS of REMO, equations and units will be used with respect to depth z only.

4.3.1 Treatment of latent heat of fusion

The consideration of the latent heat of fusion of soil water is the most important effect for the soil energy balance in cold regions. Some models use the so-called apparent heat capacity approach. Latent heat, according to the actual water content and energy supply, is giving the amount of energy released (consumed) through freezing (melting), which is added to the heat capacity that enters the diffusion equation. REMO uses the so-called Decoupled Energy Conservation Parameterization (Y. Zhang et al., 2008), which works in two steps. First, the new soil temperature is computed, accounting for pure heat diffusion. The amount of latent heat released/consumed during freeze/melt according to the actual temperature and the solid and liquid water contents from the last time step is computed in a second step:
If $T_i < T_{melt}$ and $w_{sol,i} > 0$, the amount of water that can potentially melt is calculated according to the difference between actual and melting temperature $T_i - T_{melt}$, actual volumetric heat capacity C_i, layer thickness z_i, and the latent heat of fusion L_f determine:

$$w_{melt,i} = \frac{(T_i - T_{melt})C_i z_i}{\rho L_f} \tag{4.1}$$

Layer temperature and moisture variables are updated:

$$T_i = T_{melt} \tag{4.2}$$

$$w_{sol,i} = w_{sol,i} - w_{melt,i} \tag{4.3}$$

$$w_{liq,i} = w_{liq,i} + w_{melt,i} \tag{4.4}$$

It is ensured that melting is no artificial sink for water: if $w_{sol} < 0.$, than too much ice has been melted, and water, ice, and temperature have to be adjusted:

$$T_i = T_i - w_{sol,i}\frac{\rho_{water} L_f}{C_i z_i} \tag{4.5}$$

$$w_{liq,i} = w_{liq,i} + w_{sol,i} \tag{4.6}$$

$$w_{sol,i} = 0. \tag{4.7}$$

Thus, T is adjusted according to the energy, either keeping it at the freezing point, or dampening the change in temperature. The same but vice versa is conducted for the case of freezing.

Inheriting the method from REMO5.0, the output variable of this method is the 'fraction of frozen ground':

$$fr_{froz,i} = \frac{w_{sol,i}}{w_{total,i}} \tag{4.8}$$

a dimensionless number between 0 and 1.

With the introduction of a layered soil hydrology, the change from constant to vertically varying soil moisture contents was possible, and the above written equations now use the actual water content determined with the layered hydrology scheme, thereby also considering the soil depth, or beginning of bedrock in the soil.
Therefore, the warming and cooling of sub-surface material due to latent heat effects can now vary vertically. Moreover, the blocking effect that bedrock generally imposes on percolation is represented in the model. This introduces heterogeneity in the model's sub-surface. The output variable fr_{froz} is kept for this first as well as for the second step of the model development. It is used for dividing the total water content of layer i, $w_{total,i}$, into solid and liquid phase for use in the parameterizations of thermal conductivity and heat capacity, as is pointed out in the next section.

4.3.2 Parameterization of the thermal conductivity and adaptation

Chapter 3 contains the physical principles that describe heat transfer in soils. Equation 3.12 shows that both the strength of the temperature gradient and the thermal properties determine how fast energy is transported within the matrix. As stated before in Section 3.2.1, the thermal diffusivity a is obtained dividing thermal conductivity λ by volumetric heat capacity c, and that both of these depend on the specific properties of the material. Since water and ice differ strongly in their thermal properties, and permafrost soils can contain large portions of these, it is not feasible to consider λ and c as average values only depending on soil texture type.

The thermal conductivity is the more important factor compared to the heat capacity in terms of impacting a soil model's thermal regime. E.g., Saha et al. (2007) conducted sensitivity tests with the RCM HIRHAM in order to assess the relative importance of thermal conductivity and heat capacity for simulated soil temperature. Their results revealed that in deeper soil layers (referring to depths around $> 2.50\ m$), effects through changed conductivities had greater impact on the simulated soil temperatures than changed heat capacities (both changes were in the range of observed values). They concluded that λ is more decisive for model formulations than C.

Many studies have searched for general rules that could lead into mathematical formulations for the observed behaviour of λ in unsaturated frozen and unfrozen soils (see Section 3.3.2).
The parameterization developed by Johanson (1975), which was reviewed by Farouki (1981), is a formulation frequently used in permafrost modelling, and which is being implemented more and more also in regional and global climate models (Krinner et al., 2005; Oleson et al., 2010; Verseghy, 1991).
The parameterization by Johansen and Farouki was chosen for implementation into REMO due to several reasons:

- according to literature, it performs well under conditions that are frequently observed in soils in cold and permafrost regions,
- it is easy to implement,
- it does not need more than one new input parameter.

Especially the last point can be important, since soil variables show high uncertanties (Saha et al., 2006). This can become problematic especially for vast regions with only sparse field observations, like Siberia.
The parameterization by Johansen (1975) as reviewed by Farouki (1981), or JFP during the rest of this chapter, works in several steps, linking the effects of bulk density, soil material, and the actual water and ice contents on the thermal conductivity.

Original formulation of the Johansen-Farouki Parameterization of thermal conductivity

The JFP equation for the thermal conductivity is written as follows:

$$\lambda_{total,i} = \begin{cases} Ke_i\lambda_{sat,i} + (1 - Ke_i\lambda_{dry,i}) & \text{, if } Sat_i > 10e-7 \\ \lambda_{dry,i} & \text{, if } Sat_i \leq 10e-7 \end{cases} \tag{4.9}$$

where Ke is the Kersten number, a dimensionless number between 0 and 1, λ_{sat} is the thermal conductivity of the saturated and λ_{dry} for dry soil $[W/(mK)]$, respectively. Herein several quantities can vary, depending on either actual water and/or ice content, or on the texture type of the soil, or on both.

The thermal conductivity of the dry soil material, or λ_{dry}, is computed for mineral soils as follows:

$$\lambda_{dry,i} = \frac{0.135\rho + 64.7}{2700 - 0.947\rho} \tag{4.10}$$

where the bulk density ρ is a function of the porosity:

$$\rho = 2700(1 - \theta_{sat}) \tag{4.11}$$

This parameter includes the influence of the size of the grains in the soil matrix, and of their 'spatial organisation'. λ_{dry} does not inform about heat transfer conditions inside the particles, but represents the effect due to the form of the soil pores.

For organic soils, $\lambda_{dry} = 0.05 W/mK$.

While λ_{dry} mirrors only effects through soil's properties themselves, the saturated soil conductivity λ_{sat} incorporates also effects from actual water and ice contents. Still, it also contains texture type dependent parameters. For mineral soils it is computed as follows:

$$\lambda_{sat,i} = \begin{cases} \lambda_{s,i}^{1-por_i} \lambda_{water}^{\theta_{water,i}} & \text{, if } T_i >= T_{melt} \\ \lambda_{s,i}^{1-por_i} \lambda_{water}^{\theta_{water,i}} \lambda_{ice}^{\theta_{ice,i}} & \text{, if } T_i < T_{melt} \end{cases} \tag{4.12}$$

where por_i is the porosity, λ_{water} the thermal conductivity $[W/(mK)]$ of water, λ_{ice} the thermal conductivity of ice, and λ_s is the one of the soil solids, respectively. Values for these physical constants are 0.56 for water and 2.31 $[W/(mK)]$ for ice, respectively. The saturated thermal conductivity is thus the geometric mean of the conductivities of the soil material, water, and ice, where each component consists of the respective material's conductivity as the base, and of the its volumetric content as the exponent.

The porosity *por* and the conductivity of the pure soil material, $\lambda_{s,i}$, are depending on the soil's texture type. The letter reflects that coarser soils enable faster heat diffusion than fine soils since the grains themselves are larger, and thus fewer boundaries have to be bridged over the same given distance. Moreover, coarse soils tend to high quartz contents as compared to fine soils, and quartz has a very high heat conductivity, with $7.7 W/(mK)$ one of the highest in natural materials.
The thermal conductivity of the soil solids is calculated with an empirical relationship using percentages of sand and clay contents:

$$\lambda_{s,i} = \frac{8.8(\%sand)_i + 2.92(\%clay)_i}{(\%sand)_i(\%clay)_i} \tag{4.13}$$

For organic soils a value of $0.25 W/mK$ is assumed, since organic materials are poor conductors as compared to minerals.

The JFP then weights between dry and saturated parts, in order to obtain λ_{total}. This is done using the so called Kersten number, which is a measure for the actual degree of soil saturation. In the original parameterization, a case distinction for frozen and unfrozen soils is done:

$$Ke_{fr} = Sat \tag{4.14}$$

$$Ke_{unfr} = log10(Sat) + 1. \tag{4.15}$$

Source and choice of soil parameters

Since S. Hagemann has provided a new parameter set for use in JSBACH and REMO based on a publication by Beringer et al. (2001), which enables to consider 13 (plus three additional, medium range) soil texture types instead of the formerly used five (plus peat), the soil library used for the experiments in this thesis was adapted to this parameter set. An advantage of this table is that it provides several soil variables within one data set, which otherwise have to be extracted from different sources for a given soil texture type; this would be an additional source of uncertainty in the model. The reason behind is that, depending on perspectives and background of modellers as well as of field workers, compilations of soil data often focus either on hydrological or on thermal properties. Thus a full set of soil characteristics for the use in an LSS of a climate model for a finer range of soil texture types is not easy to find.
Beringer et al. (2001) provide porosity, hydraulic conductivity, matrix potential, and more for the part of the hydrological variables, and soil solids' heat capacity and conductivity for the thermal parameters, accompanied by percentages of sand, silt, and clay, respectively. Table 4.1 shows the values that are given by Beringer et al. (2001) for the 13 soil texture types. Since Equation 4.13 only uses sand and clay and does not include silt, it was decided to conduct first JFP experiments using the values for $\lambda_{s,i}$ directly from Table 4.1, instead of computing them.
All other parameters (porosity, organic values) were used as given through the soil library and are taken from Beringer et al. (2001).

Type No.	Description	Sand (%)	Silt (%)	Clay (%)	λ_s $[W/(mK)]$
1	Sand	92	5	3	8.6143
2	Loamy sand	82	12	6	8.3991
3	Sandy loam	58	32	10	7.9353
4	Loam	43	39	18	7.0649
5	Silty loam	17	70	13	6.2520
6	Sandy clay loam	58	15	27	9.9323
7	Clay loam	32	34	34	5.7709
8	Silty clay loam	10	56	34	4.2564
9	Sandy clay	52	6	42	6.1728
10	Silty clay	6	47	47	3.5856
11	Clay	22	20	58	4.5370
12	Peat	-	-	-	0.25
13	Moss	-	-	-	0.25
14	Lichen	-	-	-	0.25

Table 4.1: Table of soil parameters taken according to Beringer et al. (2001).

Test results with original JFP

Experiments for one to two years were conducted using the above described equations and parameters for the soil properties. Analysis of time series of daily means of the conductivity, together with soil temperature and soil moisture, plotted for single grid boxes, revealed two unexpected results (Figure 4.2; for position of grid boxes see Figure 5.3) :

1. Whenever soil temperature of the respective layer crossed the 0 °C line, discontinuities occur in the timeseries of λ_{total}.

2. As can be seen from the same figure, λ_{total} was not significantly higher on average in winter than in summer; except in grid boxes with bith high moisture content and strong freezing.

Analysis and adaptation of the JFP

The results contradicted the consensus amongst field as well as laboratory investigators that frozen soils show higher thermal conductivities than unfrozen soils, based in the fact that λ_{ice} is about four times higher than λ_{water}. The sharp increase or decrease when soil temperature crossed the freezing point might not be as harmful, since it only happens during very short periods during a year, and would not influence the mean values of soil temperature. However, thermal conductivities that are, on average, during winter lower or on a similar level than during summer, miss an important and PF-specific effect, the thermal offset:
The mean T_{soil} at the depth of zero annual amplitude is noticeably lower than the mean T_{air}, because heat conduction is more efficient during winter than during summer. Thus, the cooling during the cold months is more intense than the warming during the warm period of the year. This PF-typical effect presupposes that thermal conductivities reflect the presence of soil ice. It's presence or absence can obviously be decisive for PF occurance at all. The effect of the thermal offset was described and formulated as a model by Romanovsky and Osterkamp (1995).

Kersten number

Analysis of the formulation of the Kersten number revealed at least one reason for both features. Figure 4.3 shows that for a substantial range of moisture values $Ke_{unfr} > Ke_{fr}$. Thus, whenever soil temperature changes from positive to negative values (or vice versa) at a given, medium moisture content, the Kersten number experiences a 'jump' from the unfrozen (frozen) to the frozen (unfrozen) value. This jump is small, but noticeable, and obviously the parameterization is able to produce substantial discontinuities in λ_{total}.

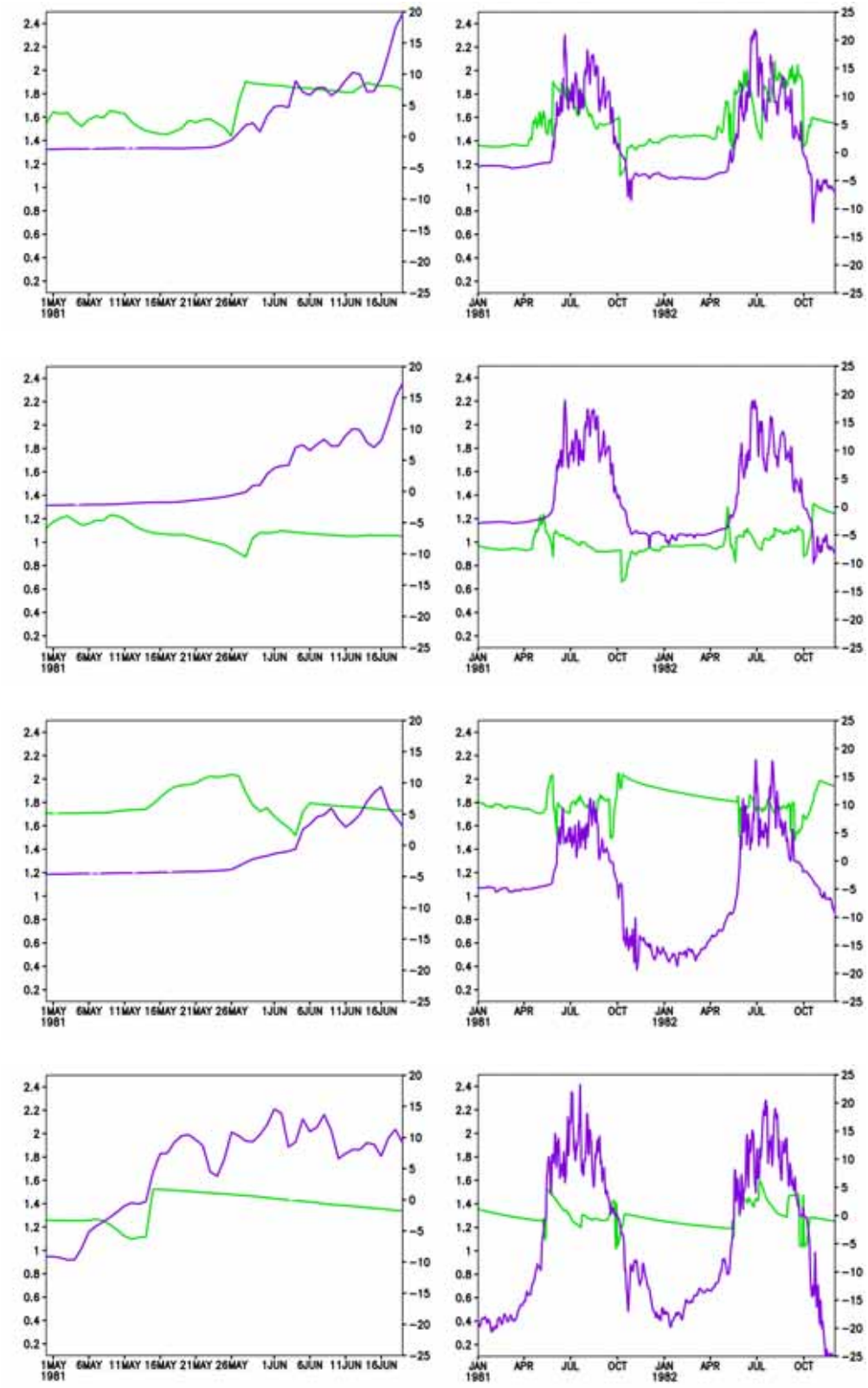

Figure 4.2: Time series of daily means of λ_{total} $[W/mK]$ (green) and soil temperature [°C] (violet) of layer 1 for example grid boxes number 3, 4, 5 and 6 (top to bottom), experiment with original JFP; displayed are melting period 1981 (left panels) and years 1981-1982 incl. (right panels).

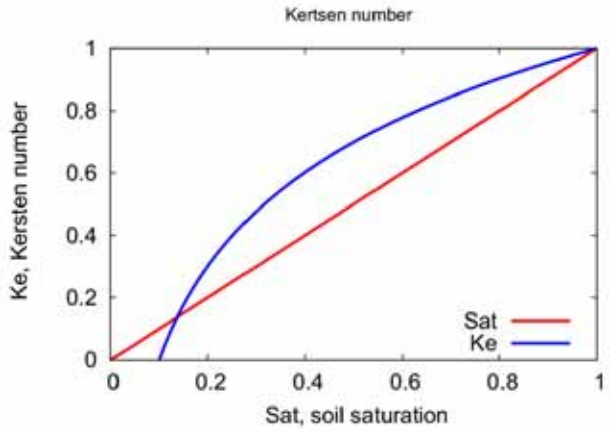

Figure 4.3: Kersten number Ke for frozen and unfrozen case as a function of Sat.

If $Ke_{unfr} > Ke_{fr}$, it also affects the total level of the final thermal conductivity (Equation 4.9). Could maybe also the second problem, the higher summer values, be attributed to this difference?

A literature search for the treatment of this variable revealed that some applications of JFP use only $Ke = Sat = Ke_{fr}$ for all soil thermal states (Gouttevin et al., 2012; Krinner et al., 2005). Therefore, tests were conducted using $Ke = Ke_{fr}$ for the full range of soil temperature. Figure 4.4 shows that this approach leads to similar conductivities in terms of their overall behaviour and magnitude, but that, on average, the simulated conductivities are now higher for winter than for summmer periods. Also, the previously abundant 'jumps' during the transition seasons disappeared.

An explanation for this behaviour can be found in the full formulation of the JFP.
The logarithmic function for the conductivity of non-frozen ground is, as described above, an important aspect. Considering a virtual soil matrix that is wetted from very dry conditions until full saturation shall explain the development of λ in dependency of increasing water content. The logarithmic course enables a model to describe the stronger-than-linear increase of λ at the beginning of wetting, when soil moisture values are still low, whereas it increases only weakly when soils are already rather wet, since then a small surplus of water has an only minor effect on heat conduction. Thus, ignoring this part in JFP will introduce a weakness in the model, which certainly is not desirable, but is left for further improvement.

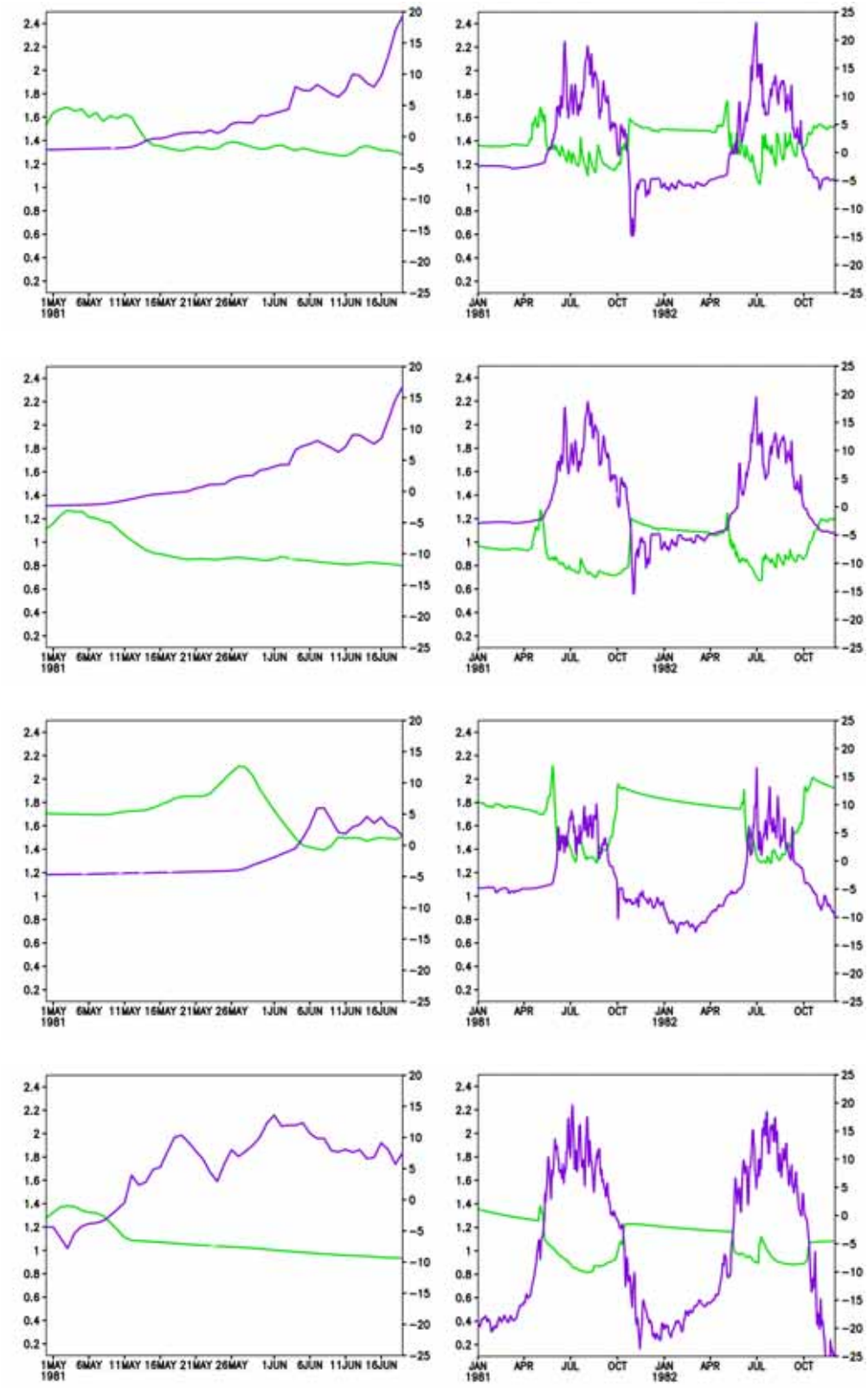

Figure 4.4: Time series of daily means of λ_{total} $[W/mK]$ (green) and soil temperature [°C] (violet) of layer 1 for example grid boxes number 3, 4, 5 and 6 (top to bottom), but for test experiment with $Ke = Sat$; displayed are melting period 1981 (left panels) and years 1981-1982 incl. (right panels).

The fact that climate models use large gridboxes of ca. 10 to more than 200 Km introduces subgrid-scale variations of the soil conditions which cannot be represented by the models' land surface schemes. It is therefore not possible to reach the same degree of accuracy with large scale models than with point scale models, with which parameterizations of soil conductivities have been developed in many cases. This justifies accepting a small error in the unfrozen conductivity.

Thermal conductivity of the soil solids

Since soil parameters might also influence the results of the JFP (see Equation 4.12), also λ_s was investigated in more detail. As λ_{dry} is of very small magnitude, and since all values for organic soil are confirmed, these parameters were not investigated further. The method to compute λ_s for mineral soils used in the original JFP is described above (see Equation 4.13), as well the reason for including this parameter through the soil library. Figure 4.5 shows the spatial distribution of λ_s for the Siberian model domain.

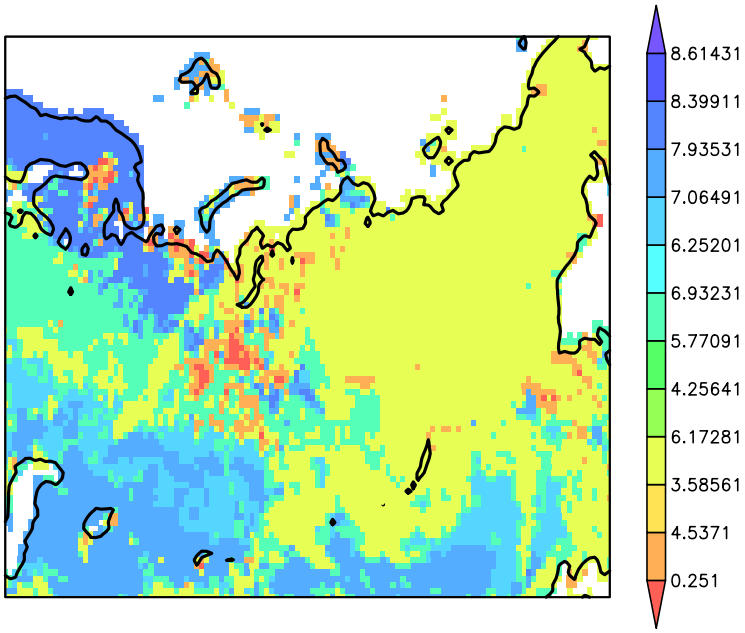

Figure 4.5: Model parameter thermal conductivity of soil solids, for the Siberian model domain, as given by the soil library.

It is noticeable that for almost all of Siberia, apart from the West-Siberian Lowlands, the same texture type is given, which can be attributed to 'sandy clay' in Table 4.1 according to Beringer et al. (2001) This type constitutes, following the table, of 52% sand, 6% silt, and 42% clay, respectively. λ_s for 'sandy clay' results in $6.1728[W/(mK)]$.
However, if Equation 4.13 is used to compute λ_s, thereby omitting the given percentage of silt, a value of ca. 4.03 evolves. The discrepancy between the two values might in part stem from the not considered silt when using Equation 4.13, but since this texture type contains more or less only sand and clay, it seemed possible that either

- the percentages are imprecise,
- λ_s are not deduced with Equation 4.13,
- or λ_s in the table and λ_s in the JFP do not have the same meaning.

A look into publications on model studies showed that it is not unusual to set λ_s to a constant value, e.g. $2.31[W/(mK)]$ in the ORCHIDEE model, the LSS of a french GCM over all grid boxes (Gouttevin et al., 2012). It is clear from Equation 4.12 that a higher λ_s shifts λ_{sat} to higher values, and, in particular, that it leads to a higher difference between frozen and unfrozen λ_{total} through the multiplication of λ_{sat} with Ke in Equation 4.9.
Tests were conducted with changed $\lambda_{s,i}$ that are lower than the ones provided by Beringer et al. (2001). Tests were made using $\lambda_{s,i} = 2.31$ ('low'), as proposed in Gouttevin et al. (2012), and with $\lambda_{s,i} = 4.3$ ('medium'), as would be received from 4.13 as above explained, respectively. Figure 4.6 illustrates that, if $Ke = Sat$ is chosen, the difference in λ as well as the differences in soil temperature between the experiments using 'low' and 'medium' $\lambda_{s,i}$ are only small.

Using different methods for obtaining the model parameter λ_s, which in each case meant a change to a (in the first one third, in the second two thirds) lower value compared to the formerly used $6.173[W/(mK)]$, lead to only small differences both in λ and in soil temperature between both of the test versions, yet markedly lower conductivities compared to using Beringer et al. (2001).
The analysis of λ_{sat} with the different values of $\lambda_{s,i}$ showed that the letter parameter, as can be expected from its role in λ_{sat}, influences the general level of the saturated thermal conductivity. Doing so, it also influences the discontinuities in λ_{total} when crossing the freezing point: since λ_{sat} is higher with higher $\lambda_{s,i}$, the jump from frozen to unfrozen values is increased with a high $\lambda_{s,i}$ value.
Furthermore, it seemed that $\lambda_{s,i}$ given in the table in Beringer et al. (2001) covers a rather high range which might not be suitable for the soils dominating the experimental region. Lower values were found to be used in e.g. Gouttevin et al. (2012) or Oleson et al. (2010), for this parameter; it was therefore decided to proceed with one of the tested, lower constants.

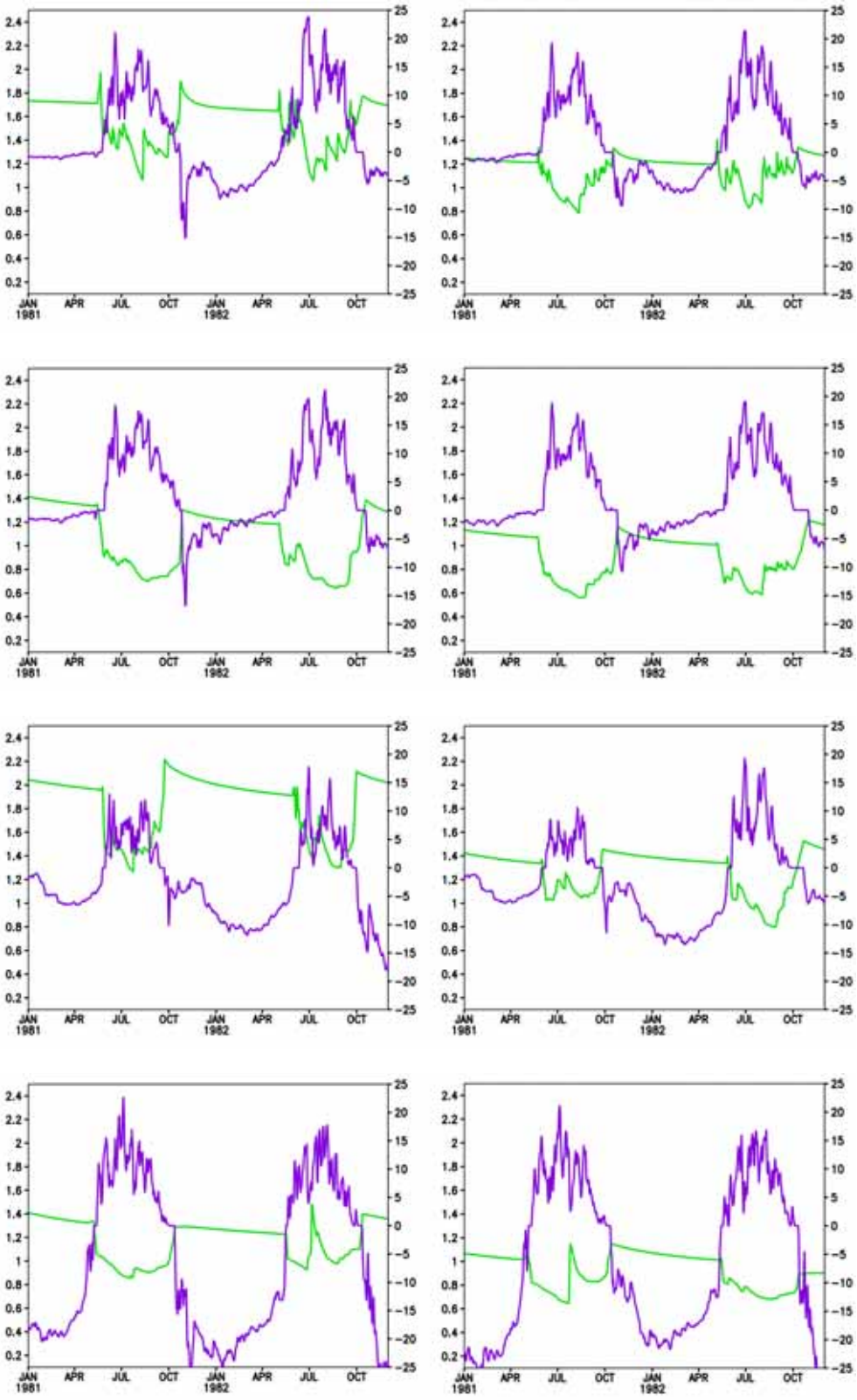

Figure 4.6: Time series of daily means of years 1981 and 1982 of λ_{total} $[W/mK]$ (green) and soil temperature [°C] (violet) of layer 1 from example grid boxes number 8, 9, 15, 18 (top to bottom); experiments with modified JFP using 'low' (left panels) and 'medium' (right panels) values of $\lambda_{s,i}$.

These aspects give arguments for a change of $\lambda_{s,i}$ to a constant value, which here was chosen to be $4.03[W/(mK)]$. The higher of the two tested values was chosen as it seemed reasonable to represent the relatively large portion of sand in the Siberian soils, with the respective higher thermal conductivity.

A clear disadvantage of a uniform $\lambda_{s,i}$ is the loss of detail with respect to soil texture type, i.e. of variation of λ with varying soils. In other words, the dependency of λ on soil texture type is reduced to varying hydrological properties and to the differences in λ_{dry}.

Taking advantages and disadvantages into consideration, it was decided for the further experiments to set $\lambda_{s,i}$ to a constant $4.03[W/(mK)]$ for the whole model domain.

4.3.3 Heat capacity

The volumetric heat capacity of soils in cold regions needs, as thermal conductivity, to include effects through soil water and ice contents. The change of C with freezing leads to a decrease of heat capacity, as $C_{ice} = 1.93 * 106\ [J/(m^3K)]$,
compared to $C_{water} = 4.18 * 106\ [J/(m^3K)]$.
A parameterization of these dependencies of C was developed, e.g., by De Vries (1963) and can be found in Moelders and Romanovsky (2006). Equation 4.16 shows the arithmetic mean that describes contributions from soil, water, and ice to the total volumetric heat capacity:

$$C_i = C_{soil,i}\theta_{soil,i} + C_{water}\theta_{water,i} + C_{ice}\theta_{ice,i}, \tag{4.16}$$

where $C_{soil,i}$, C_{water}, C_{ice} are the respective volumetric heat capacities of soil, water, and ice for layer i $[J/m^3K]$, while $\theta_{soil,i}$, $\theta_{water,i}$, $\theta_{ice,i}$ denote their respective volumetric content (which equals $1. - por$ for the case of the soil component) $[m^3/m^3]$.

4.3.4 Coupling of soil thermodynamics and hydrology

The simplified introduction of soil freezing/melting (Semmler, 2002) works under the assumption of a homogeneous soil moisture content for the whole column. As it has been implemented in a model version where no layered hydrology was present, the soil moisture content for the bucket zone was used and extrapolated to all layers:

$$Sat_{bucket} = w_{bucket}/fc_{bucket} \tag{4.17}$$

$$Sat_i \equiv Sat_{bucket} \tag{4.18}$$

$$w_i = Sat_i * fc_i \tag{4.19}$$

where Sat_{bucket} and w_{bucket} are the degree of saturation and the absolute water content of the bucket, respectively, while fc_{bucket} is its field capacity; this method leads to the assumed amount of water in a given layer for use in Equations 4.4 and 4.6.

This simplifying assumption of the sub-surface conditions results to an overestimation of the latent heat effect, since water may be frozen and melted where there is no soil. This effect occurs especially in mountainous areas, where soil depths are usually shallow.

The use of the 'bulk freezing/melting' in REMO with bucket hydrology bridged the gap between energy and water 'one-way' and ensured the dampening effect of latent heat of fusion on the seasonal cycle of soil temperatures. The reverse impacts from thermodynamics on hydrology, i.e. decreased permeability of the soil, and cryosuction (see Sections 3.3.3), could not be formulated in a realistic way, since the structures of thermodynamics and hydrology did not correspond (Figure 4.1).
Even the simplest effect of ground freezing, i.e. that only liquid water can move and is thus available for percolation, drainage and evapotranspiration, can not be assessed.

However, the effect of ground freezing on surface water had been implemented in a simple manner by H. Goettel, K. Sieck and S. Hagemann (Hagemann, pers. comm. 2011):
The 'degree of frozen ground' of layer 1 was used as a scaling factor, which reduces the infiltration of water on top of the soil, $Infil$ to $Infil_{red}$:

$$Infil_{red} = (1. - fr_{froz,1})Infil \tag{4.20}$$

Although this method is known as too strict a decrease of infiltration (Niu and Z.-L. Yang, 2006), a characteristic effect for High Northern latitudes, i.e. channelling a large amount of snow melt water into surface runoff, can be simulated with this approach.
A more sophisticated reduction of infiltration is planned for future work.

The following effects on hydrology through ground freezing were still missing:

1. restriction of water movement (percolation, drainage, diffusion, evaporation, transpiration) to its liquid phase,

2. reduced permeability when soil ice is present (see Section 3.3.3).

The realisation of these aspects was conducted as follows.

1. The most obvious and important effect of frost is the restriction of water movement to the liquid phase.
   This is obtained via substituting the variable for the water content for each layer with its liquid water content:

$$w_i = w_{liq,i} \tag{4.21}$$

   Liquid and solid water contents are obtained from the computation of freezing/melting in the thermodynamic routine, and thereafter passed into the hydrological routines.
   Parallel to that, the total water content is kept throughout the model, and it is ensured that it can only be changed due to infiltration, drainage, or percolation, yet not due to soil freezing/melting:

$$w_{total,i} = min(w_{liq,i} + w_{sol,i}, w_{total,i}) \tag{4.22}$$

   To let only liquid water move within the soil, solid and liquid water contents in a given soil layer $w_{sol,i}$, $w_{liq,i}$ are passed to the respective routines. All processes that may change water contents now merely let liquid water be treated. Affected processes are, e.g., drainage of soil water, or evaporation at the surface.
   The available pore space is reduced in most cases:

$$fc_{froz,i} = fc_i - w_{sol,i}, \tag{4.23}$$

   which can be interpreted as counting ice, if present, to the soil matrix, thereby reducing free pore volume for water abundance.

   Therefore, in order to avoid overfilling of the field capacity,

$$w_{total,i} = min(w_{total,i}, fc_i), \tag{4.24}$$

   liquid water content is restricted to the remaining field capacity:

$$w_{liq,i} = min(w_{total,i} - w_{sol,i}, fc_i - w_{sol,i}) \tag{4.25}$$

2. In order to incorporate effects of reduced permeability, approaches were chosen that can be found, i.e., in Swenson et al. (2012), Gouttevin et al. (2012), which employ approaches supported by, e.g., Niu and Z.-L. Yang (2006) and Koren et al. (1999). The equations for simulating soil water movement are based on the same formulations in the new layered hydrology scheme in REMO, which was the motivation to follow the same line. The advantage of this parameterization is that the hydrological equations in the model do not need to be changed, and that use can be made of the analogon between drying/wetting and freezing/melting of a soil, as is explained in Section 3.3.3. The effect of high suction due to a low relative moisture content is produced by setting

$$Sat_i = \frac{w_{liq,i}}{z_i} / fc_i \tag{4.26}$$

where field capacity is not reduced with soil ice. As a consequence, Sat is substantially lower with this formulation than if $w_{total,i}$ is considered, or if field capacity is reduced with soil ice. Figure 4.7 illustrates the resulting effect on the saturation.

This is important and has greatest effects in cases of high water contents and strong freezing, conditions frequently observed in permafrost soils (Farouki, 1981). It can be seen from Figure 4.7 that considering different water variables and using reduced or original field capacity is influencing the relative soil moisture Sat_i (see also Figure 3.2).

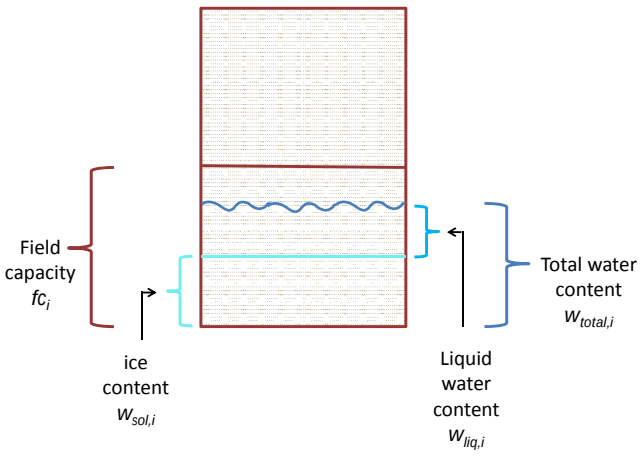

Figure 4.7: Schematic diagram of a model soil layer for sub-zero conditions, with total, liquid, and solid soil moisture values and field capacity. Choosing liquid instead of total water content in hydrological computations leads to lower hydraulic diffusivity and can impose a moisture gradient (see text for details).

4.3.5 Extension of the soil column

The soil column of REMO was extended with an additional, sixth layer below the formerly deepest, fifth layer. This was done having two aspects in mind:
Firstly, permafrost soils and soils in regions with strong seasonal freezing often show large damping depths in comparison to soils in mid latitudes due to the high thermal conductivities. In consequence, the depth of zero annual amplitude can reach down to 15 m, so that a model with merely 10 m depth misses part of the heat fluxes into and out of the ground.
Secondly, the time scales considered when analysing soil thermal dynamics depend on the period of the boundary forcing at the surface, which here is the periodic forcing through surface temperature. In other words, short term, high-frequent fluctuations of the surface temperature intrude only until very shallow depths, and the longer the period of surface forcing is, the deeper in the ground it is detectable. Thus, climatic fluctuations on time scales longer than annually influence a larger part of the soil column (Nicolsky et al., 2007). Since the scope of the development done within this work is to equip the model for studying climate change on human time scales, it was necessary to extend its depth.

The depth of the new layer was found applying an exponential fit, where the known thicknesses of the original five layers were used. The schematic Figure 4.8 shows, for all now six layers of the soil scheme, the thickness of the layer, the depth of the center of a layer, and the depth of the lower boundary, respectively.

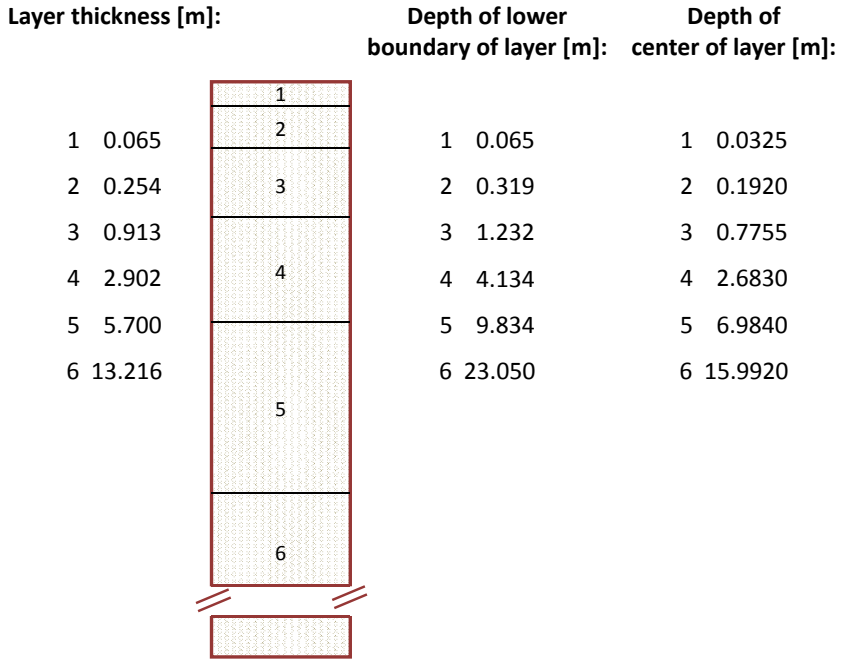

Figure 4.8: Schematic diagram of model soil column with layers, illustrating layer thickness, depth of lower boundary and depth of the center of each layer.

5 Experiments and results

5.1 Overview of experiments

Experiments were conducted for today's climate using ERA40 reanalysis data as lateral boundary forcing for the regional model. The lower boundary of the land surface is defined using the LSP2 dataset (Hagemann, 2002), which gives information about soil porosity, topography, vegetation parameters and the like. Figure 5.1 illustrates the geographic orientation of the model domain.

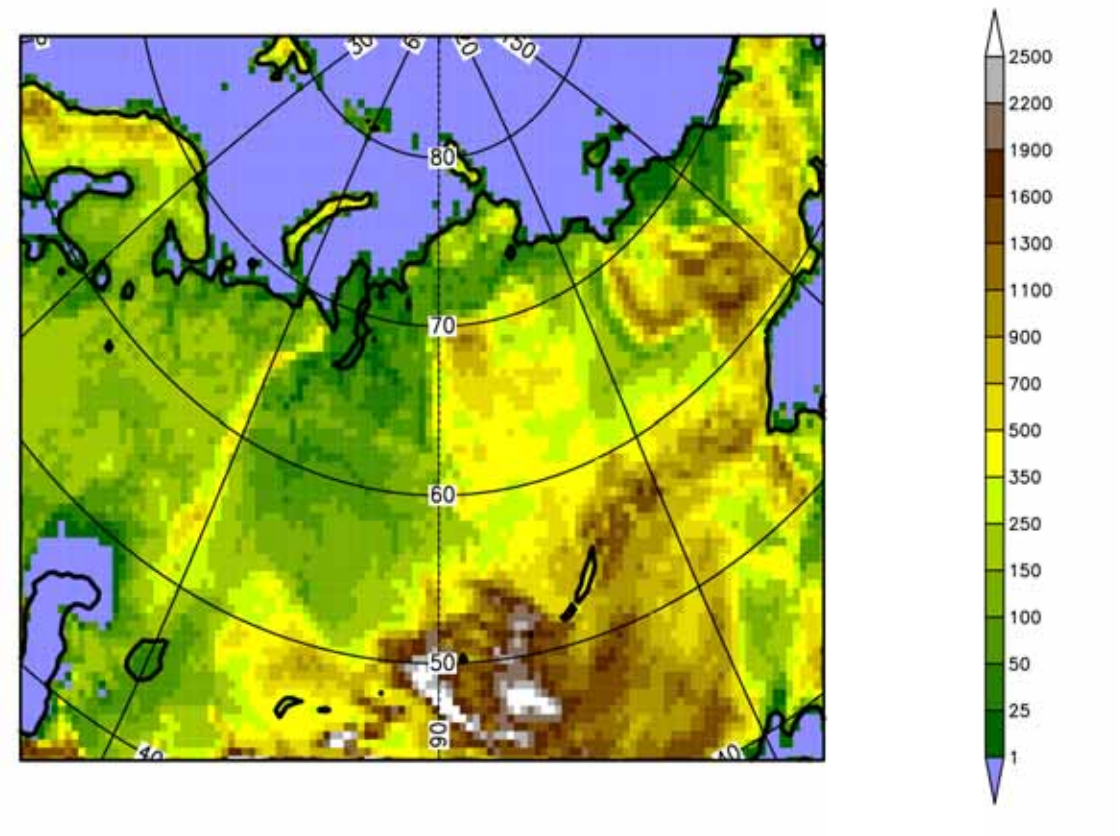

Figure 5.1: Orography [m] of model domain covering Siberia, Central Asia, and parts of Europe.

A reference run CTRL was conducted with the extended, new model version, where all frozen ground processes were disabled, which was run for a 30 year time period from 1971-2000. Twenty years were integrated for each of the experiments with the new model versions, which were run from 1971 to 1990. In the subsequent experiments, the modifications to the soil scheme were integrated step-wise as explained in detail in Section 4. The first change (experiment LAYLF) comprised the substitution of the bucket with the layered hydrology scheme and introduction of the latent heat effect within the layers; adding to this, infiltration of surface water into the ground is now scaled using the degree of freezing of the uppermost layer. In the second step, this model version was equipped with the JFP for the dependency of the thermal properties on soil water and ice content as explained in Section 4.3.2 (experiment FAROUK). The third experiment (COUP) enabled the full coupling of thermodynamics and hydrology, such that hydrological processes only act on the liquid part of soil moisture, while soil permeability is reduced if soil freezing occurs. Thereafter, an experiment with the new, sixth soil layer was conducted (experiment 6TH) using all permafrost processes as in COUP. Results from 6TH will be used for evaluation purposes within this work, while experiment LAYLF, FAROUK and COUP served to study the respective impacts through the physical processes. Table 5.1 lists the experiments and their respective names for the following analysis, and points to the added processes.

Experiment name	CTRL	LAYLF	FAROUK	COUP	6TH
Consideration of latent heat and layered hydrology	-	+	+	+	+
Varying thermal properties	-	-	+	+	+
Coupled soil heat and moisture	-	-	-	+	+
Extension of soil column	-	-	-	-	+

Table 5.1: Conducted experiments and respective processes.

5.2 Data and methods

5.2.1 Data

Gridded data

The model was forced at the lateral boundaries with reanalysis data from ECMWF Reanalysis dataset (40 years) (ERA40) (Uppala et al., 2005). This dataset was also used for comparison of surface evaporation and surface sensible and latent heat fluxes.
Several gridded observational datasets were used for the purpose of evaluation of the different model versions. E.g., simulated air temperature and total precipitation were compared to the WATCH forcing data (WFD) dataset (Weedon et al., 2010). The value of evaporation from the ERA40 data set was estimated using climatologies of total precipitation from WFD and river discharge on the basin scale for the two Siberian rivers Yenissei and Lena, thereby using the land surface water balance:

$$Precip - ET = RO \tag{5.1}$$

where the residual of precipitation and evapotranspiration equals surface runoff. This was done with the purpose of a better assessment of the ERA40 evaporation.
GlobSnow SWE data (GlobSnow) satellite observations were used for a 20-year comparison of simulated to observed snow depth (Luojus et al., 2010). The GlobSnow dataset, though running from 1981 to 2000, incorporates a discontinuity, as a change of the sensor took place in 1987. The differences between 1981-1987 and 1988-2000 mean was small though (not shown), therefore the twenty year climatology was used here for the comparison. The snow depths are given in Snow Water Equivalent (SWE), which was converted to snow depth using a factor of 3.3333 kg/m^3, as this value is given in the data documentation.
International Permafrost Association (IPA) data was used for the comparison of simulated permafrost distribution with observations (J. Brown et al., 1998).
The International Institute for Applied Systems Analysis (IIASA) provides permafrost temperature data, which cover the Russian territory (Kotlyakov and Khromova, 1997). The depth of the measurements is presumably the depth of zero annual amplitude of ground temperatures, as this is the common understanding of the term 'permafrost temperature' (Romanovsky et al., 2010). Therefore depths are very probably not uniform and are described given with 'around 12 to 15m' (D. Schepaschenko, pers. comm. 2012).

Hydrological observations

The river discharge calculated using the HD model was validated against observed climatological discharge, taken from the Global Runoff Data Center (Duemenil Gates et al., 2000).

Station measurements of soil and surface variables

Direct comparisons of climate model results with station data are somewhat difficult: Measurements are taken in one location, while the simulated variable represents a grid cell of, in this case, 50x50 km^2. The probability to match the observed details in parameters like soil porosity, water content, soil thermal conductivity etc. is therefore rather small, yet soil processes are controlled by these parameters. Moreover, climate models have a spatial uncertainty, which means that simulated atmospheric variables would be representative for the considered grid cell, but to a certain degree also also for the surrounding grid cells. Due to this, comparisons to station data often use a distance-weighted mean of 4 or 9 grid cells for comparing air temperature or precipitation.
However, for the purpose of this study it was aimed for an understanding of the reaction of the model's soil to the driving atmospheric temperature by comparing it with the observed behaviour. Smoothing over several grid points could possibly obscure effects or important differences. It was therefore decided to directly compare the respective grid cells for each station here.
The goal of the model development was to enable the soil scheme to reproduce the important processes at all (in contrast to ignoring them), while the analysis of the point measurements should reveal if there is evidence for the discussed processes, and it could not be aimed for a 'perfect match' between model and observations.

Station data used for the comparison of the mean seasonal cycle based on multi-year time series of monthly means, available from the NSIDC (Romanovsky, 2003). The mean seasonal cycle was calculated for the observations as well as for the model output, for which soil temperatures nearest to the depth of the measurements have been extracted, for the respective gridbox of the station. Figure 5.2 shows the positions of the stations in the model domain. Two of the soil temperature measurements (0.2m, 0.8m) were taken in depths that are closed to simulated soil temperatures (0.192m, 0.78,8 m) and were chosen for analysis.

Station data for comparing freezing and melting periods originate from the CALM data base (Fyodorov-Davydov et al., 2004). This evaluation has so far only been conducted with one Siberian station, Chukochya, as data with daily resolution and appropiate depths of the soil temperatures are not very frequent. The comparison was made with one more dataset of daily soil temperature measurements from Abisko, Sweden; since deviations between simulated and observed values are large, which is attributable to the detailed orography of the Abisko region, that can not be resolved by REMO at 0.5 degree spatial resolution, the comparison is not shown here.

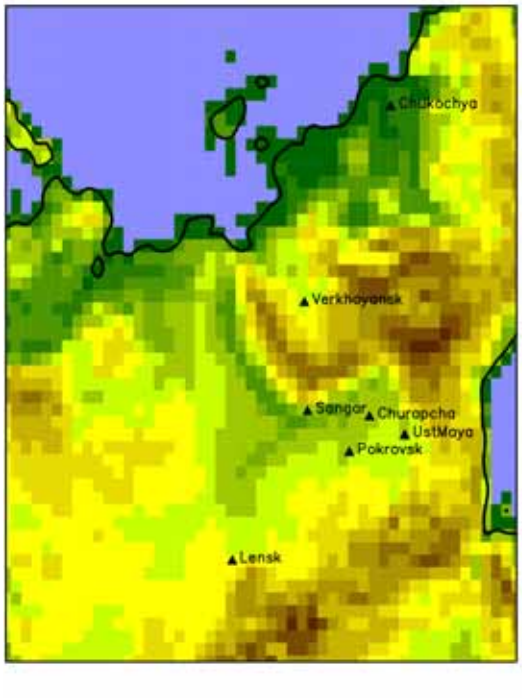

Figure 5.2: Zoom into model domain with position of stations for evaluation.

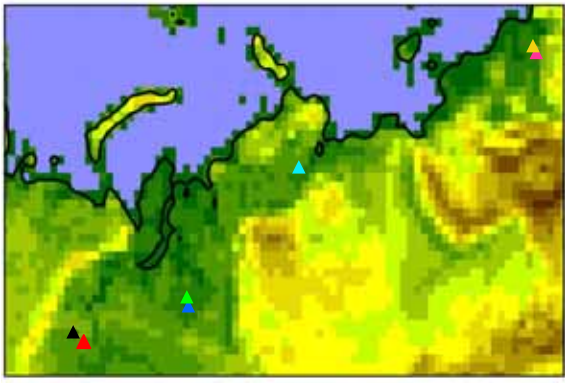

Figure 5.3: Model domain with positions of grid cells for process analysis. Grid cells are indexed as follows: black = 1, red = 2, green = 3, blue = 4, turquoise = 5, orange = 6, magenta = 7.

5.2.2 Methods

Analysis of multi-year mean spatial distributions

It was decided to display January, April, July and October for winter, spring, summer and fall, respectively, instead of the usually chosen averages over three months. This was done due to the strong impact snow cover has on the interactions between land surface and climate in this region. The transition seasons incorporate the change from snow free to snow covered land surface and vice versa, for which reason it is not recommendable to average over exactly the time period of snow cover development or ablation. An observational study by Langer et al. (2011) used two-monthly means, e.g. for the same reason.

Analysis of single grid boxes

Single gridboxes have been investigated with respect to soil variables, in order to analyse the influence of model extensions in more detail. The grid cells were chosen such that they cover different climatic zones, as Western Siberia features milder temperatures and more precipitation than the North Eastern part of Siberia. No grid boxes were chosen in mountainous regions, as here soil depths are mostly very shallow, and orographic variance is large. Shallow soil depths lead to low water contents in the soil, therefore effects of the new parameterizations will only have minor effects, apart from the high thermal conductivity of bedrock. This latter aspect can be seen nevertheless in many of the chosen grid boxes, as many of them feature bedrock below a certain depth of the column. It will be shown in Section 5.3.1 that the specific thermal properties of bedrock are properly set in the model, and that the impact on the modelled soil thermal regime is consistent with the expectations. Moreover, simulated variables have a higher uncertainty in mountaineous regions, since here horizontal variations are large in reality, yet this cannot be represented with a model resolution of roughly 50 km. Therefore, grid cells were chosen such that they are situated in relatively even topography. Figure 5.3 shows the position of the grid cells for analysis during the model development.

Hydrological discharge model

In order to compare simulated to observed river discharge, daily time series of simulated surface runoff and drainage were used to force the Hydrological Discharge model (HD model) (Hagemann and Duemenil Gates, 2001; Hagemann and Duemenil, 1998). The HD model is a routing scheme that simulates river discharge at 0.5 degree horizontal resolution, based on sub-grid scale slope information.

5.3 Results and discussion

The respective impacts due to the model extensions will be analysed following the stepwise development (see Table 5.1). In order to ensure the consistency of the new model versions with the expectations due to the physical knowledge, analysis will start with the influence on the soil and surface, with a focus on thermal and hydrologic variables (Section 5.3.1), i.e. on soil temperatures and hydrological variables as runoff and soil moisture. In Section 5.3.2, analysis of the influence on the SEB and atmosphere will follow.

5.3.1 Influence on soil and surface

Differences between experiments LAYLF and CTRL

Experiment LAYLF introduces the effect of freezing and melting of soil moisture in the soil scheme, now vertically resolved and thus varying in overall occurance, due to the influence of bedrock, and in strength, due to the influence of varying water contents. The differences in soil temperatures between experiment LAYLF and CTRL (Figures 5.4, 5.5, 5.6) show how the release of latent heat warms the soil during October and January, which represent autumn and winter, respectively.

The effects of warming due to freezing and of cooling due to melting can be attributed more clearly in layers below the uppermost soil layer, while temperature of the latter is influenced stronlgy by the atmosphere. Therefore, cooling due to melting occurs most strongly in the south-western part of the model domain during spring, indicating regions with deep soils which leads to pronounced latent heat effects. Soil cooling in the third layer can also be detected in the Northern Siberian lowlands during summer, where MAAT is low, thus AL is shallow (shown in Section 5.44); thus soil melting in this depth occurs late in the season.

Warming of the first soil layer during autumn and winter can be detected especially in Northern and Western parts of Siberia, where soils are deep and therefore water is abundant, so that the whole column is warmed from below even at the end of the winter. To the contrary, for practically all of Siberia any seasonal cooling of the uppermost layer due to melting of soil ice is superimposed by the warming due to different atmospheric conditions in LAYLF as in CTRL, which are a result of the decrease in soil moisture content due to reduced infiltration in spring. This leads to less evaporative cooling, as is shown in Section 5.3.2. The net effect is thus an increase of mean soil temperature.

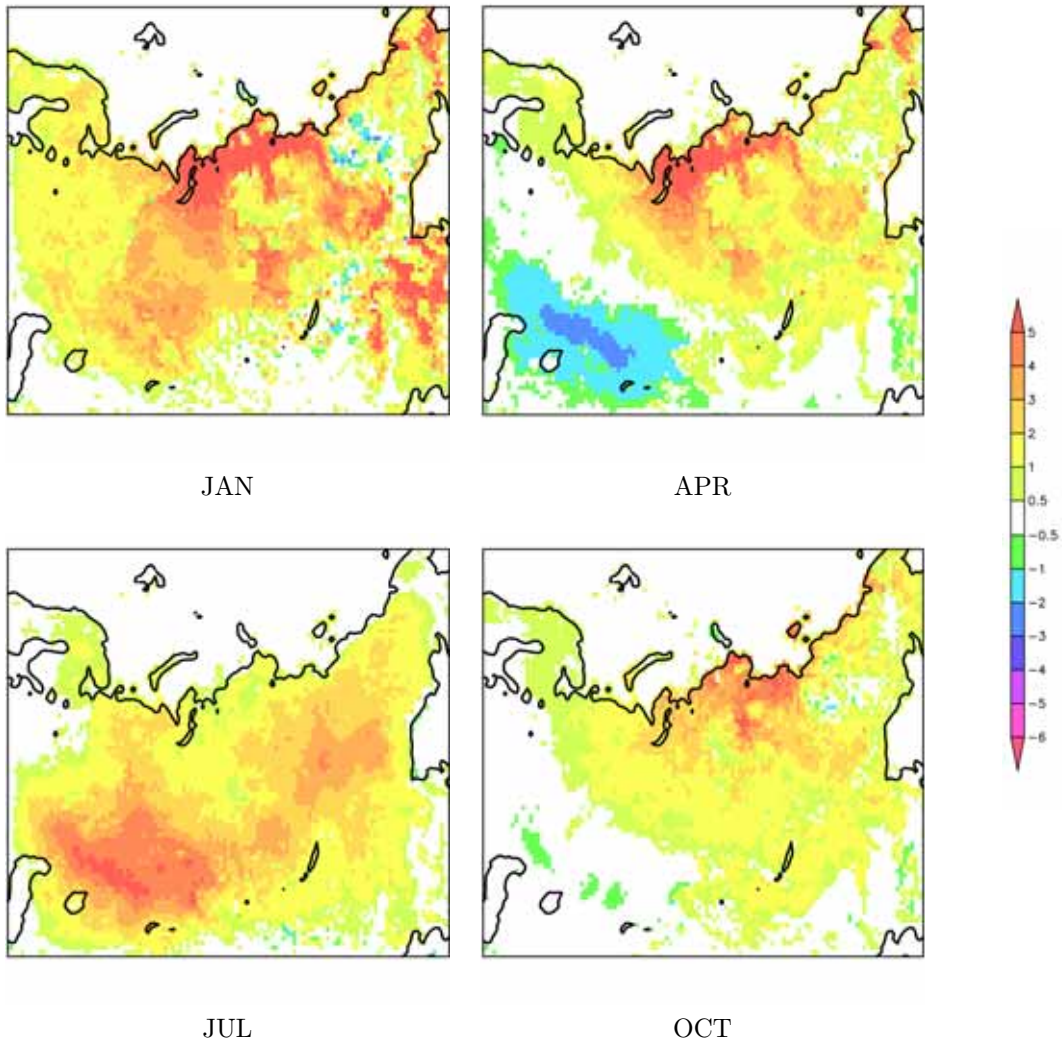

Figure 5.4: Difference in simulated soil temperature in layer 1 $[K]$, experiments LAYLF - CTRL, 1971-1990 mean, for months January (upper left), April (upper right), July (lower left), and October (lower right).

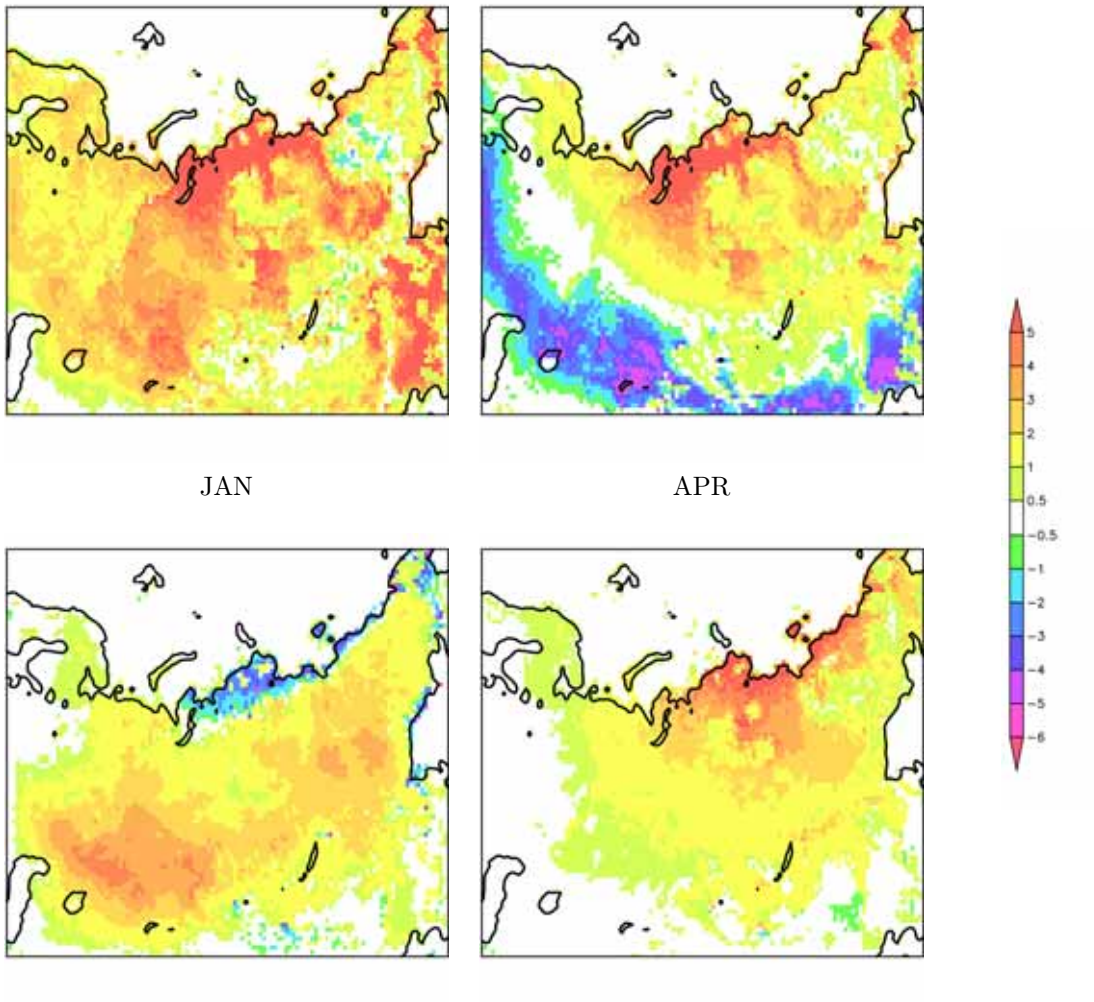

Figure 5.5: Difference in simulated soil temperature in layer 3 [K], experiments LAYLF - CTRL, 1971-1990 mean, for months January (upper left), April (upper right), July (lower left), and October (lower right).

In the fifth layer, a general warming occurs, which is attributed to the different, warmer atmospheric conditions that develop in LAYLF in summer, as explained above. A larger temperature increase occurs in the Northern part, where both freezing is strong and soils are deep enough to supply water for latent heat release. Changes in the lowest layer show only weak seasonal variation, as at this depth the seasonal cycle is stronlgy dampended (Figure 5.6). The persistent warming until the end of winter might be an effect from unrealistic percolation in the LAYLF version: Soil water can still percolate into deeper layers throughout the cold months, so that water is abundant for new freezing even in late winter to spring.

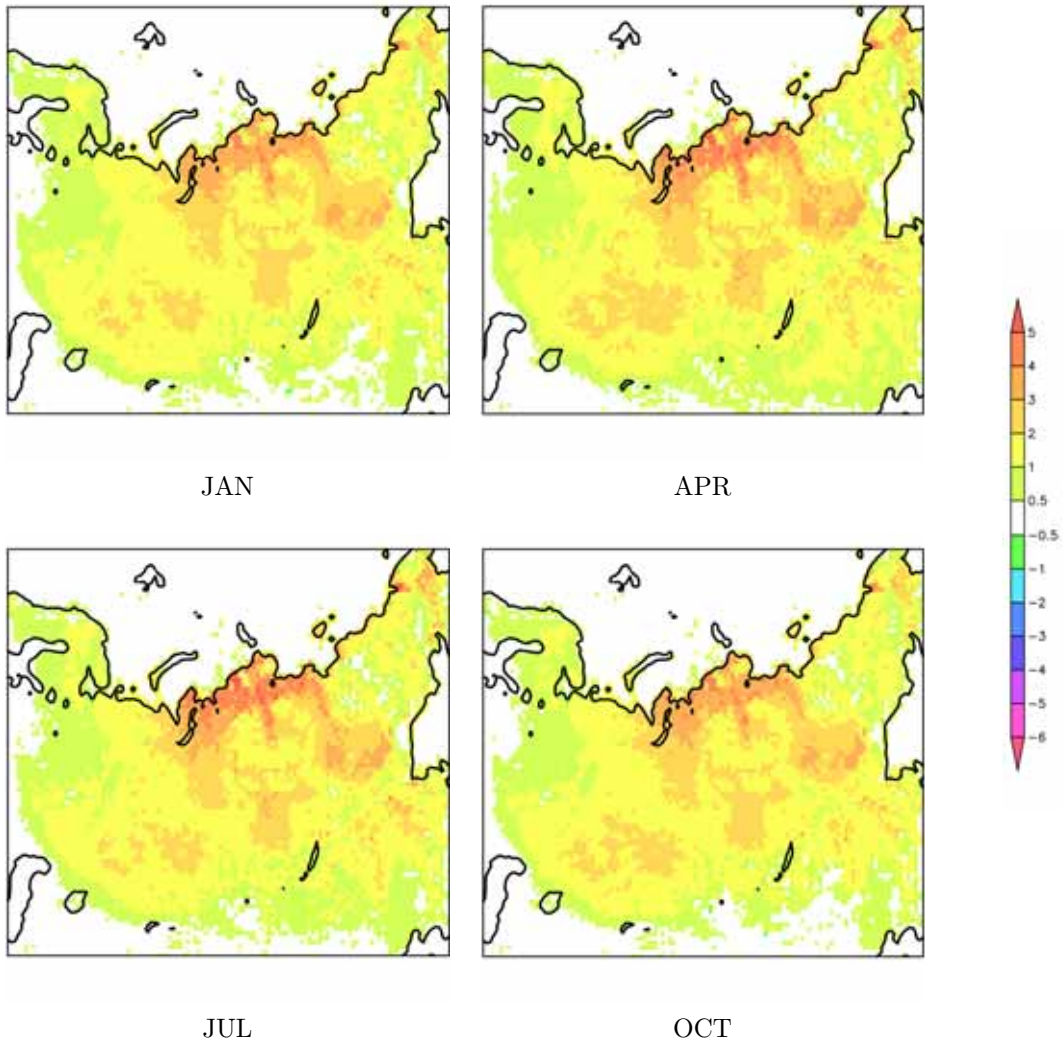

Figure 5.6: Difference in simulated soil temperature in layer 5 $[K]$, experiments LAYLF - CTRL, 1971-1990 mean, for months January (upper left), April (upper right), July (lower left), and October (lower right).

Figure 5.7 shows how simulated surface runoff reacts on the introduction of soil freezing. As explained in Chapter 4 (Section 4.3), infiltration of surface water into the soil is not influenced by the thermal state of the ground in the CTRL version. The large amount of snow melt water in spring within a short time period can freely infiltrate and replenish soils in CTRL. In LAYLF, however, infiltration is dampened when the first soil layer is frozen. This leads to a strong decrease in infiltration, whereas large part of the snow melt water is passed to surface runoff. As a consequence, root zone soil moisture is lower in LAYLF as compared to CTRL, which is shown in Section 5.3.2. Influences on SEB and atmosphere can to a large part be attributed to this effect on hydrology, which is explained in detail in Section 5.3.2.

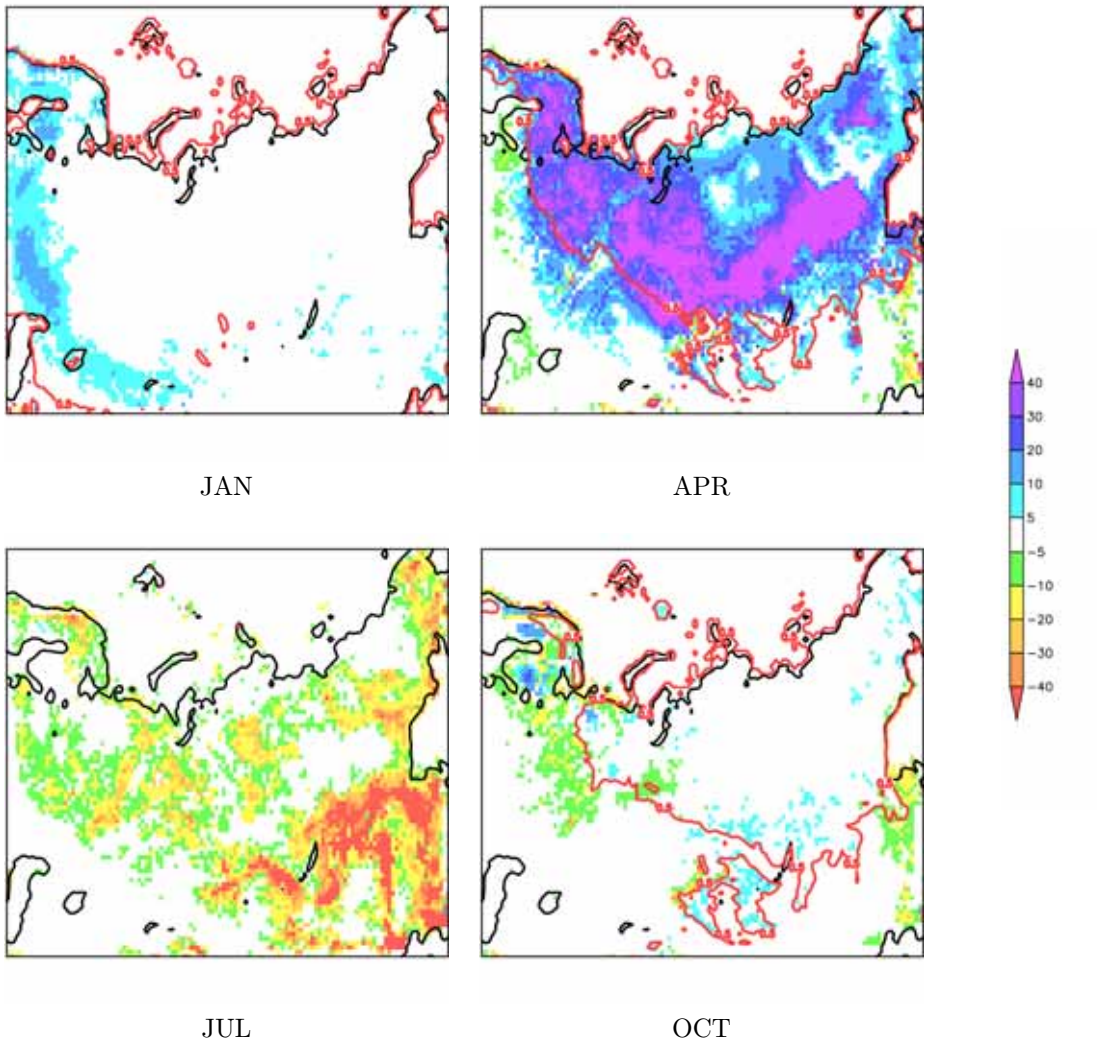

Figure 5.7: Difference in simulated surface runoff $[mm/month]$, experiments LAYLF - CTRL, 1971-1990 mean, for months January (upper left), April (upper right), July (lower left), and October (lower right).

Differences between experiments FAROUK and LAYLF

Results for simulated thermal conductivities are analysed, using multi-year mean differences in thermal conductivity for individual soil layers to the formerly used, constant values. Differences are shown for layers one and three in Figures 5.8 and 5.9; differences for the fifth layer are not shown due to its high bedrock portion.

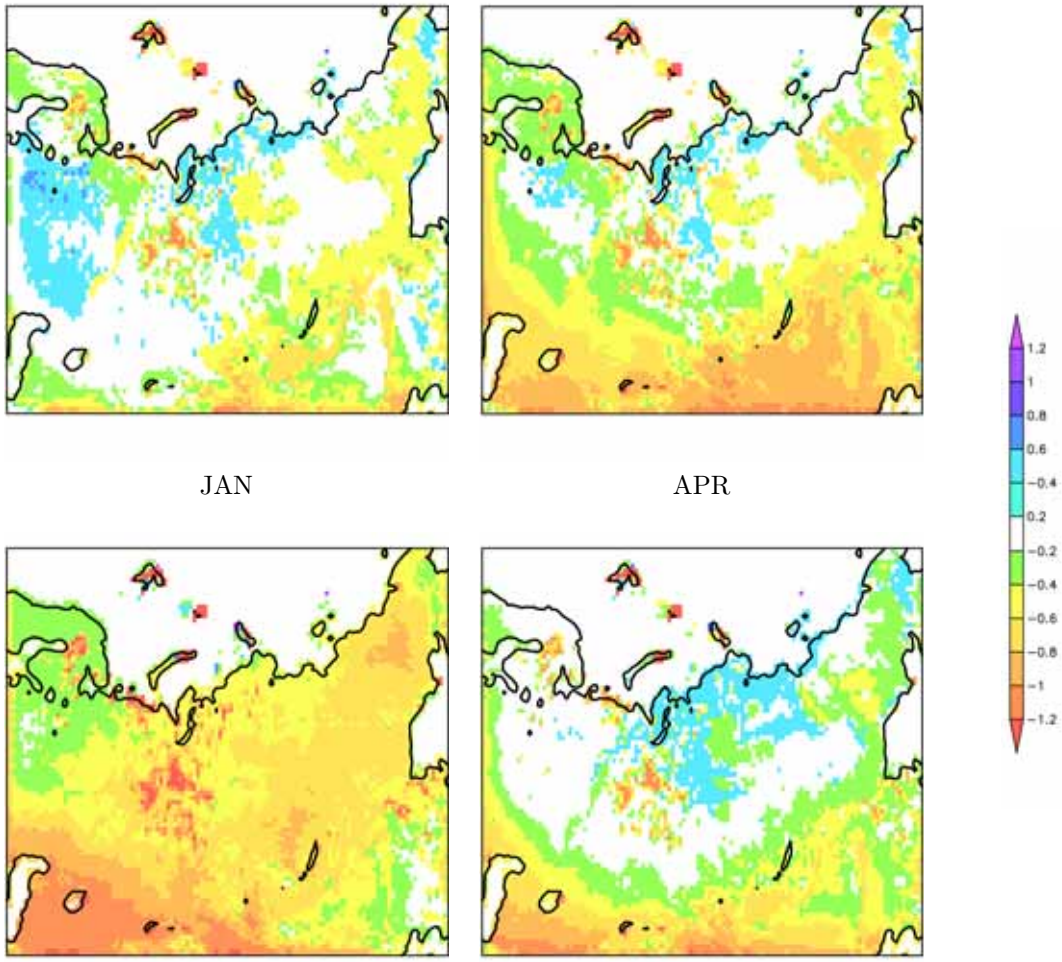

Figure 5.8: Difference in thermal conductivity λ [J/mK] of layer 1 from experiment FAROUK (1971-1990 mean) minus constant λ as given in the soil library, for months January (upper left), April (upper right), July (lower left), and October (lower right).

The thermal properties simulated with FAROUK show the expected dependencies on soil texture type, water and ice contents, and soil depth, which lead to the displayed differences, varying depending on respective season and region. The conditions of the specific grid cell are reflected, so that, e.g., the peatlands in the West Siberian lowlands

can be detected clearly, as organic material has a low thermal conductivity compared to mineral soils, regardless of its water and ice contents. The distribution of bedrock can be diagnosed from the simulated results, as they have a constant and high λ, therefore 'peaking' out of the ground with increasing layer number. The FAROUK experiment

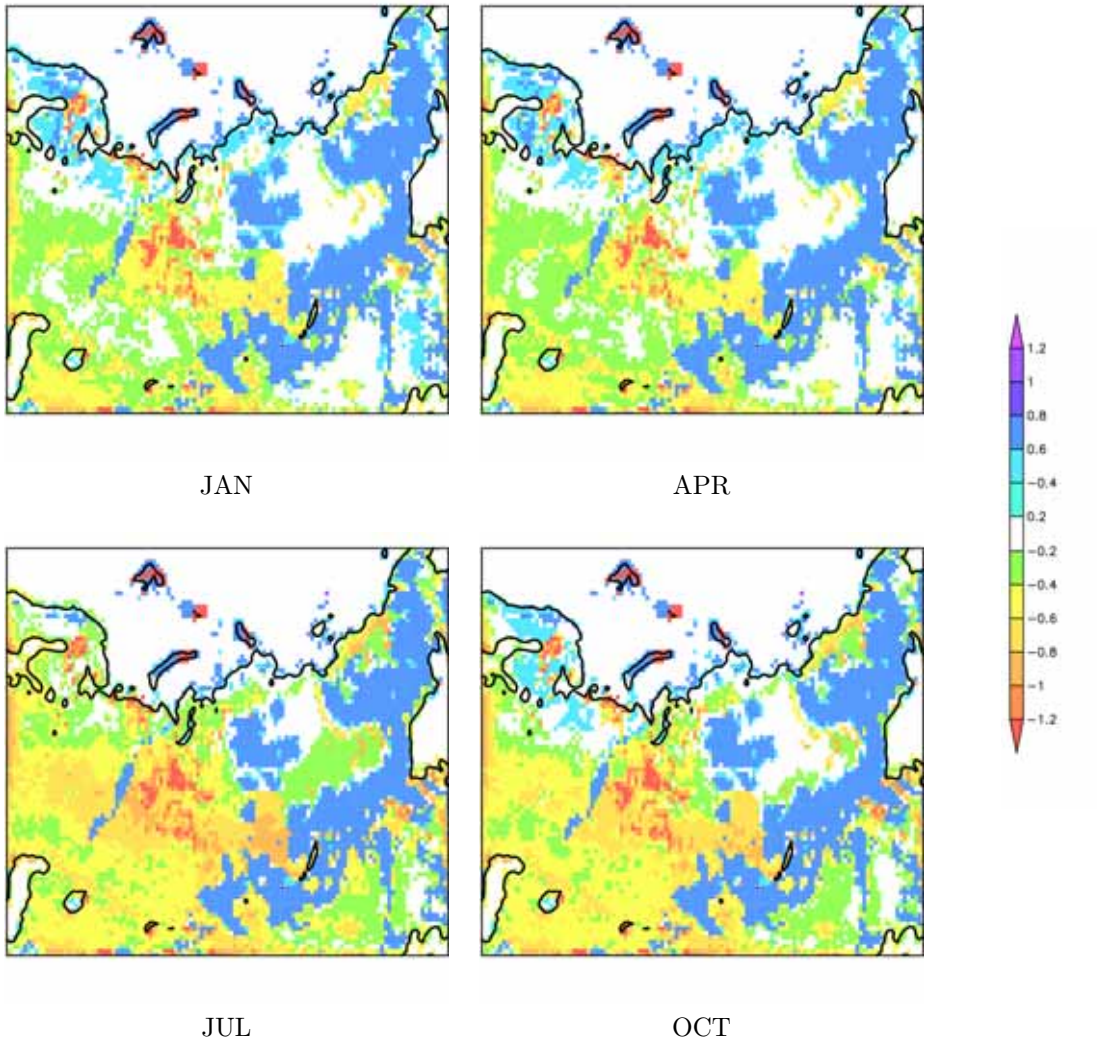

Figure 5.9: Difference in thermal conductivity λ [J/mK] of layer 3 from experiment FAROUK (1971-1990 mean) minus constant λ as given in the soil library, for months January (upper left), April (upper right), July (lower left), and October (lower right).

produces a seasonal cycle in the thermal conductivity, with the tendency to be larger than the original λ in winter, and smaller in the warm months (see also Section 4.3.2). The increase of the winter conductivity is less strong than the decrease of the summer values. A weakening of heat transfer into the ground in summer implies more favorable conditions for permafrost existence, and a more shallow AL (see Section 5.3.3). The differences in the conductivity of the uppermost layer displays more spatial heterogeneity in autumnn, winter and spring, and mirrors presence and absence of ice in the ground.

In contrast, a relatively uniform lowering of λ can be seen during summer over almost the whole model domain in the uppermost layer.
At least for the monthly means, no large changes evolve over some parts of the region. This was expected, as the original constant conductivities were chosen such that they represented a mean conductivity, fitting for a range of possible unfrozen conditions.

The different conditions for soil heat conduction in the FAROUK experiment lead to changes in the ground thermal regime, which are illustrated in Figures 5.10, 5.11, and 5.12. The simulated soil temperatures in winter decrease as compared to the LAYLF experiment, which is an effect of the higher thermal conductivity when including the influence of soil ice, or of the high thermal conductivity of bedrock now considered in the model.

When considering the temperature differences for the uppermost, the third, and the lowest layer, respectively, horizontal heterogeneity of the sub-surface material can be diagnosed, since changes in heat transport are most markable in grid cells and layers with a high portion of bedrock. Layers below the shallow uppermost soil layers in the Central Siberian mountains, e.g., feature constantly high λ values due to bedrock, and therefore effectively react on heat transport from above. This leads to an increase of the seasonal cycle of the soil temperatures in these regions.

In layers above the bedrock, heat flux into the ground is weakened during summer with FAROUK, while it is enhanced during winter. The overall effect is a shift to lower soil temperatures, which means that the model thus simulates the thermal offset effect (see Section 4.3.2).

The response of the ground temperatures incorporates both the effects from the changes in heat flow conditions and from the different mean state of the overlying atmosphere (see Section 5.3.2).
The changes in the winter patterns originate in the modified physical formulation for heat transfer in the ground, since sub-surface and atmosphere are effectively decoupled during periods with snow cover. In contrast to this, differences in summer incorporate also indirect effects, as the new parameterization impacts atmospheric variables, which in turn propagate into the ground. This can explain the 'smoothed' horizontal patterns of the differences in summer when compared to winter.

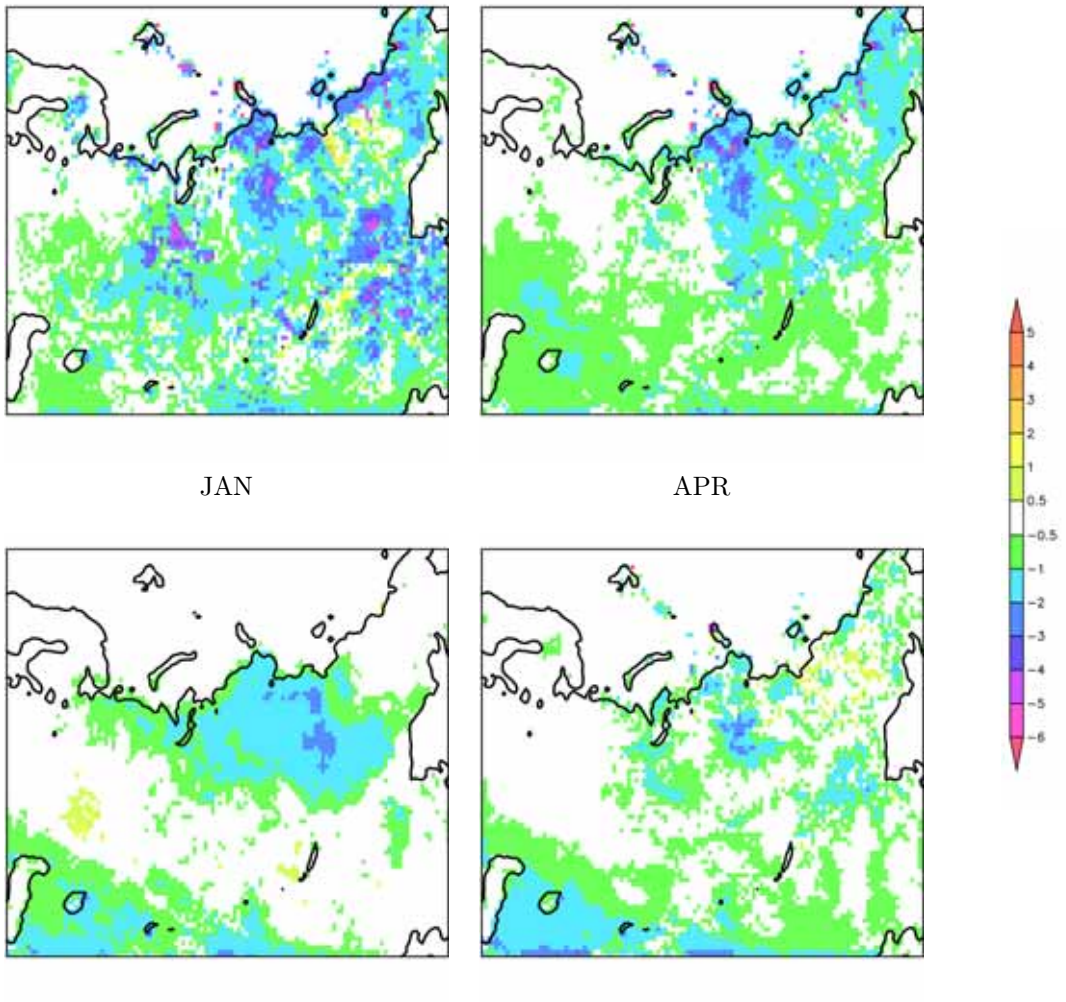

Figure 5.10: Difference in simulated soil temperature in layer 1 $[K]$, experiments FAROUK - LAYLF, 1971-1990 mean, for months January (upper left), April (upper right), July (lower left), and October (lower right).

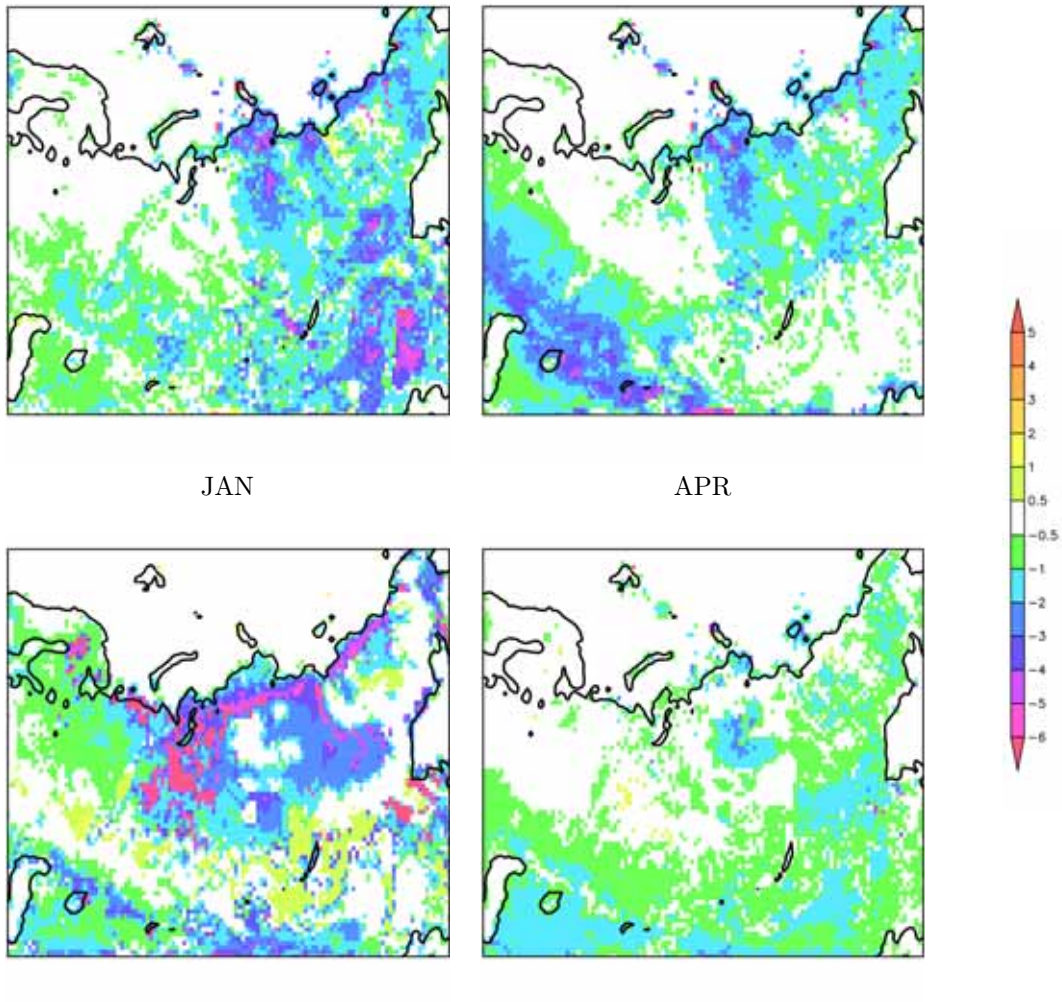

Figure 5.11: Difference in simulated soil temperature in layer 3 [K], experiments FAROUK - LAYLF, 1971-1990 mean, for months January (upper left), April (upper right), July (lower left), and October (lower right).

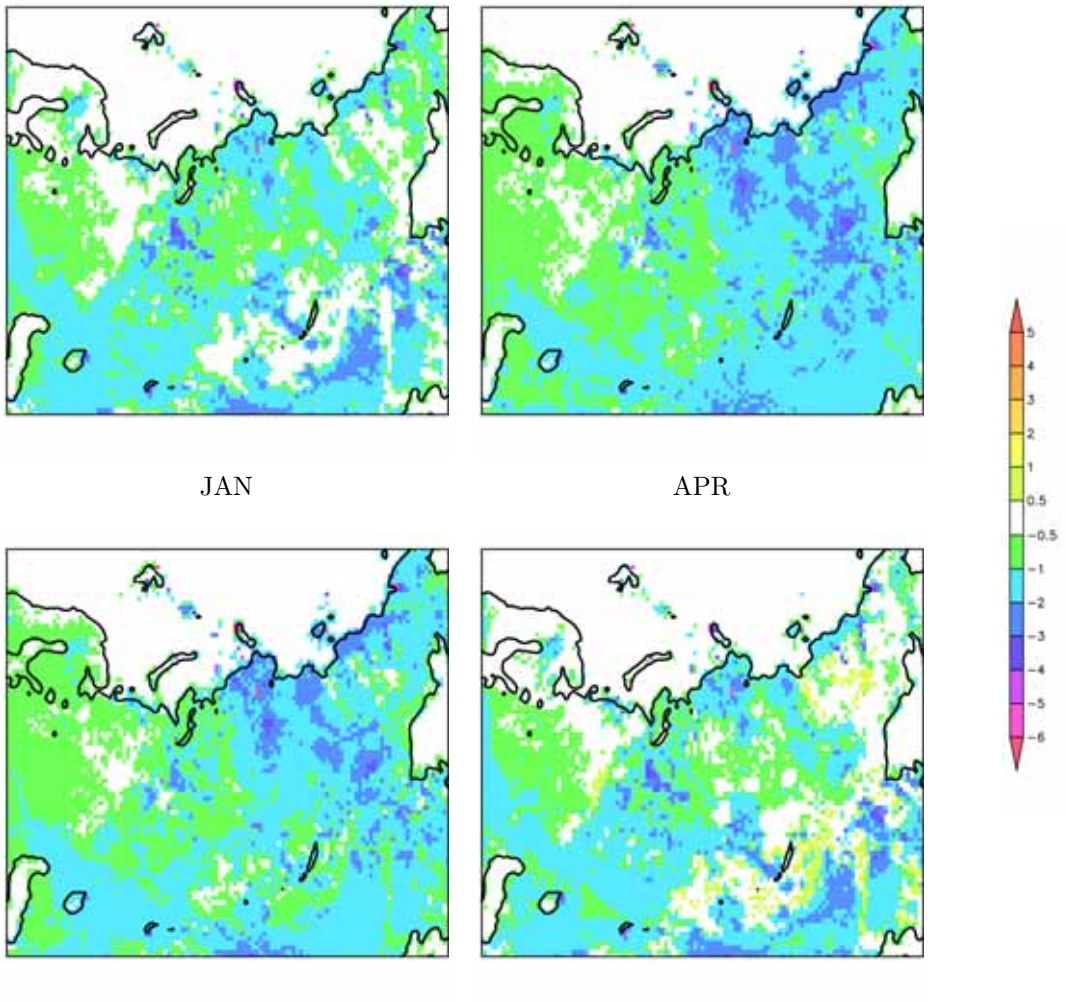

Figure 5.12: Difference in simulated soil temperature in layer 5 $[K]$, experiments FAROUK - LAYLF, 1971-1990 mean, for months January (upper left), April (upper right), July (lower left), and October (lower right).

Differences between experiments COUP and FAROUK

Spatial distribution of multi-year monthly means of the liquid and solid soil moisture in layers one and three from experiment COUP shows that moisture values follow the seasonal cycle of the energy input in a meaningful way.

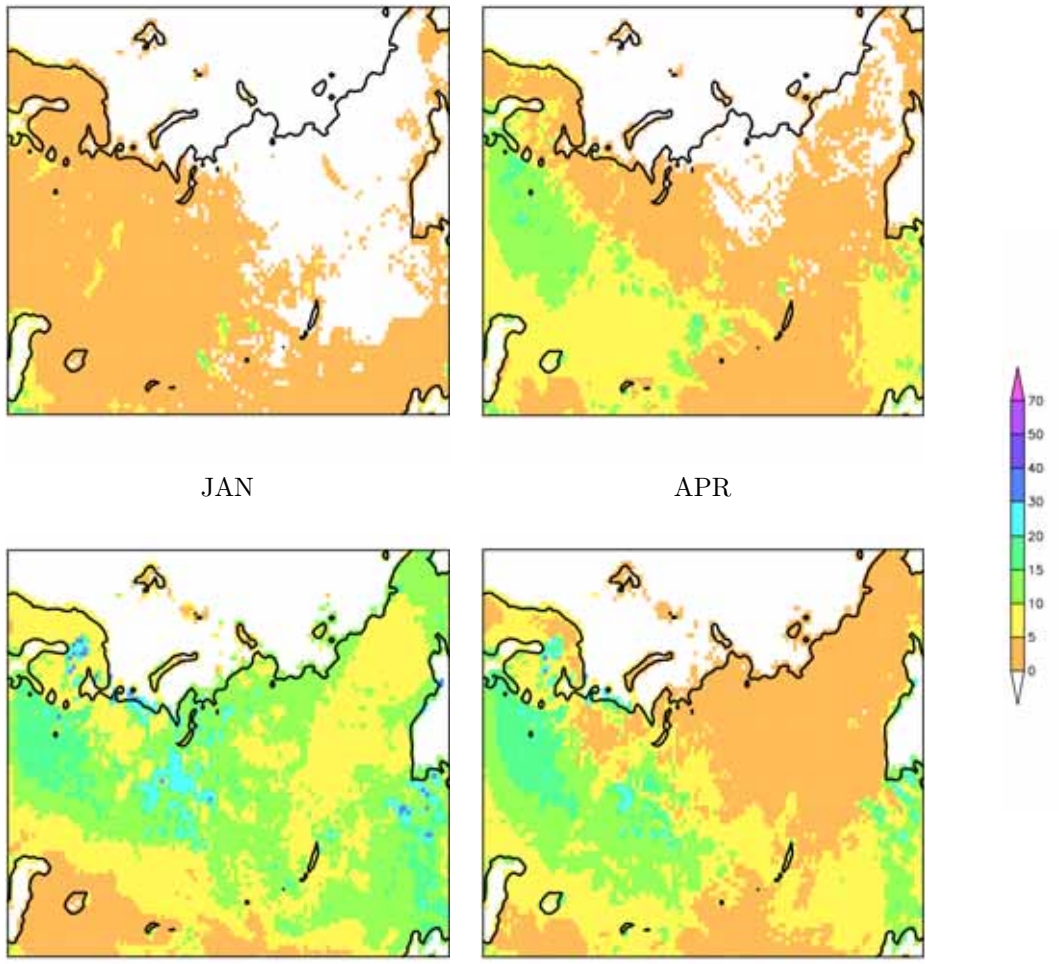

Figure 5.13: Simulated liquid soil moisture in layer 1 [mm], experiment COUP, 1971-1990 mean, for months January (upper left), April (upper right), July (lower left), and October (lower right).

Figures 5.13, 5.14, 5.15, and 5.16 display the reduction and total vanishing of liquid soil moisture during winter, and the opposite behaviour for soil moisture in the solid phase. Again, in deeper layers more and more bedrock exists, and, hence, no moisture is simulated.

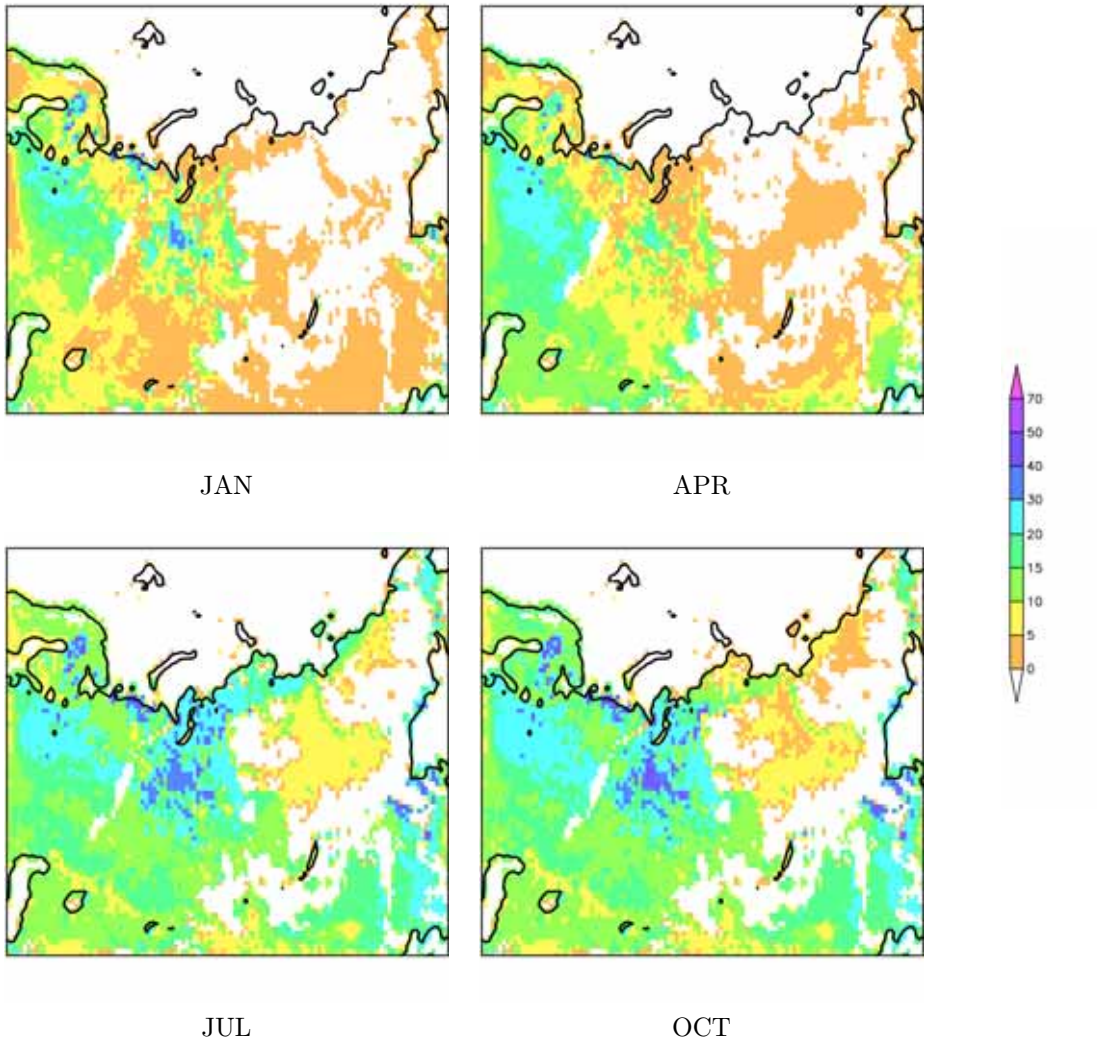

Figure 5.14: Simulated liquid soil moisture in layer 3 [cm], experiment COUP, 1971-1990 mean, for months January (upper left), April (upper right), July (lower left), and October (lower right).

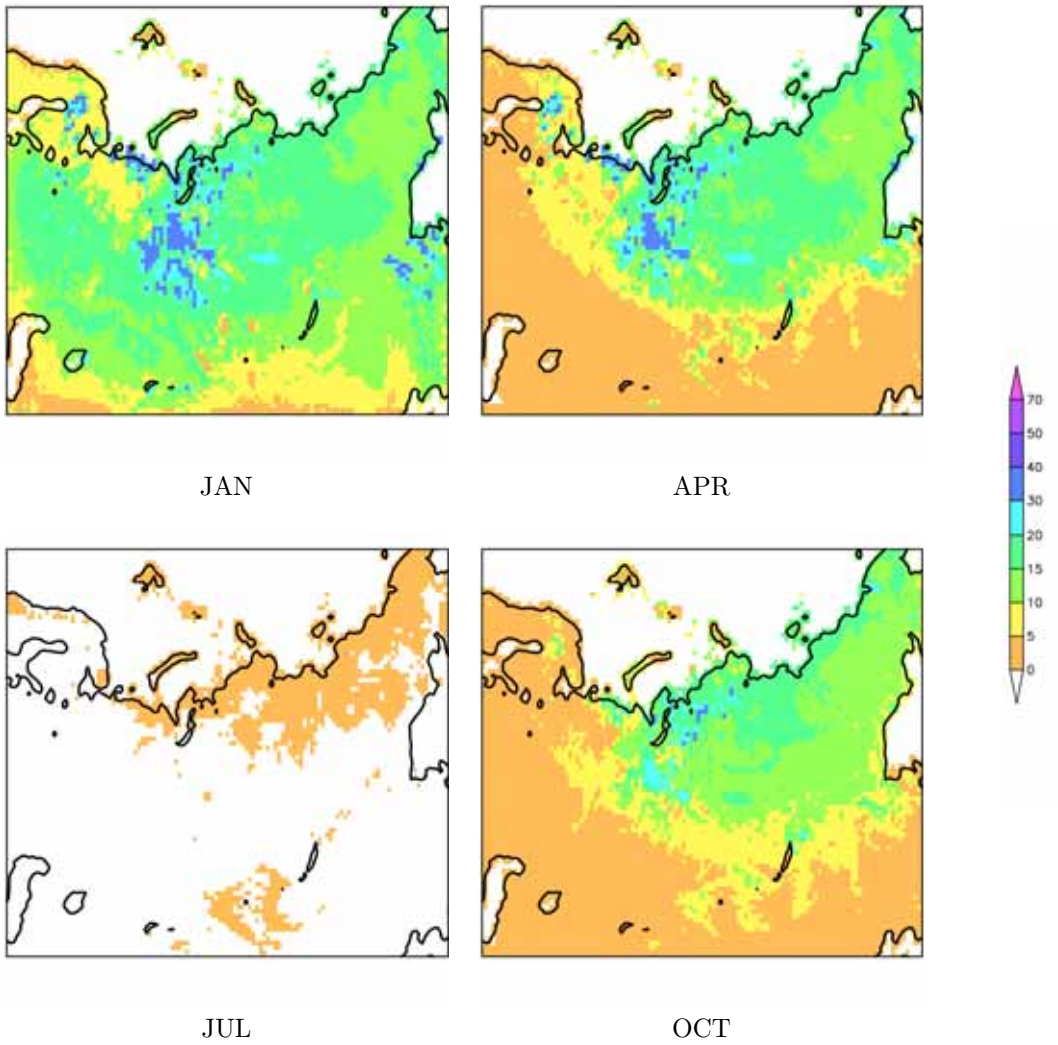

Figure 5.15: Simulated solid soil moisture in layer 1 [mm], experiment COUP, 1971-1990 mean, for months January (upper left), April (upper right), July (lower left), and October (lower right).

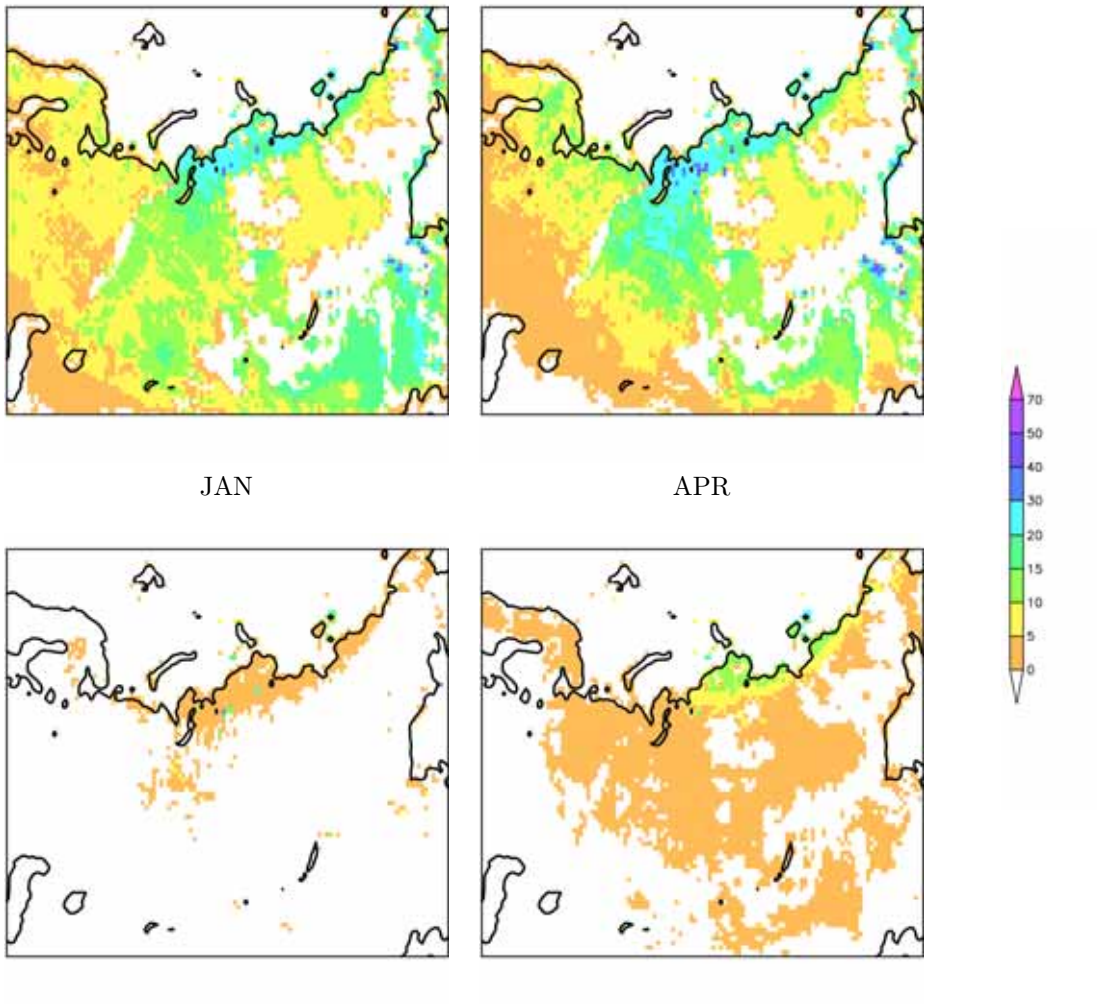

Figure 5.16: Simulated solid soil moisture in layer 3 [cm], experiment COUP, 1971-1990 mean, for months January (upper left), April (upper right), July (lower left), and October (lower right).

Spatial comparison of the climatological values of the total soil moisture content from COUP versus the respective variable from FAROUK shows an increase in overall soil moisture due to coupling of thermodynamics and hydrology (Figures 5.17 and 5.18; again the fifth layer is not shown as no large differences occur). Simulated soil moisture increases in the upper layers in COUP as compared to FAROUK in months with soil freezing, which can be attributed to restricted percolation, but also to the suction of moisture from unfrozen parts in the soil column towards the freezing front, as will be shown later in this section. In consequence, the seasonal cycle of soil moisture changes.

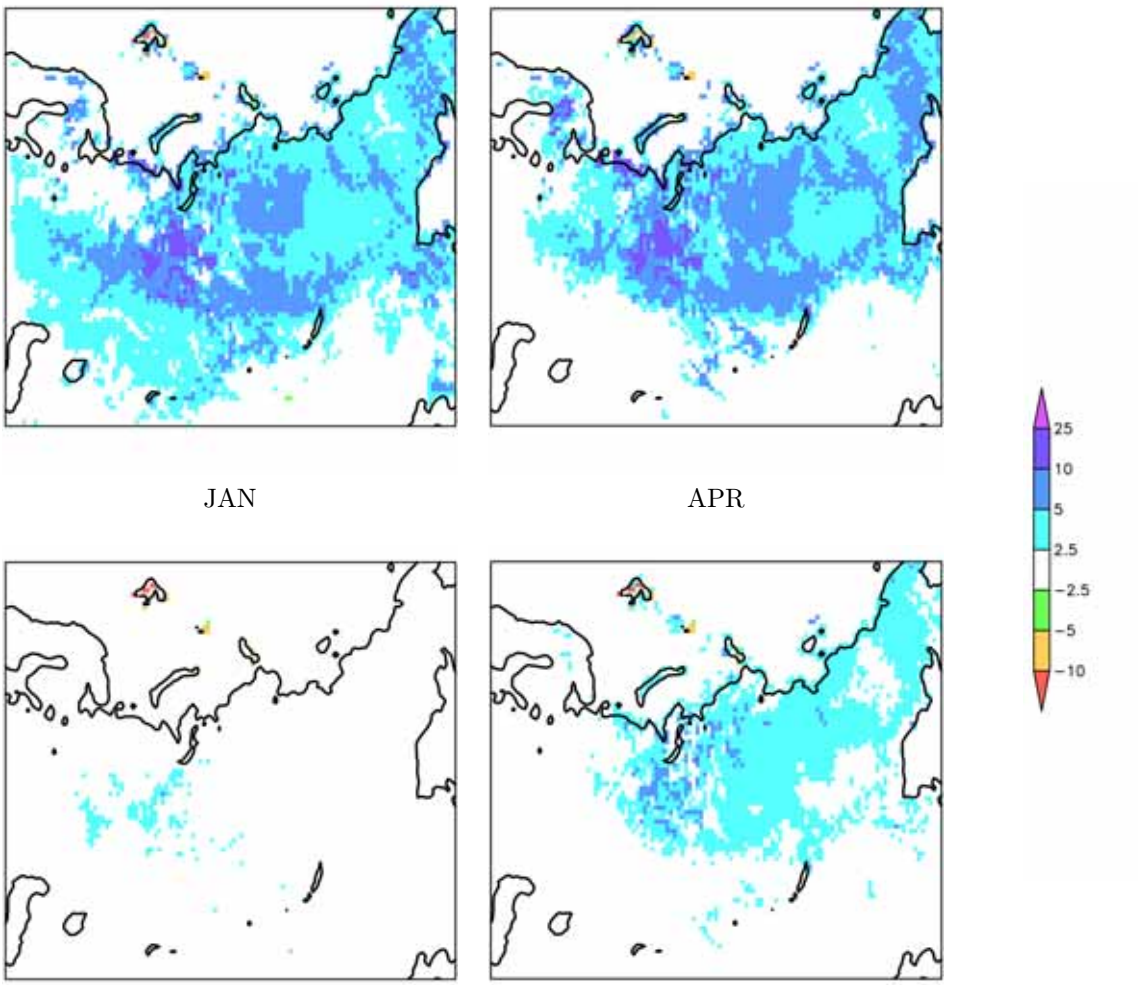

Figure 5.17: Difference in simulated total soil moisture in layer 1 [mm], experiments COUP - FAROUK, 1971-1990 mean, for months January (upper left), April (upper right), July (lower left), and October (lower right).

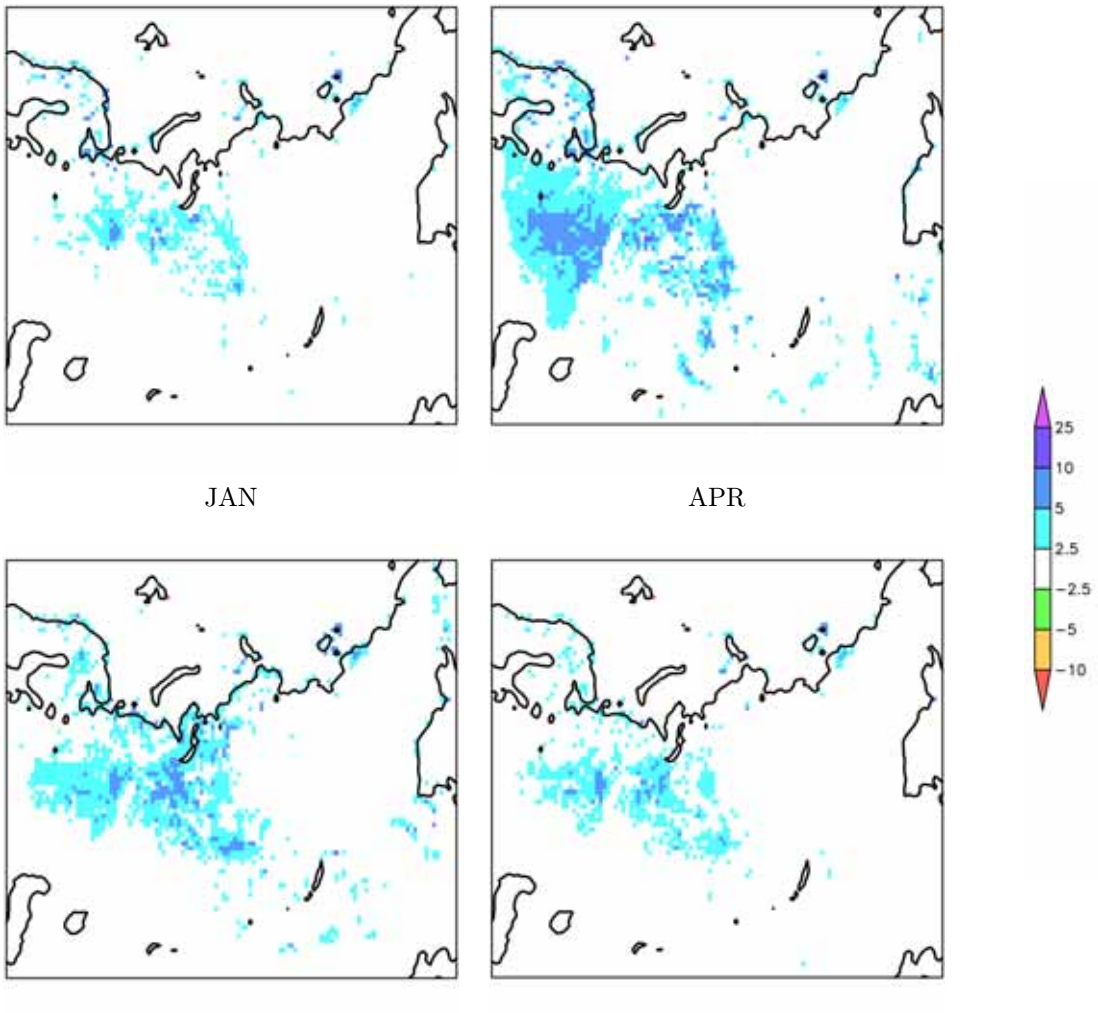

Figure 5.18: Difference in simulated total soil moisture in layer 3 [mm], experiments COUP - FAROUK, 1971-1990 mean, for months January (upper left), April (upper right), July (lower left), and October (lower right).

The mean seasonal cycle of relative soil moisture of each layer is shown in Figure 5.19 for both the FAROUK and the COUP experiment for grid boxes 1, 2, 6, and 7. Here, layers with a large portion of or within bedrock can well be recognized as they contain no water. For both experiments, the phase lag from uppermost to the successive layers is represented, and variability is dampened with increasing depth, as expected.

The minimum of water content in upper layers occurs in summer in both experiments, which is meaningful as total precipitation input is rather low, while evapotranspiration is potentially high. During the cold period only very limited or no input of liquid water from the surface is possible, since precipitation falls as snow, and since the frozen surface is blocking inflow. However, soil water can percolate from near-surface to deeper layers in FAROUK at any temperature, therefore the soil tends to dry out during winter, especially in the upper layers. Thus, the maximum soil moisture content in the FAROUK experiment occurs in autumn, due to larger amounts of water input through precipitation while soils are unfrozen. A weak secondary maximum occurs in FAROUK in spring in response to snow melt in the second layer.

The COUP model version intensifies the seasonal cycle in the upper layers and leads to differences in their temporal dynamics.
While summer months display lowest values in COUP as in FAROUK in the first and second layer, the winter values are clearly higher in COUP than in FAROUK.

The spring peak due to snow melt water is hardly detectable in the third layer in FAROUK while it is the yearly maximum in COUP.
In general, the behaviour of the upper three layers in autumn and winter point to a slow depletion of soil moisture from near-surface towards more deeper layers with FAROUK, whereas the third layer rather acts as a storage for water movement towards upper layers during winter in COUP.
Moreover, in the western grid cells (number 2 and 4), soil moisture content in the deeper layers increases clearly in COUP as compared to FAROUK, which was already shown in Figure 5.18. Soil depth reaches the deepest, fifth layer in this grid box, so that the binding of water during winter in COUP increases moisture substantially when compared to FAROUK.

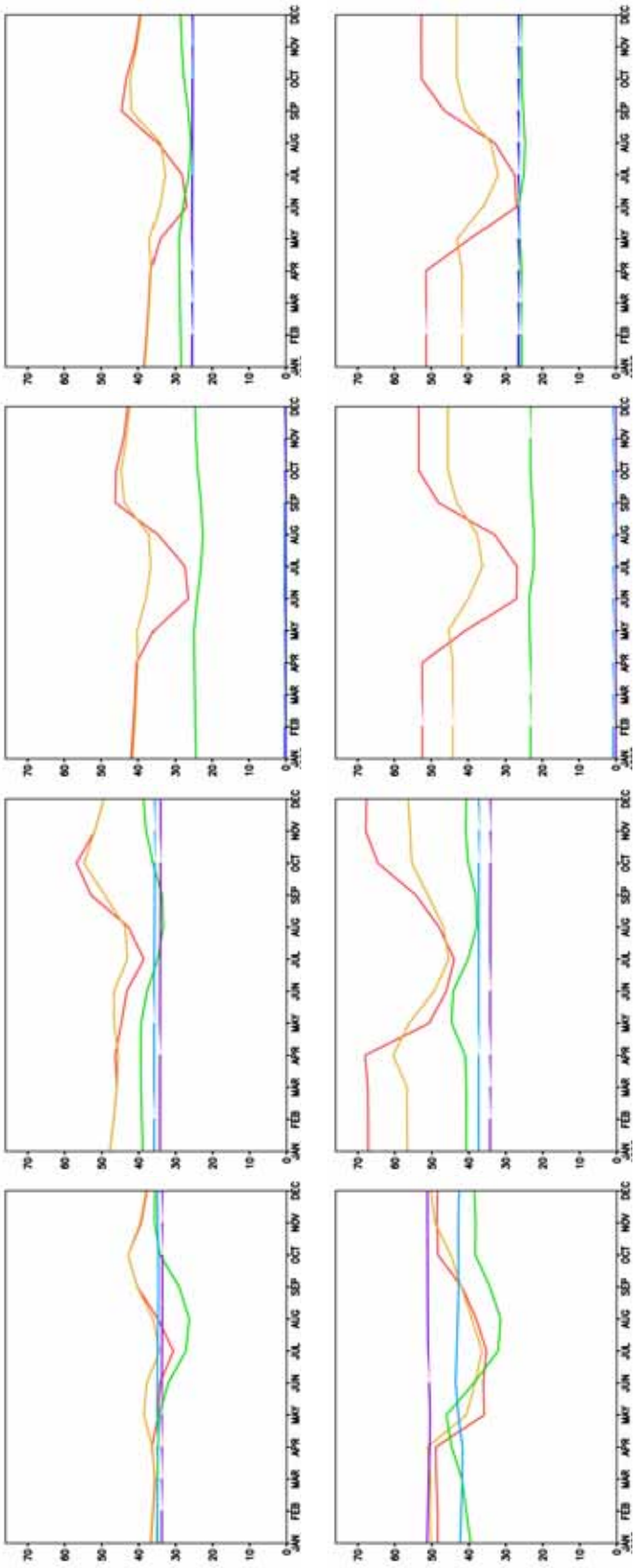

Figure 5.19: Seasonal cycle of relative soil moisture [%] in grid box 1, 2, 6, and 7 (from left to right) from experiment FAROUK (upper row) and COUP (bottom row), of layers 1 (red), 2 (yellow), 3 (green), 4 (blue), and 5 (violet); 1971-1990 mean.

The behaviour of the new scheme with regard to freezing periods is analysed on the basis of time series of daily means. (The analysis of its behaviour during melting is shown in the context of model evaluation using station data, see Section 5.3.3 and Figure 5.51). Soil water contents and temperatures for the upper three layers from individual grid cells are shown in Figure 5.20.
Autumn period shows important differences between FAROUK and COUP in the dynamics of soil moisture in the upper three layers when freezing occurs.
Soil water contents of the uppermost layers clearly vary in response to water input from above the surface in both experiments, as the coincidence with liquid precipitation indicates. The latter decreases to zero as weather conditions become more cold, and the soil temperatures drop to the freezing point and/or below. After the beginning of soil freezing, short term soil water variations cease, since synoptic activity does not deliver liquid water to the surface any more, and since the surface starts to become impermeable. From the start of freezing, FAROUK simulates depletion of water from layers one and two towards the third layer.
To the contrary, the COUP version maintains moisture contents in upper layers, or even increases them (depending on the respective layer), at the expense of water contents in layers below. This hints to the ability of the COUP model version to simulate cryosuction. The total water content of the third layer in COUP shows a somewhat different behaviour in terms of inertia and response to changes. A generally faster reaction seems to occur, for which to find the reason is subject to future studies.

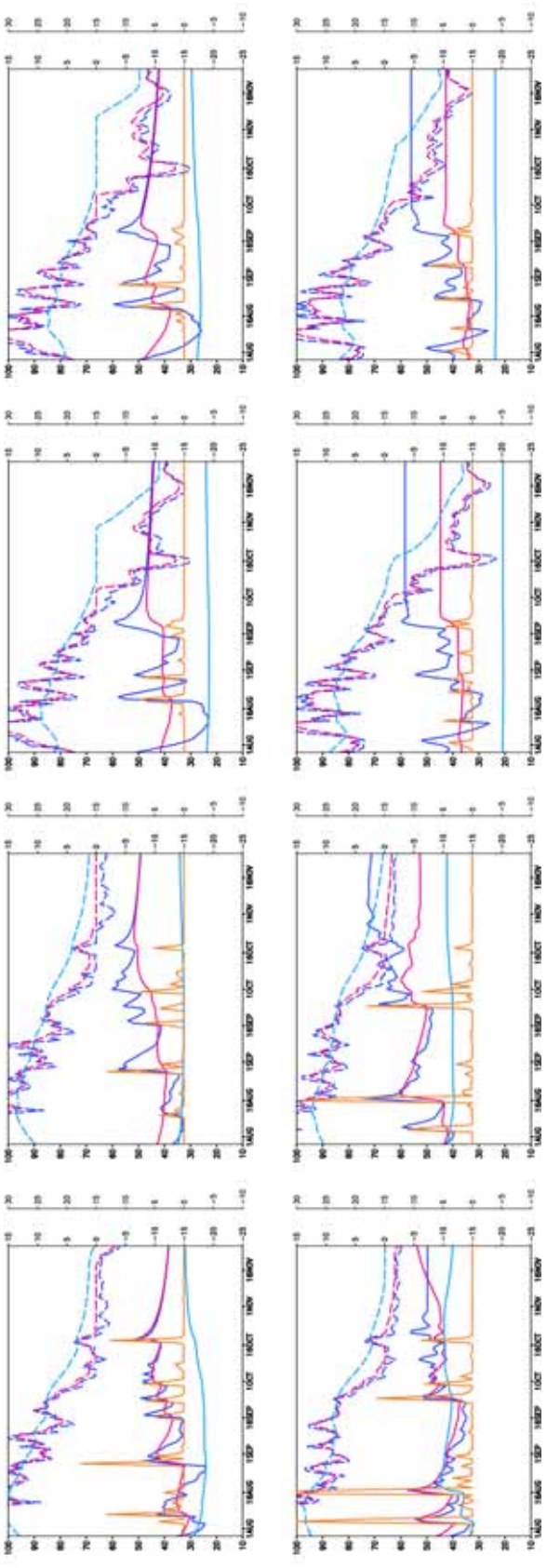

Figure 5.20: Time series of daily means of simulated relative soil moisture [%] (solid, left y-achsis) and temperature [K] (dashed, right y-achsis) in layers 1 (dark blue), 2 (magenta), and 3 (blue) from grid boxes 1, 2, 6, and 7 (from left to right) as simulated with FAROUK (upper row) and COUP (bottom row). Solid orange line shows liquid precipitation (second right y-achsis). Displayed is freezing period 1985.

The changes in soil hydrology are expected to impose two effects on soil temperatures:

1. more pronounced and prolongued freezing (melting) in winter and autumn (spring and summer), due to an enlarged latent heat release (consumption) in upper layers, where moisture contents increase;

2. a net cooling, as increased total water contents in the near-surface soil layers increase λ in winter, which would enhance the thermal offset effect (see Section 4.3.2).

Differences of thermal diffusivities between COUP and FAROUK are displayed in Figures 5.21 and 5.22.

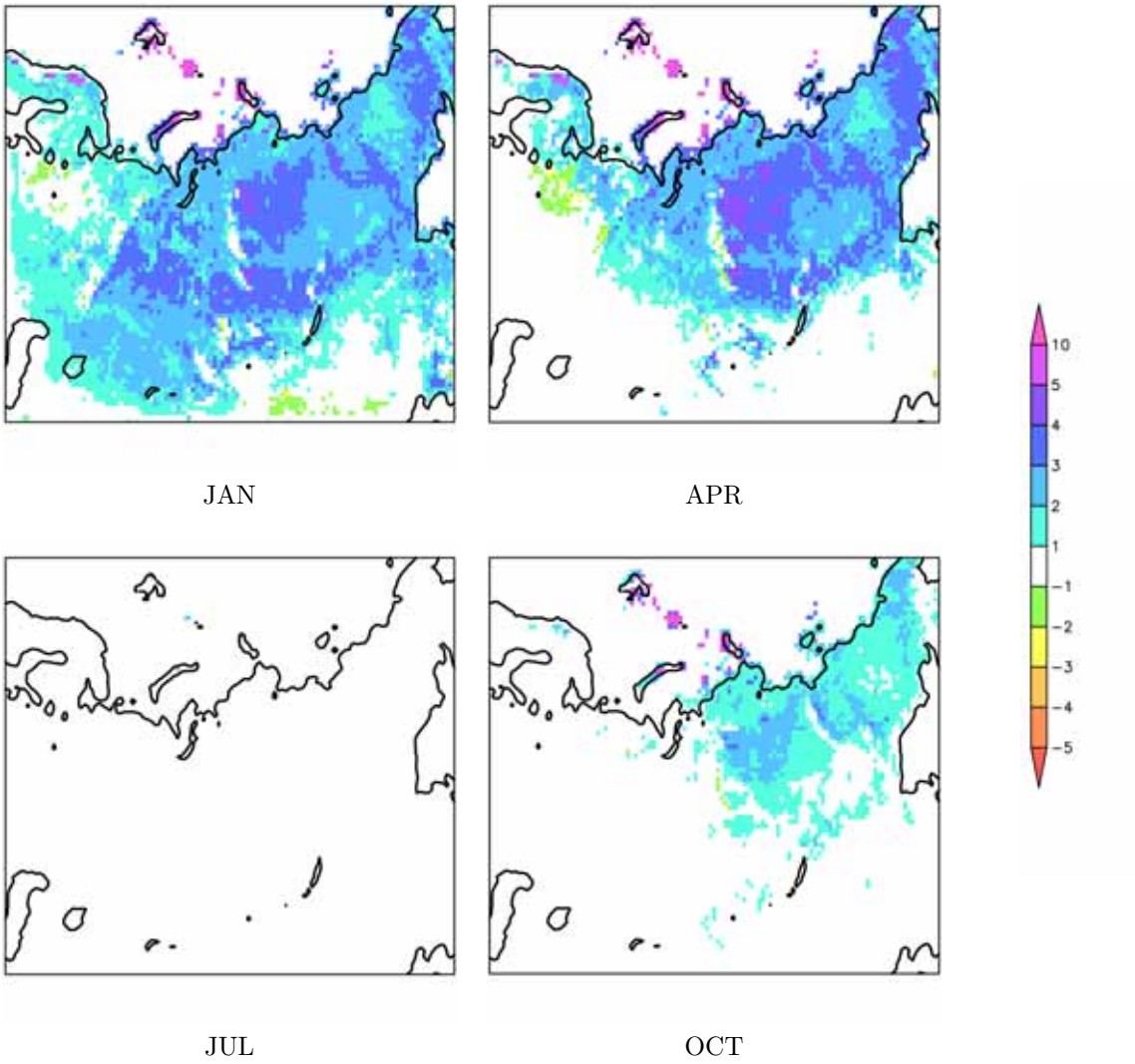

Figure 5.21: Difference in thermal diffusivity a of layer 1 $[10^{-7}m^2/s]$, experiments COUP - FAROUK (1971-1990 mean), for months January (upper left), April (upper right), July (lower left), and October (lower right).

The effect due to full coupling is a clear increase of a during seasons when soil freezing is dominant. Therefore, using COUP introduces the thermal offset effect to a larger degree than the FAROUK version.

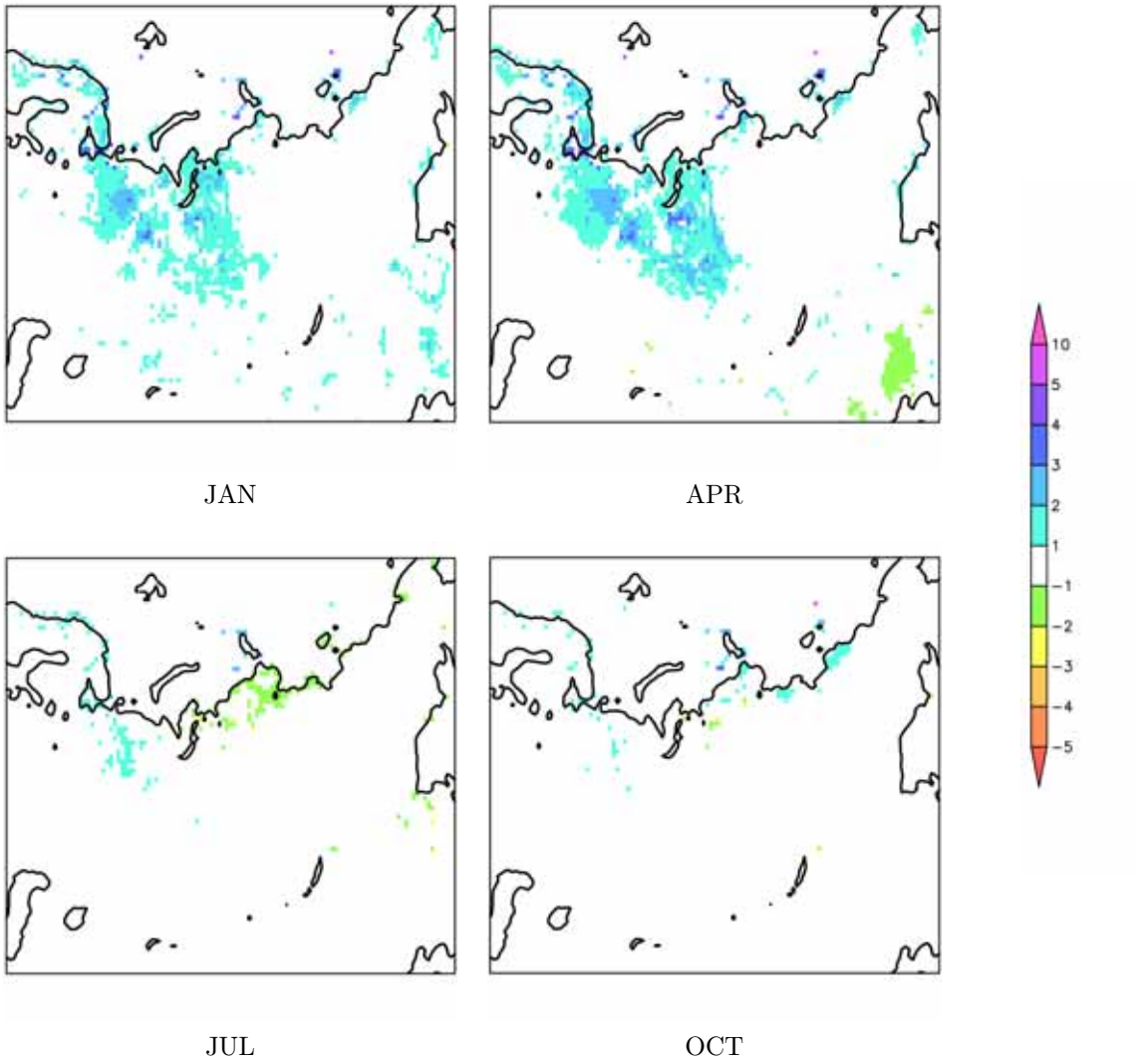

Figure 5.22: Difference in thermal diffusivity a of layer 3 $[10^{-7}m^2/s]$, experiments COUP - FAROUK (1971-1990 mean), for months January (upper left), April (upper right), July (lower left), and October (lower right).

This has consequences for the simulated soil thermal regime, as now winter cooling is more effective over large regions of the model domain as compared to results from FAROUK. Figures 5.23 and 5.24 show differences of soil temperatures between COUP and FAROUK for layers one and three. They illustrate the cooling effect due to higher λ during the cold seasons of the year.

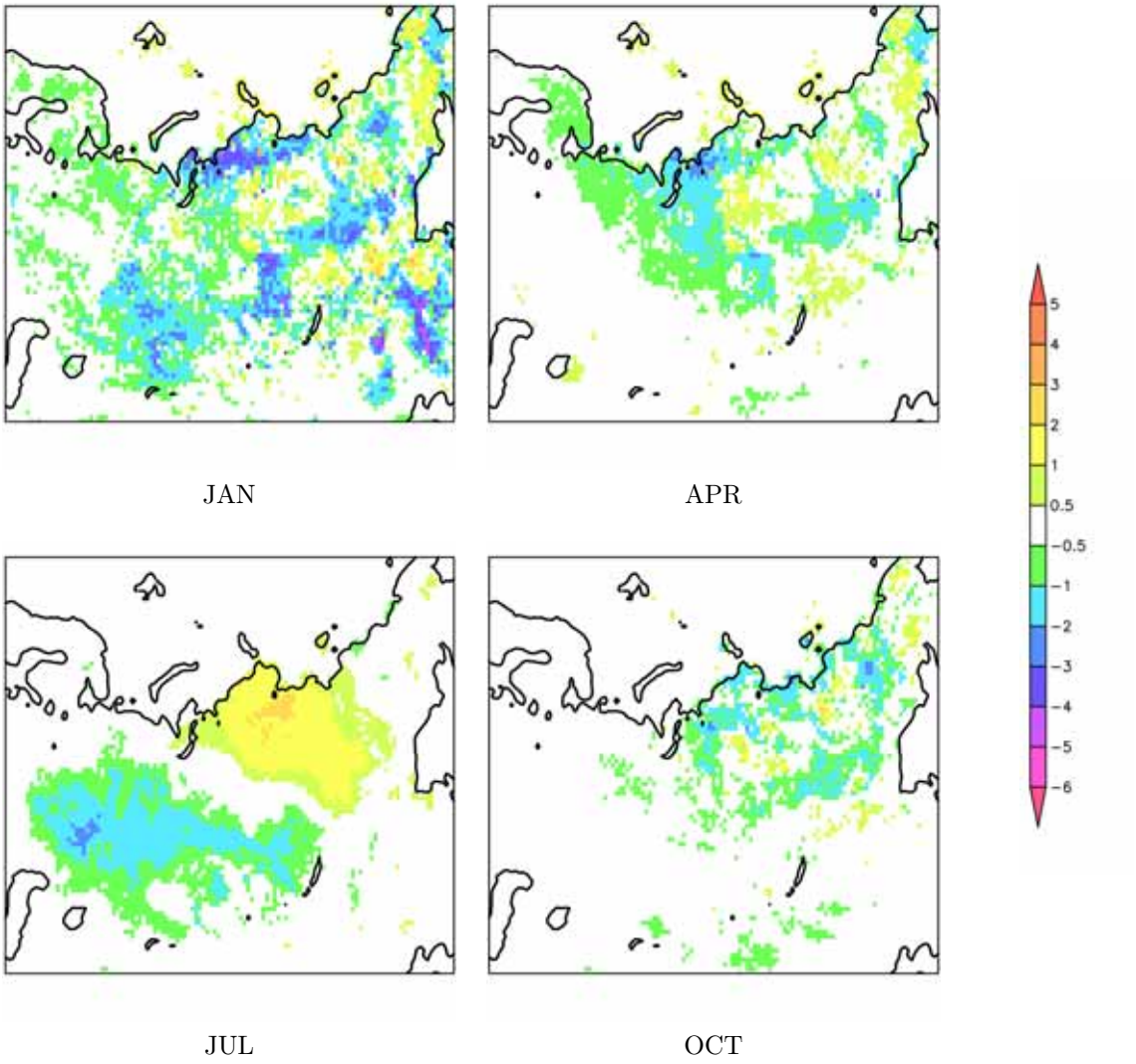

Figure 5.23: Difference in simulated soil temperature of layer 1 $[K]$,
experiments COUP - FAROUK (1971-1990 mean), for months January (upper left), April (upper right), July (lower left), and October (lower right).

To the contrary, summer soil temperatures in the third layer show an increase also in Northern parts of Siberia, regions where both simulations do not show relevant atmospheric temperature differences. Therefore, this is an effect of enhanced intrusion of the summer heat wave due to higher λ as compared to FAROUK. This is related to the higher soil moisture contents in COUP.
The differences in the fifth layer are not shown, since only minor changes occur due to the large bedrock portions.

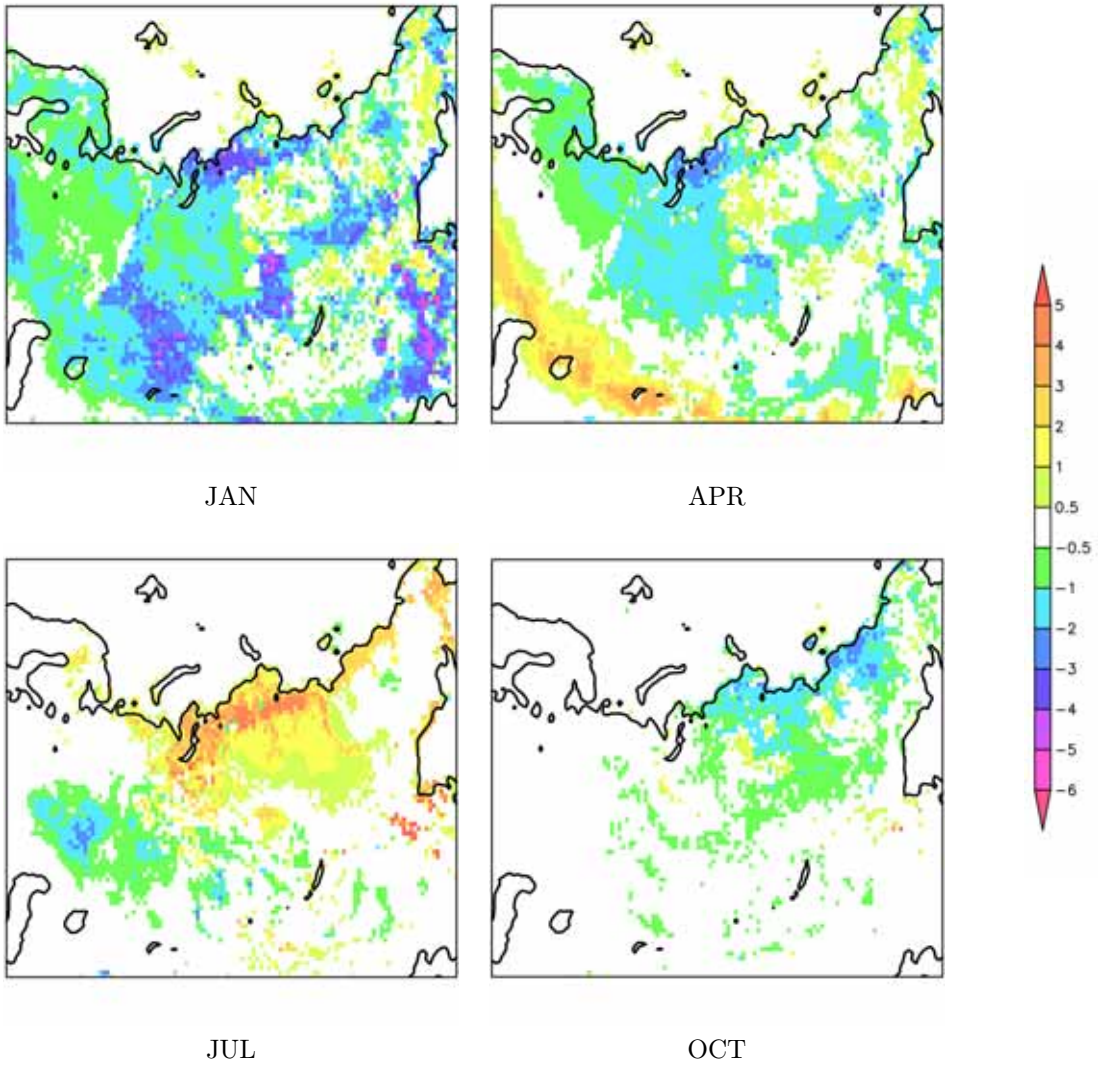

Figure 5.24: Difference in simulated soil temperature of layer 3 [K], experiments COUP - FAROUK (1971-1990 mean), for months January (upper left), April (upper right), July (lower left), and October (lower right).

5.3.2 Influence on surface energy balance and atmosphere

It was demonstrated in the previous section that the implemented processes work in a physically meaningful way. How does the simulated climate react on the implementation of permafrost processes with regard to the SEB and the near-surface atmosphere?

As was shown in figure 5.7, the intrusion of soil freezing and melting markedly impacts the surface water balance especially in spring, due to reduced input of snow melt water into the still frozen, less permeable ground. This has consequences for the water cycling in the simulated climate system, as the effect on soil water is quantitatively large. The different soil moisture state that develops when using the new model versions impacts the partitioning of energy at the surface into sensible and latent heat fluxes. This in turn changes both atmospheric moisture and temperature, which also influences total precipitation (see the end of this section).

The analysis will concentrate on differences between COUP and CTRL experiments, since impacts due to the combined model extensions are of interest. Where necessary, differences between intermediate versions will be used in order to clarify effects, or to ensure the origin of changes.

Winter climate is influenced only weakly by the changes in the soil scheme of the model, since snow cover decouples ground and atmosphere, which is therefore not shown.
Important differences occur during summer, yet originate to a large part in the changed infiltration in spring. The analysis therefore will trace the changes to individual processes for multi-year means of March, April, May and June, respectively.

Figure 5.25 displays absolute snow depth from COUP, as well as the differences in surface runoff and soil moisture between COUP and CTRL for the months March until June. It illustrates how snow still covers almost the entire domain in March, thereafter retracting successively north- and eastwards in April, May and June, when it has almost fully vanished.
Melting of the snow increases water supply for infiltration on top of the ground surface. Panels in the center column of figure 5.25 demonstrate how surface runoff increases in COUP when compared to CTRL in areas where soils are frozen, which is indicated by the red contour. This illustrates how the degree of freezing of the uppermost soil layer controls the partitioning of snow melt water into runoff and infiltration: Inside the frozen area, runoff production is large and the difference between COUP and CTRL is highly positive, whereas it even changes sign and becomes negative in regions where the uppermost soil layer has already melted. This can be attributed to the undersaturation, relative to the CTRL experiment, of the soil that develops due to the increased infiltration (refer to Section 5.3.1). Therefore, runoff production is lower in COUP as compared to CTRL throughout the rest of the warm season (July, August are not displayed yet show the same signals). Nevertheless, surface water input through precipitation during the remaining warm months is too low to catch up with CTRL, and the large difference

in the amount of infiltrated water during spring imposes a fundamental shift on the modelled soil moisture status for large parts of the domain.

The root zone soil moisture (right column) is a more inert state variable, therefore the difference between COUP and CTRL shows less variation during the course of the year, than fluxes as e.g. runoff.
The south-western part of the domain features the most prominent decrease in soil moisture, which is detectable throughout the spring, yet the peak occurs in June. The graphs also reveal that the lowering pattern of soil moisture follows the difference in snow melt. In the South-West, changes are large probably due to the deep root zone in this area, therefore the reduced infiltration induces large absolute differences here.

Figure 5.26 illustrates the influence on latent and sensible turbulent heat fluxes (left and right panels, respectively). The latent turbulent heat flux (L) decreases in COUP as compared to CTRL wherever the soil moisture has decreased. Therefore, the strongest impact occurs over exactly the South-Western region of the domain that showed largest deviations in soil moisture in figure 5.25. Less L in May and June yet occurs over almost entire Siberia. July and August feature the same signal (not shown).
Over the Western part of the domain, the European part of Russia, L increases. This might be due to the principally different hydrology scheme in COUP, which, where soils are deep enough as in this respective region, provides a deep 'buffer' layer, that enables evapotranspiration in periods when the simple bucket scheme has already reached the wilting point, and thus limits further moisture flux to the atmosphere. These effects might be more important here due to the more moderate climate, because soil freezing in spring is not as decisive for the surface water balance west of the Urals as in Siberia. Moreover, albeit these regions are not within the permafrost zones, they still feature cold winter climate with temperatures well below 0°C, thus part of the soil moisture cannot percolate and drain during winter in the COUP version. Thus, the change from CTRL to COUP induces moister soils in this region.

The sensible turbulent heat flux (S) mirrors the discussed changes in the expected manner, i.e. it increases over areas with drier soils in experiment COUP. In the south-western part of the model domain, however, it decreases in April due to enlarged evaporation. This is probably a consequence of changes in the soil moisture regime induced by the substitution of the bucket with the layered soil hydrology scheme, since in these regions root zones are deep (reaching into the fourth layer), yet soil depths are deeper (reaching into the fifth layer). Therefore, in these areas, which have already thawed at that time, the buffering effect due to deeper, slow-reacting soil layers might be the reason for an increase of evaporation and thus L over this region in April.

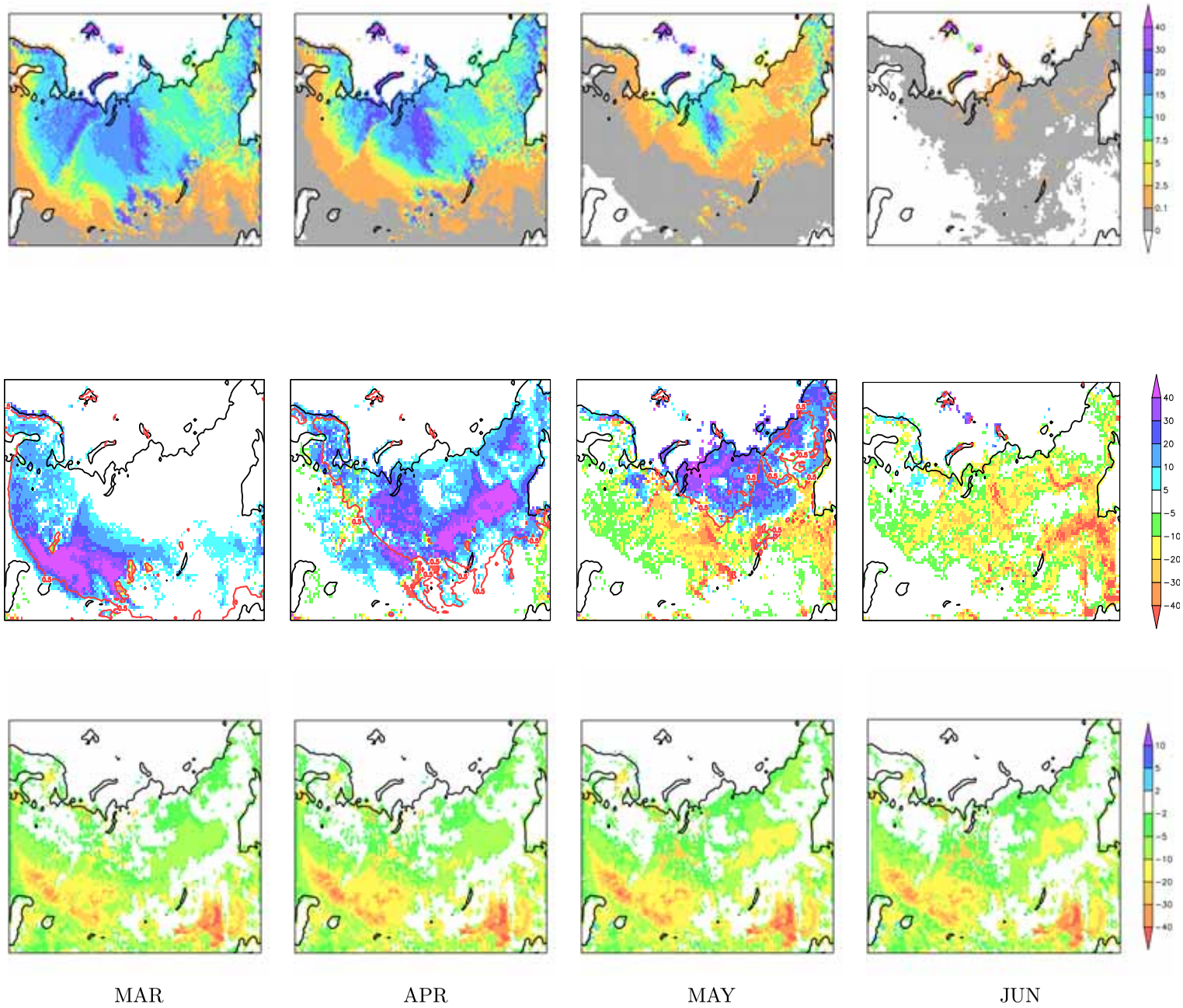

Figure 5.25: Snow depth [cm WE] from COUP (top), difference COUP - CTRL in surface runoff [$mm/month$] (center) and root zone soil moisture [cm] (bottom), for March, April, May, and June (left to right), 1971-1990 mean. Red contour ontop of surface runoff encloses area where fraction of frozen soil f_{froz} in first layer > 0.5.

Figure 5.26: Difference in simulated latent (top) and sensible (bottom) turbulent heat flux [W/m^2], experiments COUP - CTRL (1971-1990 mean), for months April, May, June and July (left to right).

In consequence of the changes imposed on the soil and surface variables and on the SEB, the near-surface air temperatures follow these changes, and increase in COUP over large parts of the domain during May and June (Figure 5.27). COUP thus simulates a drier atmosphere, which can be seen from the reduced cloud cover and total precipitation (Figure 5.27, center and right panels). A Student t-test was conducted for the 2m air temperature and the total precipitation, and the significance at the 95% level is displayed in the respective panels of figure 5.27. The warmer LS in summer also warms the atmosphere up to heights of about 500 gpm (not shown).

The intermediate model versions simulate the discussed surface and atmospheric variables slightly different, depending on the respective represented physical processes. The differences are yet small as compared to the differences between any of the new and the CTRL version (not shown).
E.g., FAROUK features increased sensible turbulent heat fluxes in summer, which satisfies the principles of the SEB, as a less effective ground heat flux leads to enlarged heat transport into the atmosphere. Since moisture supply for evaporation is similar in LAYLF and in FAROUK, sensible heat flux is increasing, and in consequence air temperatures are warmer, and less precipitation is simulated.
The COUP version introduces the opposite effect in turbulent heat fluxes. Since soils are wetter in this experiment, latent heat fluxes increase to the expense of the sensible heat flux, air temperatures decrease, and precipitation increases.

Influence during autumn is small, as is shown in Figures 5.28 and 5.29. Areas with more significant changes again are the regions in the south-western part of the domain, were evaporation increases in COUP as compared to CTRL. This again can be attributed to the principally different soil hydrology schemes, of which the new layered scheme is able to deliver moisture from deeper zones to near-surface layers when these are already dry, whereas evapotranspiration is more limited when using the bucket scheme. This is similar to the differences detected for April, it is independent of freezing and melting processes, and occurs in regions with relatively mild climate and large soil and root zone depths.
The 2m air temperature displays statistically significant warming over Siberia in all months, which propagates from mountaineous regions, where it begins in September, thereafter spreading allmost all of West Siberia in October, while it vanishes in November and December. This can be interpreted as an effect of the latent heat release in the ground due to freezing at that time of the year. Large portions of ground heat flux towards the atmosphere during autumn, originating from the heat release of the phase change in the ground, are reported by e.g. Langer et al. (2011) from their measurements conducted in the Lena river delta.

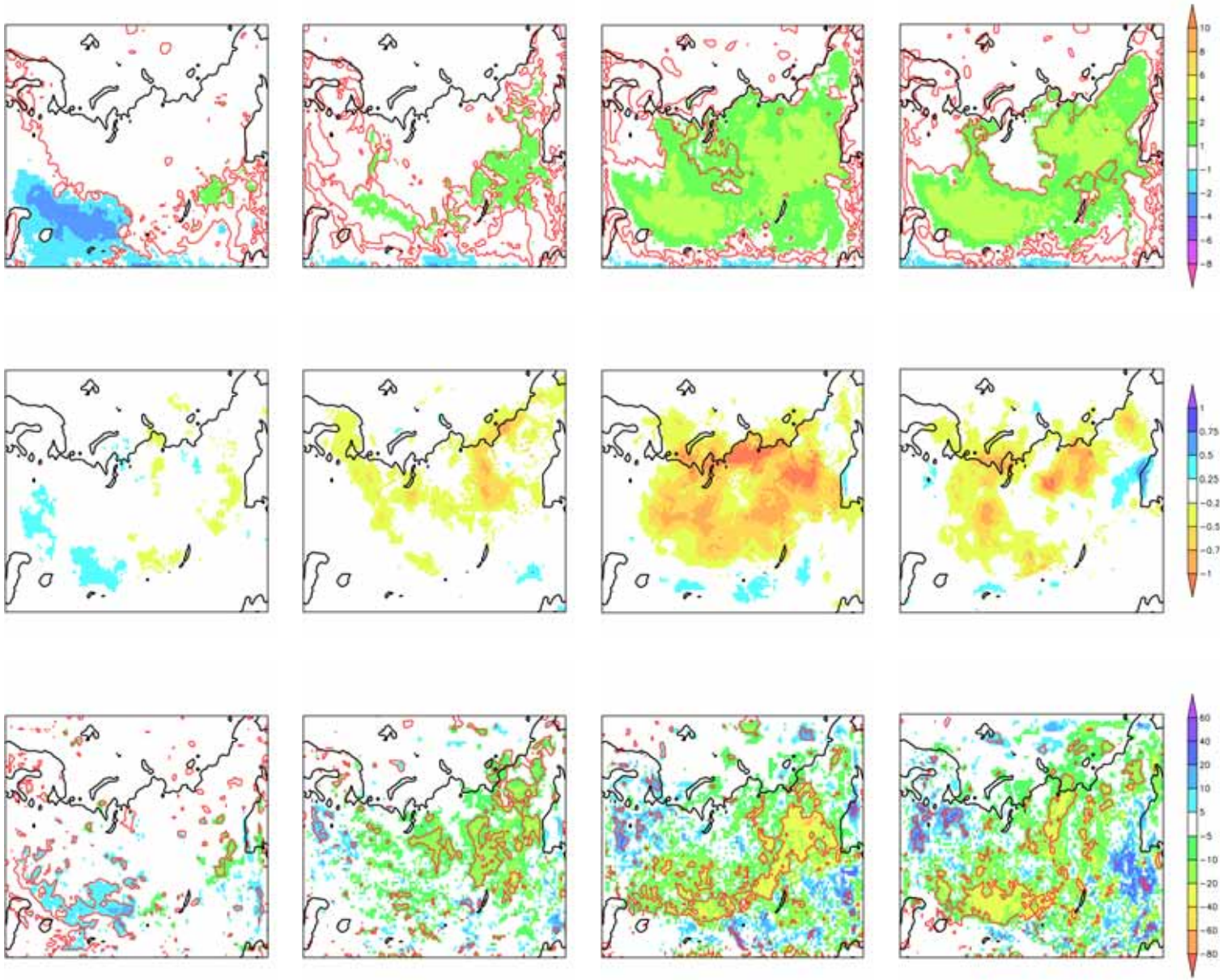

Figure 5.27: Difference COUP - CTRL in 2m air temperature [K] (top), cloud cover [fract.] (center) and total precipitation [$mm/month$] (bottom), for April, May, June and July (left to right), 1971-1990 mean. Red contour denotes the 95% significance level.

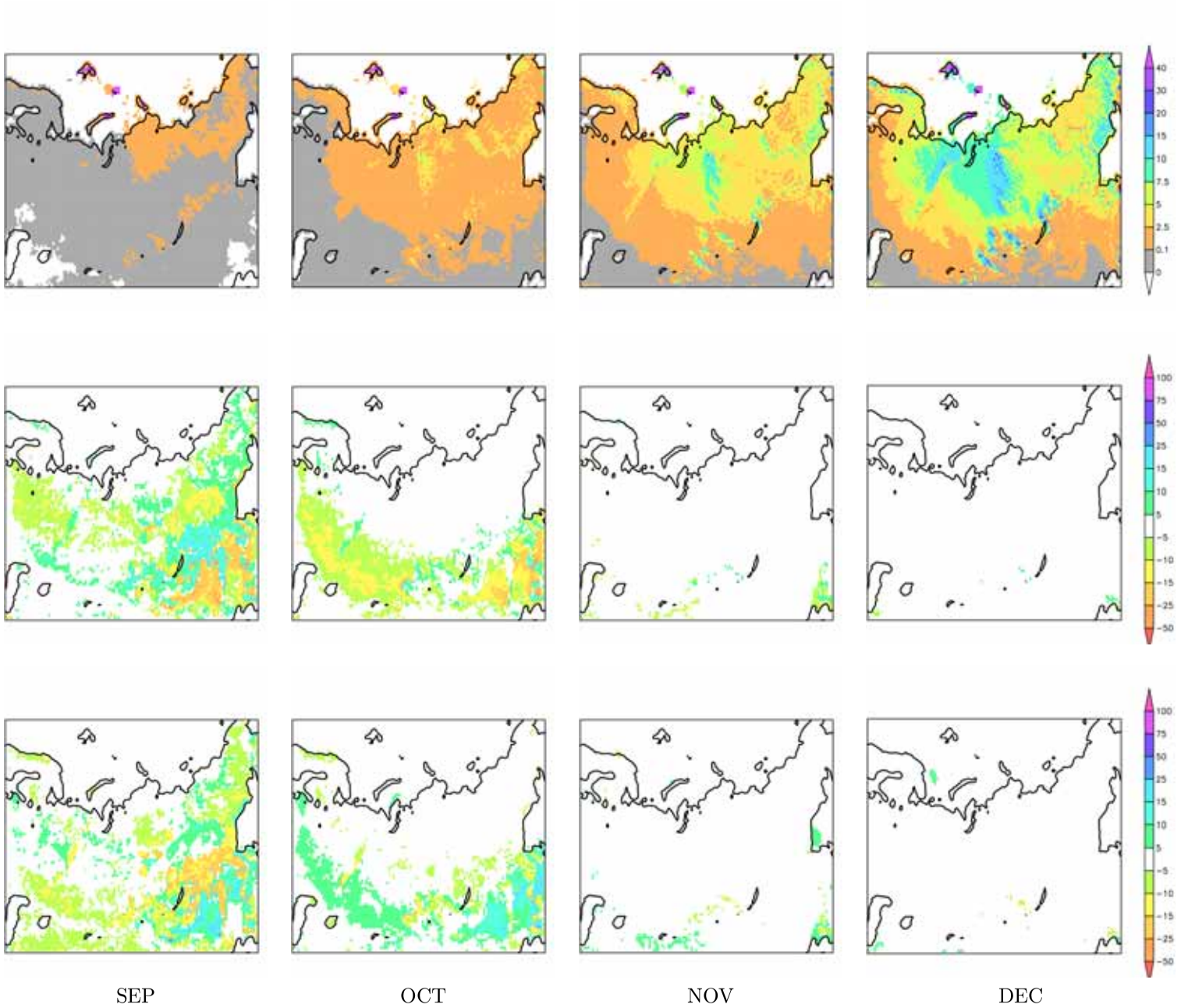

Figure 5.28: Snow depth [cm] in COUP (top) and difference COUP - CTRL in latent (center) and sensible (bottom) heat flux $[W/m^2]$, for September, October, November, December (left to right), 1971-1990 mean.

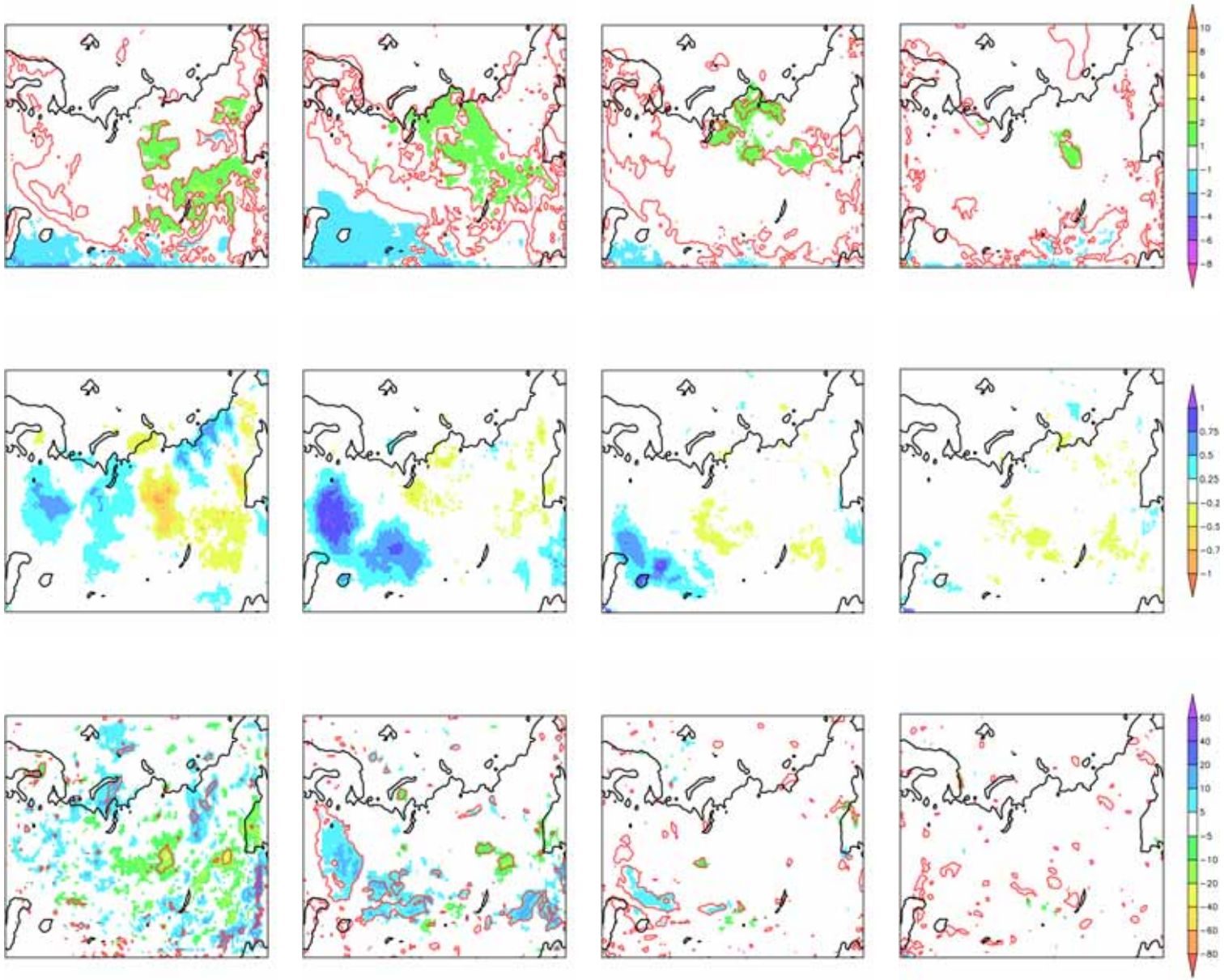

Figure 5.29: Difference COUP - CTRL in 2m air temperature $[K]$ (top), cloud cover [fract.] (center) and total precipitation $[mm/month]$ (bottom), for September, October, November, December (left to right), 1971-1990 mean. Red contour denotes the 95% significance level.

5.3.3 Model evaluation

Results of an evaluation of the reference experiment CTRL and of the final model version COUP are shown in the following. Differences between model and observations in the South and South-East of the model domain are not discussed further, as it is difficult for a climate model to capture the observed state over such an orographically pronounced area at a spatial resolution of 0.5 degree.

2m air temperature

Figure 5.30 shows the average simulated 2m air temperatures over Siberia according to WFD. The graphs illustrate strong continentality, which increases with latitude and longitude. The monthly 2m air temperature differences between CTRL and WFD data are shown in Figure 5.31.

There are substantial biases detectable in the simulated winter temperatures. A strong warm bias of more than 8 K is simulated over the North-Eastern part of Siberia for January, which is similar in the months December and February (not shown).
In April, the warm bias disappears and is much weaker. However, simulated temperatures are too cold in the more southern and western parts of the domain.
The biases in summer are much weaker and mainly consist of slightly too warm temperatures in the Eastern part of Eurasia, and a weak cold bias around the Ural region. In the North, a small region with too cold simulated temperatures can be seen in the Lena delta region and along the cost towards the East.

When compared directly to the ERA40 driving data, winter warm bias in East-Siberia is weaker, where as the cold bias in the Western part is more pronounced (not shown). Summer warm biases are weaker against ERA40 than against the two observational data sets. It can thus be concluded that ERA40 is warmer than WFD2 and WFD. Therefore, one reason for the strong winter biases in the simulated air temperatures seems to be the too warm driving data. Moreover, deficiencies related to the atmospheric heat transport seem to lead to the large warm bias in Eastern Siberia, as was investigated by D. Sein (pers. comm., 2011). Tests revealed that the use of a gravity wave drag parameterization improved the bias. The noticeable bias also affects global model runs with ECHAM6, and is subject to further investigation (S. Hagemann, pers. comm., 2012).

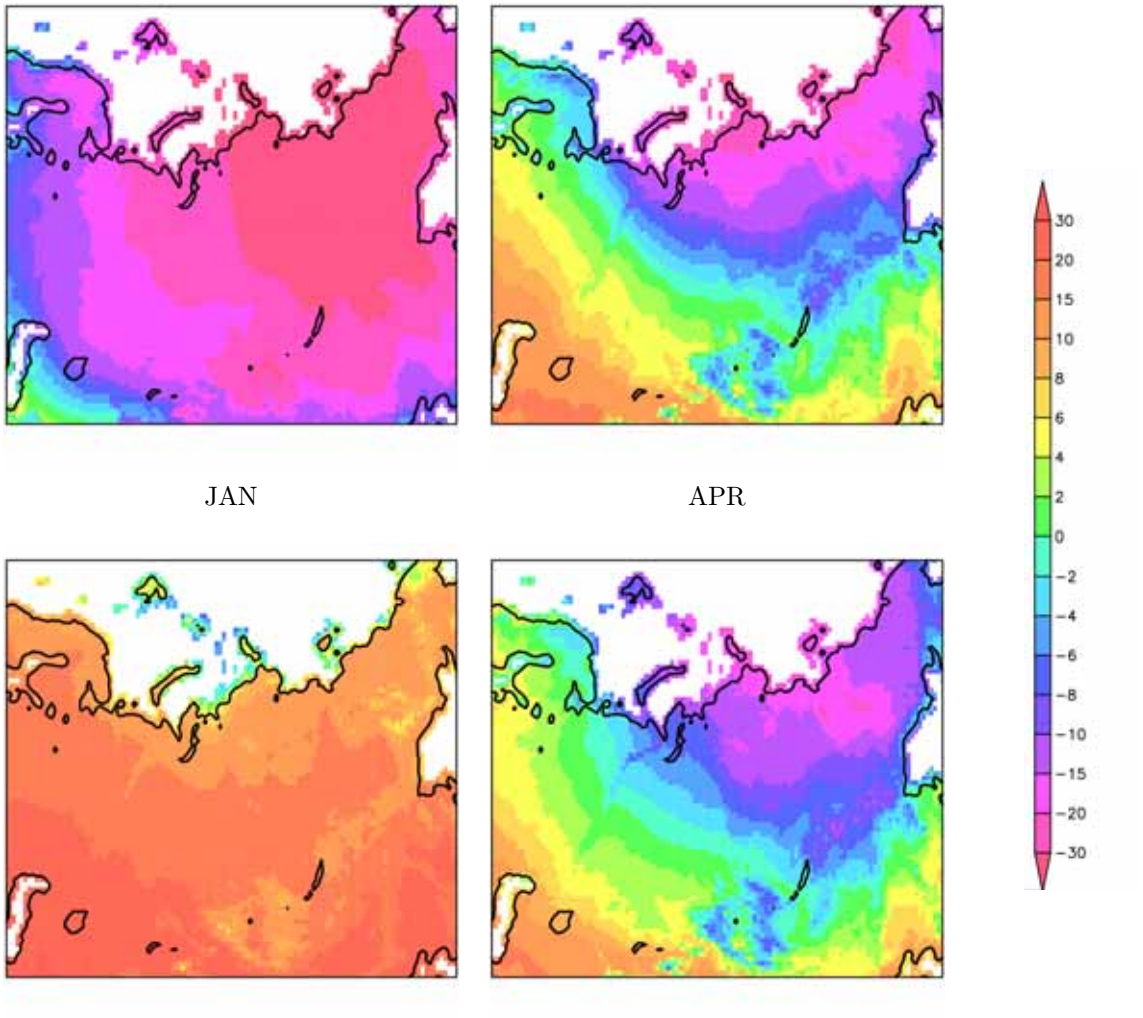

Figure 5.30: Observed 2m air temperature [°C] from WFD, 1971-1990 mean, for months January (upper left), April (upper right), July (lower left), and October (lower right).

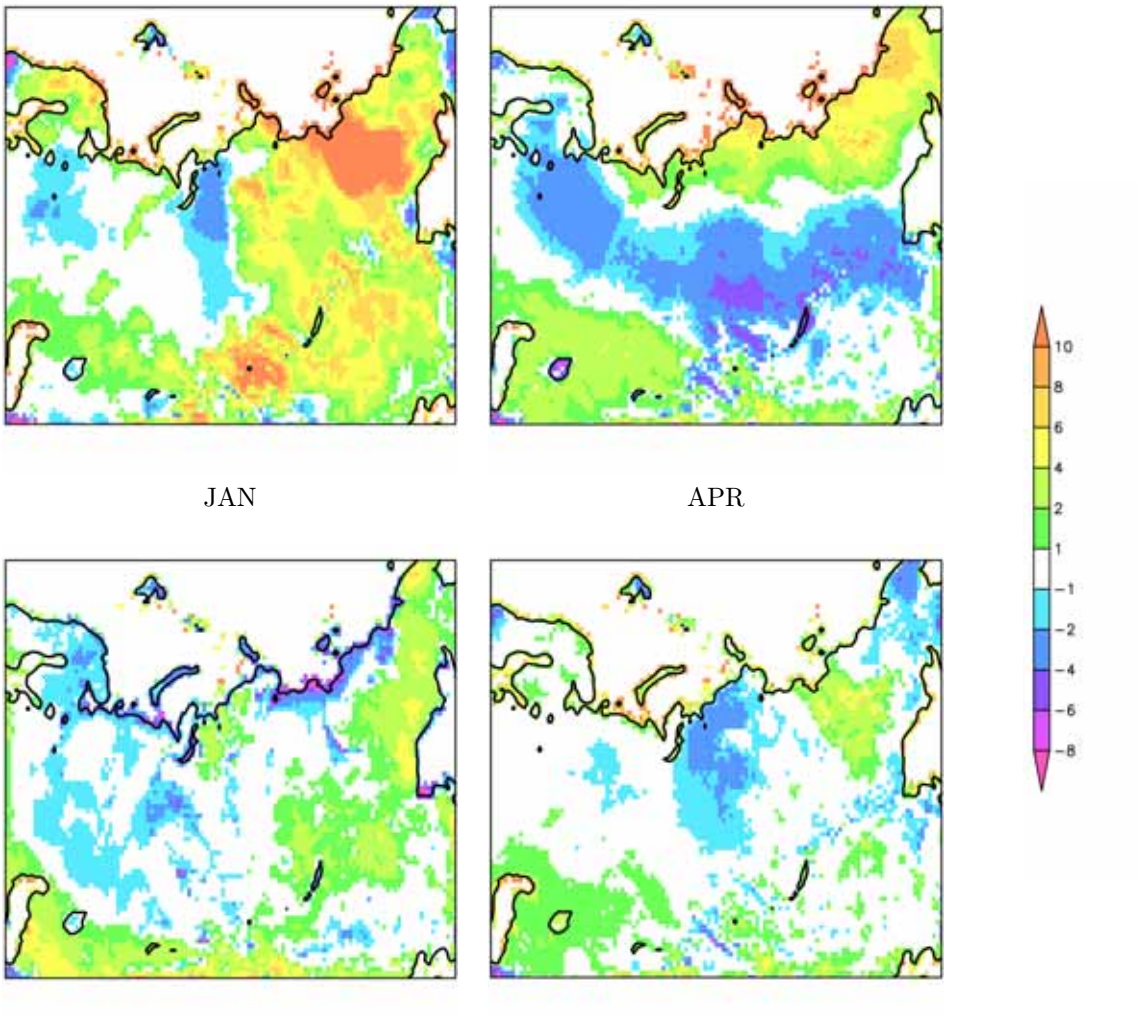

Figure 5.31: Difference between simulated and observed 2m air temperature $[K]$, CTRL - WFD, 1971-1990 mean, for months January (upper left), April (upper right), July (lower left), and October (lower right).

Precipitation

Figure 5.32 shows the total precipitation over Siberia according to WFD, while Figure 5.33 illustrates the differences between mean simulated and observed total precipitation. The

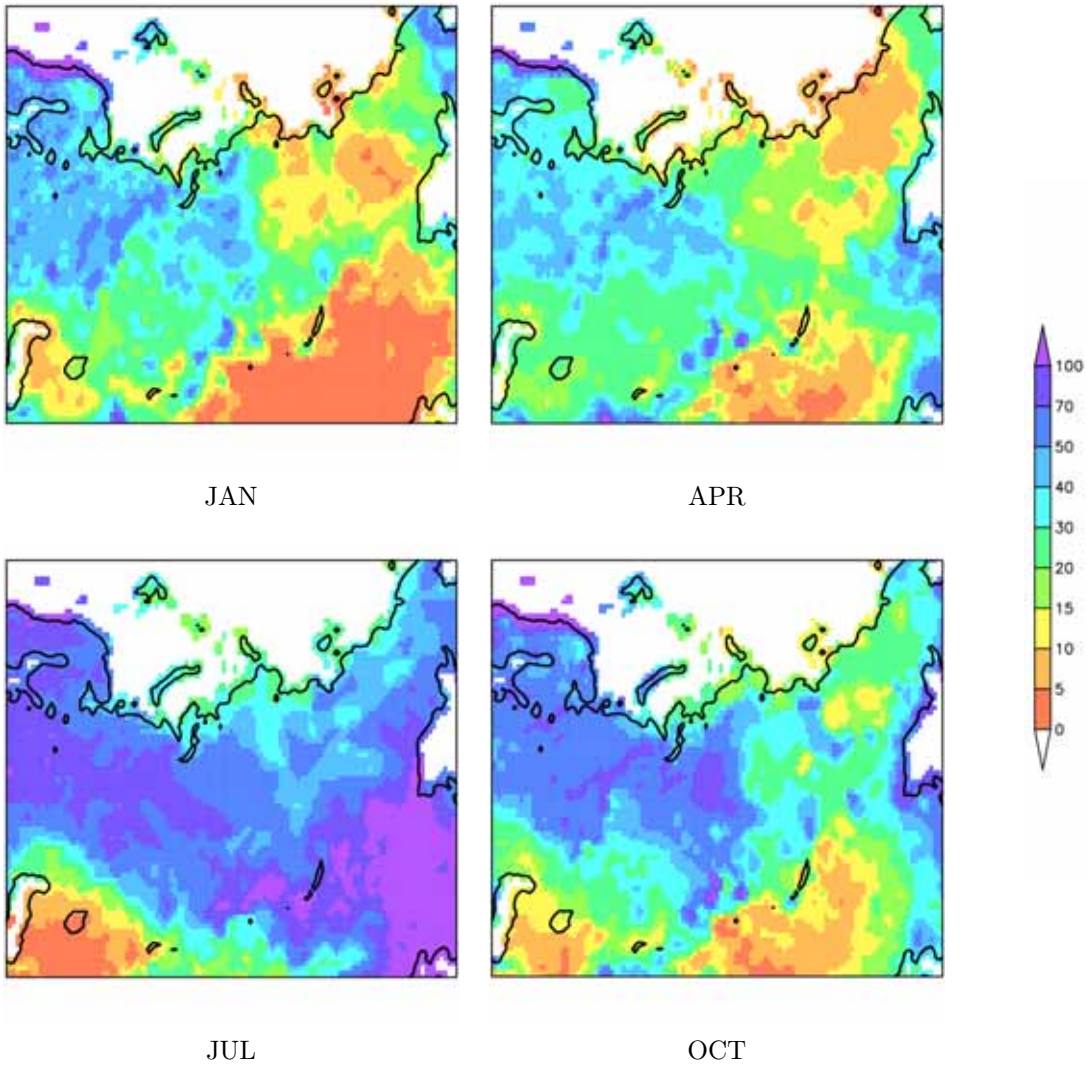

Figure 5.32: Observed total precipitation [$mm/month$] as observed from WFD, 1971-1990 mean, for months January (upper left),
April (upper right), July (lower left), and October (lower right).

model is in good accordance with the observations in winter. Total precipitation is overestimated by the model in April over large parts of Siberia, and the same signal can be seen over Scandinavia. The more northern parts of Siberia show weaker deviation from the observed values. In summer, biases are weaker. A small dry bias can be detected over Russia (west of the Ural), western Siberia, and parts of eastern and southern Siberia. At the same time, the amount of simulated precipitation is too large over the Central Siberian Plateau, and north of it. The model simulates slightly too high total precipitation

amounts for autumn over most of the domain. Yet then the simulated precipitation seems to decrease again towards winter values, which were modelled satisfyingly. Simulated precipitation in july is too low in north-western Russia and East Siberia, while Central Siberia and the region north of the Caspian Sea show overestimation of total precipitation.

To summarize the comparison of baseline results with gridded observations, simulated precipitation seems satisfying during winter. During transition seasons, the precipitation amounts are too high, which occurs especially in spring. Deviations in summer precipitation are more spatially heterogeneous and generally mostly small, where the bias it negative; to the West of the Central Siberian mountains, however, precipitation is overestimated in the same range as for the wet bias in spring.

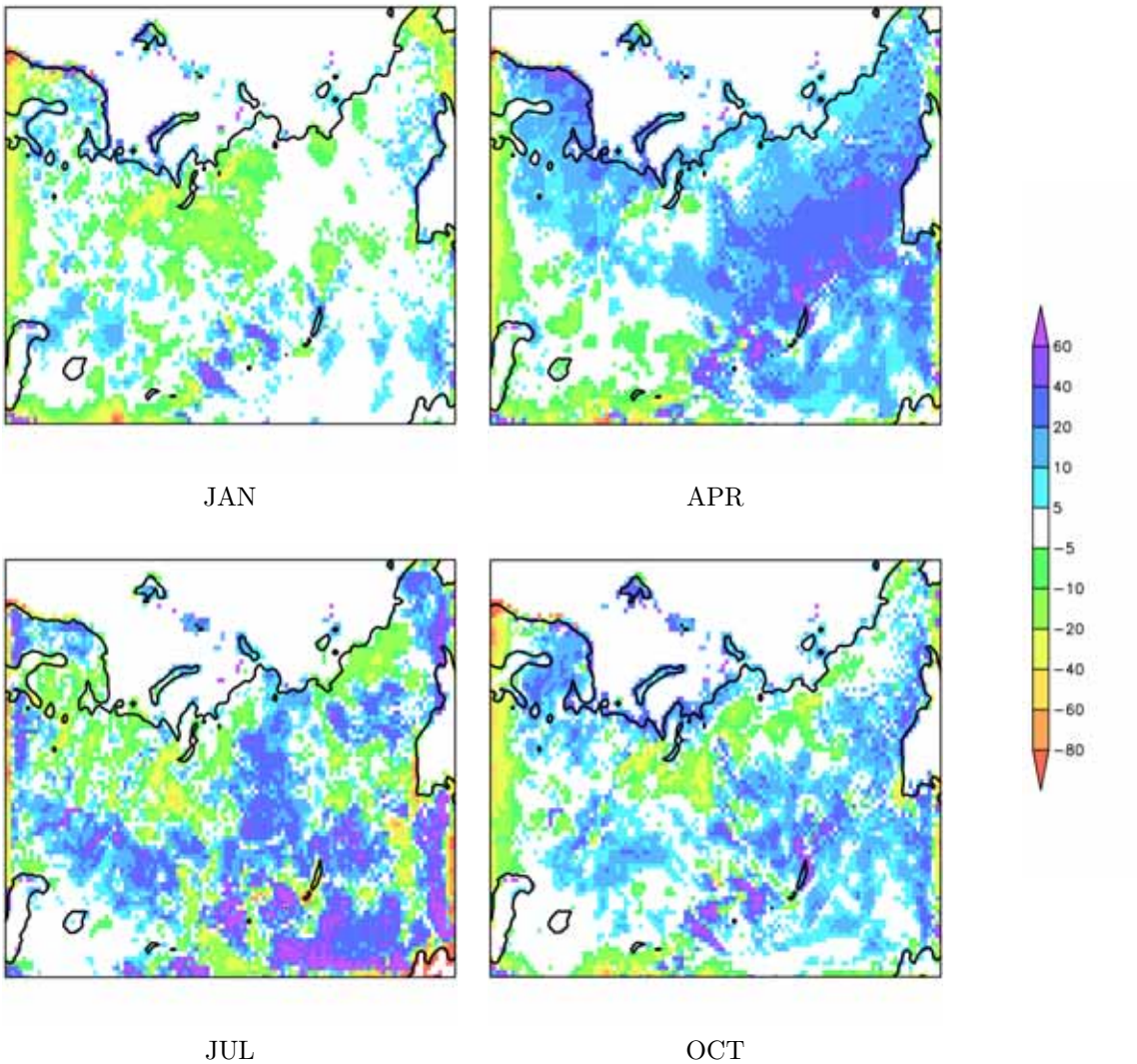

Figure 5.33: Difference between simulated and observed total precipitation [$mm/month$], CTRL - WFD, 1971-1990 mean, for months January (upper left), April (upper right), July (lower left), and October (lower right).

Evaporation

Figure 5.34 shows the differences between simulated and ERA40 evaporation. As expected, winter evaporation is almost zero over land in both ERA40 and model data. This changes as snow cover vanishes and land surface starts to evaporate, which is lower in ERA40 than in the simulation. This difference is most pronounced during summer, and reaches up to ca. 50 mm/month, which corresponds to a 100% overestimation (not shown).

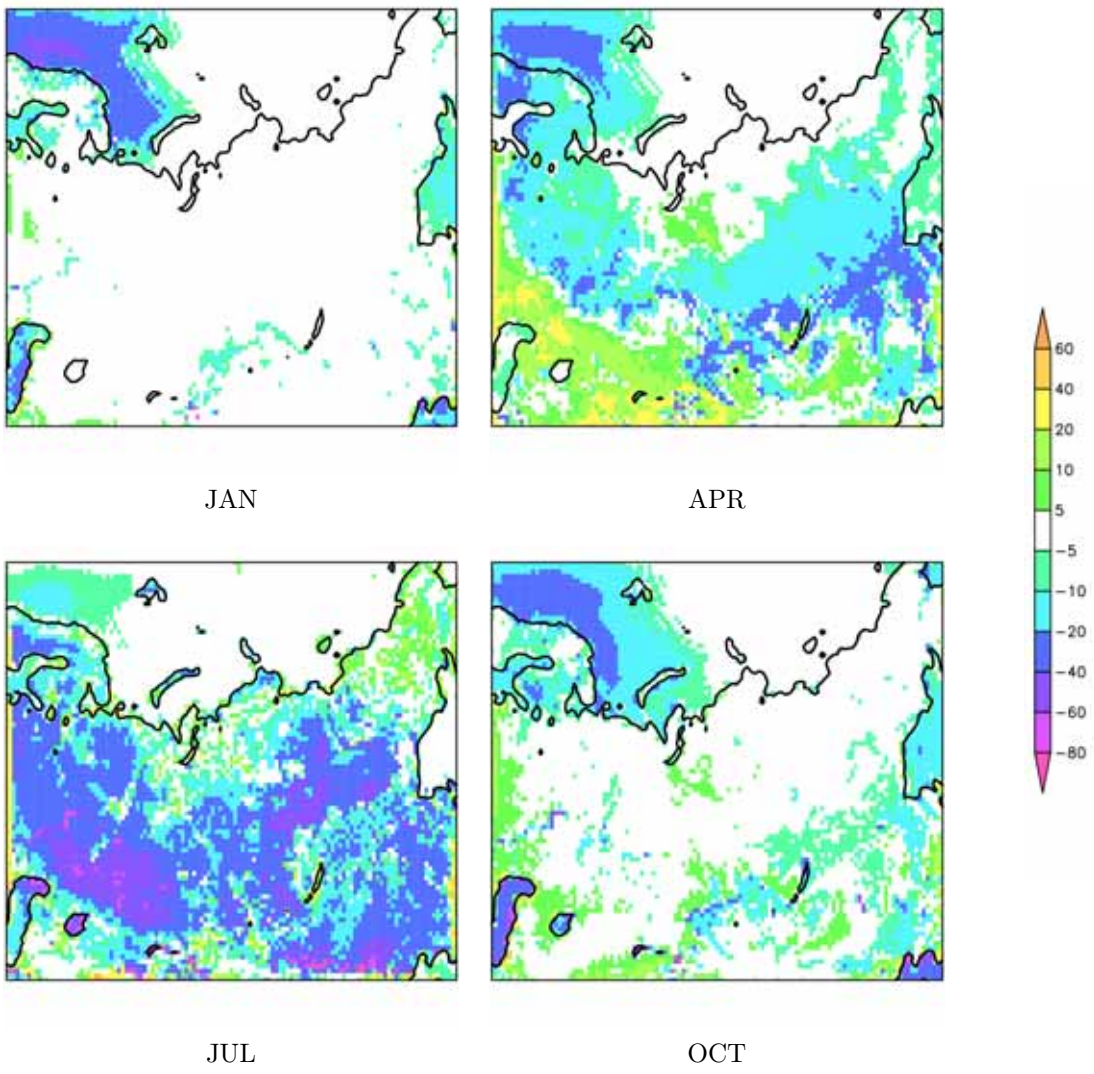

Figure 5.34: Difference between simulated and ERA40 evaporation [*mm/month*], CTRL - ERA40, 1971-1990 mean, for months January (upper left), April (upper right), July (lower left), and October (lower right).

Modelled summer evaporation is higher over almost all parts of Russia, while simulated values agree well with the ERA40 data in the North and East of Siberia. Recalling that ERA40 are reanalysis and therefore another type of model data, an estimation for evapotranspiration was applied in order to better estimate the quality of simulated evaporation. The equation for the surface water balance,

$$Precip - ET = RO \tag{5.2}$$

was used, where $Precip$ is total precipitation, ET means evapotranspiration, and RO denotes surface runoff, respectively. Using WFD precipitation data and hydrological discharge observations for the runoff part, ET can thus be obtained in a more observationally constrained manner. Results are shown in Table 5.2.

Hydrological Variable [mm/d]	River Basin	Observations	CTRL	COUP
Precipitation	Jenissei	490	621	578
	Lena	388	526	484
Evapotranspiration	Jenissei	251	345	320
	Lena	188	332	277
Surface runoff	Jenissei	239	271	255
	Lena	200	191	206

Table 5.2: Climatologies for precipitation, evapotranspiration, and surface runoff, derived from observations, and from experiments CTRL and COUP for Jenissei and Lena river basins (1971-1990 mean).

The method showed that the ERA40 data overestimate evaporation, thus the deviation in the CTRL experiment can be seen as proofed. Moreover, introducing the new COUP version leads to improved model results, mainly for the water variables. This indicates to the fact that the changes in surface runoff and infiltration, which led to the discussed shifts in latent and sensible heat fluxes, improve the model with respect to the hydrological cycle. These findings are supported by the comparison to river discharge data which is shown later in this section.

Turbulent heat fluxes

Comparison of simulated turbulent heat fluxes with data from ERA40 (Figures 5.35, 5.35) reveal that modelled sensible heat fluxes are too low during summer, while in the meantime the latent heat flux is overestimated. These deficiencies are clearly linked with the too high amounts of evaporation in the CTRL experiment when compared also to ERA40 data. In the West of the model domain, sensible heat flux is simulated too low during summer, while it is rather too high in Central, Northern and Eastern Siberia.

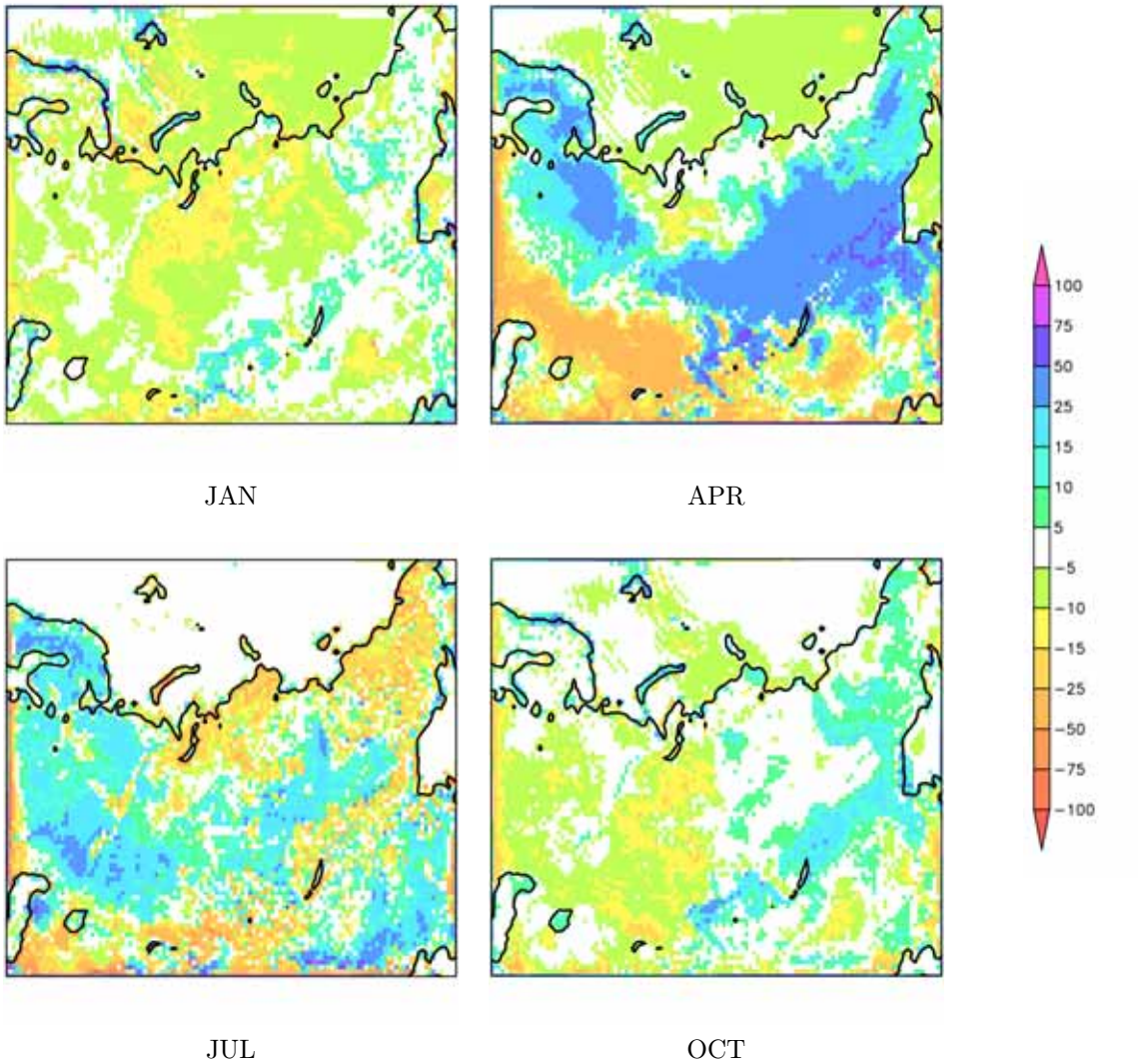

Figure 5.35: Difference between simulated and ERA40 sensible heat flux $[W/m^2]$, CTRL - ERA40, 1971-1990 mean, for months January (upper left), April (upper right), July (lower left), and October (lower right).

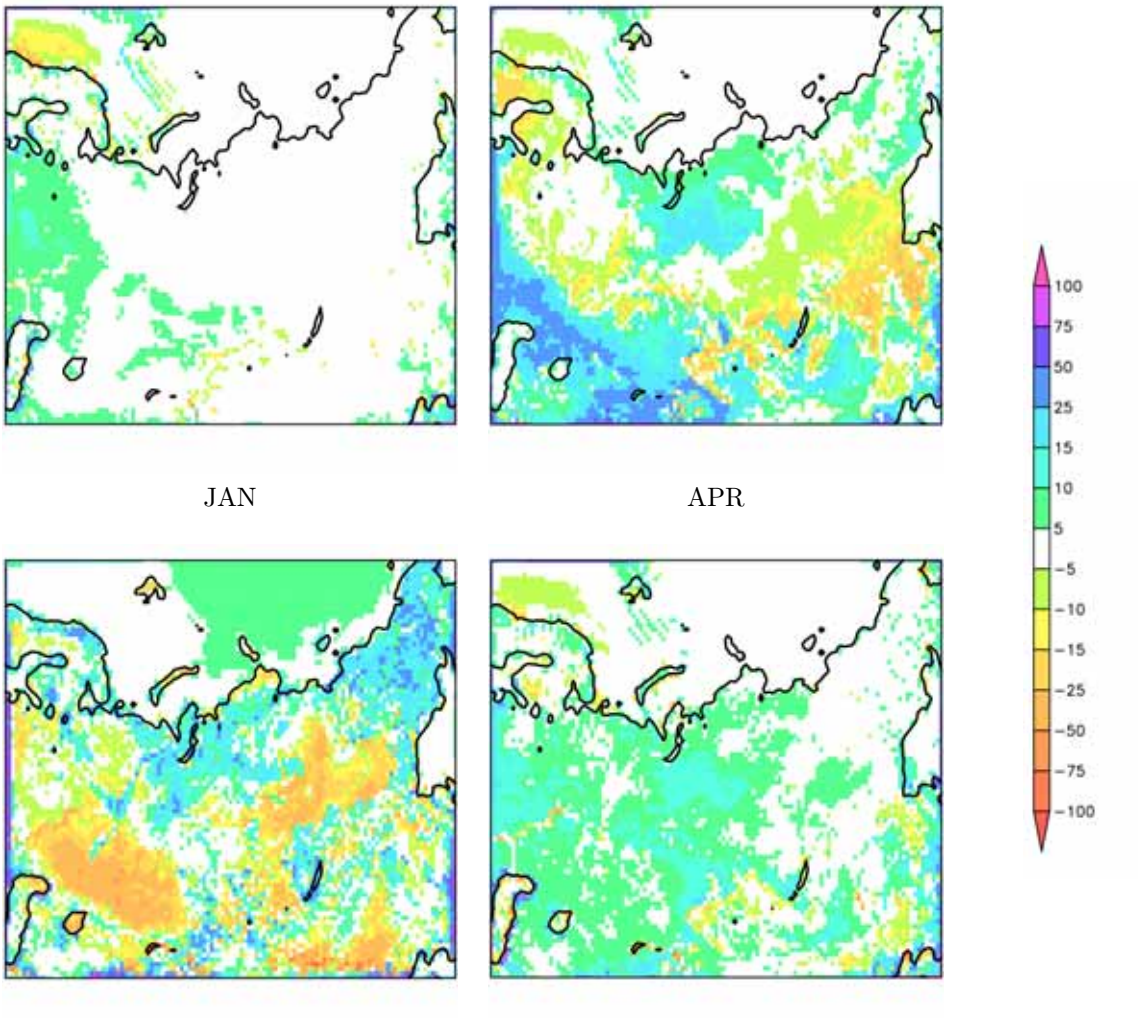

Figure 5.36: Difference between simulated and ERA40 laten heat flux $[W/m^2]$, CTRL - ERA40, 1971-1990 mean, for months January (upper left), April (upper right), July (lower left), and October (lower right).

Snow

Absolute distribution of snow depth from satellite observations is shown in Figure 5.37 for snow months October (upper left) to May (lower right panel). Figure 5.38 shows the differences between mean observed and simulated snow depth. Snow depth is derived from snow water equivalent via multiplication with a factor that represents an assumed snow density, which was 3.333 g/cm^3 in this case.

Triangles mark stations where climatological measurements of air and snow temperatures and of snow depth were taken, which are used for point-to-point comparison (see sect. 5.3.3). It is obvious that most of the stations are situated in areas where simulated snow depth is too low when compared to the GlobSnow data. The same deviation is obtained from the point-to-point evaluation in the same section, which supports the result of the large-scale comparison with GlobSnow data. A probable source of error might be the used factor for the conversion of SWE into snow depth.

The evaluation using the gridded GlobSnow data gives useful hints to possible mismatches of the simulations with reality, which is important for the development of the ground temperatures in the cold months. As mentioned, use will be made of the data within the comparison of simulated surface and soil variables to station measurements.

The large scale comparison shows a region covering the Central Siberian Plateau where snow depth from REMO is lower than from GlobSnow throughout the winter. This holds also for North Eastern Siberia.
The North Western part of Siberia, to the contrary, as well as the Luv of the Urals, and Western Russia, feature too high snow depths. This is also the case in late winter and early spring in the Western Siberian Lowlands.
All in all, the differences are related to orography, as in the Luv of mountaineous regions snow depth is overestimated, while this might be the reason for the too low simulated snow depth over regions in the East, thus in Lee of mountaineous areas.
At the end of the snow season, larger areas show overestimated snow depth in the simulation, which is most prominent in May and in West Sibera.

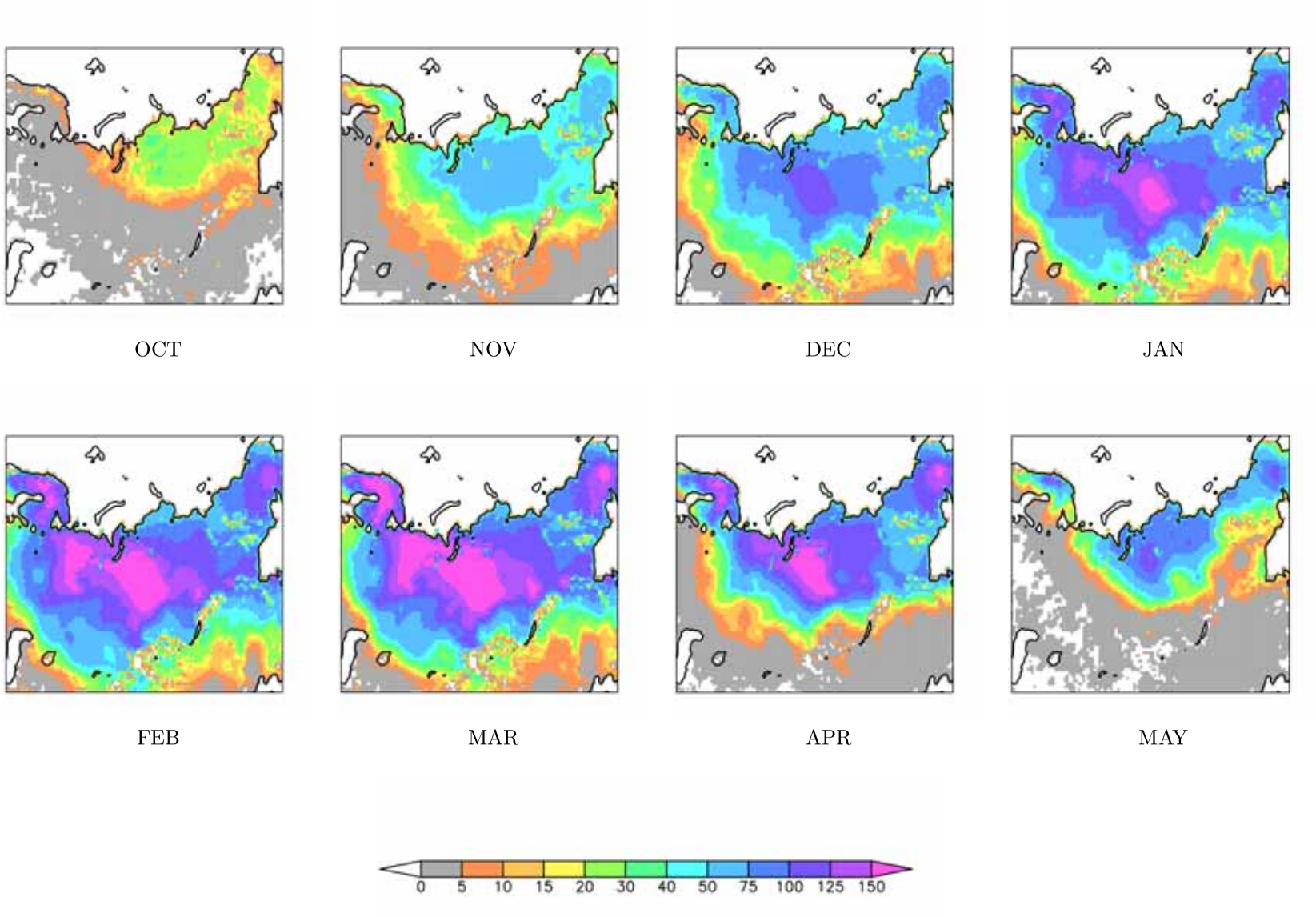

Figure 5.37: Observed snow water equivalent [mm] from GlobSnow, 1981-2000 mean, for months October until May (upper left to lower right).

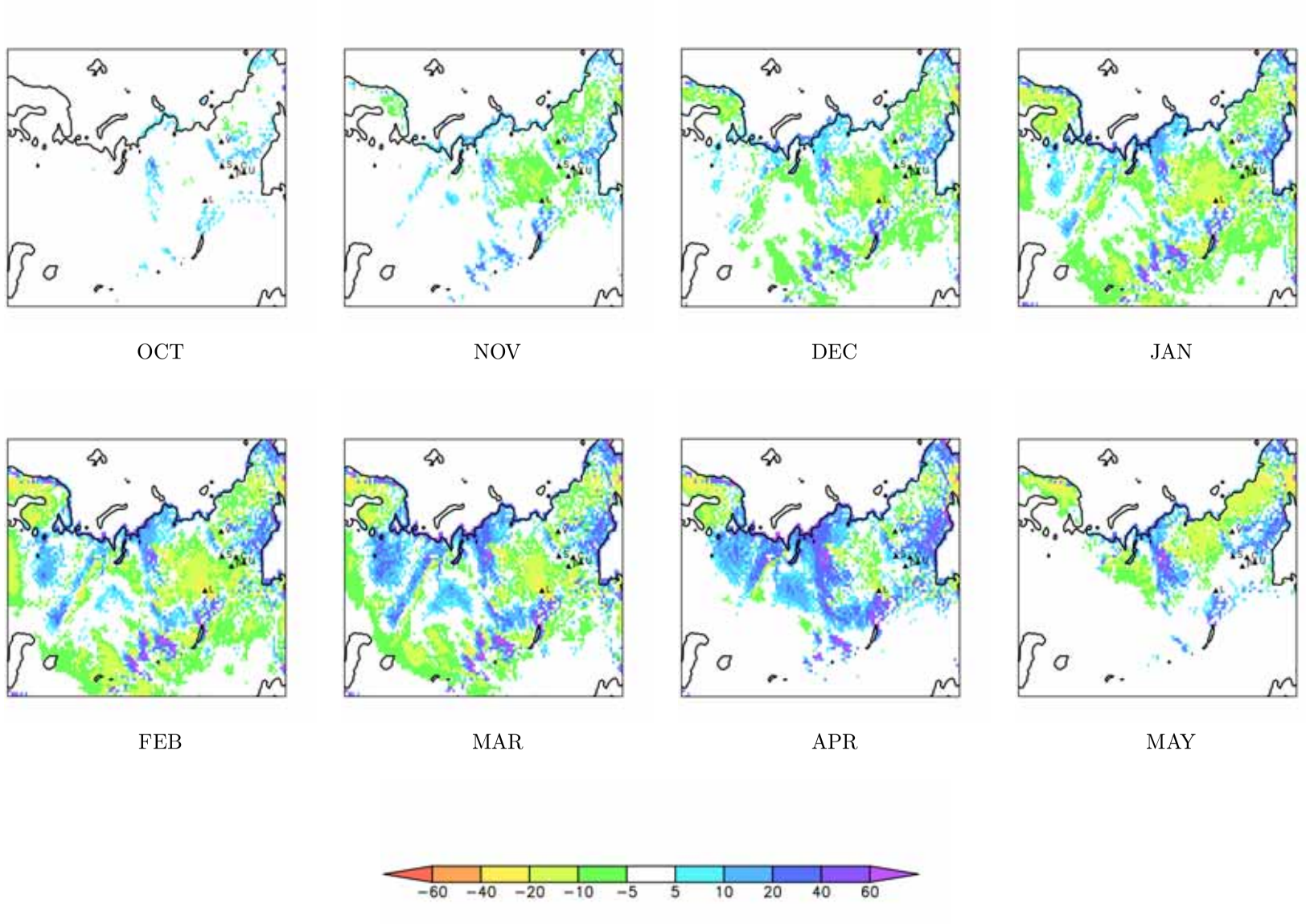

Figure 5.38: Difference between simulated and observed snow depth [mm], CTRL - GlobSnow, 1981-2000 mean, for months October until May (upper left to lower right).

Consequences of changes for model biases

The changes imposed through the implementation of permafrost processes in part lead to improvements of the biases of the simulated climate shown for the CTRL experiment. Figure 5.39 illustrates that modelled surface evaporation improves when compared to ERA40 data with the use of permafrost processes, as the overestimation in summer is decreasing in COUP as compared to CTRL over large parts of Siberia (refer to Figure 5.34).

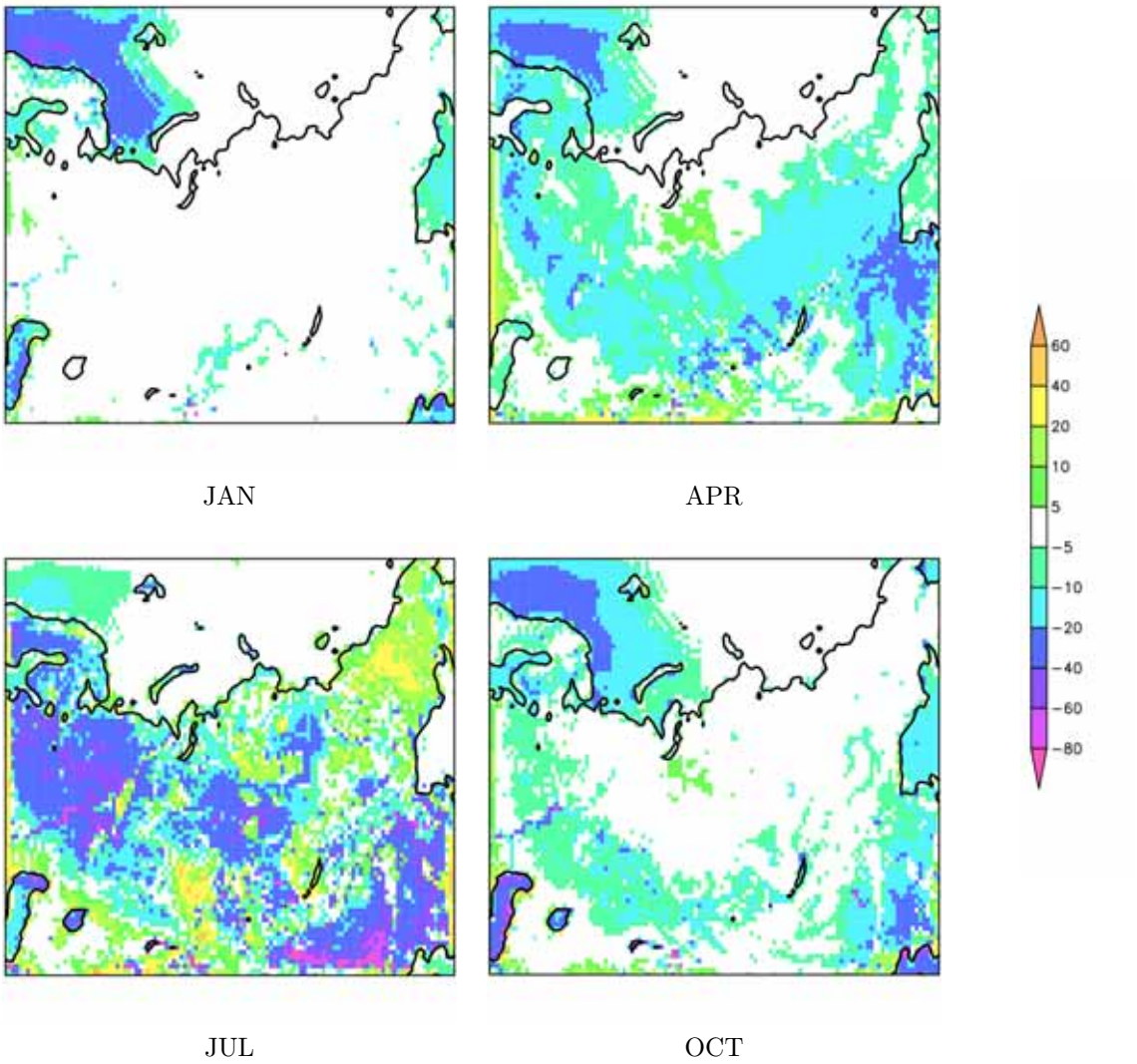

Figure 5.39: Difference between simulated and ERA40 surface evaporation [$mm/month$], COUP - ERA40, 1971-1990 mean, for months January (upper left), April (upper right), July (lower left), and October (lower right).

To the contrary, some regions even show a negative deviation in the COUP version, mainly Eastern Siberia and smaller areas in the central part of Siberia. This does not hold, however, for the Western part of the domain, the European part of Russia,

where evaporation is still subtantially overestimated. No large influence can be detected for April. The discussed resulting warming of the near-surface air temperatures in summer brings about a more widespread warm bias with respect to WFD data in COUP (Figure 5.40) as compared to CTRL (see Figure 5.31). A slight improvement can be detected over Western Siberia in autumn, as the cold bias is less widespread and reduced in magnitude. This might be attributable to latent heat release due to freezing, which may warm the near-surface atmosphere at the beginning of the freezing season even though snow cover develops.

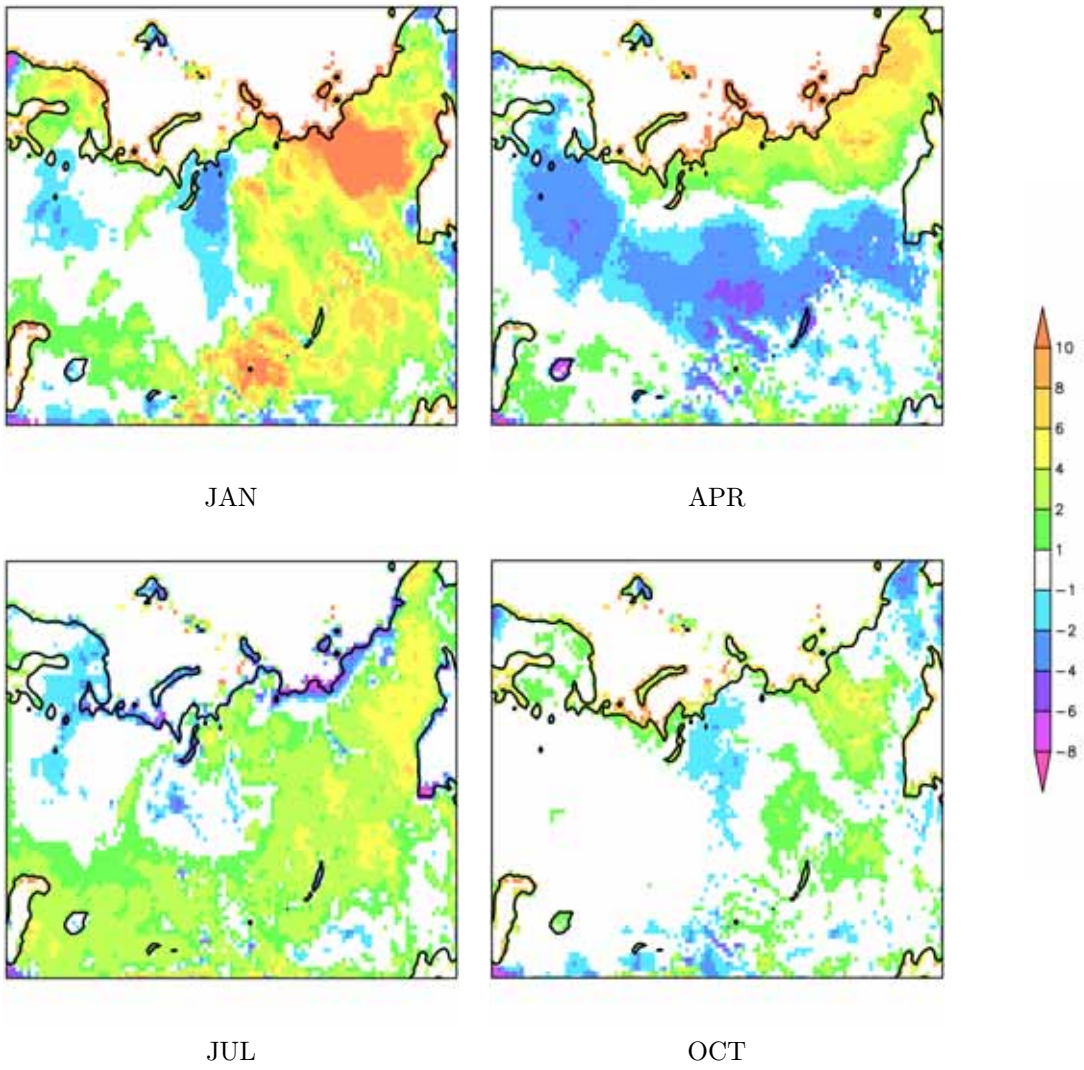

Figure 5.40: Difference between simulated and observed 2m air temperature $[K]$, COUP - WFD, 1971-1990 mean, for months January (upper left), April (upper right), July (lower left), and October (lower right).

The warmer and drier summer climate in the COUP experiment also leads to some changes to the biases in total precipitation between model and observations (Figure 5.41). As shown in sect. 5.3.2 (Figure 5.25) shifts in variables related to the surface water balance mainly affect spring and summer. Improvements of the biases in evaporation and total precipitation also occur in the same months.

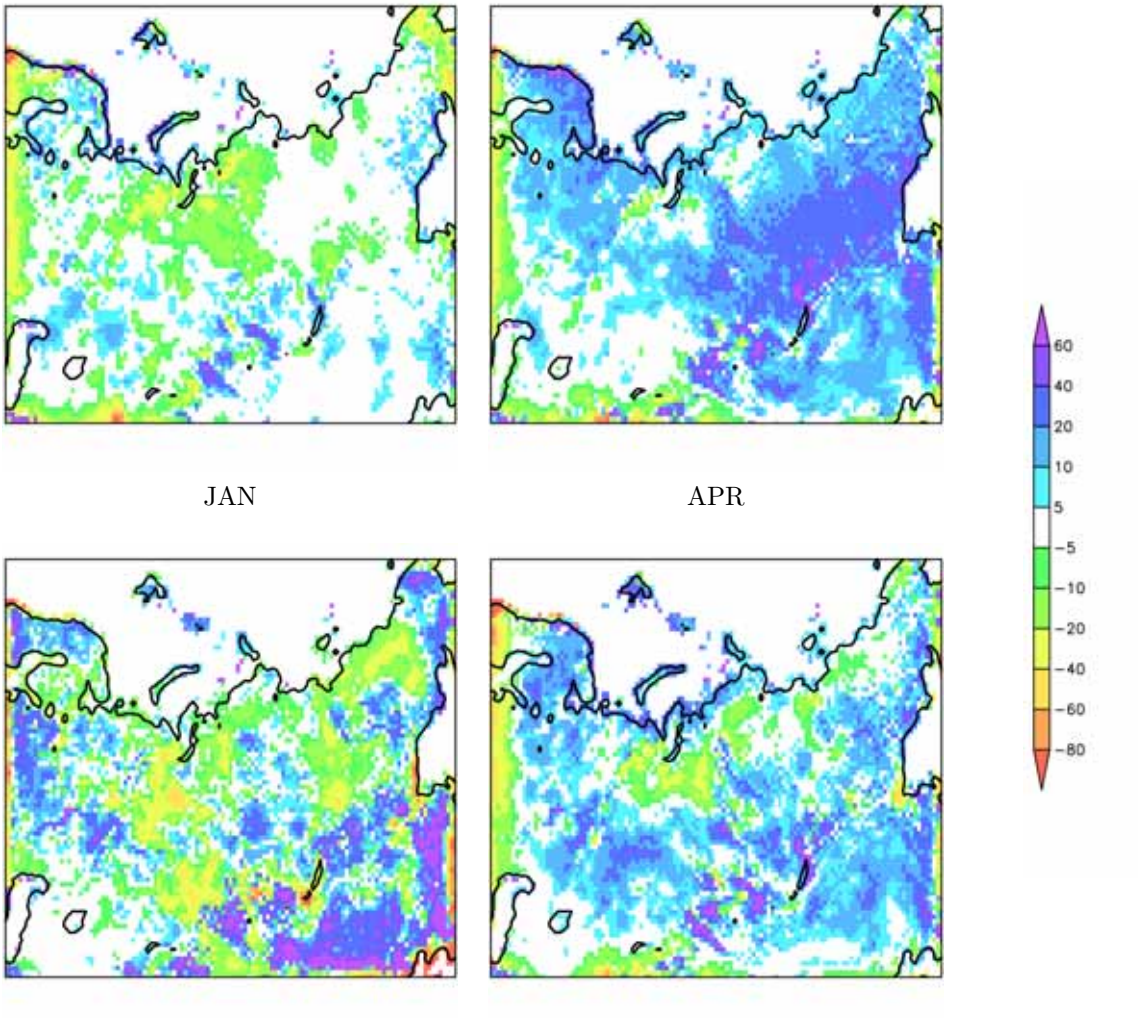

Figure 5.41: Difference between simulated and observed total precipitation [$mm/month$], COUP - WFD, 1971-1990 mean, for months January (upper left), April (upper right), July (lower left), and October (lower right).

Permafrost characteristics

Figure 5.42 shows the spatial distribution of permafrost in the model domain in absolute values (left panel), and a comparison of the simulated extent to IPA observations (right panel). The reader is reminded to the differences between observed and simulated values with regard to the information they contain. The observed permafrost distribution assigns a value such as e.g. "discontinuous permafrost" to each grid cell, which corresponds to a spatial percentage of permafrost coverage (see Section 2.2). In REMO, however, soil variables are computed for one point for each grid cell, so that it can only be flagged as "permafrost" or "no permafrost", and the subgrid-scale heterogeneity cannot be represented.
In order to determine permafrost occurance for a grid cell, the temperature of the deepest layer is used, the center of which is located in 6.984m depth in the COUP version. A grid cell is defined as permafrost if the respective value constantly stayed below 0°C for at least the two preciding years. This diagnosis was conducted with timeseries of daily means of the soil temperature. For displaying the observed permafrost distribution, the continuous class was chosen, as it is not meaningfull to compare the simulated permafrost extent to low spatial permafrost cover, as explained above.

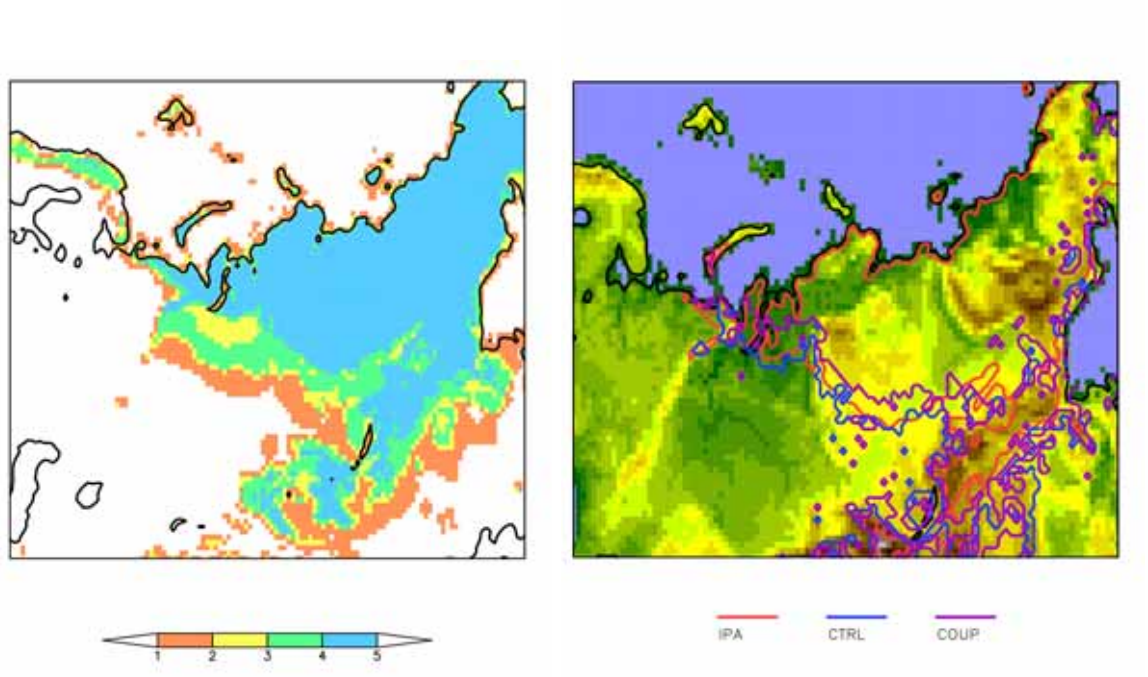

Figure 5.42: Left panel: permafrost distribution as observed from IPA (zones with isolated (1), sporadic (2), discontinuous (3), continuous (4) permafrost); right panel: outer boundary of the continuous zone (IPA, red) vs simulated permafrost distribution from experiments CTRL (blue) and COUP (violet).

The comparison shows that the overall occurance of continuous permafrost is matched satisfyingly by the model over Siberia. The comparison also reveals that permafrost is observed in regions more to the South and West (the discontinuous areas), where the model obviously cannot simulate permafrost. This might be attributed to the most part to the warm bias in air temperature. Also, in Western Siberia the permafrost is more discontinuous, originating partly in the last glacial time period and the Little Ice Age (Romanovsky et al., 2010) , which is not reproduceable by this experimental setup. Simulated permafrost extent is slightly larger in the CTRL experiment than in COUP, which is not only a result of the changes to the soil model, but is attributable to the warmer summer climate that develops in COUP due to the impacts of the new scheme on the SEB (see Section 5.3.2).
The ability to reproduce practically the same permafrost distribution with COUP than with CTRL, despite of the significantly warmer summer climate in the COUP experiment, implies that typical aspects of the High Norther latitudes are represented in the new scheme. These would be processes that control the coupling between air and ground thermal regimes, as e.g. the thermal offset effect.

A similar observational data set, permafrost temperatures provided by IIASA (see Section 5.2.1), was used for a comparison of the simulated permafrost temperature using the new deepest, sixth soil layer. The term "permafrost temperature" usually refers to the ground temperature at a depth of zero annual amplitude, which is said to be at 12 to 15 m depth (Romanovsky et al., 2010). Thus, the depth of the center of the newly implemented sixth soil layer, 15.99m, can well be used for an evaluation of simulated deep soil temperatures in the permafrost regions.

As Figure 5.43 illustrates, the pattern of observed permafrost temperature show a gradient from South to North and from West to East, which reflects the increasing continentality of Siberian climatic conditions. Permafrost is coldest in Northern Siberia at the Laptev Sea coast, where in some areas temperatures are as low as -15 °C.

The field is very homogeneous over large areas, which is attributable to data scarcity, and is rather unlikely to reflect the "full truth". This is especially valid when considering the pronounced orography in large parts of Central and Eastern Siberia. This is probably due to the lack of spatially more detailed information to feed into the IIASA dataset, and extrapolation leads to such homogeneous belts of constant temperatures over much of Siberia.

A general warm bias is obvious in the model, which can be attributed firstly to the warm bias in the simulated winter climate (see Figure 5.3.3), secondly to the fact that substantial parts of permafrost are not in equilibrium with today's climate, but reflect past, colder conditions. Especially the Northern Siberian Lowlands show very cold permafrost with temperatures lower than -10°C.

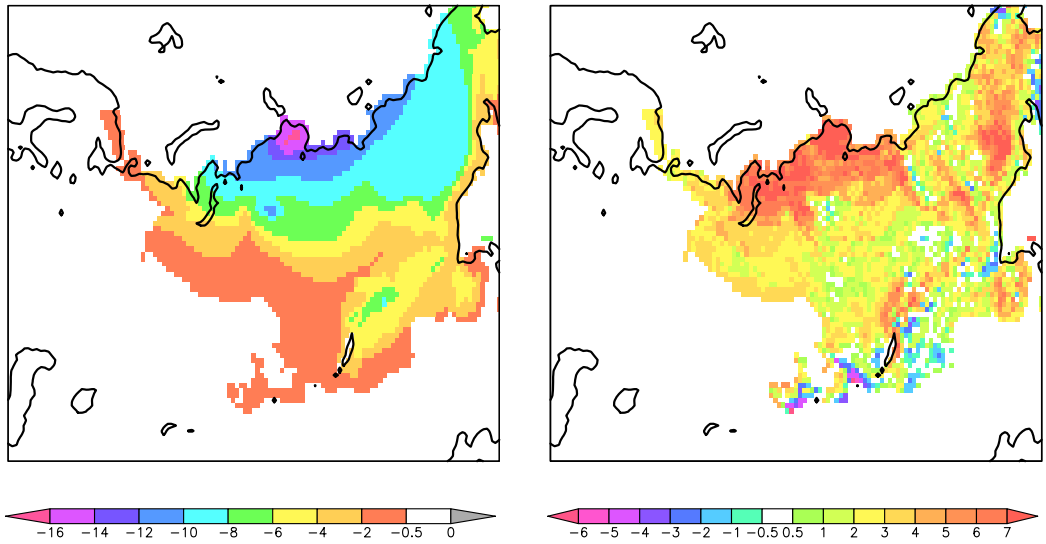

Figure 5.43: Horizontal distribution of 'permafrost temperature' [°C] as observed by IIASA (left), difference between simulated multi-year mean (1981-1990) and observed deep soil temperatures [K] (right).

Nevertheless, some gridboxes show a negative difference, meaning that here the model produces lower soil temperatures than IIASA provides. This can be attributed to the spatial homogeneity in the IIASA data (see above), while REMO simulates very cold ground temperatures in mountaineous regions due to elevation effects and the constantly high thermal conductivity of the bedrock.

The Depth of the Active Layer is compared between model versions CTRL and COUP (Figure 5.44). The overall pattern do not differ much, which would be expected as winter climate is largely identical in both experiments, while summer air temperatures are warmer in COUP than in CTRL. As for permafrost distribution, this result is satisfying insofar as the new scheme is able to reproduce similar permafrost specifics while it features a warmer summer climate. Nevertheless, there are areas where COUP simulates a deeper AL (at the southern boundary of its permafrost distribution), yet in the Northern Siberian lowlands it shows more shallow AL.

A comparison with observed AL data was not conducted due to two reasons. Firstly, no REMO output variable could be directly compared to the AL depth, as soil temperatures at distinct depths are calculated, instead of a certain isotherm, and as the above comparison of the deep soil temperature to the IIASA data revealed, REMO seems to be too warm in the permafrost region. However, comparison with AL measurments will be done in the future.

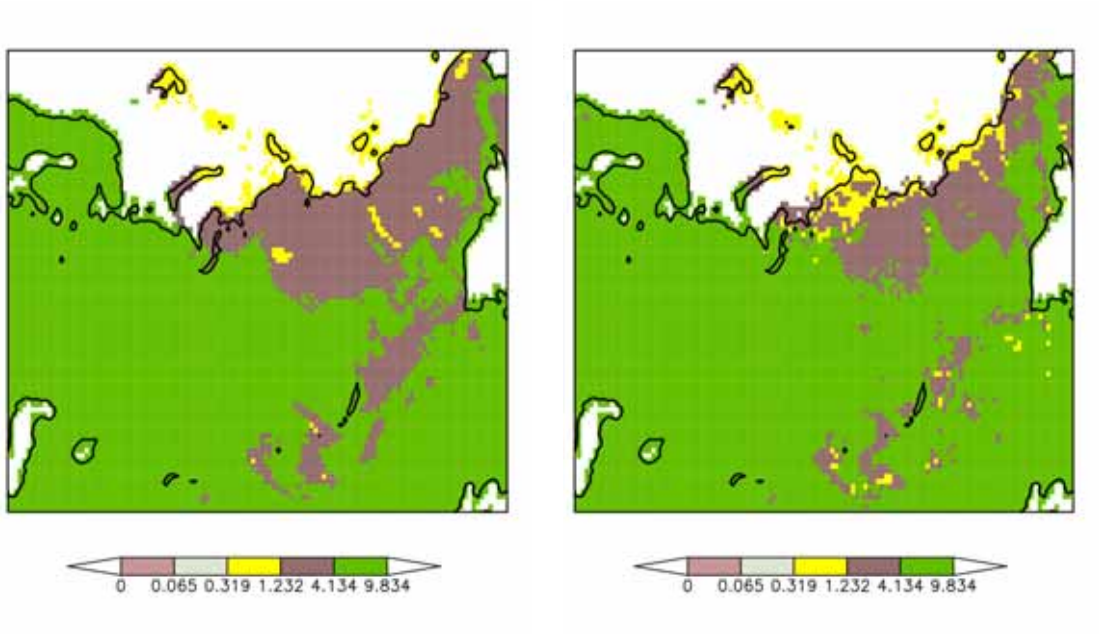

Figure 5.44: Simulated Active Layer Depth [m] from CTRL (left) and COUP (right), 1971-1990 mean; scale is set according to lower boundaries of the layers of the soil scheme.

Comparison of river discharge

In order to evaluate the impacts of the new model formulations on regional scale hydrological variables, simulated river discharge is compared to observations for the Lena and the Yenissei river basins, respectively (Figure 5.45).

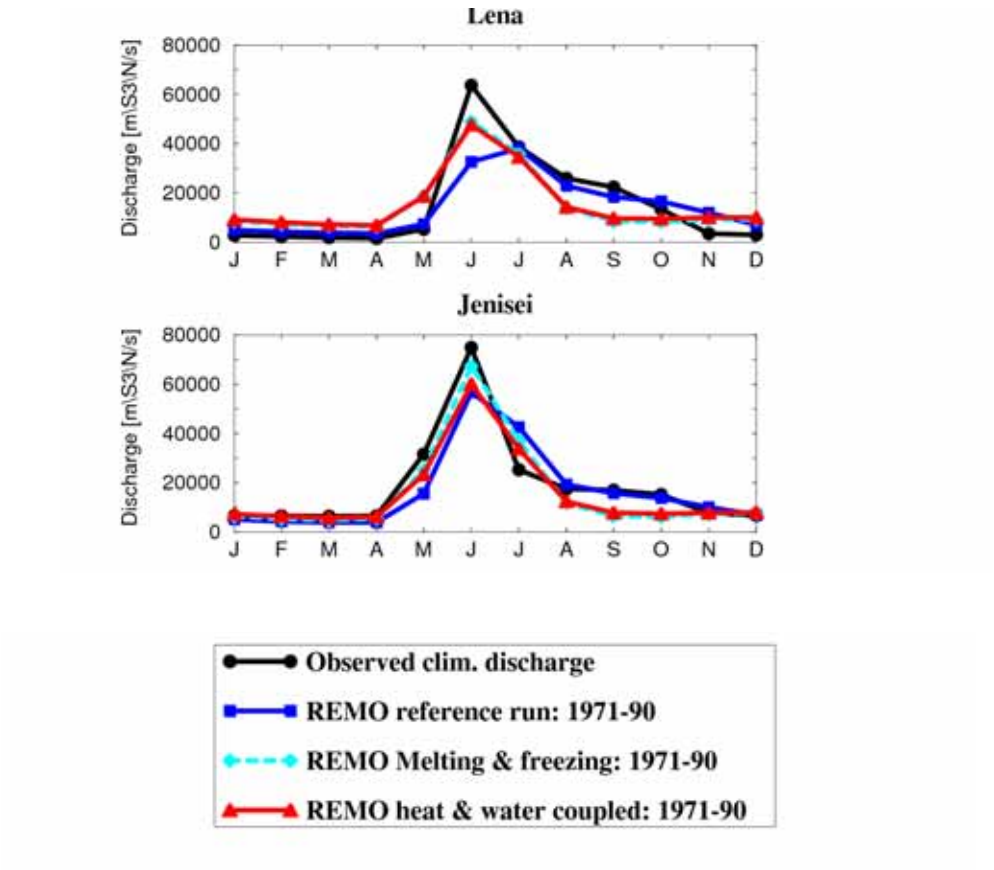

Figure 5.45: Simulated and observed river discharge $[m^3/s]$ from Yenissei (top) and Lena (bottom), model results from experiment CTRL (dark blue), LAYLF (light blue) and COUP (red), 1971-1990 mean.

The seasonal cycle is improved with introduction of freezing and melting, as both curves show a shift of the peak towards one month earlier (Lena) or a sharpening of the peak (Lena and Yenissei). The low flow during winter is simulated to be smaller when freezing and melting is introduced. This effect seems to be equally strong in both FAROUK and COUP.
Thus, the main effect from the model extensions on discharge is the reduced infiltration of surface water when soil is frozen, since this exactly reproduces the distinct and large spring peak of the observations.

Comparison to station measurements - Mean seasonal cycle

A comparison is made for soil temperatures in depths 0.2m and 0.8m, at the stations Churapcha, Lensk, Sangar, Ust Maya, Verkhoyansk, and Pokrovsk. These stations were chosen as they show typical biases, and provide useful insight into how the model extensions work and differ, as well as possible reasons for still occuring mismatches between model and observations. Temperatures are corrected using a lapse rate of 0.65K/100m for stations Sangar, Verkhoyansk and Churapcha to the elevation of the respective REMO grid cell. All stations have measured snow depths which are also provided as monthly means.

Summer air temperatures are simulated too warm by all model versions at almost all stations. Hereby, the CTRL experiment is closest to the observations, whereas the implementation of permafrost processes increases or introduces a warm bias. This can be explained with the general warming of near-surface atmosphere in all new model versions due to the reduced soil moisture and thus less evaporative cooling, as shown in Section 5.3.2. As an exception from this, stations Lensk and Sangar show the opposite effect, and all new versions capture observed air temperature better than the CTRL version, in which a cold bias can be seen.

In most cases the comparison shows how the known winter warm bias of the air temperature (see Section 5.3.3) affects the respective grid cells. The warm biases in winter air temperature are much more pronounced than the summer biases in all stations (apart from Lensk).
The comparison reveals that changes to the model do not noticeably impact the winter atmospheric climate, as all experiments simulate the winter air temperature almost identically.

Similarly, simulated snow depths vary only weakly between all model versions.
At all stations, simulations underestimate the observed snow depth. Moreover, a phase lag can be seen in the comparison, meaning that snow cover develops too late in REMO in fall, while it melts too late in spring. The possible consequences for the simulated soil temperatures are discussed below.
Note that the conversion of model output from SWE to snow depths, however, might introduce an error and at least uncertainty: It represents an assumption on the snow density, a variable that in reality is not constant and shows a marked range (T. Zhang, 2005). The observed snow probably had, e.g., different snow densities in fall than in spring. These effects are ignored with the method used here for snow evaluation.

Simulated summer soil temperatures are too warm as compared to the measurements in most cases. This might be due to the missing organic layer on top of the soil that is frequently observed in sub-Arctic and Arctic regions. Organic top layers lead to enhanced insulation of the soil layers below and thus dampen the annual minima and maxima (see Section 2.3.3).

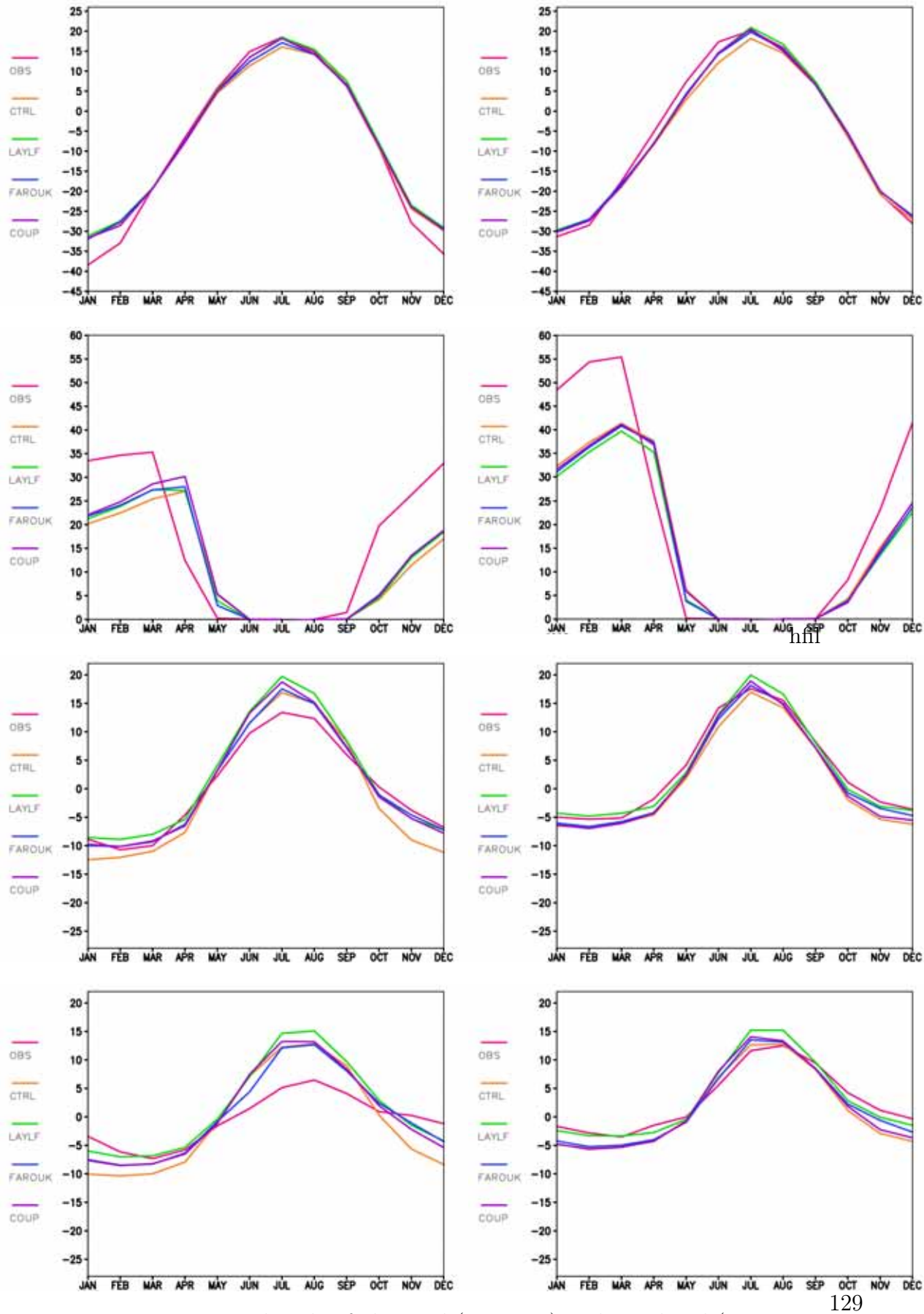

Figure 5.46: Mean seasonal cycle of observed (magenta) and simulated (orange, green, blue, violet) 2m air and soil temperature [°C] in 0.2m and 0.8m depth (first, third, and fourth row) and snow depth [cm] (second row) for Sangar (left) and Lensk (right), 1971 - 1990 mean.

Due to the warm bias in air temperatures, simulated soil temperatures are too warm in winter in some cases (Verkhoyansk, Pokrovsk).
As an exception from this the Station Lensk shows a generally good accordance of the simulations with the observations.
Interestingly, warm winter bias in air T often is reversed in the soil, i.e. a cold bias evolves, as can be seen for Sangar, Verkhoyansk, Churapcha, and Ust Maya, respectively. This tends to strengthen with depth, i.e. the model shows a cold bias which is increasing with depth, despite too warm simulated air temperatures (stations Ust Maya, Churapcha, e.g.).
As for the summer temperatures, this can be attributed to soil properties of the model that do not capture the characteristics of the observations. Soils at the stations Churapcha, Sangar and Ust Maya are described e.g. as mineral soil texture types, but "with organic inclusions" or peat on top. Since the model soil column is vertically homogeneous, such effects cannot be represented with neither of the model versions, but it is expected to improve with the planned introduction of an organic top layer in permafrost regions.
Adding to this, the cold bias that appears in many of the graphs can be attributed to deficiencies of the snow in the model. The comparison to GlobSnow data shows that in all of the cases simulated snow underestimates the measurements, which leads to less insulation of the ground, and thus enhanced heat loss.

In the following, differences between individual model versions will be analysed in more detail.
In general, the new model versions are relatively close to each other at most of the stations during the summer months. As no freezing and melting occurs during that time of the year, neither latent heat effects nor changes in λ through presence or absence of ice could strongly modify heat conduction in the ground. The largest change can be seen between the new versions and the CTRL version, which is due to differences in summer climate that develop with the implementation of permafrost processes (see Section 5.3.2. Nevertheless, some effects can be detected and attributed to the respective change to the physical formulations. E.g., the first change, implementation of the latent heat effect, led to enhanced summer air temperatures, which are dampened in the ground through the use of the FAROUK and a thus decreased summer thermal conductivity in FAROUK, which can well be seen in all stations in the soil temperatures. The effect of this second change enhances with depth, as would be expected. Also, FAROUK is often slightly colder than COUP during summer, which can be explained with the higher soil moisture level in COUP, which in turn increases λ.
During winter, larger differences between inividual new model versions evolve. The higher total soil moisture in COUP as compared to FAROUK explains the decrease in winter soil temperatures from FAROUK to COUP, as it leads to increased λ and a thus more effective cooling (see Ust Maya, Pokrovsk, and Churapcha).
All in all, simulated winter soil temperatures decrease with each each new process implemented.

The introduction of permafrost processes function in the expected way, as was shown above. In some cases, the implementation of permafrost processes leads to an improvement of the simulated soil temperatures, which in part counterbalance the deviations of atmospheric climate from the observations. In other cases, the new model versions show increased deviations from the observations, which can be traced to either biases in the atmosheric (air temperature) and surface (snow) climatic conditions, that drive and modulate the ground thermal regime, and to specifics of the soil, which are not represented in the model (organic top layer and/or organic inclusions). It is concluded that the comparison of the mean seasonal cycle to station measurements supported the understanding of the functioning of the new model versions, as these behave in a physically meaningfull manner.

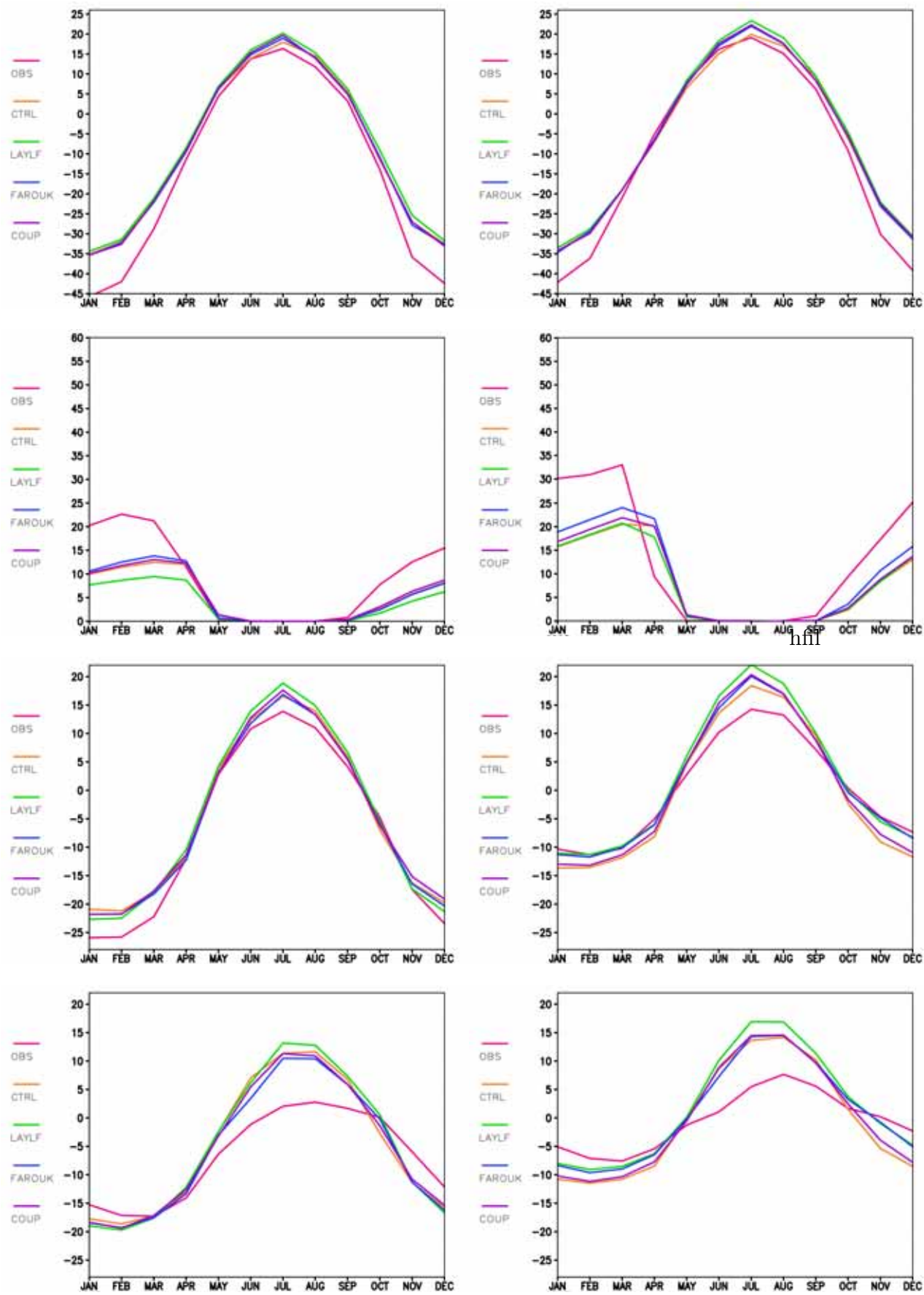

Figure 5.47: Mean seasonal cycle of observed (magenta) and simulated (orange, green, blue, violet) 2m air and soil temperature [°C] in 0.2m and 0.8m depth (first, third, and fourth row) and snow depth [cm] (second row) for Verkhoyansk (left) and Churapcha (right), 1971 - 1990 mean.

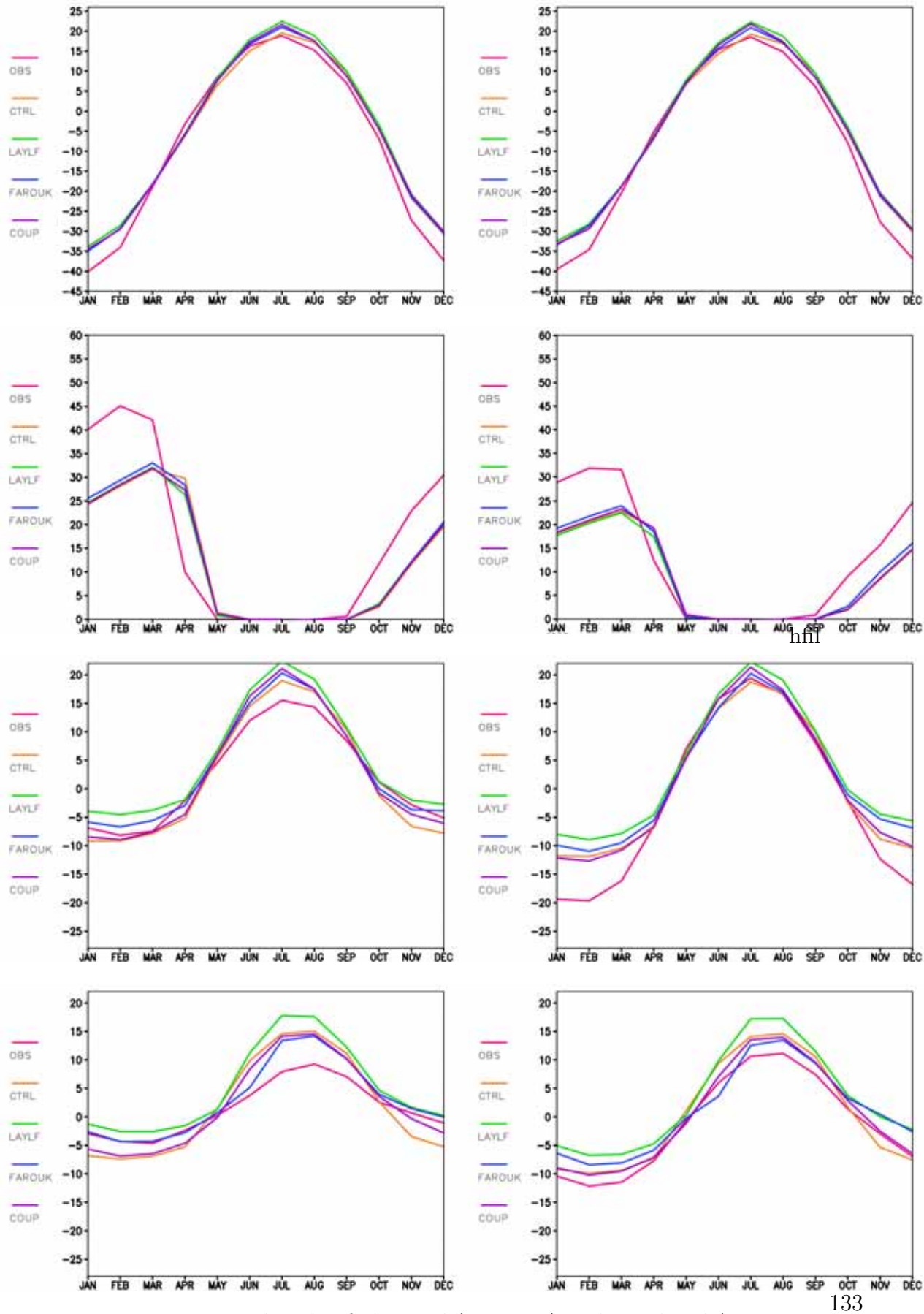

Figure 5.48: Mean seasonal cycle of observed (magenta) and simulated (orange, green, blue, violet) 2m air and soil temperature [°C] in 0.2m and 0.8m depth (first, third, and fourth row) and snow depth [cm] (second row) for Ust Maya (left) and Pokrovsk (right), 1971 - 1990 mean.

Comparison to station measurements - freezing and melting periods

Comparisons were made for surface and soil temperatures against daily measurements from two autumn and spring seasons, respectively, in order to investigate the model's behaviour during the key periods of freezing and melting. Snow cover will first be analysed as herein reasons can be found for possible deviations between model and observations. No snow measurements were taken at this station, therefore GlobSnow data for the respective gridcell and time period was extracted for the evaluation of modelled snow depth. Figure 5.49 gives an overview of how the simulated snow depth behaves compared with satellite observations from GlobSnow for the complete period of station observations. Data are extracted again for the respective grid cell for Chukochya.

In principle, simulated snow depth is capturing the observed amount; however, snow depth is simulated too high in the first winter, while it is underestimated in the second winter by the model. In both spring periods, snow melt occurs too early in the model.

Chukochya station provides observations of temperatures in 2m height above the surface and in a soil depth of 0.2 m, the latter of which can well be compared to the model's second soil layer.
Figure 5.50 displays the freeze-up of the years 1998 and 1999.
The observed soil temperatures feature a pronounced zero-curtain, which is not detectable in the CTRL experiment, as no latent heat of fusion is considered. The new model versions, to the contrary, reproduce the zero-curtain, as is seen in formerly discussed results (see Section 5.3.1). Unfortunately, observations start in the first freezing period during freeze-up, and it is thus not possible to decide whether model or observations are retained longer at 0°C. However, the zero-curtain situation lasts considerable time in the observations in the second autumn (1999), which is not that pronounced in neither of the new model versions.
The time period of latent heat release is more pronounced in COUP than in FAROUK, which would match the expectations, as COUP has a generally higher soil moisture level.
While in both years the simulated surface temperature drops faster than the observed one after freeze-up, soil temperatures behave differently:
In 1998, observed soil temperature cools faster than the simulated soil temperature, while in 1999, soil temperatures decrease faster in the model than in the observations.

Differences between REMO and GlobSnow can partly explain deviations of modelled and observed soil temperatures. In autumn 1998, soil temperatures are too warm, which is especially the case for the new model versions due to release of latent heat. All simulations show higher snow depths, and the snow cover starts to develop earlier than in the observations. Both leads to enhanced insulation of the ground in the model, thereby keeping simulated soil temperatures on a higher level.

In the second winter, REMO generally seems to underestimate snow depth. The onset of freezing coincides with a gap in the GlobSnow data, but from the general underestimation

of snow depth in REMO (Figure 5.49) during the second winter, it can be assumed that this was also the case in autumn.
This could explain in part the too fast decrease of the simulated soil temperature, while the observed values are higher including after the freeze-up, i.e. when they start to drop below 0°C, they do so slower than the model.

Snow depths at this site are shallow and vary around critical values of some centimeters, barely reaching 20 cm. Thus, small differences can have important effects on the soil thermal regime (see Section 2.3.2), since the insulating effect depends critically on the snow depth until it reaches roughly 40 cm (T. Zhang (2005) and references therein).

Figure 5.51 shows the same variables, yet for the melting periods of 1999 and 2000, respectively. The most prominent feature is a strong warm bias of the model in both surface and soil temperatures in both years (surface temperature data was missing for spring 1999).
The new model versions produce a zero-curtain, but to a much smaller degree than the observations. Melting of the soil only lasts some days in the model, while it takes about three weeks in the observations. The zero-curtain seem to be stretched and smoothed in the observations, i.e. less sharply distinguishable than in autumn seasons.
The smoothing of the latent heat effect in COUP is recognisable, as energy release or consumption is delivered over a temperature range of 2K.
The deficiencies of the model during both spring seasons can also be attributed to differences in snow cover (see below).

Several general statements can be drawn from this comparison.
The graphs display how soil temperature follows surface temperature in a dampened form. Yet the degree of dampening is weaker in the model than in the observations, i.e. the model shows stronger variability than the measured variables.

The most important effect of the model extensions, i.e. simulating the zero-curatin, is reproduced, and simulated soil temperatures stay at (or around) the freezing point for a marked time. This fundamental change in model behaviour has important consequences for the upper soil layers' thermal regime, as was also shown in Section 5.3.1.
The generally too warm temperatures in the simulations can be attributed to the warm bias of the 2m air temperature in this region in winter (see Section 5.3.3, Figure 5.31). They may also contribute to the markedly earlier thawing in the simulations, in spring 1999 even almost one month.
More importantly, large deviations of the simulated from the observed soil temperature in both spring seasons can be explained by the differences in snow cover between model and observations. Figure 5.49 shows, despite many data gaps, that snow melt occurs too early in the model. This leads to enhanced energy input into the ground in the simulations as compared to the observations, as at this time ot the year incoming solar radiation is already large. Thus, the early and intense warming in REMO can be traced to biases in the modelled snow cover.

Observed soil temperatures hint to large amounts of moisture in the ground, which lead to such a long zero-curtain situation.
Moreover, the rather gradual and slow increase of the observations in spring, now without a distinct zero-curtain, may be a sign of substantial amounts of supercooled, unfrozen water, which delays the melting, and which smoothes the latent heat effect by distributing it over a temperature range, instead of letting all ice melt at 0°C sharply. Data documentation reveals that this is probably the reason behind, as "soil texture / type" is given as "loamy", and fine grained soils hold significant portions of water in unfrozen state down to roughly -5 °C (Romanovsky and Osterkamp, 1995).
This process is only weakly represented in REMO in the COUP version, as here the release of latent heat of fusion is distributed over a 'freezing window' of 2 K below 0°C. The implementation of a freezing point depression equation for determining the liquid water content at sub-zero temperatures, and thus a restriction of complete freezing for fine grained, not too cold soils, is planned for future work.

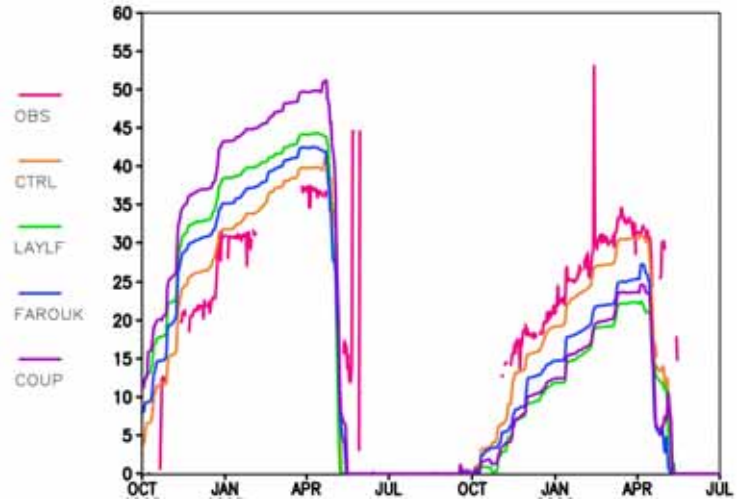

Figure 5.49: GlobSnow (magenta) and simulated (orange, green, blue, violet) snow depth [cm] for the grid cell of Chukochya, complete period of soil observations (1998 - 2000).

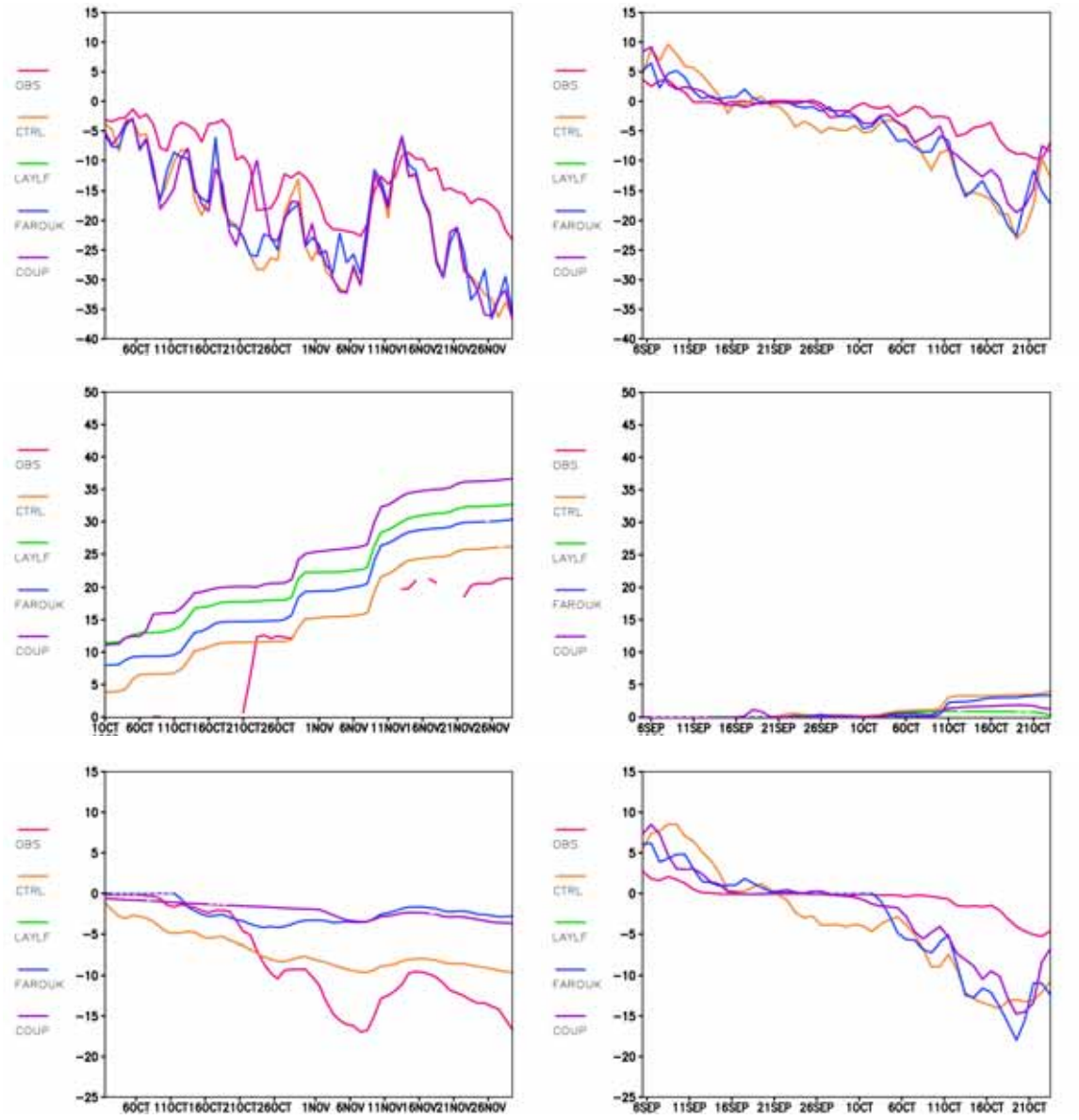

Figure 5.50: Oberved (magenta) and simulated (orange, green, blue, violet) surface (upper panels) and soil (lower panels) temperatures [°C] and snow depth [*cm*] (center panels) for Chukochya, freezing periods 1998 (left) and 1999 (right).

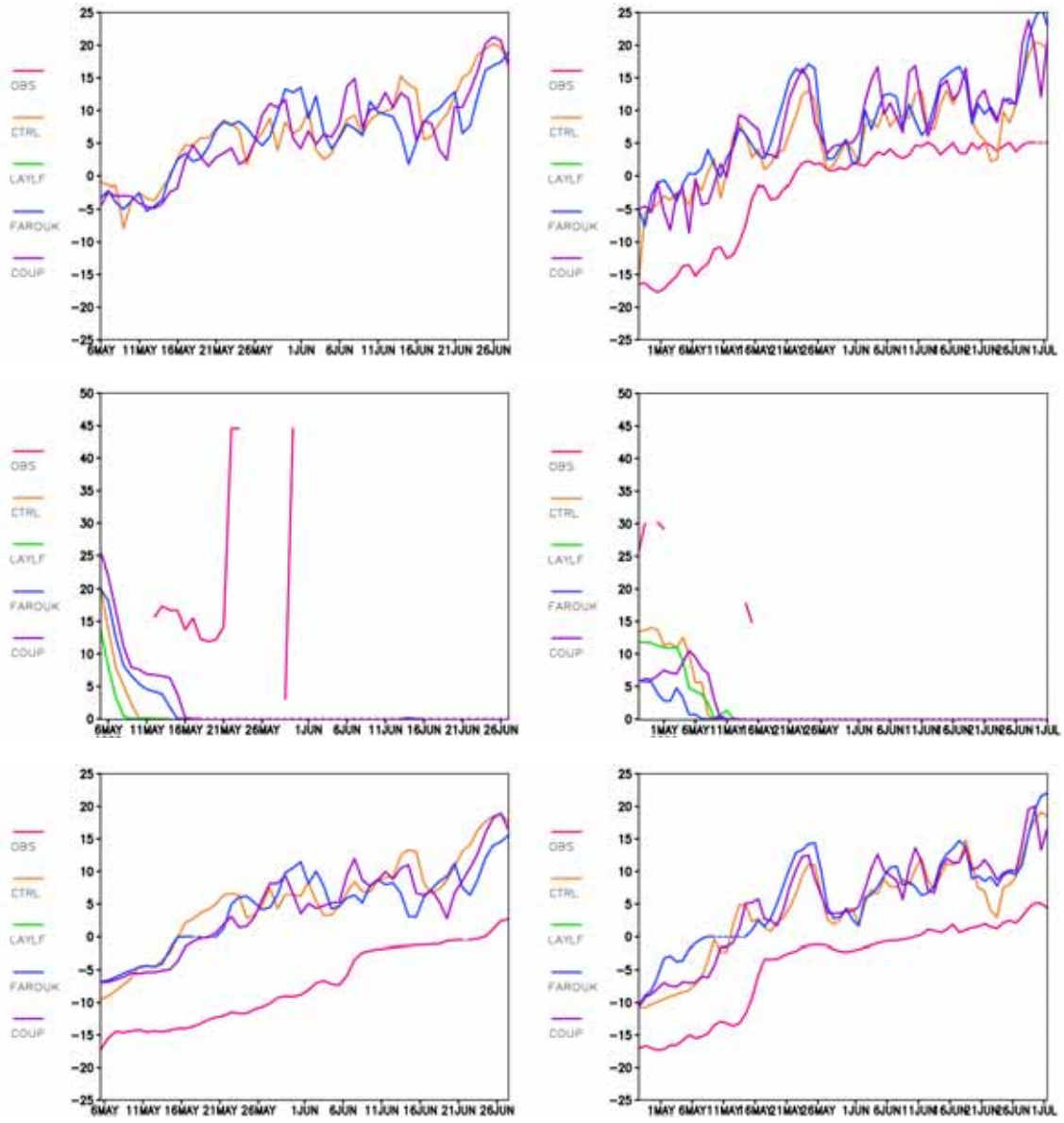

Figure 5.51: Oberved (magenta) and simulated (orange, green, blue, violet) surface (upper panels) and soil (lower panels) temperatures [°C] and snow depth [cm] (center panels) for Chukochya, melting periods 1999 (left) and 2000 (right).

6 Summary, conclusions, and outlook

6.1 Summary

It was the aim of this PhD study to understand how different processes that are dominant in permafrost soils impact the regional climate of Siberia in terms of simulated energy and water cycles.
Interactions between the land surface and the atmosphere should be investigated, which was realised with the use of a regional climate model. This was done because of the advantage of the constraining, 'perfect' lateral boundary forcing and the high horizontal resolution, which is especially important when feedbacks between land surface and atmosphere are considered.
Relevant soil and surface processes with regard to permafrost on the larger scale are the freezing and melting of soil moisture, thereby modulating the energy balance of the ground, a reduced infiltration capacity of the land surface to surface water, thermal properties that vary with changing soil water and ice contents, and reduced soil water movement.

Though many aspects of cold regions' soil physics are well known, it has not yet been analysed how individual processes influence the regional climate in terms of their relevance, and which of these are dominating others. This was the aim and outcome of the present study.

For investigating the influence of permafrost processes on the changed land surface-atmosphere interactions, these processes were implemented into the soil scheme of the REMO model. In order to be able to attribute resulting changes, it was decided to follow a step-wise method, such that the coupling of energy and water within the soil, that is expressed in the above listed processes, is enabled successively during the course of the model development.
A detailed analysis of the respective impact of the different permafrost processes that link energy and water was thus possible, and was conducted within this PhD for the first time.
The successive implementation method allowed to attribute changes in the simulated climate to specific processes. Therefore, the analysis within this work followed the steps described in Section 4, yet first concentrating on soil and surface variables, whereafter it was focussed on the surface energy balance and climate. In the last part of the analysis, an evaluation of the baseline as well as of the new model versions was conducted using

gridded observational, reanalysis and station measurement data.

6.2 Conclusions and outlook

Three research questions were defined (Section 1.4) which guided analysis and discussion of the results of the experiments in Chapter 5. Condensing results and findings from chapter 5, these questions will be answered in the following.

Research question 1

The first question queried how different permafrost properties and processes influence states of energy and water in the soil and at the land surface. The implementation of specific processes known to be important in permafrost soils led to different changes in soil and surface temperature and moisture variables, that in part counterbalanced each other.

The first incorporated processes were the latent heat of fusion in the energy balance in the ground, in combination with the reduction of surface water infiltration for frozen soils. Namely the reduced infiltration of the spring snow melt water led to a substantially lower root zone soil moisture, which in turn impacted the surface energy balance during the warm months.
The above mentioned first implemented processes demonstrated the expected behaviour, as the latent heat effect dampened the annual amplitude of soil temperatures, and typical permafrost features, as the pronounced stay at 0°C (zero-curtain) were reproduced by the model. However, the influence of the latent heat was dominated by the different summer climate that resulted from the changed surface water balance. Thus, soils warmed in general, and over large parts of Siberia ground cooling in spring and early summer due to melting of soil ice was reversed through warmer air temperatures that developed with the markedly reduced soil moisture.

The dependency of the soil thermal processes on soil water and ice contents, which were implemented in the second step, mainly modulated the soil temperatures, as they now dampen the intrusion of heat into the ground in summer, while they enhance heat loss in winter. This process is typical for high northern latitudes and leads to a net soil cooling. Therefore, REMO is now able to simulate soil properties that tend to stabilize permafrost, which is a gain in realism for this region.

The full coupling of soil thermodynamics and hydrology led to substantially higher moisture values in near-surface soil layers. This was attributable to the binding of water in its solid phase during the cold season, but also to the migration of liquid soil water towards the freezing front (cryosuction). Therefore, the model is now able to reproduce a process frequently observed in permafrost soils, which has an important impact on the

soil moisture profile.
The coupling of soil energy and water led to lower soil temperatures, as it increased the thermal offset effect, meaning increasing soil thermal conductivities due to more soil moisture especially during winter.
For the basin scale hydrology, the cold regions soil processes led to an improved behaviour with respect to river discharge. Again, the consideration of soil freezing led to a clear change which was only modulated through the coupling. The different partitioning of surface water into surface runoff and infiltration increased runoff in spring, while decreased runoff was simulated during the rest of the year. Therefore, soil and land surface variables were simulated more realistically when permafrost processes were represented in the model.

Research question 2

The second question asked how permafrost impacts seasonal variations of energy and water fluxes on the regional scale.
It was answered by analysing the consequences that the process implementation had for the surface energy balance and atmospheric variables such as air temperature, cloud cover, and precipitation.

The change in surface runoff due to the first process implementation is the most important, as the resulting decrease in root zone soil moisture markedly influences the partitioning of energy at the land surface into sensible and latent heat fluxes during summer.
Less moisture supply from the ground reduces the latent heat flux, while the sensible heat flux increases. The changed energy and moisture fluxes lead to higher near-surface air temperatures, which is detectable until heights of about 500 gpm, and to less atmospheric moisture, which consequently reduces cloudiness and precipitation.
These effects occur throughout the warm season, yet are most pronounced during early summer, as then the difference between experiments with permafrost processes and the baseline experiment are largest in terms of the changed surface water budget.

In fall, the discussed warming is weaker, yet supported by enhanced ground heat flux and thus warming of the atmosphere from below due to latent heat release in the soil. The coupling counterbalances this warming through the increase in soil moisture, and thus more evaporative cooling than in the first experiment.

The second and third change, respectively, imposed smaller differences on the surface energy balance and climate, which again emphasizes the dominance of the changed surface water partitioning in spring.

The surface energy balance was affected by the new, varying soil thermal properties, yet not as strongly as by the infiltration reduction. It showed a slight increase in near-surface air temperatures, as sensible heat flux needs to increase in order to counterbalance the reduced ground heat flux in summer.

The higher soil moisture values in turn counterbalanced the impacts due to the former discussed process implementations, as this more moist land surface showed an increased evaporation when compared to the preciding experiment.

Research question 3

The third question asked for the ability of the new REMO model to simulate cold regions' soil processes. Therefore, results from all including the baseline experiments were compared to different datasets; part of these data were chosen especially with respect to permafrost and a validation of soil variables.

Most importantly, a strong warm bias occurs over North- and East Siberia, which led to substantially too high simulated soil temperatures when compared to station measurements in the respective region. As the model extensions did not impact the winter atmospheric climate, this warm bias affects all experiments.
A marked wet bias occurs in precipitation during spring and early summer, concomittand with too high simulated evapotranspiration as compared to ERA40 data as well as to observations.

The comparison of baseline and coupled experiments to observations of continuous permafrost from the International Permafrost Association revealed that, despite the winter warm bias, the overall distribution is satisfyingly captured by both model versions.
Interestingly, the final, coupled version is able to simulate almost the same permafrost extent as the baseline experiment, albeit it featured a clearly warmer summer and fall climate. This indicates that the implemented processes enable REMO to simulate lower mean annual ground temperatures than the respective mean annual air temperatures are, due to the changed physical formulations. It is concluded that the new model version reproduces soil physical processes that are observed to be important in permafrost soils, as they modulate the ground thermal regime in a distinct way which cannot be reproduced without the respective processes.

Also the small changes induced on the Active Layer Depth can be attributed to the thermal offset effect, which leads to a now more shallow Active Layer in Northern Siberia in the new model as compared to the baseline experiment, albeit the Active Layer deepens in some more southernly regions.

The analysis of details of the freezing period for the model version including changes 2 and 3 revealed that the third, final model version maintains high total water contents throughout the cold season, and that it is able to simulate cryosuction or soil water migration from unfrozen layers towards the freezing front. The latter process is important in cold regions' soils, as it supports the high soil moisture levels frequently observed despite low precipitation.

Last, a comparison to station measurements on daily basis in order to validate the model's behaviour during freezing and melting periods showed the fundamental improvement of the simulated soil temperatures. The key property, the pronounced stay of the soil temperature at the freezing point (zero-curtain), can now be now simulated with REMO.

It can be concluded that the implementation of the most important permafrost processes into REMO led to improvements for the simulated soil variables and enabled the representation of processes that were neglected before.

Concluding remarks

The new model version is capable to simulate characteristic processes, such as the latent heat effects on the soil temperatures during freezing and melting and the cooling of ground with respect to air temperatures due to the specific behaviour of the soil thermal properties in cold regions. These properties are specific to soils in high latitudes, and importantly modulate the ground thermal regime.
Similarly, the regional hydrology improves noticeably with the implemented permafrost processes, which produce the typical spring peak in surface runoff with good realism due to the effects of soil freezing on surface water infiltration.

In summary, the work disentangled the impacts that different permafrost processes have on the regional cycles of energy and water within the ground, as well as between land surface and atmosphere. Moreover, it could be shown that the inclusion of permafrost processes in REMO led to improved soil and surface variables, and partially also to better simulated atmospheric variables.
Thus, it is concluded that permafrost processes might not only be decisive in the context of global Carbon modelling, but that their implementation is highly recommended for any study on land surface-atmosphere interactions in the high northern latitudes.

Outlook

Although permafrost processes in REMO improved the model with respect to cold regions' soil and land surface processes, there are still aspects that have not yet been considered, which will be outlined in the following.
It is planned, e.g. to incorporate an organic top layer into the soil scheme, which would decrease the intrusion of heat flux into the ground, especially during summer, thus leading to a stronger dampening of soil temperatures with depth. This would be a further improvement, as it showed a too large annual amplitude in the comparison to station measurements. It potentially also decreases near-surface air temperature due to enhanced evaporative cooling.

Another process that will be implemented in the future is the limitation of freezing through use of a freezing point depression equation. This could lead to an even better fit

of the freezing and melting curves, for which the comparison with the Chukochya station gave evidence. Moreover, this next step could further improve hydrological variables as it would influence soil water diffusivity.

It would be interesting and helpful to have more than one dataset of soil parameters, in order to evaluate the reliability of these.
It is recommended to study the influence of the soil column extension on simulated soil temperatures. Additional extension is planned, as it is recommended by permafrost scientists (V. Romanovsky, pers. comm., 2012).
An important aspect of permafrost regions is the treatment of the snow cover. It would therefore be advantageous to further validate the REMO snow scheme in order to improve it.

Eidesstattliche Erklärung

Hiermit versichere ich, dass ich vorgelegte Dissertation selbständig verfasst habe.
Alle Bezugsquellen der von mir benutzten Daten sind explizit in der vorgelegten Dissertation aufgeführt.

Tanja Blome

7 Acknowledgements

During the course of my PhD, I was supported by many people. First of all, I would like to thank my supervising panel, Stefan Hagemann, Daniela Jacob and Martin Claussen, for giving me this interesting research topic. They always had important and helpful remarks, and I learned a lot.
Thanks, Stefan for always having an open ear and for your patience! Moreover, I want to thank Martin Claussen for supporting me, and for helpful comments to keep on track. Daniela, thank you so much for trusting in me.
I would like to acknowledge the financial support during the final year of my PhD study by the European Union FP7-ENV project PAGE21 under contract number GA282700.
I am so thankful for all the technical and editorial advice that Tobias gave to me. Also, I would like to say thanks to the THY group, for giving interesting comments and hints. The same to the REMO group! A special thanks to Bjoern and Juliane, for your help with the data. And Swantje, what would I have done without you? I really don't know ... A very warm thanks to Ute, who helped me so much and was just calm. And always had interesting comments.
Diana and Fahad, it was so good to have you when last winter was darkest... I also need to thank Andreas, with whom to share the office was really a pleasure.
Thanks to Altug Ekici and Isabelle Gouttevin for helpful, open and interesting discussions! It was pleasure to work with you.
The same goes to Annette Rinke, which was always interested in what I am doing. And to Julia Boike, for always providing advice, and also data.
The meetings with Lars Kutzbach led to important ideas - thanks for the inspiring view of a permafrost observer.
Antje, I am so glad that you felt responsible also for me, for taking care for the bureaucratic stuff, and for being so encouraging.
Thanks for reading and commenting to Philip, Ute, Holger, Tobias, which was so helpfull. A very special thanks I want to dedicate to Ralf, who was so supporting. I hope you are fine where you are.
I really don't know how I could have managed to finish without all these people who looked after our kids. It was wunderful to feel that you cared, Nicole and Simon, Maja and Api, Birga, Holger and Maret, and Nicky of course. And thanks to my mom, who also helped us in this respect! Thanks to both of my parents, for help and support. The deepest gratefullness I feel for Heiko. Thank you for being with me.

Bibliography

Abu-Hamdeh, Nidal H. and Randall C. Reeder (2000). Soil Thermal Conductivity Effects of Density, Moisture, Salt Concentration, and Organic Matter. *Soil Science Society of America Journal* 64(4), pp. 1285–1290 (cit. on p. 36).

ACIA (2005). Arctic Climate Impact Assessment. Scientific Report (22). Cambridge University Press,1042p. (cit. on p. 3).

Anisimov, O.A. and F.E. Nelson (1997). Permafrost zonation and climate change in the northern hemisphere: Results from transient general circulation models. *Climatic Change* 35(2), 241–258. ISSN: 0165-0009. DOI: {10.1023/A:1005315409698}.

Baehr, H.D. and K. Stephan (2010). Waermeleitung und Diffusion. German. In: *Waerme- und Stoffuebertragung*. Springer Berlin Heidelberg, pp. 117–297. ISBN: 978-3-642-05500-3. DOI: 10.1007/978-3-642-10194-6_2. URL: http://dx.doi.org/10.1007/978-3-642-10194-6_2 (cit. on p. 30).

Beringer, J., A.H. Lynch, F.S. Chapin, M. Mack, and G.B. Bonan (2001). The representation of arctic soils in the land surface model: The importance of mosses. *Journal of Climate* 14(15), 3324–3335. ISSN: 0894-8755. DOI: {10.1175/1520-0442(2001)014<3324:TROASI>2.0.CO;2} (cit. on pp. 56, 62).

Brown, J., O.J. Ferrians, J.A.Jr. Heginbottom, and E.S. Melnikov (1998). Circum-arctic map of permafrost and ground ice conditions. Technical Reports (22). Boulder, CO: National Snow and Ice Data Center (cit. on pp. 3, 11, 71).

Brown, R.J.E. (1960). The distribution of permafrost and its relation to air temperature in Canada and the U.S.S.R. *Arctic*, pp. 163–177. ISSN: 13-3 (cit. on p. 15).

Cannone, N., J. C. Ellis Evans, R. Strachan, and M. Guglielmin (2006). Interactions between climate, vegetation and the active layer in soils at two Maritime Antarctic sites. *Antarctic Science* 18(3), 323–333. ISSN: 0954-1020. DOI: {10.1017/S095410200600037X}.

Carslaw, H.S. and J.C. Jaeger (1959). Conduction of heat in solids. Ed. by 2nd. Edn. Oxford University Press (cit. on pp. 33, 36).

Christiansen, H. H., B. Etzelmuller, K. Isaksen, H. Juliussen, H. Farbrot, O. Humlum, M. Johansson, T. Ingeman-Nielsen, L. Kristensen, J. Hjort, P. Holmlund, A. B. K. Sannel, C. Sigsgaard, H. J. Akerman, N. Foged, L. H. Blikra, M. A. Pernosky, and R. S. Odegard (2010). The Thermal State of Permafrost in the Nordic Area during the International Polar Year 2007-2009. *Permafrost and Periglacial Processes* 21(2, SI), 156–181. ISSN: 1045-6740. DOI: {10.1002/ppp.687}.

De Vries, D. A. (1963). Thermal properties of soils. In: *Physics of Plant Environment*. Ed. by W.R. Van Wijk. Amsterdam: North-Holland Publ Co. (cit. on pp. 37, 38, 64).

DeConto, R.M., S. Galeotti, M. Pagani, D. Tracy, K. Schaefer, T. Zhang, D. Pollard, and D.J. Beerling (2012). Past extreme warming events linked to massive carbon release from thawing permafrost. *Nature* 484(7392), pp. 87+. ISSN: 0028-0836. DOI: {10.1038/nature10929} (cit. on p. 13).

Duemenil Gates, L., S. Hagemann, and C. Golz (2000). Observed historical discharge data from major rivers for climate model validation. Scientific Report (22). Max Planck Institute for Meteorology, Hamburg (cit. on p. 71).

Dunne, J.P., J.G. John, A.J. Adcroft, S.M. Griffies, R.W. Hallberg, E. Shevliakova, R.J. Stouffer, W. Cooke, K.A. Dunne, M. J. Harrison, J.P. Krasting, S.L. Malyshev, P.C. D. Milly, P.J. Phillipps, L.T. Sentman, B. L. Samuels, M.J. Spelman, M. Winton, A. T. Wittenberg, and N. Zadeh (2012). GFDL's ESM2 Global Coupled Climate-Carbon Earth System Models. Part I: Physical Formulation and Baseline Simulation Characteristics. *Journal of Climate* 25(19), 6646–6665. ISSN: 0894-8755. DOI: {10.1175/JCLI-D-11-00560.1} (cit. on p. 46).

Ekici, A., C. Beer, S. Hagemann, J. Boike, M. Langer, and C. Hauck (2014). Simulating high-latitude permafrost regions by the JSBACH terrestrial ecosystem model. *Geosci. Model Dev.* 7 631–647. ISSN: 2. DOI: {10.5194/gmd-7-631-2014} (cit. on pp. 46, 50).

Farouki, O. (1981). The thermal properties of soils in cold regions. *Cold Reg.Sci. Technol.* 5(20), pp. 67–75. ISSN: 0094-8276. DOI: {10.1029/2006GL027484} (cit. on pp. 36, 37, 41, 54, 67).

Finney, D. L., E. Blyth, and R. Ellis (2012). Improved modelling of Siberian river flow through the use of an alternative frozen soil hydrology scheme in a land surface model. *The Cryosphere* 6(4), pp. 859–870. DOI: 10.5194/tc-6-859-2012. URL: http://www.the-cryosphere.net/6/859/2012/ (cit. on p. 41).

French, Hugh M. (2007). Editorial. *Permafrost and Periglacial Processes* 1(1), pp. 1–1. ISSN: 1099-1530. DOI: 10.1002/ppp.3430010102. URL: http://dx.doi.org/10.1002/ppp.3430010102 (cit. on pp. 3, 12, 25, 44).

Fyodorov-Davydov, D.G., V.A. Sorokovikov, V.E. Ostroumov, A.L. Kholodov, I.A. Mitroshin, N.S. Mergelov, S.P. Davydov, and A.I. Zimov S.A. & Davydova (2004). Spatial and Temporal Observations of Seasonal Thaw in the Northern Kolyma Lowland. *Polar Geography* 28(4), 308–325 (cit. on p. 72).

Gouttevin, I., G. Krinner, P. Ciais, J. Polcher, and C. Legout (2012). Multi-scale validation of a new soil freezing scheme for a land-surface model with physically-based hydrology. English. *Cryosphere* 6(2), 407–430. ISSN: 1994-0416. DOI: {10.5194/tc-6-407-2012} (cit. on pp. 37, 38, 41, 46, 59, 62, 67).

Haeckel, H. (2008). Meteorologie. Ed. by korrigierte Auflage 6. Stuttgart : Ulmer (cit. on p. 17).

Hagemann, S. (2002). An improved land surface parameter dataset for global and regional climate models. MPI-Report (336). Hamburg, Germany: Max Planck Institute for Meteorology (cit. on p. 69).

Hagemann, S., T. Blome, F. Saeed, and T. Stacke (2013). Perspectives in modelling climate-hydrology interactions. *Surveys in Geophysics* 35(ISSI special issue on Hydrological Cycle). DOI: 10.1007/s10712-013-9245-z (cit. on p. 6).

Hagemann, S. and L. Duemenil Gates (2001). Validation of the hydrological cycle ECMWF and NCEP reanalyses using the MPI hydrological discharge model. *J. Geophys. Res. D Atmos.* 106(2), pp. 1503–1510. DOI: 10.1029/2000JD900568 (cit. on p. 74).

Hagemann, S. and L. Duemenil (1998). A parametrization of the lateral waterflow for the global scale. *Clim. Dyn.* 14(1), pp. 17–31. DOI: 10.1007/s003820050205 (cit. on p. 74).

Hagemann, S. and T. Stacke (2013). Impact of the soil hydrology scheme on simulated soil moisture memory. *Climate Dynamics, in review* (cit. on pp. 40, 49, 51).

Hall, A. and X. Qu (Feb. 2006). Using the current seasonal cycle to constrain snow albedo feedback in future climate change. *Geophysical Research Letters* 33(3), p. L03502. DOI: 10.1029/2005GL025127 (cit. on p. 5).

Halliwell, D. H. and W. R. Rouse (1987). Soil heat flux in permafrost: Characteristics and accuracy of measurement. *Journal of Climatology* 7 pp. 571–584 (cit. on p. 29).

Heginbottom, J.A. (2002). Permafrost mapping: a review. *Progress in Physical Geography* 26(4), 623–642. ISSN: 0309-1333. DOI: {10.1191/0309133302pp355ra} (cit. on pp. 9, 11, 44).

Hillel, Daniel (1980). Fundamentals of soil physics. Ed. by Academic Press. New York [u.a.]: Academic Press (cit. on pp. 33, 35).

IPCC (1990). Report prepared for Intergovernmental Panel on Climate Change by Working Group I. Ed. by S. Solomon, D. Qin, M. Manning, Z. Chen, M. Marquis, K.B. Averyt, M. Tignor, and H.L. Miller. Cambridge, UK and New York, USA: Cambridge University Press (cit. on p. 43).

– (1995). Contribution of Working Group I to the Second Assessment Report of the Intergovernmental Panel on Climate Change. Ed. by S. Solomon, D. Qin, M. Manning, Z. Chen, M. Marquis, K.B. Averyt, M. Tignor, and H.L. Miller. Cambridge, UK and New York, USA: Cambridge University Press (cit. on pp. 11, 43).

– (2007). Contribution of Working Group I to the Fourth Assessment Report of the Intergovernmental Panel on Climate Change. Ed. by S. Solomon, D. Qin, M. Manning, Z. Chen, M. Marquis, K.B. Averyt, M. Tignor, and H.L. Miller. Cambridge, UK and New York, USA: Cambridge University Press (cit. on pp. 3, 10, 13, 22, 23).

Jacob, D. (2001). A note to the simulation of the annual and inter-annual variability of the water budget over the Baltic Sea drainage basin. *Meteorology and Atmospheric Physics* 77(1-4), 61–73. ISSN: 0177-7971. DOI: {10.1007/s007030170017} (cit. on pp. 7, 49).

Jacob, D. and R. Podzun (1997). Sensitivity studies with the regional climate model REMO. *Meteorology and Atmospheric Physics* 63(1-2). International Workshop on Limited-Area and Variable Resolution Models, BEIJING, PEOPLES R CHINA, OCT, 1995, 119–129. ISSN: 0177-7971. DOI: {10.1007/BF01025368} (cit. on p. 49).

Johansen, O. (1975). Thermal conductivity of soils. PhD thesis. Trondheim, Norway (cit. on p. 37).

Kersten, M.S. (1949). Laboratory research for the determination of the thermal properties of soils. Tech. rep. Corps of Engineers, USArmy (cit. on p. 37).

Koren, V., J. Schaake, K. Mitchell, Q.Y. Duan, F. Chen, and J.M. Baker (1999). A parameterization of snowpack and frozen ground intended for NCEP weather and

climate models. English. *Journal of Geophysical Research-Atmospheres* 104(D16), 19569–19585. ISSN: 0747-7309. DOI: {10.1029/1999JD900232} (cit. on p. 67).

Kotlarski, S. (2007). A Subgrid Glacier Parameterisation for Use in Regional Climate Modelling A Subgrid Glacier Parameterisation for Use in Regional Climate Modelling. PhD thesis. University of Hamburg. Max Planck Institute for Meteorology (cit. on p. 49).

Kotlyakov, V. and T. Khromova (1997). Land Resources of Russia. Technical Reports (22). International Institute for Applied Systems Analysis (cit. on p. 71).

Koven, Charles D., W.J. Riley, and A. Stern (2013). Analysis of Permafrost Thermal Dynamics and Response to Climate Change in the CMIP5 Earth System Models. *Journal of Climate* 26(6), 1877–1900. ISSN: 0894-8755. DOI: {10.1175/JCLI-D-12-00228.1} (cit. on pp. 6, 46, 47).

Kraus, Helmut (2008). Grundlagen der Grenzschicht-Meteorologie. URL: http://ebooks.ub.uni-muenchen.de/16702/ (cit. on pp. 29, 30, 32, 36).

Krinner, G., N. Viovy, N. de Noblet-Ducoudre, J. Ogee, J. Polcher, P. Friedlingstein, P. Ciais, S. Sitch, and I.C. Prentice (2005). A dynamic global vegetation model for studies of the coupled atmosphere-biosphere system. *Global Biogeochemical Cycles* 19(1). ISSN: 0886-6236. DOI: {10.1029/2003GB002199} (cit. on pp. 46, 54, 59).

Landerer, F.W., J.O. Dickey, and A. Guentner (2010). Terrestrial water budget of the Eurasian pan-Arctic from GRACE satellite measurements during 2003-2009. *Journal of Geophysical Research-Atmospheres* 115 ISSN: 2169-897X. DOI: {10.1029/2010JD014584} (cit. on p. 26).

Langer, M., S. Westermann, S. Muster, K. Piel, and J. Boike (2011). The surface energy balance of a polygonal tundra site in northern Siberia - Part 2: Winter. *Cryosphere* 5(2), 509–524. ISSN: 1994-0416. DOI: {10.5194/tc-5-509-2011} (cit. on pp. 74, 104).

Lawrence, D.M., K.W. Oleson, M.G. Flanner, P.E. Thornton, S.C. Swenson, P.J. Lawrence, X. Zeng, Z.-Liang Yang, S. Levis, K. Sakaguchi, G.B. Bonan, and A.G. Slater (2011). Parameterization Improvements and Functional and Structural Advances in Version 4 of the Community Land Model. *Journal of Advances in Modeling Earth Systems* 3 ISSN: 1942-2466. DOI: {10.1029/2011MS000045} (cit. on p. 46).

Luo, L.F., A. Robock, K.Y. Vinnikov, C.A. Schlosser, A.G. Slater, A. Boone, H. Braden, P. Cox, P. de Rosnay, R.E. Dickinson, Y.J. Dai, Q.Y. Duan, P. Etchevers, A. Henderson-Sellers, N. Gedney, Y.M. Gusev, F. Habets, J.W. Kim, E. Kowalczyk, K. Mitchell, O.N. Nasonova, J. Noilhan, A.J. Pitman, J. Schaake, A.B. Shmakin, T.G. Smirnova, P. Wetzel, Y.K. Xue, Z.L. Yang, and Q.C. Zeng (2003). Effects of frozen soil on soil temperature, spring infiltration, and runoff: Results from the PILPS 2(d) experiment at Valdai, Russia. English. *Journal of Hydrometeorology* 4(2), 334–351. ISSN: 1525-755X. DOI: {10.1175/1525-7541(2003)4<334:EOFSOS>2.0.CO;2} (cit. on p. 47).

Luojus, K., J. Pulliainen, and the GlobSnow Consortiuum (2010). Global Snow Monitoring for Climate Research: Snow Water Equivalent. Tech. rep. Finnish Meteorological Institute, Helsinki, Finland (cit. on p. 71).

Majewski, D. (1991). The Europa-Modell of the Deutscher Wetterdienst. *ECMWF Seminar on Numerical Methods in Atmospheric Models* 2 147–191 (cit. on p. 49).

Matthes, H., A. Rinke, P.A. Miller, P. Kuhry, K. Dethloff, and A. Wolf (2012). Sensitivity of high-resolution Arctic regional climate model projections to different implementations of land surface processes. *Climatic Change* 111(2), 197–214. ISSN: 0165-0009. DOI: {10.1007/s10584-011-0138-1} (cit. on pp. 47, 48).

McClelland, J.W., R.M. Holmes, B.J. Peterson, and M. Stieglitz (2004). Increasing river discharge in the Eurasian Arctic: Consideration of dams, permafrost thaw, and fires as potential agents of change. English. *Journal of Geophysical Research-Atmospheres* 109(D18). ISSN: 0148-0227. DOI: {10.1029/2004JD004583} (cit. on p. 26).

McGuire, A. David, Leif G. Anderson, Torben R. Christensen, Scott Dallimore, Laodong Guo, Daniel J. Hayes, Martin Heimann, Thomas D. Lorenson, Robie W. Macdonald, and Nigel Roulet (2009). Sensitivity of the carbon cycle in the Arctic to climate change. English. *Ecological Monographs* 79(4), 523–555. ISSN: 0012-9615. DOI: {10.1890/08-2025.1} (cit. on pp. 3, 22).

Mickley, A.S. (1951). The thermal conductivity of moist soil. *Am. Inst. Elect. Engrs. Transactions* 70 pp. 1789–1797 (cit. on p. 37).

Moelders, N. and V.E. Romanovsky (2006). Long-term evaluation of the Hydro-Thermodynamic Soil-Vegetation Scheme's frozen ground/permafrost component using observations at Barrow, Alaska. *Journal of Geophysical Research-Atmospheres* 111(D4), n/a–n/a. ISSN: 2156-2202. DOI: 10.1029/2005JD005957. URL: http://dx.doi.org/10.1029/2005JD005957 (cit. on pp. 37, 64).

Nelson, F.E. (2003). (Un)frozen in time. *Science* 299(5613), 1673–1675. ISSN: 0036-8075. DOI: {10.1126/science.1081111} (cit. on pp. 12, 15).

Nelson, F.E. and S.I. Outcalt (1987). A computational method for prediction and regionalization of permafrost. *Arctic and alpine research* 19(3), 279–288. ISSN: 0004-0851. DOI: {10.2307/1551363} (cit. on p. 45).

Nicolsky, D.J., V.E. Romanovsky, V.A. Alexeev, and D.M. Lawrence (2007). Improved modeling of permafrost dynamics in a GCM land-surface scheme. *Geophysical Research Lettters* 34(8). ISSN: 0094-8276. DOI: {10.1029/2007GL029525} (cit. on p. 68).

Niu, G.-Y. and Z.-L. Yang (2006). Effects of frozen soil on snowmelt runoff and soil water storage at a continental scale. English. *Journal of Hydrometeorology* 7(5), 937–952. ISSN: 1525-755X. DOI: {10.1175/JHM538.1} (cit. on pp. 40, 65, 67).

Oleson, K.W., D.M. Lawrence, G.B. Bonan, M.G. Flanner, E. Kluzek, P.J. Lawrence, S. Levis, S.C. Swenson, and P.E. Thornton (2010). Technical Description of version 4.0 of the Community Land Model (CLM). Technical Reports. National Center for Atmospheric Research (cit. on pp. 54, 62).

Peterson, B.J., R.M. Holmes, J.W. McClelland, C.J. Vörösmarty, R.B. Lammers, A.I. Shiklomanov, I.A. Shiklomanov, and S. Rahmstorf (2002). Increasing River Discharge to the Arctic Ocean. *Science* 298(5601), pp. 2171–2173. DOI: 10.1126/science.1077445. URL: http://www.sciencemag.org/content/298/5601/2171.abstract (cit. on p. 25).

Pitman, A. J. (2003). The evolution of, and revolution in, land surface schemes designed for climate models. *International Journal of Climatology* 23(5), pp. 479–510. ISSN: 1097-0088. DOI: 10.1002/joc.893. URL: http://dx.doi.org/10.1002/joc.893 (cit. on p. 43).

Preuschmann, S. (2012). Regional surface albedo characteristics - analysis of albedo data and application to land-cover changes for a regional climate model. *Reports on Earth System Science* 117 p. 160. URL: http://www.mpimet.mpg.de/fileadmin/publikationen/Reports/WEB_BzE_117.pdf (cit. on p. 49).

Raddatz, T. J., C. H. Reick, W. Knorr, J. Kattge, E. Roeckner, R. Schnur, K.-G. Schnitzler, P. Wetzel, and J. Jungclaus (2007). Will the tropical land biosphere dominate the climate-carbon cycle feedback during the twenty-first century? *Climate Dynamics* 29(6), 565–574. ISSN: 0930-7575. DOI: {10.1007/s00382-007-0247-8} (cit. on p. 46).

Rechid, D. (2009). On biogeophysical interactions between vegetation phenology and climate simulated over Europe. *Reports on Earth System Science* 61 p. 130 (cit. on p. 49).

Rinke, A., P. Kuhry, and K. Dethloff (2008). Importance of a soil organic layer for Arctic climate: A sensitivity study with an Arctic RCM. *Geophysical Research Letters* 35(13). ISSN: 0094-8276. DOI: {10.1029/2008GL034052}.

Rinke, A., H. Matthes, J.H. Christensen, P. Kuhry, V.E. Romanovsky, and K. Dethloff (2012). Arctic RCM simulations of temperature and precipitation derived indices relevant to future frozen ground conditions. *Global and Planetary Change* 80-81 136–148. ISSN: 0921-8181. DOI: {10.1016/j.gloplacha.2011.10.011}.

Riseborough, D., N. Shiklomanov, B. Etzelmuller, S. Gruber, and S. Marchenko (2008). Recent advances in permafrost modelling. *Permafrost and Periglacial Processes* 19(2), 137–156. ISSN: 1045-6740. DOI: {10.1002/ppp.615} (cit. on pp. 3, 6, 9, 44, 46, 47).

Romanovsky, V.E. (2003). East Siberian Air, Ground Temperature, and Snow Depth Measurements, 1882-1994. Technical Reports (22). NSIDC: National Snow and Ice Data Center (cit. on p. 72).

Romanovsky, V.E. and T.E. Osterkamp (1995). Interannual variations of the thermal regime of the active layer and near-surface permafrost in northern Alaska. *Permafrost and Periglacial Processes* 6(4), 313–335. ISSN: 1045-6740. DOI: {10.1002/ppp.3430060404} (cit. on pp. 57, 136).

– (2000). Effects of unfrozen water on heat and mass transport processes in the active layer and permafrost. *Permafrost and Periglacial Processes* 11(3), 219–239. ISSN: 1045-6740. DOI: {10.1002/1099-1530(200007/09)11:3<219::AID-PPP352>3.0.CO;2-7} (cit. on p. 41).

Romanovsky, V.E., S.L. Smith, and H.H. Christiansen (2010). Permafrost thermal state in the polar Northern Hemisphere during the international polar year 2007-2009: a synthesis. *Permafrost and Perciglacial Processes* 21 pp. 106–116. URL: http://dx.doi.org/10.1002/ppp.689.

Saha, S.K., A. Rinke, K. Dethloff, and P. Kuhry (2006). Influence of a complex land surface scheme on Arctic climate simulations. *Journal of Geophysical Research-Atmospheres* 111(D22). ISSN: 2169-897X. DOI: {10.1029/2006JD007188} (cit. on pp. 37, 47, 54).

Sazonova, T.S., V.E. Romanovsky, J.E. Walsh, and D.O. Sergueev (2004). Permafrost dynamics in the 20th and 21st centuries along the East Siberian transect. *Journal of Geophysical Research-Atmospheres* 109(D1). ISSN: 2169-897X. DOI: {10.1029/2003JD003680}.

Schuur, E.A.G., J. Bockheim, J.G. Canadell, E. Euskirchen, C.B. Field, S.V. Goryachkin, S. Hagemann, P. Kuhry, P.M. Lafleur, H. Lee, G. Mazhitova, F. E. Nelson, A. Rinke, V.E. Romanovsky, N. Shiklomanov, C. Tarnocai, S. Venevsky, J.G. Vogel, and S.A. Zimov (2008). Vulnerability of permafrost carbon to climate change: Implications for the global carbon cycle. English. *Bioscience* 58(8), 701–714. ISSN: 0006-3568. DOI: {10.1641/B580807} (cit. on pp. 3, 11).

Semmler, T. (2002). Der Wasser- und Energiehaushalt der arktischen Atmosphaere. PhD thesis. Max-Planck-Institut fuer Meteorologie (cit. on pp. 49–51).

Seneviratne, S.I., T. Corti, E.L. Davin, M. Hirschi, E.B. Jaeger, I. Lehner, B. Orlowsky, and A.J. Teuling (2010). Investigating soil moisture-climate interactions in a changing climate: A review. *Earth-Science Reviews* 99(3-4), pp. 125–161. ISSN: 0012-8252. DOI: 10.1016/j.earscirev.2010.02.004. URL: http://www.sciencedirect.com/science/article/pii/S0012825210000139 (cit. on p. 5).

Serreze, M.C., D.H. Bromwich, M.P. Clark, A.J. Etringer, T.J. Zhang, and R. Lammers (2002). Large-scale hydro-climatology of the terrestrial Arctic drainage system. English. *Journal of Geophysical Research-Atmospheres* 108(D2). ISSN: 0148-0227. DOI: {10.1029/2001JD000919} (cit. on pp. 25, 26).

Shiklomanov, N.I. (2005). From exploration to systematic investigation: Development of Geocryology in 19th-and early-20th-century Russia. English. *Physical Geography* 26 (4), pp. 249–263. ISSN: 1028-334X. DOI: 10.2747/0272-3646.26.4.249 (cit. on pp. 9, 15, 44).

Slater, A. and D. Lawrence (2013). Diagnosing Present and Future Permafrost from Climate Models. DOI: {10.1175/JCLI-D-12-00341.1} (cit. on pp. 46, 47).

Smith, S.L., V.E. Romanovsky, A.G. Lewkowicz, C.R. Burn, M. Allard, G.D. Clow, K. Yoshikawa, and J. Throop (2010). Thermal State of Permafrost in North America: A Contribution to the International Polar Year. *Permafrost and Periglacial Processes* 21(2, SI), 117–135. ISSN: 1045-6740. DOI: {10.1002/ppp.690}.

Staehli, M., P.-E. Jansson, and L.-C. Lundin (1999). Soil moisture redistribution and infiltration in frozen sandy soils. *Water Resources Research* 35 (1), pp. 95–104. DOI: 10.1029/1998WR900045 (cit. on p. 40).

Sturm, M., J.P. McFadden, G.E. Liston, F.S. Chapin, C.H. Racine, and J. Holmgren (2001). Snow-shrub interactions in Arctic tundra: A hypothesis with climatic implications. *Journal of Climate* 14(3), 336–344. ISSN: 0894-8755. DOI: {10.1175/1520-0442(2001)014<0336:SSIIAT>2.0.CO;2} (cit. on p. 27).

Sturm, M., J. Schimel, G. Michaelson, J.M. Welker, S.F. Oberbauer, G.E. Liston, J. Fahnestock, and V.E. Romanovsky (2005). Winter biological processes could help convert arctic tundra to shrubland. *Bioscience* 55(1), 17–26. ISSN: 0006-3568. DOI: {10.1641/0006-3568(2005)055{[}0017:WBPCHC]2.0.CO;2} (cit. on p. 27).

Sugimoto, A., N. Yanagisawa, D. Naito, N. Fujita, and T.C. Maximov (2002). Importance of permafrost as a source of water for plants in east Siberian taiga. *Ecological Research* 17(4), 493–503. ISSN: 0912-3814. DOI: {10.1046/j.1440-1703.2002.00506.x} (cit. on p. 28).

Sushama, L., R. Laprise, and M. Allard (2006). Modeled current and future soil thermal regime for northeast Canada. *Journal of Geophysical Research-Atmospheres* 111(D18). ISSN: 2169-897X. DOI: {10.1029/2005JD007027}.

Sushama, L., R. Laprise, D. Caya, D. Verseghy, and M. Allard (2007). An RCM projection of soil thermal and moisture regimes for North American permafrost zones. *Geophysical Research Letters* 34(20). ISSN: 0094-8276. DOI: {10.1029/2007GL031385}.

Swenson, S.C., D.M. Lawrence, and Hanna Lee (2012). Improved simulation of the terrestrial hydrological cycle in permafrost regions by the Community Land Model. *Journal of Advances in Modeling Earth Systems* 4 ISSN: 1942-2466. DOI: {10.1029/2012MS000165} (cit. on pp. 24, 25, 41, 67).

Takata, K., S. Emori, and T. Watanabe (2003). Development of the minimal advanced treatments of surface interaction and runoff. *Global and Planetary Change* 38(1-2), 209–222. ISSN: 0921-8181. DOI: {10.1016/S0921-8181(03)00030-4} (cit. on p. 46).

Takata, K. and M. Kimoto (2000). A numerical study on the impact of soil freezing on the continental-scale seasonal cycle. *Journal of the Meteorological Society of Japan* 78(3), 199–221. ISSN: 0026-1165 (cit. on p. 48).

Tarnawski, V.R. and B. Wagner (1993). Modeling the thermal conductivity of soils. *Cold Regions Science and Technology* 22 pp. 19–31 (cit. on p. 37).

Tarnocai, C., J.G. Canadell, E.A.G. Schuur, P. Kuhry, G. Mazhitova, and S. Zimov (2009). Soil organic carbon pools in the northern circumpolar permafrost region. *Global Biogeochemical Cycles* 23 ISSN: 0886-6236. DOI: {10.1029/2008GB003327} (cit. on p. 3).

Uppala, S.M., P.W. Kållberg, A.J. Simmons, U. Andrae, V. da Costa Bechtold, M. Fiorino, J.K. Gibson, J. Haseler, A. Hernandez, G.A. Kelly, X. Li, K. Onogi, S. Saarinen, N. Sokka, R.P. Allan, E. Andersson, K. Arpe, M.A. Balmaseda, A.C.M. Beljaars, L. van de Berg, J. Bidlot, N. Bormann, S. Caires, F. Chevallier, A. Dethof, M. Dragosavac, M. Fisher, M. Fuentes, S. Hagemann, E. Hólm, B.J. Hoskins, L. Isaksen, P.A.E.M. Janssen, R. Jenne, A.P. McNally, J.-F. Mahfouf, J.-J. Morcrette, N.A. Rayner, R.W. Saunders, P. Simon, A. Sterl, K.E. Trenberth, A. Untch, D. Vasiljevic, P. Viterbo, and J. Woollen (2005). The ERA-40 re-analysis. *Q. J. R. Meteorol. Soc.* 131(612), pp. 2961–3012. DOI: 10.1256/qj.04.176 (cit. on p. 71).

Verseghy, D.L. (1991). Class Canadian land surface scheme for GCMS. I. Soil model. *International Journal of Climatology* 11(2), pp. 111–133. ISSN: 1097-0088. DOI: 10.1002/joc.3370110202. URL: http://dx.doi.org/10.1002/joc.3370110202 (cit. on pp. 46, 54).

Volodin, E.M., N.A. Dianskii, and A.V. Gusev (2010). Simulating present-day climate with the INMCM4.0 coupled model of the atmospheric and oceanic general circulations. *Izvestiya Atmospheric and Oceanic Physics* 46(4), 414–431. ISSN: 0001-4338. DOI: {10.1134/S000143381004002X} (cit. on p. 46).

Warnecke, G. (1997). Meteorologie und Umwelt: eine Einfuehrung. Ed. by 2nd. Edn. Berlin (u.a.): Springer (cit. on p. 38).

Weedon, G.P., S. Gomes, P. Viterbo, H. Österle, J.C. Adam, N. Bellouin, O. Boucher, and M. Best (2010). The WATCH Forcing Data 1958-2001: A Meteorological Forcing

Dataset for Land Surface- and Hydrological-Models. Technical Reports (22). WATCH (cit. on p. 71).

Yang, D., D.L. Kane, L.D. Hinzman, X. Zhang, T. Zhang, and H. Ye (2002). Siberian Lena River hydrologic regime and recent change. *Journal of Geophysical Research* 107 (D23). DOI: 10.1029/2002JD002542 (cit. on p. 26).

Yi, S., M.-K. Woo, and M.A. Arain (2007). Impacts of peat and vegetation on permafrost degradation under climate warming. *Geophysical Research Letters* 34(16). ISSN: 0094-8276. DOI: {10.1029/2007GL030550} (cit. on p. 27).

Zech, R., Y. Huang, M. Zech, R. Tarozo, and W. Zech (2011). High carbon sequestration in Siberian permafrost loess-paleosols during glacials. *Climate of the Past* 7(2), 501–509. ISSN: 1814-9324. DOI: {10.5194/cp-7-501-2011} (cit. on pp. 13, 22).

Zhang, N., T. Yasunari, and T. Ohta (2011). Dynamics of the larch taiga-permafrost coupled system in Siberia under climate change. *Environmental Research Letters* 6(2). ISSN: 1748-9326. DOI: {10.1088/1748-9326/6/2/024003} (cit. on p. 28).

Zhang, T.J. (2005). Influence of the seasonal snow cover on the ground thermal regime: An overview. *Reviews of Geophysics* 43(4). ISSN: 8755-1209. DOI: {10.1029/2004RG000157} (cit. on pp. 16, 128, 135).

Zhang, Y., S.K. Carey, and W.L. Quinton (2008). Evaluation of the algorithms and parameterizations for ground thawing and freezing simulation in permafrost regions. *Journal of Geophysical Research-Atmospheres* 113(D17). ISSN: 2169-897X. DOI: {10.1029/2007JD009343} (cit. on p. 52).

Zimov, S.A., S.P. Davydov, G.M. Zimova, A. I. Davydova, E.A.G. Schuur, K. Dutta, and F.S. Chapin III (2006). Permafrost carbon: Stock and decomposability of a globally significant carbon pool. *Geophysical Research Letters* 33(20). ISSN: 0094-8276. DOI: {10.1029/2006GL027484} (cit. on pp. 3, 22, 23).

Die gesamten Veröffentlichungen in der Publikationsreihe des MPI-M
„Berichte zur Erdsystemforschung“,
„Reports on Earth System Science“,
ISSN 1614-1199

sind über die Internetseiten des Max-Planck-Instituts für Meteorologie erhältlich:

http://www.mpimet.mpg.de/wissenschaft/publikationen.html



ISSN 1614-1199